

- I. AN $^{18}\text{O}/^{16}\text{O}$ INVESTIGATION OF THE LAKE CITY CALDERA,
SAN JUAN MOUNTAINS, COLORADO

- II. $^{18}\text{O}/^{16}\text{O}$ RELATIONSHIPS IN TERTIARY ASH-FLOW TUFFS FROM
COMPLEX CALDERA STRUCTURES IN
CENTRAL NEVADA AND THE SAN JUAN MOUNTAINS, COLORADO

Thesis by

Peter Brennan Larson

In Partial Fulfillment of the Requirements

for the Degree of

Doctor of Philosophy

California Institute of Technology

Pasadena, California

1983

(Submitted September 19, 1983)

ACKNOWLEDGEMENT

Throughout my stay at Caltech, Profesor Hugh Taylor has provided useful and timely advice. He originally suggested this thesis project and gave me the freedom to pursue it as I saw fit. I especially thank him for the time and effort he put into this manuscript and for insis-ting on perfection throughout its preparation.

Support and fruitful discussions have been provided by many of the faculty. Professors Silver, Stolper, Rossman, Epstein, Sieh, and Saleeby have been most helpful at various times during my stay.

This thesis would not have been possible without the technical aid provided by Joop Goris, John Coulson, Mike Carr, and Art Chodos. The secretarial and administrative staff always cheerfully provided help, with special thanks to Dorothy Coy, Cheryl Contopulos, and Elaine Thompson. Some of the drafting was kindly provided by Jan Mayne and Kathi Kronenfeld. I thank you all.

My fellow students at Caltech deserve much credit for valuable dis-cussions and support in many aspects of this work. Jim Conca, Robert Hill, Ray Weldon, Cleve Solomon, George Gehrels, and John Jones were especially helpful. Bob Criss deserves a special mention and a special thanks for much useful advice.

Ken Hon was kind enough to provide some of his own samples, as well as providing samples from the Amoco Red Mountain drill core; he also provided some of the results of his mapping of the Lake City caldera. Discussions with him provided much insight concerning the geology of the caldera.

The Anaconda Company was kind enough to support me for one summer

of field work without any stipulations. John King was instrumental in providing this aid.

The most important person in my life throughout my four years at Caltech has been my wife, Meredith. None of what I have accomplished since coming to Caltech would have been possible without her. She has graciously postponed her goals so that I could achieve mine. Also, special thanks go to four animals (Toivola, Columbine, Sutter, and Thomasina) for always smiling. Meredith's parents, Mr. and Mrs. Marshall Brown, were also very supportive and deserve acknowledgment.

Support for this work was provided by N.S.F. Grant EAR-78-16874 and D.O.E. Grant EX-76-G-03-1305. A Penrose Grant from the Geological Society of America helped provide field expenses.

ABSTRACT

Part I. $^{18}\text{O}/^{16}\text{O}$ analyses were made on 355 samples in and around the 11 by 14 km Lake City caldera, which formed 23 m.y. ago in response to the eruption of the rhyolitic Sunshine Peak Tuff. All of the major lithologies and hydrothermal alteration facies were analyzed, and a detailed $\delta^{18}\text{O}$ map was made of the caldera and its surroundings. Intracaldera facies Sunshine Peak Tuff consists of three members interbedded with landslide debris and megabreccias shed into the caldera during eruption and collapse. Asymmetric resurgence within the Lake City caldera followed collapse and was accompanied by intrusion of a flat-topped, granitic magma centered in the resurgent dome. Ring magmatism produced dike-like intrusions along the northern ring fault and the Red Mountain-Grassy Mountain quartz latite ring dome on the eastern caldera margin. The caldera was emplaced into older Tertiary volcanic rocks and Precambrian granitic rocks.

Based on analyses of outflow-facies samples and of the least altered intracaldera facies, we can demonstrate that the caldera-fill Sunshine Peak Tuff originally was isotopically very homogeneous, with an initial igneous $\delta^{18}\text{O}$ value of +7.2 to +7.3. Thus, ^{18}O depletions in the hydrothermally altered tuff could be compared without worrying about the complicating factor of different initial $\delta^{18}\text{O}$ values. Nearly all the rocks within the caldera and outside the caldera within at least 3 km of the ring fault were altered by meteoric-hydrothermal fluids, and depleted in ^{18}O down to values as low as $\delta^{18}\text{O} = -3.1$. Erosion has exposed the hydrothermally altered caldera-fill rocks and the upper

contact of the altered resurgent intrusion in the western and central part of the caldera, providing about 2 km of vertical exposure. Because of post-alteration regional eastward tilting, the eastern part of the caldera has not been extensively eroded, and the original topography of the ring dome and the top of the caldera-fill rocks are locally preserved. This differential erosion from west to east furnishes a unique opportunity to study water-rock interactions in a caldera-type hydrothermal system from near-surface environments down through 3 km into the sub-volcanic intrusion that drove the hydrothermal convection.

Elevation and proximity to fractures exerted the strongest control on ^{18}O -depletions in the Precambrian granite and the older volcanic rocks. The lowest $\delta^{18}\text{O}$ values are found in rocks from the Eureka graben, a highly-fractured and extensively altered zone that extends SW from the caldera. Low $\delta^{18}\text{O}$ values also occur adjacent to the caldera ring fault. Those samples of the Precambrian granite and of the older volcanic rocks that are located at the greatest depths below the mid-Tertiary erosion surface have the lowest $\delta^{18}\text{O}$ values. At present-day, constant elevations, $\delta^{18}\text{O}$ values are lowest in the western part of the study area than in the eastern part; this is a result of the regional eastward tilting. The above effects are best interpreted as indicating higher water/rock ratios near the permeable fractures and higher temperatures at greater depth.

The $\delta^{18}\text{O}$ values within the Lake City caldera are controlled by elevation, proximity to permeable zones, and proximity to the resurgent intrusive rocks. $\delta^{18}\text{O}$ values decrease systematically with stratigraphic depth within the caldera. The lowest $\delta^{18}\text{O}$ values are found along the

western ring fault, along resurgence-related fractures, in the permeable megabreccia units, and along the contact of the resurgent intrusion. Mineralogic alteration facies within the caldera show complementary patterns. Intense argillization is found along fractures near the resurgent intrusion. Rocks adjacent to the resurgent intrusion have been hornfelsed but not intensely mineralogically altered. Weak argillization in stratigraphically shallow Sunshine Peak Tuff grades into both of these alteration regimes and also grades downward into chlorite-calcite alteration. These data show that the resurgent intrusion was the "heat engine" that drove the Lake City hydrothermal system. Alteration in and near the intrusion occurred at high temperatures ($\approx 400^{\circ}\text{C}$) and intermediate water/rock ratios. Away from the resurgent intrusion, water-rock interaction in the permeable zones (megabreccia units and fractures) occurred at lower temperatures (200°C to 300°C) and high water/rock ratios. The regional eastward tilting has raised low- ^{18}O rocks in the western part of the caldera to higher elevations than stratigraphically equivalent rocks in the eastern part of the caldera. Mineralogical alteration patterns are also similarly displaced.

Near-surface solfataric alteration is centered on a brecciated zone in the Red Mountain-Grassy Mountain quartz-latitude dome on the eastern caldera margin. $\delta^{18}\text{O}$ values of hydrothermal quartz from this alteration zone are high ($> +11$) and decrease gradationally with depth. Vein quartz $\delta^{18}\text{O}$ values from deeper levels within the caldera lie on the deeper projection of the solfataric quartz $\delta^{18}\text{O}$ trend. These data can be successfully modelled using an upward-flowing, boiling, ^{18}O -shifted meteoric water as a hydrothermal fluid. This model shows that the same

fluids responsible for vein quartz precipitation also produced the shallow solfataric alteration. High $\delta^{18}\text{O}$ values were also measured from a number of other solfatarically altered areas in the San Juan Mountains (Red Mountain district near Silverton, Calico Peak near Rico, Engineer Pass, Carson Camp, and the Summitville district). These alteration zones, some of which are economically mineralized, were also apparently produced by boiling meteoric-hydrothermal fluids.

Deeply-circulated, ^{18}O -shifted, meteoric waters were the primary source of hydrothermal fluids in the Lake City hydrothermal system. By analogy with other deeply eroded caldera hydrothermal systems studied by other workers, such fluids probably rose along deep extensions of the fractured, permeable Lake City ring fault zone. At the present level of exposure, fluids in the Lake City hydrothermal system were apparently drawn into the central part of the resurgent dome along the permeable, outward-dipping, megabreccia units. Flow was directed upward along permeable fractures where these fractures intersected the megabreccia units. A strong thermal gradient existed around and over the resurgent intrusion. Recharge into this hydrothermal system was basically radially inward toward the caldera, but flow was greatly enhanced through the permeable, highly fractured, Eureka graben.

Part II. Oxygen isotope studies were made on 60 samples from the central Nevada caldera complex, which consists of three nested calderas that erupted from 32 to 25 m.y. ago. $^{18}\text{O}/^{16}\text{O}$ analyses were also made on 96 samples from the central San Juan caldera complex, Colorado, which contains 7 ash-flow tuffs, each erupted from separate, nested collapse structures between 28 and 26 m.y. ago. The sequence of ash-flow tuffs

erupted from the earliest of the three central Nevada calderas began with the giant Tuff of Williams Ridge and Morey Peak (+ 2500 km³), followed by the Monotony Tuff (3000 km³), and finally by various ash-flow tuffs erupted from the youngest caldera (400 km³). In the San Juan complex, the earliest ash-flow was the Fish Canyon Tuff, which is also the largest of these ash-flows (> 3000 km³). Of the six other major ash-flow tuffs erupted from the central San Juan complex, none exceeds 1000 km³ in volume.

Previous studies of other complex calderas at Yellowstone National Park and in southwest Nevada indicated that the later eruptions have $\delta^{18}\text{O}$ values 3 per mil lower than rocks erupted early in the cycles. However, in the present study, no large negative shifts in $\delta^{18}\text{O}$ were found. The various eruptions in both central Nevada and the central San Juans were remarkably uniform in $^{18}\text{O}/^{16}\text{O}$, although small shifts of about -0.2 to -0.3 per mil were found in both suites of rocks in going from the early ash-flows to a later set. The indicated range of $\delta^{18}\text{O}$ values of these quartz-latitude and rhyolite magmas was 9.1 to 9.8 in the central Nevada complex and 6.6 to 7.5 in the central San Juan complex. The higher $\delta^{18}\text{O}$ values in central Nevada probably indicate melting of sedimentary or metasedimentary country rocks at depth, whereas in Colorado, the low- ^{18}O , lower part of the craton was very likely involved in the melting process.

$\delta^{18}\text{O}$ fractionations between coexisting phenocryst minerals in all of the ash-flow tuffs and lava flows from these two complexes are larger at the bases of the units (tops of the magma chambers) and smaller at the tops of the units (deeper levels of the magma chambers). These

relationships show that temperature gradients existed in virtually all these magmas prior to eruption (cooler at the top and hotter at deeper levels).

It is not clear why some complex caldera magmas become depleted in ^{18}O with time, and others do not. No relationship exists between the duration of caldera magmatism and low- ^{18}O rocks, nor between the size of the eruptions and these ^{18}O depletions. However, the large ^{18}O depletions found to date occur only in caldera complexes younger than about 15 to 20 m.y., corresponding to the initiation of Basin-Range extension in the western United States. Perhaps Basin-Range faults allow meteoric fluids to penetrate deeply into fairly high-temperature regions of the crust. These younger magmas might then be able to melt or assimilate larger amounts of altered, ^{18}O depleted rocks during their ascent. A correlation also appears to exist between the ^{18}O depletions and the major-element chemistry of the rocks. All of the low- ^{18}O ash-flow tuffs contain abundant high-silica rhyolites (consistently ranging up to or above 77 percent SiO_2). The large silica contents of these magmas indicate very strong differentiation, suggesting prolonged assimilation-fractional crystallization in a stable magma chamber without the renewed addition much primitive, unfractionated magma having a "normal" $\delta^{18}\text{O}$ value. It is tentatively concluded that ash-flow magmas strongly depleted in $\delta^{18}\text{O}$ will be produced only if: (1) there is a pre-history of intense fracturing, caldera collapse, and extensive meteoric-hydrothermal activity, followed by (2) the development of a stable, strongly differentiated, zoned magma chamber, whose roofward portion is in close proximity to low- ^{18}O , hydrothermally altered

roof rocks for an extended interval of time (> 100,000 years?).

TABLE OF CONTENTS

	<u>Page</u>
PART I	1
1 INTRODUCTION	2
1.1 Object of Research	2
1.2 Previous Stable Isotopic Investigations of Water-Rock Interaction in the Western San Juan Mountains	4
2 GEOLOGIC SETTING OF THE LAKE CITY CALDERA	21
2.1 Introduction	21
2.2 San Juan Regional Geology	24
Pre-Mid-Tertiary Development	24
Tertiary Magmatic Evolution of the San Juan Volcanic Field	28
Tertiary Mineralization and Alteration in the Western San Juans	32
2.3 Geology of the Lake City Caldera	43
Magmatic Evolution of the Lake City Caldera	43
Hydrothermal Alteration in the Lake City Caldera	48
3 OXYGEN ISOTOPIC ANALYSES OF ROCKS FROM THE LAKE CITY CALDERA	56
3.1 Sampling Program and Sample Preparation	56
3.2 Analytical Procedures	59
3.3 Data from the Lake City Caldera	60
4 OXYGEN ISOTOPE RELATIONSHIPS IN METEORIC WATERS AND ROCKS IN THE VICINITY OF THE LAKE CITY CALDERA	95
4.1 Meteoric Water as a Hydrothermal Fluid	95
Oxygen Isotope Relationships in Meteoric- Hydrothermal Systems	95
Isotopic Composition of Tertiary Meteoric Water in the Western San Juan Mountains	99
Meteoric Water as a Fluid Reservoir for the Lake City Caldera Hydrothermal System	100
4.2 $\delta^{18}\text{O}$ Variations in the Precambrian Granite of Cataract Gulch	104
Initial Magmatic Isotopic Composition	104
Mineral-Mineral Isotopic Relationships	106
Water/Rock Ratios and Mineral Alteration	119
Effects of Fractures and Faults on Fluid Flow	130

	Effect of Grain Size	139
	Effect of Elevation on the $^{18}\text{O}/^{16}\text{O}$ Ratio	143
	Structural Interpretation of $\delta^{18}\text{O}$ Values	153
	Comparison with $^{18}\text{O}/^{16}\text{O}$ Data from the Idaho Batholith	160
4.3	$\delta^{18}\text{O}$ Variations in Older Volcanic Rocks Outside the Lake City Caldera	164
5	ISOTOPIC STUDIES OF QUARTZ VEINS AND SOLFATARIC ACTIVITY ACTIVITY IN THE SAN JUAN MOUNTAINS	176
5.1	Alteration and Vertical Isotopic Gradients in the Ring Domes of the Lake City Caldera	176
	Initial Isotopic Composition	176
	Vertical Extent of the Red Mountain Alteration System	177
	Vertical Variations in Oxygen Isotopic Compositions of Alteration Minerals	181
5.2	$^{18}\text{O}/^{16}\text{O}$ Variations in Vein Quartz	187
	Data Obtained in the Present Study	187
	Comparison with Fluid Inclusion Data	190
	Temperatures of Formation of Quartz and $\delta^{18}\text{O}$ of Fluids, Lake City Caldera	192
5.3	Boiling in an Upflowing Fluid as a Model for the Red Mountain Solfataric Alteration	194
	Solfataric Alteration in Present-Day Hot Springs	194
	Temperature-Depth Model of the Red Mountain Solfataric System	195
5.4	Solfataric Alteration Elsewhere in the San Juan Mountains	211
	Localities Studied in This Work	211
	Characteristic Features of the Six Localities	212
	Discussion of the Isotope Data	216
6	$^{18}\text{O}/^{16}\text{O}$ RELATIONSHIPS WITHIN THE LAKE CITY CALDERA	225
6.1	Initial Oxygen Isotopic Composition of the Intra- Caldera Volcanic and Volcaniclastic Rocks	225
	Initial $\delta^{18}\text{O}$ Values of the Sunshine Peak Tuff and Resurgent Intrusive Rocks	225
	Initial $\delta^{18}\text{O}$ Values of the Sunshine Peak Tuff Megabreccia	228
6.2	Variations in Alteration Mineralogy and $\delta^{18}\text{O}$ in the Megabreccia	229
6.3	Mineralogical Alteration of the Sunshine Peak Tuff	234
6.4	Correlation between $\delta^{18}\text{O}$ Values and Alteration Assemblages	238
6.5	Geometry of $^{18}\text{O}/^{16}\text{O}$ Variations in and around the Lake City Caldera	251
	$\delta^{18}\text{O}$ Contour Map	251
	Shape of the Resurgent Intrusion	257

	Radial Cross Sections	260
	Structural Cross Sections	271
	Effect of Asymmetric Uplift and Tilting	273
	Effect of Proximity to the Resurgent Intrusions	276
	Effect of Topography	282
	Effect of the Ring Fault	283
	Does a $\delta^{18}\text{O}$ Discontinuity Exist along the Ring Fault ?	284
	Effects of Other Faults and Fractures	285
	Effect of Mineralogy and Lithology	286
7	HYDROTHERMAL CIRCULATION IN THE LAKE CITY CALDERA	289
7.1	A Review of Caldera-Related Hydrothermal Systems	289
	Shallow, Caldera-Related Hydrothermal Activity in the Western United States	289
	Long Valley Caldera, California	289
	Yellowstone Caldera, Wyoming	295
	Valles Caldera, New Mexico	299
	Oxygen Isotopic Evidence for Deep Meteoric- Hydrothermal Fluid Circulation in Eroded Calderas	307
	Summary of Caldera-Related Meteoric-Hydrothermal Systems	311
7.2	The Meteoric-Hydrothermal System Associated with Lake City Caldera	320
	Introduction	320
	A Circulation Model for the Lake City Hydro- thermal System	320
7.3	Implications for Mineralization in Shallow Volcanic Environments	341
8	SUMMARY AND CONCLUSIONS	346
PART II		
1	INTRODUCTION	354
1.1	Object of the Research	354
1.2	Low- ^{18}O Igneous Rocks	355
1.3	Previous $\delta^{18}\text{O}$ Studies of Ash-Flow Tuffs	357
2	CENTRAL NEVADA CALDERA COMPLEX	361
2.1	Evolution of the Central Nevada Caldera Complex	361
2.2	Oxygen Isotopic Analyses of Coexisting Minerals from the Central Nevada Caldera Complex	368
2.3	Possible Effects of Post-Magmatic Alteration on the $^{18}\text{O}/^{16}\text{O}$ Ratios	373

2.4	Oxygen Isotopic Fractionations Among Coexisting Minerals	377
	General Statement	377
	Early Eruptive Sequence	381
	The Middle Eruptive	382
	Late Eruptive Sequence	383
2.5	$\delta^{16}\text{O}$ Variations in the Eruptive Units with Time	383
2.6	$^{18}\text{O}/^{16}\text{O}$ Variations within Individual Ash-Flow Tuffs	388
3	CENTRAL SAN JUAN CALDERA COMPLEX	393
3.1	Evolution of the Central San Juan Caldera Complex	393
3.2	Oxygen Isotopic Analyses of Coexisting Minerals from the Central San Juan Caldera Complex	402
3.3	Possible Effects of Post-Magmatic Alteration on the $^{18}\text{O}/^{16}\text{O}$ Ratios	408
3.4	Oxygen Isotopic Fractionations among Coexisting Minerals and Rocks	414
3.5	$\delta^{18}\text{O}$ Variations in the Eruptive Units with Time	419
3.6	$^{18}\text{O}/^{16}\text{O}$ Variations within Individual Ash-Flow Tuffs	422
3.7	Possible Complications Attributable to High Fluorine Contents in the Biotites	427
4	CONCLUSIONS	432
4.1	Comparison with Plutonic Rocks	432
4.2	Temperatures of the Ash-Flow Magmas	438
4.3	The Problem of Low- 18 Magmas	440
	REFERENCES CITED	453

FIGURES

	<u>Page</u>
1.1 Oxygen isotopic analyses of rocks from the western San Juan Mountains	5
1.2 A highly schematic cross section showing oxygen isotopic data in and around the Stony Mountain complex	9
1.3 Oxygen isotopic analyses of vein quartz, and calculated $\delta^{18}\text{O}$ values of ore fluids, from the Sunnyside vein system	13
1.4 Model plan groundwater flow pattern for the Sunnyside mineralizing hydrothermal system	15
1.5a Geologic cross section through the San Juan and Silverton calderas	17
1.5b Model cross sectional ground water flow pattern for the Sunnyside mineralizing hydrothermal system	17
2.1 Map of the San Juan volcanic field showing calderas	22
2.2 Generalized geologic map of the western San Juan volcanic field	25
2.3 Relationships between volume and age of the calc-alkaline and bimodal igneous suites in the western San Juan volcanic field	29
2.4abc Schematic development of the western San Juan caldera complex	34
2.5 Geologic map showing structure in the Silverton caldera area	39
2.6 Generalized geologic map of the Lake City caldera	44
2.7 Schematic distribution of intensely altered areas within the Lake City caldera	49
2.8 Diagrammatic E-W cross section through the Lake City caldera	53
3.1 Map of the Lake City caldera showing topography	57
4.1 Oxygen and hydrogen isotopic analyses of fluids discharging in active geothermal areas	97

4.2	Histogram showing all whole-rock oxygen isotopic analyses made in this study from outcrop samples in the Lake City caldera area	101
4.3	Oxygen isotopic analyses of quartz-orthoclase pairs from the Precambrian granite of Cataract Gulch	107
4.4	Oxygen isotopic analyses of quartz-feldspar pairs from the Idaho batholith	109
4.5	Oxygen isotopic compositions of minerals from the Precambrian granite of Cataract Gulch	112
4.6	Mineral-mineral fractionation factors	114
4.7	Idealized $\delta^{18}\text{O}$ versus W/R ratio plot for the Precambrian granite of Cataract Gulch	121
4.8abc	Hypothetical whole-rock $\delta^{18}\text{O}$ variations as a function of the degree of mineralogical alteration of biotite in the Cataract Gulch granite	125
4.9	Whole rock isotopic compositions of the Precambrian granite of Cataract Gulch as a function of the degree of mineralogic alteration of the biotite	128
4.10	Map of the Precambrian granite showing sample locations, structure, and composite mineralogic alteration effects	131
4.11	Map of the Precambrian granite showing contours of whole-rock $\delta^{18}\text{O}$ values	133
4.12	Variations in whole-rock $\delta^{18}\text{O}$ values of the Precambrian granite as a function of sample elevation and distance from the graben axis	135
4.13	Map of the Precambrian granite showing contours of average grain size of the samples	140
4.14	Geographic subdivisions of sample locations within the Precambrian granite	144
4.15	$\delta^{18}\text{O}$ values of the Precambrian granite plotted as a function of the sample elevation	146
4.16	Whole-rock $\delta^{18}\text{O}$ values of the Precambrian granite plotted as a function of the degree of mineralogic alteration of the biotite	151
4.18	Structural contours on the upper contact of the Cataract Gulch granite	154

4.18	Variation of the $\delta^{18}O$ values of the Cataract Gulch granite as a function of the depth of the sample location beneath the Tertiary-Precambrian unconformity	158
4.19	Comparison of hydrothermally altered rocks from the Cataract Gulch granite and the Idaho batholith	162
4.20	Location of samples of the Sapinero Mesa Tuff collected north and west of the Lake City ring fault	166
4.21	Relationships between sample elevation and distance from the Lake City ring fault	169
4.22	Plot of $\delta^{18}O$ versus elevation for samples of volcanic rocks older than the Sunshine Peak Tuff	172
5.1	Map showing the geology, hydrothermal alteration, sample locations, and $\delta^{18}O$ data from the Red Mountain lava dome	178
5.2	$^{18}O/^{16}O$ ratios in altered rocks and hydrothermal quartz from the Red Mountain fossil hydrothermal system, as a function of the elevation at which the samples were collected	182
5.3	A $\delta^{18}O$ -elevation plot for the Red Mountain lava ring dome, showing water/rock ratios	185
5.4	Histogram of the oxygen isotopic analyses of vein quartz from the Lake City caldera	188
5.5	Model for boiling of meteoric-hydrothermal fluids rising along the hydrostatic boiling curve	196
5.6	Pressure-enthalpy diagram for the system water-steam	200
5.7	Plot of temperature ($^{\circ}C$) vs. mole fraction of vapor in the closed steam-water systems	203
5.8	Calculated hydrothermal quartz $^{18}O/^{16}O$ ratios for the three model fluids, compared with the observed $\delta^{18}O$ variations in samples from the Red Mountain solfataric zone	206
5.9	Oxygen isotopic fractionation curves used in the Red Mountain solfataric model	208
5.10	Locations of solfatarically altered areas in the San Juan Mountains from which oxygen isotopic data have been obtained	214

5.11	Histograms comparing oxygen isotopic analyses of samples from solfatarically altered areas in the San Juan Mountains	217
5.12	$\delta^{18}\text{O}$ values of solfataric quartz from Summitville and altered rocks and ksolinite from the Alamosa River stock, plotted as functions of sample elevation	222
6.1	Comparison between $\delta^{18}\text{O}$ values of megabreccia and tuff in the southwest quarter of the Lake City caldera	231
6.2	Histograms of whole-rock $\delta^{18}\text{O}$ values of the Sunshine Peak Tuff and resurgent intrusive rocks as a function of the type and facies of mineralogic alteration	239
6.3	$\delta^{18}\text{O}$ whole-rock values of hornfelsed tuff, chlorite/calcite altered tuff, and resurgent intrusive rocks, plotted as a function of the degree of mineralogical alteration of K feldspar	242
6.4	Whole-rock $\delta^{18}\text{O}$ values of argillically altered zones I through V tuff plotted as a function of the degree of mineralogical alteration of sanidine	244
6.5a	Stability fields of K feldspar, sericite, kaolinite, and pyrophyllite as functions of temperature and $m_{\text{KCL}}/m_{\text{HCL}}$	246
6.5b	Plausible fluid trajectories for the Fracture Regime and Intrusive Regime alteration plotted as functions whole-rock $\delta^{18}\text{O}$ and the amount of sanidine alteration	246
6.6	Contour of $\delta^{18}\text{O}$ values in the Lake City caldera area	254
6.7	Structural contours drawn on the top of the Lake City caldera resurgent intrusion	258
6.8	A composite radial cross section that includes all samples studied in this work from within the Lake City caldera	261
6.9	Lithology plotted on the composite radial cross section	263
6.10	Alteration facies of the Sunshine Peak Tuff plotted on the composite radial cross section	265
6.11	Contours of $\delta^{18}\text{O}$ values plotted on the composite radial cross section	267
6.12	The present erosional surface of the Lake City caldera, after adjustment to remove the eastward, post-alteration tilting	274

6.13	Sample height above the resurgent intrusion plotted versus the whole-rock $\delta^{18}\text{O}$	278
6.14	Sample height above the resurgent intrusion plotted versus whole-rock $\delta^{18}\text{O}$, with the alteration facies indexed for each Sunshine Peak Tuff sample	280
7.1	Distribution of hot springs in the Long Valley caldera	292
7.2	Distribution of hot springs in the Yellowstone National Park	297
7.3	Map of the Valles caldera	301
7.4	Whole-rock $\delta^{18}\text{O}$ values from the Baca no. 7 drill hole	304
7.5	Generalized hydrothermal flow pattern associated with the Scottish Hebridian ring dike complexes	309
7.6	Generalized hydrothermal flow pattern associated with Eocene calderas of the Idaho batholith	312
7.7	Comparison of the sizes and hydrothermal flow patterns of caldera-related hydrothermal systems	315
7.8	Model of the meteoric-hydrothermal fluid flow patterns associated with resurgent calderas	317
7.9	Schematic distribution of alteration regimes within the Lake City caldera	322
7.10	Calculated water/rock ratios for altered Sunshine Peak Tuff	326
7.11	300°C and 400°C isotherms associated with the resurgent intrusion	328
7.12	A schematic cross section showing the distribution of isotherms in the Lake City hydrothermal system	330
7.13	Contours of water/rock ratios above the resurgent intrusion, along the present day erosion surface within the Lake City caldera	333
7.14	Hydrothermal flow model for the Lake City caldera	335
7.15	Relationships between vein mineralization and solfataric mineralization	342
1.1ab	$\delta^{18}\text{O}$ values of phenocrysts separated from some low- ^{18}O ash-flow tuffs and associated lavas from the western United States	359

2.1	Structural evolution of the central Nevada caldera complex	363
2.2	$\delta^{18}\text{O}$ of quartz and feldspar plotted vs. the $\delta^{18}\text{O}$ of biotite for the central Nevada caldera complex samples	374
2.3	$\Delta^{18}\text{O}$ quartz-biotite fractionations plotted vs. $\Delta^{18}\text{O}$ quartz-feldspar fractionations for ash-flow tuffs from the central Nevada complex, the central San Juan complex, and other published studies of ash-flow tuffs	378
2.4	Mineral $\delta^{18}\text{O}$ values from central Nevada complex rocks plotted as a function of stratigraphic height	385
2.5	$\Delta^{18}\text{O}$ quartz-feldspar and quartz-biotite fractionations for the central Nevada complex plotted as a function of relative height of the sample	389
3.1	Evolution of the central San Juan caldera complex	395
3.2	Mineralogy of some of the ash-flows and lavas erupted from the central San Juan caldera complex	399
3.3	$\delta^{18}\text{O}$ of quartz and feldspar plotted vs. the $\delta^{18}\text{O}$ of biotite for the central San Juan complex samples	410
3.4	$\delta^{18}\text{O}$ whole-rock values from the central San Juan complex plotted vs. $\delta^{18}\text{O}$ values of feldspar, hornblende, and pyroxene	417
3.5	$\delta^{18}\text{O}$ values of the mineral separates of rocks from the central San Juan caldera complex plotted as a function of stratigraphic position	423
3.6	$\Delta^{18}\text{O}$ feldspar-biotite and $\Delta^{18}\text{O}$ quartz-biotite fractionations plotted vs. relative sample height for the central San Juan complex	425
3.7	$\Delta^{18}\text{O}$ feldspar-biotite values plotted vs. F formula positions for three samples of Fish Canyon Tuff	429
4.1	$\Delta^{18}\text{O}$ quartz-biotite values plotted vs. the $\delta^{18}\text{O}$ values of biotites, for a granodiorite pluton from the Southern California batholith and for various ash-flow tuffs	433
4.2	$\Delta^{18}\text{O}$ feldspar-biotite values from the Southern California batholith and ash-flow tuffs plotted vs. the $\delta^{18}\text{O}$ values of biotite	435

4.3	$\delta^{18}\text{O}$ feldspar values plotted vs. $\delta^{18}\text{O}$ biotite values for ash-flow tuffs	442
4.4	$\delta^{18}\text{O}$ feldspar values from ash-flows plotted vs. the age of the ash-flow eruptions	445

TABLES

	<u>Page</u>
1.1 Oxygen Isotopic Analyses of Rocks from the Lake City Caldera and Solfatarically Altered Areas, San Juan Mountains, Colorado	61
4.1 Isotopic, petrographic, and location data for samples of the Precambrian granite of Cataract Gulch	105
4.2 Oxygen isotopic fractionation temperatures for mineral pairs from the Precambrian granite of Cataract Gulch	117
5.1 Calculated fluid oxygen isotopic compositions for selected QBP and fluorite-carbonate veins associated with the Lake City caldera	193
5.2 Characteristics of three fluids used to model the solfataric alteration at Red Mountain	198
5.3 Summary of characteristics of some solfatarically altered areas in the San Juan Mountains	213
6.1 Progressive alteration mineralogy in argillized Sunshine Peak Tuff away from the quartz veins	236
6.2 Characteristics of alteration regimes in the Sunshine Peak Tuff of the Lake City caldera	252
7.1 Stages in the development of resurgent cauldrons	290
2.1 Volumes and ages of rocks erupted from the central Nevada caldera complex	362
2.2 Oxygen isotopic analyses of rocks and mineral separates from the central Nevada caldera complex	369
3.1 Volumes and ages of rocks erupted from the central San Juan caldera complex	394
3.2 Oxygen isotopic analyses of rocks and mineral separates from the central San Juan caldera complex	403

PLATES

- | | | |
|---|--|-----------|
| 1 | Geologic map of the Lake City caldera, showing locations and $\delta^{18}\text{O}$ values of samples | in pocket |
| 2 | Alteration map of the Lake City caldera | in pocket |
| 3 | $\delta^{18}\text{O}$ contours in the Lake City caldera | in pocket |
| 4 | Structural cross sections of the Lake City caldera showing $\delta^{18}\text{O}$ contours | in pocket |
| 5 | Composite radial cross section of the Lake City caldera showing $\delta^{18}\text{O}$ contours | in pocket |

PART I

AN $^{18}\text{O}/^{16}\text{O}$ INVESTIGATION OF THE LAKE CITY CALDERA,
SAN JUAN MOUNTAINS, COLORADO

CHAPTER 1

INTRODUCTION

1.1 Object of Research

A primary goal of this research is to evaluate the fluid flow regime and water-rock interactions in a relatively shallow paleo-hydrothermal system. The Lake City caldera, western San Juan Mountains, southwestern Colorado, provides a unique environment in which to pursue this goal. Erosion within this caldera has exposed a variety of levels within the paleo-system, from a shallow solfataric environment formed within a few tens of meters of the original topographic surface, stratigraphically downward about 2000 m into the resurgent intrusive rocks within the caldera; the latter served as "heat engines" to drive the hydrothermal convective circulation.

In a now classic paper, Smith and Bailey (1968) outlined a general model for the evolution of resurgent cauldrons. Stage VII of this model consists of terminal hot spring and solfataric activity. This hot spring activity represents the surface manifestation of large, convectively driven, meteoric-hydrothermal systems. In recent years, isotopic, mineralogic, and theoretical studies that describe and measure the dynamics and chemistry of fluid flow and water-rock interaction have been developed and applied to a number of paleo-hydrothermal systems. Most of these studies have been concerned with the deeper portions of such systems.

Calderas and their related magmatic rocks hold no exclusive patent on the generation of convective meteoric-hydrothermal systems. The

caldera environment, however, provides a number of advantages for studying the relatively shallow levels of a hydrothermal system: 1) the structural and magmatic evolution of calderas, or resurgent cauldrons, has been formulated into a general model that seems to have wide applicability (Smith and Bailey, 1968). The Lake City caldera conforms almost perfectly to this idealized model. 2) Several recent calderas in the western United States, the Long Valley caldera, California, the Yellowstone caldera, Wyoming, and the Valles caldera, New Mexico, are currently in stage VII of the Smith and Bailey (1968) model, terminal solfataric and hot spring activity. These well-documented systems provide modern analogues with which the Lake City system can be compared. 3) Hydrothermal systems associated with the roots of deeply eroded calderas have been mapped using stable isotopic analyses of the rocks altered in these environments. For example, systems at depths of about 2 to 3 km and 5 to 7 km, respectively, have been studied in the Tertiary Scottish Hebridian province (Taylor and Forester, 1971) and in Tertiary intrusive centers in the Idaho batholith (Criss and Taylor, 1983). The Lake City caldera, exposed by erosion to depths of 0 to 2 km, provides access to that link in caldera-related hydrothermal systems between the near-surface, active hot-spring and solfataric stage VII, and the circulation patterns inferred for deeply eroded calderas.

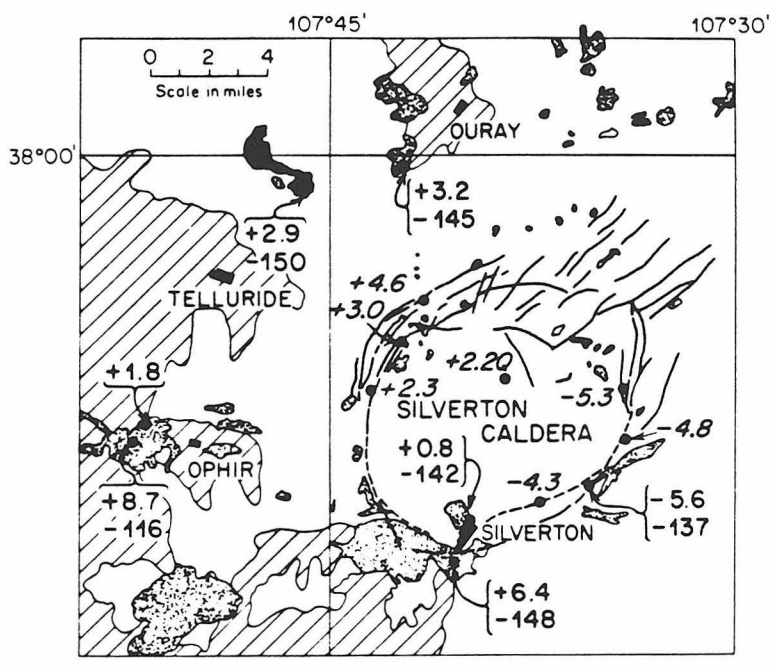
Several other aspects of the Lake City caldera make it an attractive candidate for extensive research. The caldera is situated in the western San Juan Mountains, on the margin of an area of extensive hydrothermal alteration and mineralization. This area includes the historically productive base and precious metal mining districts of

Henson Creek, Lake City, Eureka, Silverton, South Silverton, Telluride, Red Mountain, and Ouray, among others. The economic mineralization and volcanic geology of the San Juan Mountains has drawn numerous geologic investigators to this region; these earlier studies provide a substantial geologic and geochemical data base upon which we can build. The Lake City caldera is associated with the largest silicic magmatic event in the western San Juan area that can be shown to be temporally associated with abundant economic mineralization. Although the Lake City caldera is itself not extensively mineralized, a study of the hydrothermal alteration of the caldera ought to provide some insight into the relationship between fluid circulation and ore deposition.

1.2 Previous Stable Isotopic Investigations of Water-Rock Interaction in the Western San Juan Mountains

Samples of altered rocks from the Silverton caldera, from the Ouray area, and from diorite porphyry intrusions emplaced into Paleozoic and Mesozoic sedimentary rocks in the western San Juan Mountains, were analyzed by Taylor (1974a) (Fig. 1.1). The isotopic compositions of samples from the Silverton caldera show depletions in both ^{18}O and deuterium relative to "normal" unaltered igneous rocks. Samples collected along the eastern Silverton caldera ring fault exhibit the greatest ^{18}O depletions, with four samples having an average $\delta^{18}\text{O} = -5$. Stocks emplaced into sedimentary rocks in the western San Juans show only minor ^{18}O depletions. Taylor (1974a) explains such relationships as indicating that the sedimentary rocks were either (1) much less permeable to hydrothermal fluid flow than the highly jointed and

Figure 1.1 Isotopic analyses of rocks from the western San Juan Mountains (from Taylor, 1974a). The plotted $\delta^{18}\text{O}$ analyses are for whole-rock samples, except that Q=quartz. The analyses of volcanic rocks are given in italics, those on intrusive rocks in regular lettering. The large negative numbers (-142, etc.) are δD values of biotite or chlorite. The intrusions are shown in a stippled pattern, the volcanic rocks in blank pattern, and Paleozoic and Mesozoic sedimentary rocks in a diagonal-lined pattern. The Stony Mountain intrusive complex (Fig. 1.2) is shown in solid black in the upper left corner of the map. The geology is generalized after Luedke and Burbank (1968).



fractured volcanic rocks associated with the Silverton caldera, or (2) they contained pore waters with much higher $\delta^{18}\text{O}$ and δD values (saline formation waters ?).

Taylor (1974a) identified meteoric water as the primary source for the hydrothermal fluids involved in the alteration of the western San Juan volcanic and intrusive rocks. Using δD analyses of hydrous alteration minerals, Taylor (1974a) calculated the D/H ratio of the fluid with which these minerals had equilibrated. From this calculation, and using the meteoric water equation of Craig (1961), Taylor (1974a) estimated that mid-Tertiary western San Juan meteoric water had an initial δD of about -115 per mil and an initial $\delta^{18}\text{O}$ of about -16 per mil.

Because the fluids involved in alteration had been ^{18}O shifted to a $\delta^{18}\text{O} \approx -5$, Taylor (1974a) suggests that the hydrothermal fluids must have circulated to depths of at least several kilometers, and interacted with a large volume of rock. Water/rock ratios were at least on the order of 0.5 to 1.0, and were locally greater than 5.

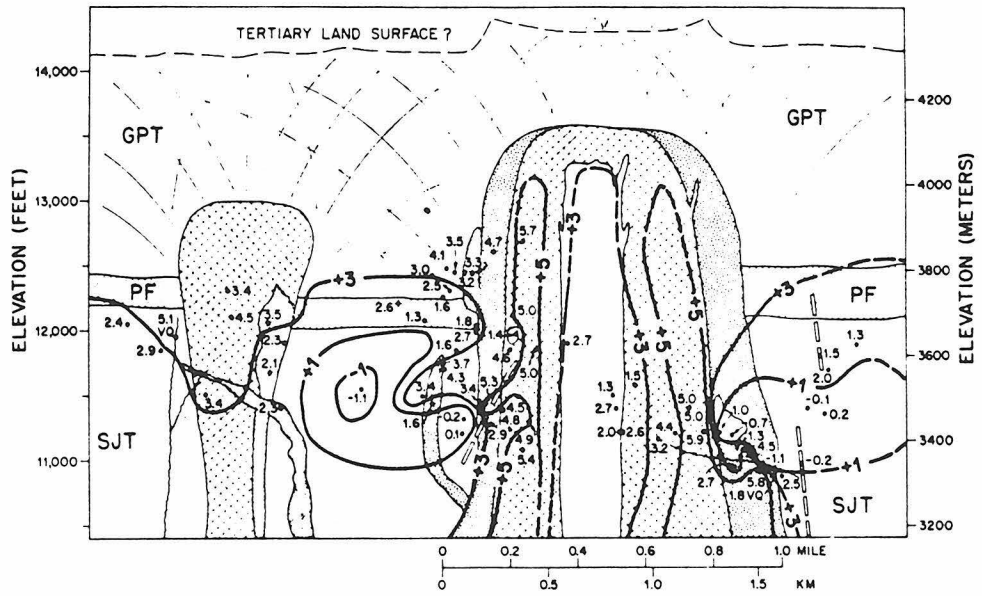
The Stony Mountain intrusive complex, southwest of Ouray in the western San Juan Mountains, was isotopically studied by Forester and Taylor (1972, 1980). This composite gabbro-diorite-granodiorite stock intrudes horizontal, highly jointed, volcanic rocks that are strongly depleted in ^{18}O within 2 to 3 kilometers of the stock, with an average $\delta^{18}\text{O}$ of about -1.5. D/H ratios in biotites from the stock lie well below "normal" igneous values, with $\delta\text{D} = -135$ to -145 . Both of these features indicate exchange with heated meteoric-hydrothermal fluids. Water/rock ratios in this system were calculated to be in the range 0.1 to 0.8.

Forester and Taylor (1972) constructed a schematic vertical section illustrating the $\delta^{18}\text{O}$ values associated with the intrusive complex (Fig. 1.2). The most ^{18}O -depleted volcanic unit, the lowermost San Juan tuff, is considered to have been the main aquifer in the region. Pronounced ^{18}O depletions along the margins of the stock resulted from high fluid fluxes along the stock-host rock contacts (Forester and Taylor, 1980).

Forester and Taylor (1972, 1980) noted that coexisting minerals typically exhibit disequilibrium ^{18}O fractionations, indicating that the rock-forming minerals underwent variable exchange rates with the hydrothermal fluids. The order of increasing resistance to ^{18}O exchange in this hydrothermal environment is: alkali feldspar-plagioclase-pyroxene-biotite-magnetite-quartz. Forester and Taylor (1972, 1980) also noted that $\delta^{18}\text{O}$ values of the altered rocks decrease with decreasing grain size.

Jackson et al (1980) and Ringrose et al (1981) briefly report the results of stable isotopic analyses of hydrothermally altered volcanic and intrusive rocks in the western San Juan Mountains, west of the Silverton caldera. Regionally propylitized volcanic rocks in this area exhibit the characteristic ^{18}O depletions (to $\delta^{18}\text{O} = -1.3$ per mil) that are typical of alteration by meteoric-hydrothermal fluids. However, several local zones within the regionally propylitized areas are intensely altered to clays and sericite and contain stockwork molybdenum mineralization. The δD values of fluid inclusions in quartz veinlets from these localities range from -109 to -73, and $\delta^{18}\text{O}$ of the vein quartz ranges from +7.6 to +9.5. Jackson et al (1980) and

Figure 1.2 A highly schematic cross section showing oxygen isotopic data in and around around the Stony Mountain complex (from Forester and Taylor, 1972). All samples are plotted at their exact elevation, but have been projected onto the plane of the section. The volcanic units are: GPT, Gilpin Peak Tuff; PF, Picayune Formation; SJT, San Juan Tuff. In the intrusion, the central diorite is shown in blank pattern, the gabbro is crosshatched, and the outer diorite is stippled.



Ringrose et al (1981) conclude from their isotopic data that the stockwork veinlets formed from an aqueous fluid dominantly composed of magmatic water. Jackson et al (1980) and Ringrose et al (1981) invoke the general hydrothermal model proposed by Sheppard et al (1969; 1971) and Taylor (1974a) for porphyry copper systems: 1) a magmatic fluid is released by a crystallizing stock, producing stockwork molybdenite mineralization, 2) adjacent to the stock, this magmatic fluid mixes with meteoric-hydrothermal fluids, derived from the surrounding convective circulation system, and 3) with time, the meteoric-hydrothermal circulation collapses inward during cooling of the stock, imprinting a late-stage, meteoric-hydrothermal "signature" throughout the intrusion. In this model, Pb-Zn-pyrite mineralization is precipitated in veins peripheral to the stock where the two fluids mix.

Oxygen isotopic analyses of epithermal vein quartz from the western San Juan Mountains has been reported by Taylor (1974a), Forester and Taylor (1972, 1980), Casadevall and Ohmoto (1977), and Ringrose et al (1981). A conclusion reached by all these authors is that meteoric water was the fluid from which all these quartz veins precipitated, including both barren and mineralized veins. Three veins associated with the Stony Mountain complex yield $\delta^{18}\text{O}$ values of -1.8, -1.7, and +5.1 per mil (Forester and Taylor, 1980). Vein quartz from the Gold King mine, 10 km north of Silverton, has a $\delta^{18}\text{O}$ value of 2.2 per mil (Taylor, 1974a). Ringrose et al (1981) state that vein quartz along the north side of the Sultan Mountain stock, west of Silverton, has $\delta^{18}\text{O} = -2.8$ to +9.7.

Casadevall and Ohmoto (1977) analyzed a number of vein samples

from the Sunnyside vein system, within the Silverton caldera. Six successive periods of vein mineralization were recognized in the Sunnyside system. Periods 1 through 5 contain the quartz-sulfide ores. Period 6 contains fluorite, quartz, carbonates, and sulfates, but only traces of sulfides. The $\delta^{18}\text{O}$ values of quartz in period I to V ores (Fig. 1.3) range from -1.2 to +1.8, and decrease slightly but systematically from period 1 to period 5. Period 6 quartz has $\delta^{18}\text{O} = -5.0$ to -0.4.

Based on the evolved nature of the meteoric-hydrothermal fluids from which the Sunnyside vein quartz was deposited, and on a number of other geochemical lines of evidence, Casadevall and Ohmoto (1977) suggest that the fluids involved in the Sunnyside mineralization circulated deeply into the crust prior to entering the Sunnyside vein system. Meteoric fluid sources were in volcanic and Precambrian crystalline highlands peripheral to the Silverton caldera. Casadevall and Ohmoto's (1977) fluid circulation model is reproduced in Figures 1.4 and 1.5.

Farther east, in the Creede mining district, central San Juan Mountains, Bethke and Rye (1979) found that the δD and $\delta^{18}\text{O}$ values of the fluids from which different vein minerals formed (sphalerite, quartz, illite/chlorite, carbonate minerals) seemed to have differed substantially from one another. Bethke and Rye (1979) drew the remarkable conclusion that water from three coexisting reservoirs alternately and episodically fed the Creede vein system, and that little mixing of the fluids occurred. Carbonate-producing fluids had an isotopic composition consistent with a deep-seated, probably magmatic origin. Quartz-

Figure 1.3 Oxygen isotopic analyses of vein quartz, and calculated $\delta^{18}\text{O}$ values of ore fluids, from the Sunnyside vein system (from Casadevall and Ohmoto, 1977). The numbers refer to the period of mineralization. Open circles are quartz analyses. Closed circles are fluid compositions calculated from fluid inclusion filling temperatures and the quartz analyses. Vertical bars indicate uncertainty. Horizontal bars for period 6 are calculated water $\delta^{18}\text{O}$ values for calcite, and x's are calculated water $\delta^{18}\text{O}$ values for rhodochrosite.

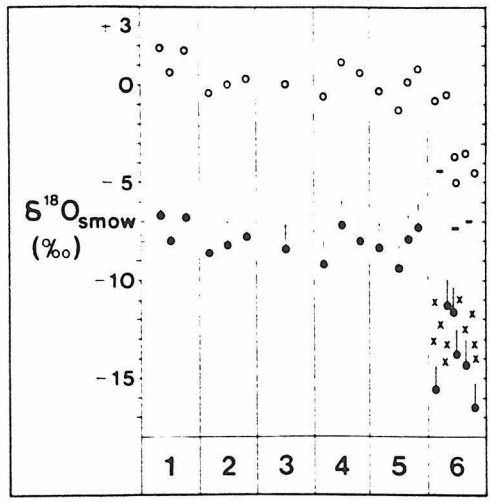


Figure 1.4 Model plan groundwater flow pattern for the Sunnyside mineralizing hydrothermal system (from Casadevall and Ohmoto, 1977). Locations are: MS, Mount Sneffels; O, Ouray; CB, Camp Bird mine; T, Telluride; I, Idarado mine; SIL, Silverton; S, Sunnyside mine; B, Beartown.

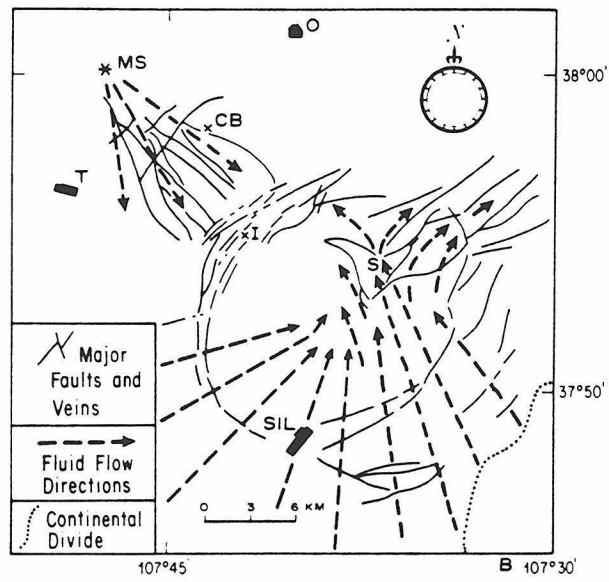
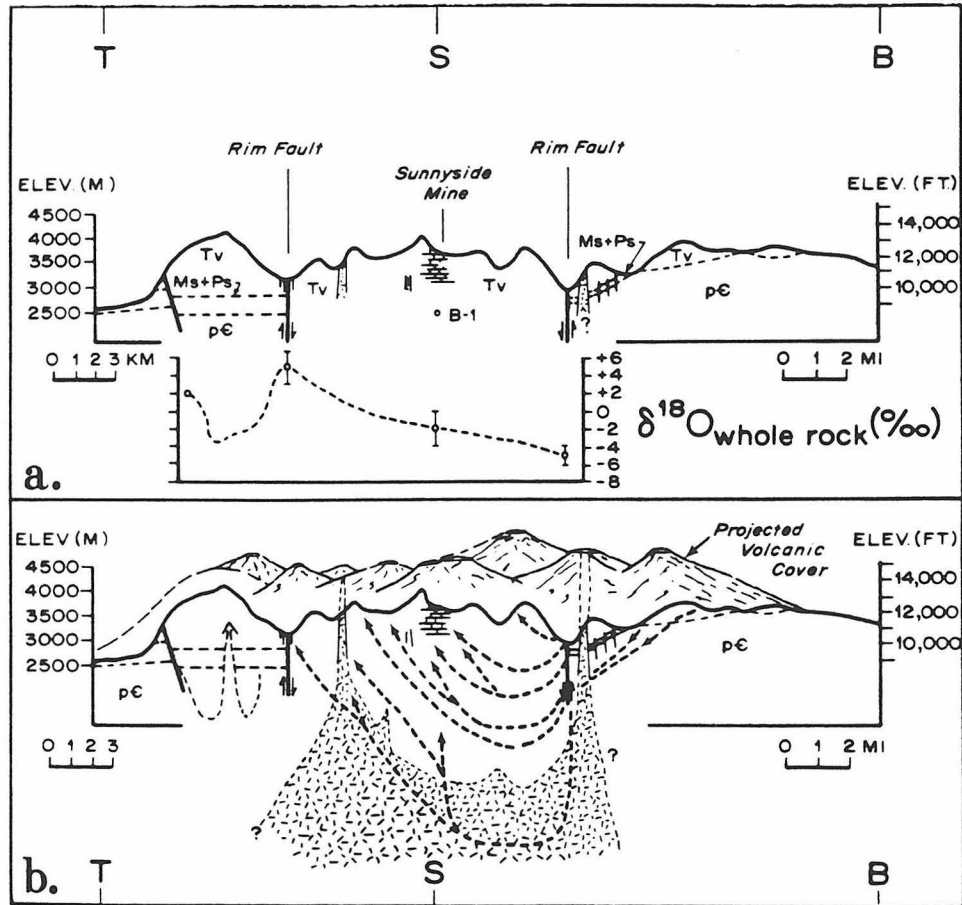


Figure 1.5 a. Geologic and topographic cross section through the San Juan and Silverton calderas along section T-S-B (Telluride-Sunnyside-Beartown) of Figure 1.4 (from Casadevall and Ohmoto, 1977). Whole-rock $\delta^{18}O$ values are from Taylor (1974a) and Casadevall and Ohmoto (1977)

b. Model cross sectional ground water flow pattern for the Sunnyside mineralizing hydrothermal system (from Casadevall and Ohmoto, 1977). Dashed arrows indicate suggested groundwater flow and convective fluid flow during mineralization.



producing fluids were low-D meteoric, and may have entered the vein system from topographically high areas to the north. Sphalerite and illite/chlorite fluids were higher-D meteoric, and may have entered the vein system from topographically low areas to the south. The low area may have been a closed-basin lake filling the structural moat of the Creede caldera. Bethke and Rye (1979) suggest that a large δD difference between the two meteoric water sources may have resulted from evaporation from the lake, which would fractionate D and H between the vapor and the lake.

Measurements of the isotopic composition of Pb in ore deposits throughout the San Juan Mountains (Doe et al, 1979) have shown that the ore lead is more radiogenic than the lead in the associated Tertiary igneous rocks (Lipman et al, 1978). The ore lead is isotopically similar to lead in the Precambrian crystalline rocks and Phanerozoic sedimentary rocks, suggesting that the ore-depositing fluids leached lead from the basement below the volcanic rocks. Such interaction requires deep circulation of meteoric water in the hydrothermal systems (Doe et al, 1979).

In summary, except for some very localized stockwork Mo deposits, the sources for hydrothermal fluids involved in convective systems in the western San Juan Mountains are nearly entirely meteoric in nature. These fluids circulated deeply into the crust, and they may have interacted extensively with the basement rocks prior to involvement with the alteration and mineralization currently exposed. In the local areas where magmatic fluids appear to have been present, they were responsible for only limited amounts of water-rock interaction for relatively short

periods of time.

CHAPTER 2

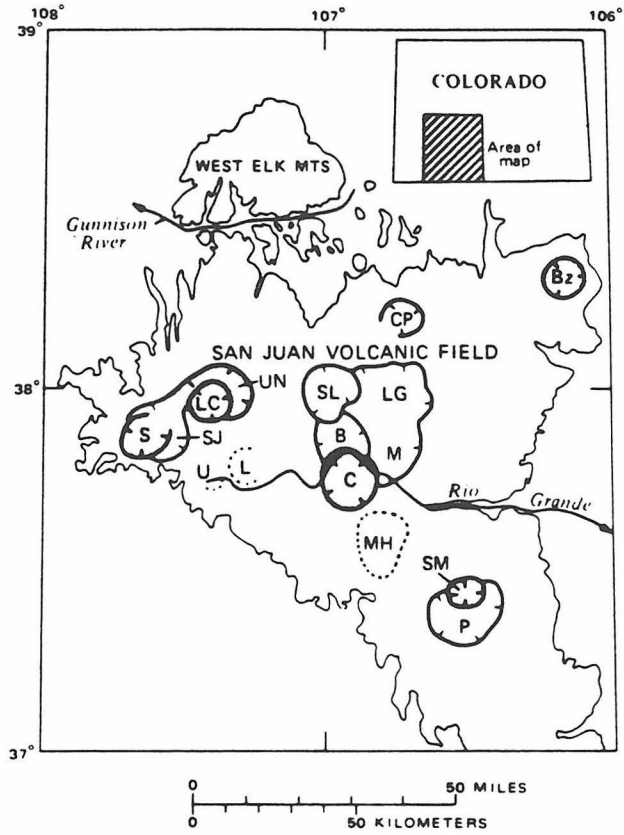
GEOLOGIC SETTING OF THE LAKE CITY CALDERA

2.1 Introduction

The Lake City caldera is the youngest of 15 mid-Tertiary volcanic collapse structures (Fig. 2.1) recognized in the San Juan volcanic field, southwestern Colorado (Steven and Lipman, 1976). This volcanic field comprises volcanic, volcanoclastic, and shallow plutonic rocks emplaced in Oligocene to Pliocene time. These rocks now cover approximately 25000 km² in southwestern Colorado and adjacent New Mexico, locally to thicknesses in excess of 2 km. Prior to erosion, the volcanic rocks were much more extensive. The basement rocks upon which the volcanic field was erupted range in age from Precambrian to Tertiary. The pre-volcanic topography varied considerably as a result of episodes of uplift, deformation, and erosion extending back into the Precambrian. One such cycle immediately preceded the initiation of volcanic activity. Now, the San Juan Mountains are quite rugged, with numerous glaciated peaks rising to elevations above 4000 meters.

Hydrothermal alteration and mineralization are widespread in the volcanic province. The mineralization is typically vein controlled, but replacement, porphyry, and chimney deposits are also present. The discovery and exploitation of some of these high-grade bonanza deposits in the late nineteenth century initially stimulated geologic investigations in this region. A series of five folios produced by the United States Geological Survey (Cross and Hole, 1910; Cross and Howe, 1905; Cross et al, 1905; Cross et al, 1907; Cross and Puring-

Figure 2.1 Map of the San Juan volcanic field showing calderas (from Steven et al, 1974): S, Silverton; LC, Lake City; SJ, San Juan; UN, Uncompahgre; CP, Cochetopa Park; Bz, Bonanza; SL, San Luis; B, Bachelor; C, Creede; LG, La Garita; M, general area of Mammoth Mountain caldera; U, Ute Creek; L, Lost Lake; MH, Mount Hope; SM, Summitville; P, Platoro. Solid caldera boundaries indicate known or readily inferred calderas, dotted boundaries indicate buried calderas.



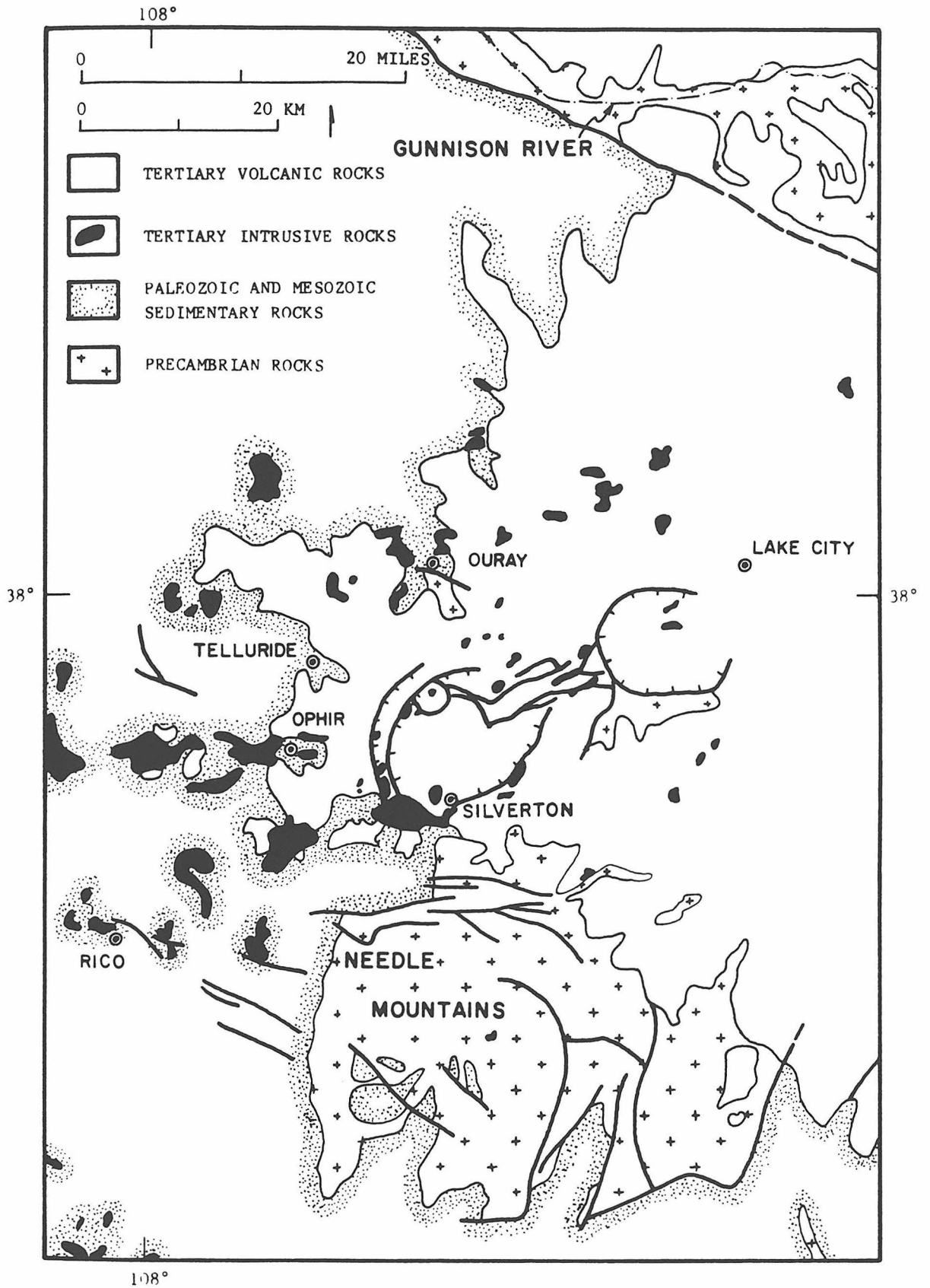
ton, 1899) are monumental achievements when one considers the hardships of working without modern transportation in the extremely rugged and oftentimes nearly inaccessible terrain. This early work served as a foundation upon which later studies of the geology and volcanic stratigraphy were based (Cross and Larsen, 1935; Larsen and Cross, 1956; Luedke and Burbank, 1963, 1968). More recent detailed mapping of volcanic rocks, coupled with radiometric age determinations, have led to major revisions of the volcanic stratigraphy, and to recognition of large-scale volcanic eruptive structures, the calderas (Lipman et al, 1970, 1973; Steven and Lipman, 1976). These more recent studies place the hydrothermal alteration and mineralization within the framework of the magmatic evolution of the volcanic province (Steven et al, 1974; Lipman et al, 1976). Although lacking the insight provided by radiometric dating, the work of Larsen and Cross (1956) remains a classic piece of descriptive geology; that paper was consulted constantly during the course of this study.

2.2 San Juan Regional Geology

2.2.1 Pre-Mid-Tertiary Development

The San Juan volcanic field was deposited on rocks ranging from Precambrian crystalline basement to Eocene conglomerate (Fig 2.2). Extensive exposures of Precambrian crystalline rocks are found along the northern (Gunnison River area) and southwestern (Needle Mountains) margins of the volcanic field. Rocks in both areas are lithologically and temporally similar (Silver and Barker, 1967; Bickford et al, 1967; Hansen and Peterman, 1968; Bickford et al, 1969; Barker, 1969). Barker

Figure 2.2 Generalized geologic map of the western San Juan volcanic field (from Burbank and Luedke, 1969). Areas of Precambrian exposure in the Needle Mountains and Gunnison River area are shown. Faults are shown in heavy black lines. Ring faults of the Silverton (western) and Lake City (eastern) calderas are indicated by hachures. Intrusive rocks in the Ouray area, at Rico, and in the southwestern corner of the map are latest Cretaceous (Laramide) in age.



(1969) has summarized the history of the Precambrian rocks in the Needle Mountains; deformed mafic and intermediate volcanic and clastic sedimentary rocks, the oldest recognized rocks in the area, have been intruded by 1.7 to 1.8 b.y. old quartz diorites, granodiorites, and granites. The thick, clastic Uncompahgre Formation, subsequently deformed in a second tectonic event, was deposited on an erosion surface developed on these older rocks. Postkinematic plutons ranging in composition from gabbro to granite (1.45 b.y. old) intrude the Uncompahgre Formation and older rocks. Finally, the mineralogically distinctive two-mica Trimble granite (1.35 b.y. old) intrudes the older postkinematic rocks. The Trimble granite petrographically resembles the Precambrian granite exposed along the southwestern margin of the Lake City caldera (granite of Lake Fork, Larsen and Cross, 1956; or granite of Cataract Gulch, Lipman, 1976a), these two plutons are believed to be contemporaneous. Precambrian rocks exposed along the Gunnison River are correlative with those in the Needle Mountains. One such intrusive rock, the Curecanti granite (1.42 b.y. old, Hansen and Peterman, 1968), is also a two-mica granitic rock similar petrographically to the Trimble granite (Larsen and Cross, 1956; Hansen, 1971).

Sedimentary rocks of Paleozoic and Mesozoic age are exposed along the flanks of the Needle Mountains, and underlie the western and south-southwestern margins of the volcanic field. These rocks are described in detail by Burbank (1930) and Larsen and Cross (1956). The Paleozoic rocks, approximately 1.8 km thick, were deposited on a smooth erosional surface cut on the Precambrian basement. Devonian and Mississippian marine limestone and shale overlie a basal Cambrian sandstone, and are

overlain unconformably by Pennsylvanian interbedded coarse clastic sediments and limestone. These grade upward into Permian continental red beds.

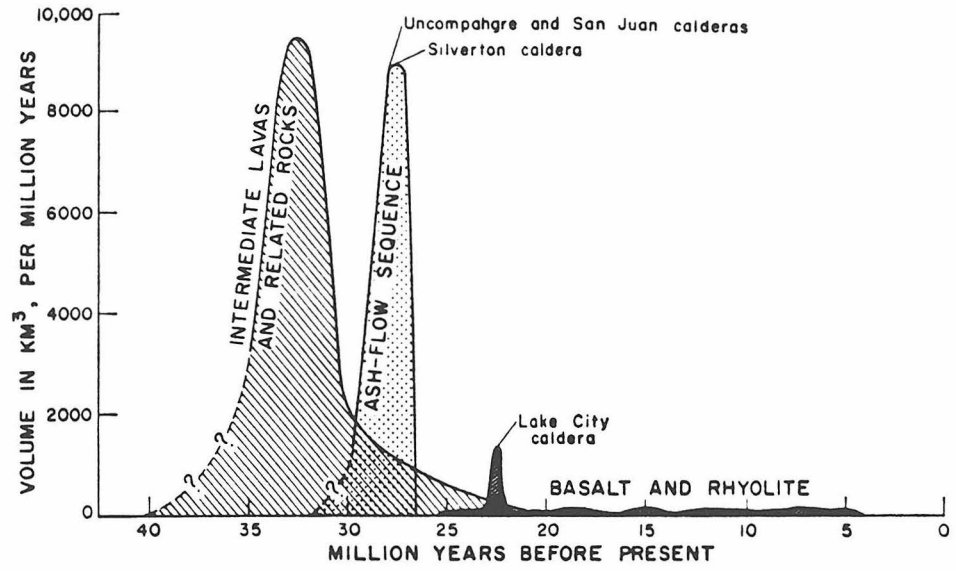
Prior to the deposition of the Mesozoic rocks, the Paleozoic rocks in the western San Juans were uplifted, and the area southeast and east of Ouray was eroded to expose Precambrian basement. Late Triassic to Late Cretaceous sediments were deposited on the Paleozoic and Precambrian rocks. Triassic and Jurassic rocks consist of red beds, aeolian sandstone, and other non-marine sedimentary rocks. An unconformity separates the Jurassic from the Triassic, and another occurs within the Late Jurassic. Cretaceous clastic marine sediments unconformably overlie the Late Jurassic non-marine rocks.

Doming recurred east of Ouray in latest Cretaceous (Laramide) time (Dickenson et al, 1968), and was accompanied by intermediate intrusions and lava flows in the Ouray area (Luedke and Burbank, 1962). Subsequent erosion exposed the Precambrian core of this Laramide dome. Erosional debris was deposited as a conglomeratic apron (Eocene Telluride Conglomerate) on the flanks of the uplift (Steven et al, 1967).

2.2.2 Tertiary Magmatic Evolution of the San Juan Volcanic Field

The San Juan volcanic field is composed of two petrologically and temporally distinct magmatic suites (Fig. 2.3) (Lipman et al, 1978). The older, more voluminous, calc-alkaline suite is Oligocene in age. It began with the eruption of intermediate-composition lavas and volcaniclastic rocks from volcanoes scattered throughout the field. The magmas evolved to more silicic ash-flow tuffs and related rocks erupted

Figure 2.3 Relationships between volume and age of the calc-alkaline and bimodal igneous suites in the western San Juan volcanic field (from Lipman et al, 1970; Lipman et al, 1976). Note that the earlier calc-alkaline lavas and ash-flow tuffs were erupted in much greater quantities than those associated with the younger Lake City event.



from caldera environments. Fourteen calderas related to these ash-flow eruptions have been recognized (Steven and Lipman, 1976). The younger Miocene-Pliocene suite comprises a bimodal basalt-rhyolite assemblage that initially formed a thin veneer of dominantly basaltic rocks over much of the older Oligocene volcanic field. Rhyolites associated with the younger suite form local accumulations, but one large eruption, the Sunshine Peak Tuff, was related to the collapse of the Lake City caldera. K-Ar dating of volcanic rocks from the San Juan volcanic field (Lipman et al, 1970) has shown that the early calc-alkaline intermediate lavas erupted from about 35 to 30 m.y. ago, the calc-alkaline ash-flow tuffs erupted from about 30 to 26 m.y. ago, and the bimodal suite erupted from about 24 to 3 m.y. ago.

The evolution of the Oligocene magmatism, from the early andesitic volcanism to later more silicic ash-flow tuff eruptions, is interpreted by Lipman et al (1978) to represent the rise, differentiation, and crystallization of a large composite batholith beneath the San Juan volcanic field. Lipman et al suggest that the Oligocene magmas were probably related to subduction along the western margin of the American plate. They interpret compositional and Pb and Sr isotopic patterns in the earlier andesitic volcanic rocks to indicate high-pressure fractionation of these magmas during melting in a subducted oceanic slab or upper mantle, and major interaction between these mantle-derived magmas and lower crustal rocks. Oligocene caldera development followed the andesitic volcanism as a large batholith was emplaced beneath the volcanic field. Lipman et al suggest that compositional trends in the ash-flow sheets reflect low-pressure fractional crystallization, and more radio-

genic Pb and Sr isotope compositions resulted from interaction with the upper crust. The regional gravity low centered on the calderas within the volcanic field is attributed to the presence of this batholith (Plouff and Pakiser, 1972).

The Miocene-Pliocene volcanic rocks were emplaced during intraplate extension and are not related to plate convergence and subduction (Christiansen and Lipman, 1972). Lipman et al (1978) suggest that the basaltic rocks originated as upper mantle partial melts. The associated rhyolitic rocks are dominated by non-radiogenic Pb and Sr, and thus are interpreted by Lipman et al to have been generated as lower crustal partial melts that did not interact with upper crustal rocks, perhaps because they were shielded by the Oligocene batholith.

2.2.3 Tertiary Mineralization and Alteration in the Western San Juans

Many of the economically important mining districts associated with the San Juan volcanic rocks are located in and around the western San Juan caldera complex, which includes the Uncompahgre, San Juan, Silverton, and Lake City calderas (Vanderwilt, 1947; Burbank and Luedke, 1968; Steven et al, 1974). The deposits are all hydrothermal in origin, and consist dominantly of veins filling faults and fractures, although chimney (vertical pipes of concentrated ore minerals), replacement, and porphyry stockwork deposits are present and have locally been historically productive. The four-county area encompassing the western San Juan caldera complex has a reported total production, through 1964, of gold, silver, lead, copper, and zinc in excess of 500 million dollars (Burbank and Luedke, 1968). This includes more than 7 million ounces

of gold and 160 million ounces of silver.

Radiometric and fission-track dating of minerals associated with the ore deposits and altered rocks in this area have shown that most of these hydrothermal systems were associated with the younger bimodal magmatism, not the older, calc-alkaline, caldera-forming magmatism (Lipman et al, 1976). However, the vein mineralization follows structures developed during the evolution of the older calderas.

Some hydrothermal activity was associated with the older calc-alkaline suite. Minor mineralization occurred during development of the pre-caldera, calc-alkaline, intermediate volcanoes. The cores of three such volcanic centers, the Carson, Cimmaron, and Larsen centers, are altered and mineralized, although metal production from these areas has been minimal. Mineralization and alteration contemporaneous with the western San Juan calc-alkaline calderas is best developed in the Uncompahgre caldera. Altered and mineralized rocks near Capitol City, an area of minor economic production within the Uncompahgre caldera, are truncated by the 23 m.y. old Lake City caldera (Lipman et al, 1976). The Golden Fleece vein, south of Lake City on the eastern margin of the Uncompahgre caldera, is also clearly truncated by the Lake City caldera eruptive rocks (Lipman et al, 1982). In this area, the intensely altered rocks of Slungullion Pass, which include rocks of the Uncompahgre caldera, are overlain by unaltered Sunshine Peak Tuff, which erupted from the Lake City caldera (Lipman et al, 1976).

The faults and fractures within which most of the veins were deposited were formed during resurgence and doming in the San Juan-Uncompahgre-Silverton caldera cycle (Fig. 2.4abc) (Burbank and Luedke,

Figure 2.4abc Schematic development of the western San Juan caldera complex (from Steven and Lipman, 1976). (a) Initial magmatism in the western San Juans produced the precaldera volcanoes at the Carson center (lower), the Larsen center (upper right), and the Cimarron center (upper center). These were followed by the eruption of the Sapinero Mesa Tuff and the contemporaneous collapse of the San Juan and Uncompahgre calderas. (b) Shortly after collapse of the San Juan-Uncompahgre calderas, eruption of the Crystal Lake Tuff resulted in collapse of the Silverton caldera, nested within the San Juan caldera. This was followed by general resurgence of the collapsed area and development of the apical Eureka graben. Intrusive rocks were emplaced along the ring faults of the calderas. (c) After a lapse of about 5 m.y., the Sunshine Peak Tuff erupted from the Lake City caldera, which collapsed within the southern part of the Uncompahgre caldera. Resurgent and ring fracture magmas were emplaced within the Lake City caldera. About 5 m.y. after collapse of the Lake City caldera, a string of intrusive rhyolites was emplaced along the northern margin of the Uncompahgre caldera.

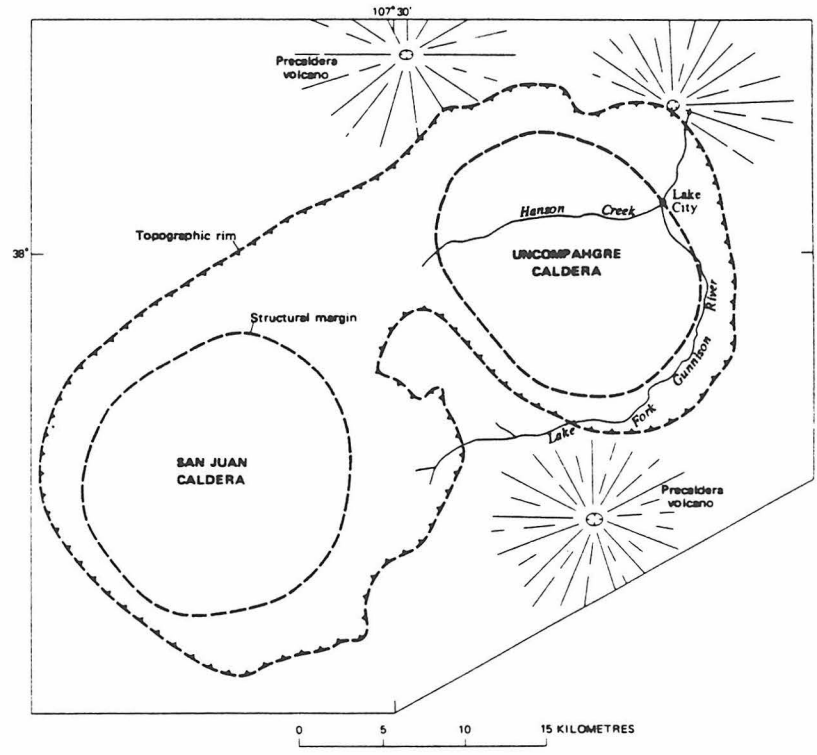


Figure 2.4a

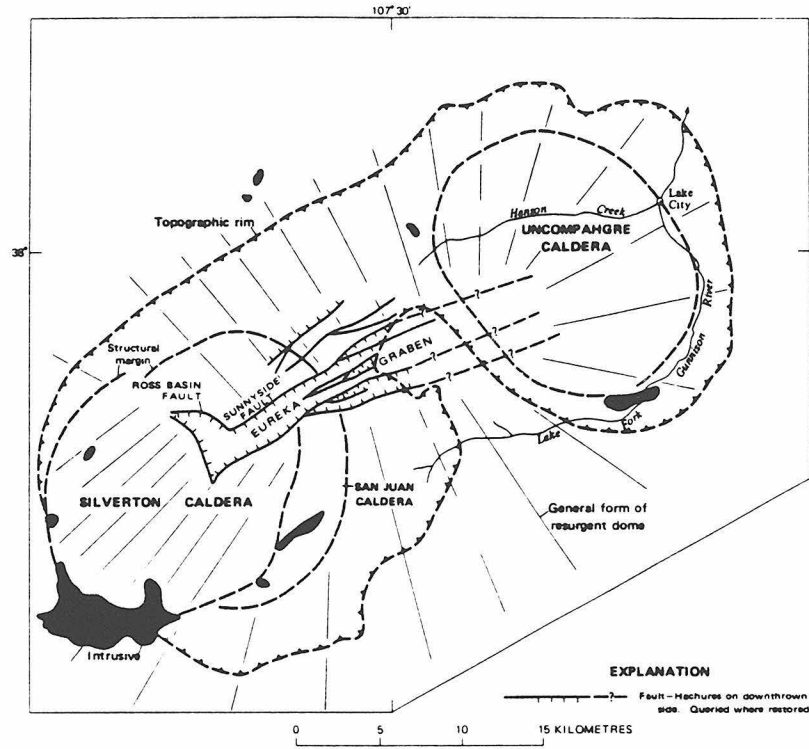


Figure 2.4b

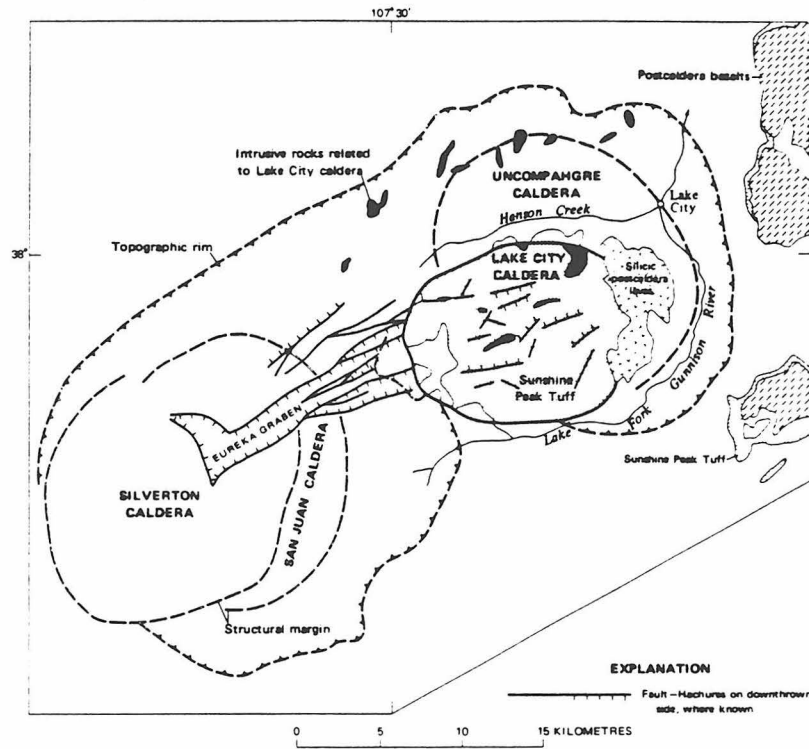


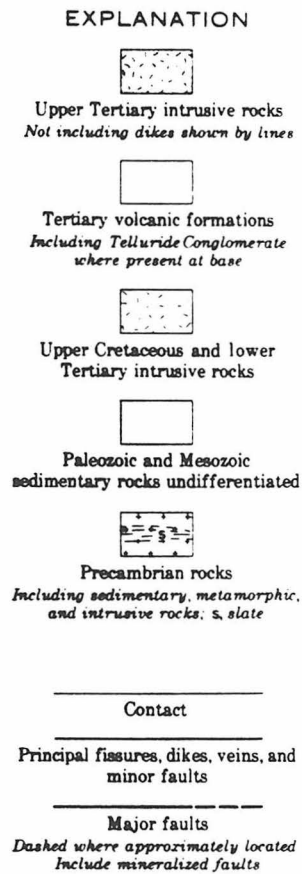
Figure 2.4c

1968; Steven et al, 1974). Veins occupying radial fissures occur in two areas: in a broad belt northwest of the Silverton caldera between the towns of Telluride and Ouray, in the vicinity of the Stony Mountain intrusive complex (Forester and Taylor, 1972, 1980; Fig. 2.5), and south of the Silverton caldera southeast of the town of Silverton (Fig. 2.5). Veins are also found filling faults and fractures in the Eureka graben, which developed along the crest of the resurgent dome that uplifted the collapsed blocks of the San Juan, Uncompahgre, and Silverton calderas. Economically less important veins fill fractures along the northern and eastern margins of the Uncompahgre caldera (Irving and Bancroft, 1911; Slack, 1980).

Alteration associated with these vein systems consists of narrow (<5 m) selvages of quartz, sericite, and pyrite (Burbank, 1950). This alteration is superimposed upon a pre-vein regional propylitization, which has been called pre-ore propylitization by Burbank (1960). This alteration is characterized by quartz, chlorite, epidote, calcite, and pyrite. In the area of the Sunnyside vein system in the Eureka graben, this assemblage changes with depth to an assemblage that also includes tremolite and anhydrite but lacks calcite (Burbank and Luedke, 1968; Casadevall and Ohmoto, 1977).

K-Ar and fission track ages of vein and alteration minerals from deposits in the radial fissures range from about 10 to 17 m.y. (Lipman et al, 1976). Rb/Sr isotopic analyses of minerals from the Sunnyside vein system define an apparent isochron between 13.0 and 16.6 m.y. (Casadevall and Ohmoto, 1977). These veins occur in rocks and structures related to the 27 to 29 m.y. San Juan-Uncompahgre-Silverton cal-

Figure 2.5 Geologic map showing structure in the Silverton caldera area (from Burbank and Luedke, 1969). The 10 km diameter area defined by circular structures in the central part of the figure is the Silverton caldera. Many of the faults and fissures are now mineralized, and represent host structures for many economically important veins.



dera cycle, but are also spatially related to small, contemporaneous, silicic intrusions of the bimodal suite, which are scattered throughout the mineralized area (Lipman et al, 1976).

The veins in the western San Juan Mountains consist dominantly of quartz and sulfides with local concentrations or minor occurrences of manganese carbonates and silicates, calcite, ankerite, fluorite, adularia, and barite. Abundant hypogene sulfides include pyrite, chalcopyrite, sphalerite, galena, and tetrahedrite, with minor arsenopyrite, gold and silver tellurides, silver sulfosalts, and free gold (Burbank and Luedke, 1968, 1969).

Replacement deposits occur in the Eocene Telluride Conglomerate, beneath the volcanic rocks where the veins in the radial fissures between Telluride and Ouray intersect the conglomerate (Mayor and Fisher, 1972). These deposits consist of 70 to 80 per cent massive concentrations of sphalerite, galena, chalcopyrite, and pyrite, with quartz, epidote, chlorite, rhodonite, and carbonate gangue minerals. Minor replacement ores are also found in the underlying Permian Cutler Formation and the Triassic Dolores Formation.

Chimney deposits occur in the Red Mountain district in an arc along the northwestern margin of the Silverton caldera, and are associated with brecciated cores within latite intrusive plugs (Ransome, 1901; Burbank, 1941, 1950; Burbank and Luedke, 1968, 1969). Massive pyrite and enargite with chalcopyrite, sphalerite, and copper and silver sulfosalts form significant ore bodies within the breccias. The chimneys lie within solfatarically altered volcanic rocks, which consist of pervasive zones of hydrothermal quartz, dickite, kaolinite, alunite, diasporite, and

pyrophyllite. The solfataric alteration grades outward into typical propylitization. Burbank (1950) interpreted this alteration to have formed in an acid-sulfate hot spring environment, based on the similarity of the alteration mineralogy to that described in modern acid-sulfate hot spring areas. Similarly altered areas are found throughout the San Juan Mountains, including, among others, Red Mountain near Lake City, Carson Camp, Summitville, Bonanza, and Calico Peak near Rico (Larsen, 1913; Serna-Isaza, 1971).

Eruption of the Sunshine Peak Tuff and the concurrent collapse of the Lake City caldera at 23 m.y. (Mehnert et al, 1973a) initiated the bimodal magmatism in the western San Juans. Alteration within the Lake City caldera, not an economically productive area, is centered on a granitic resurgent intrusion within the caldera. Alunite in the solfatarically altered breccia within the Red Mountain quartz latite dome on the eastern Lake City caldera ring fault yields a K-Ar age of about 23 m.y. (Mehnert et al, 1980), identical with that of the Sunshine Peak Tuff and the quartz latite dome (Mehnert et al, 1973a). Outside the northern margin of the Lake City caldera, radial veins that cut the volcanoclastic debris within the Uncompahgre caldera exhibit systematic mineralogic zonation concentric to the Lake City caldera (Slack, 1980), suggesting a genetic relationship. A sericite stringer from one such vein, the Hidden Treasure vein, yields a K-Ar age of 20.3 m.y., considered to be a minimum age because of the fine-grained nature of the sericite and the possibility of argon loss (Lipman et al, 1976). Quartz latite intrusions, spatially related to the chimney deposits in the Red Mountain district on the northwestern margin of the Silverton

caldera, yield concordant K-Ar and fission-track ages that also cluster around 22.5 m.y. (Lipman et al, 1976).

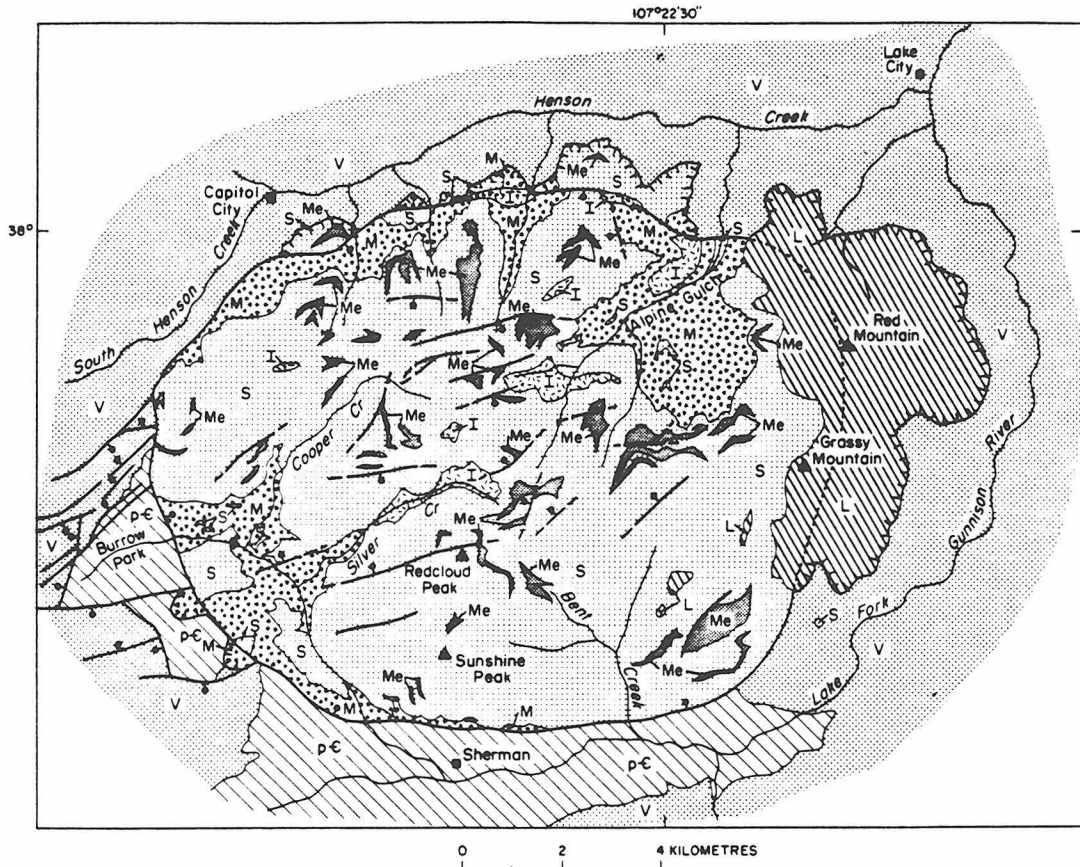
Occurrences of porphyry-type stockwork molybdenum mineralization are also present, although none have been productive. Several such areas occur between Silverton and Ophir (Jackson et al, 1980; Ringrose et al, 1981). A tabulation of stockwork molybdenum deposits in western North America by Clark (1972) includes Matterhorn Peak, just north of the Uncompahgre caldera, although other work in this area mentions only anomalous Mo-rich stream silt analyses (Fischer et al, 1968). South of Silverton, in the Precambrian crystalline rocks of the Needle Mountains, stockwork molybdenum is associated with a 9 m.y. rhyolite stock at Chicago Basin (Schmitt and Raymond, 1977). The Silverton-Ophir and Chicago Basin occurrences comprise thin quartz veinlets containing pyrite and molybdenite enclosed in wall rocks pervasively altered to quartz, sericite, pyrite, and, locally, kaolinite.

2.3 Geology of the Lake City Caldera

2.3.1 Magmatic Evolution of the Lake City Caldera

The Lake City caldera formed in response to the eruption of the Sunshine Peak Tuff 23 m.y. ago (Lipman et al, 1973; Mehnert et al, 1973a; Steven and Lipman, 1976; Hon et al, 1983). The caldera has been mapped by Lipman (1976a), and more recent work by Hon et al (1983) has defined detailed stratigraphic relationships within the caldera-fill Sunshine Peak Tuff (Fig. 2.6). The collapsed block, 11 by 14 km, is nested within the southern part of the Uncompahgre caldera, and truncates the eastern extension of the Eureka graben. The caldera ring

Figure 2.6 Generalized geologic map of the Lake City caldera (from Lipman, 1976b). Displacement on resurgence-related faults is no more than meters or tens of meters. Several hundred meters of uplift in the central part of the caldera has resulted from resurgence.



EXPLANATION

TERTIARY	I	Resurgent granitic intrusions	} LAKE CITY CALDERA-FILL SEQUENCE		Contact
	L	Caldera-filling lavas			Fault--Bar and ball on downthrown side. Dashed where approximately located; dotted where concealed
	S	Sunshine Peak Tuff (Intracaldera ash-flow tuff)			Remnants of topographic wall
	Me	Mesobreccia			
	M	Megabreccia			
	V	Precaldera volcanic rocks			
	p-C	Precambrian rocks			

fault is exposed for about 300° of arc around the caldera, and is a single, steeply inward-dipping, narrow fault. Various older volcanic rocks of the San Juan volcanic field are exposed along the margins of the caldera. Also, the crystalline basement is exposed in a structural high along the southern and southwestern margin of the caldera (the Precambrian granite of Cataract Gulch, Lipman, 1976a).

Intracaldera Sunshine Peak Tuff comprises three gradational facies with an overall thickness greater than 1300 m (Hon et al, 1983): the lower member is a high-silica, alkali rhyolite containing quartz, sanidine, and rare biotite phenocrysts (76 percent SiO₂); the middle member is a rhyolite containing quartz, sanidine and biotite phenocrysts (74 percent SiO₂); and the upper member is a quartz trachyte containing sanidine, plagioclase, quartz, and biotite phenocrysts (68 percent SiO₂). Outflow Sunshine Peak Tuff is only locally preserved, and is exclusively the early high-silica alkali rhyolite. Within the caldera, caldera-collapse breccias were shed into the downdropped block from the oversteepened caldera walls, and are interbedded with the three tuff units (Lipman, 1976b). These megabreccias contain fragments of volcanic rocks and Precambrian granitic rocks now exposed along the margins of the caldera. Megabreccia in the northwestern part of the caldera contains clasts of altered rhyolite that closely resemble altered rocks of the Capitol City area, just to the north outside the caldera. The stratigraphically higher breccia units contain smaller clasts than the lower units (Lipman, 1976b).

Ring-fracture domes, the quartz latites of Red Mountain and Grassy Mountain (63 percent SiO₂: Hon et al, 1983) were erupted on the eastern

caldera ring fracture shortly after the ash-flow eruptions, but it is not clear whether they predate or postdate resurgent doming of the down-dropped block (Steven and Lipman, 1976). A flat-topped quartz syenite intrusion (65 percent SiO_2 ; Hon et al, 1983) accompanied resurgence in the north-central part of the caldera. The caldera resurged asymmetrically, as indicated by variable displacements of the tuff units along the caldera walls. A maximum uplift of 700 m occurred along the northern wall, which corresponds to the highest level of emplacement of the resurgent intrusion (Hon et al, 1983). A discontinuous ring dike is exposed along the northern ring fault of the caldera (Steven and Lipman, 1976). A zone of faulting related to resurgence trends east-northeast across the resurgent dome, parallel to the extension of the Eureka graben.

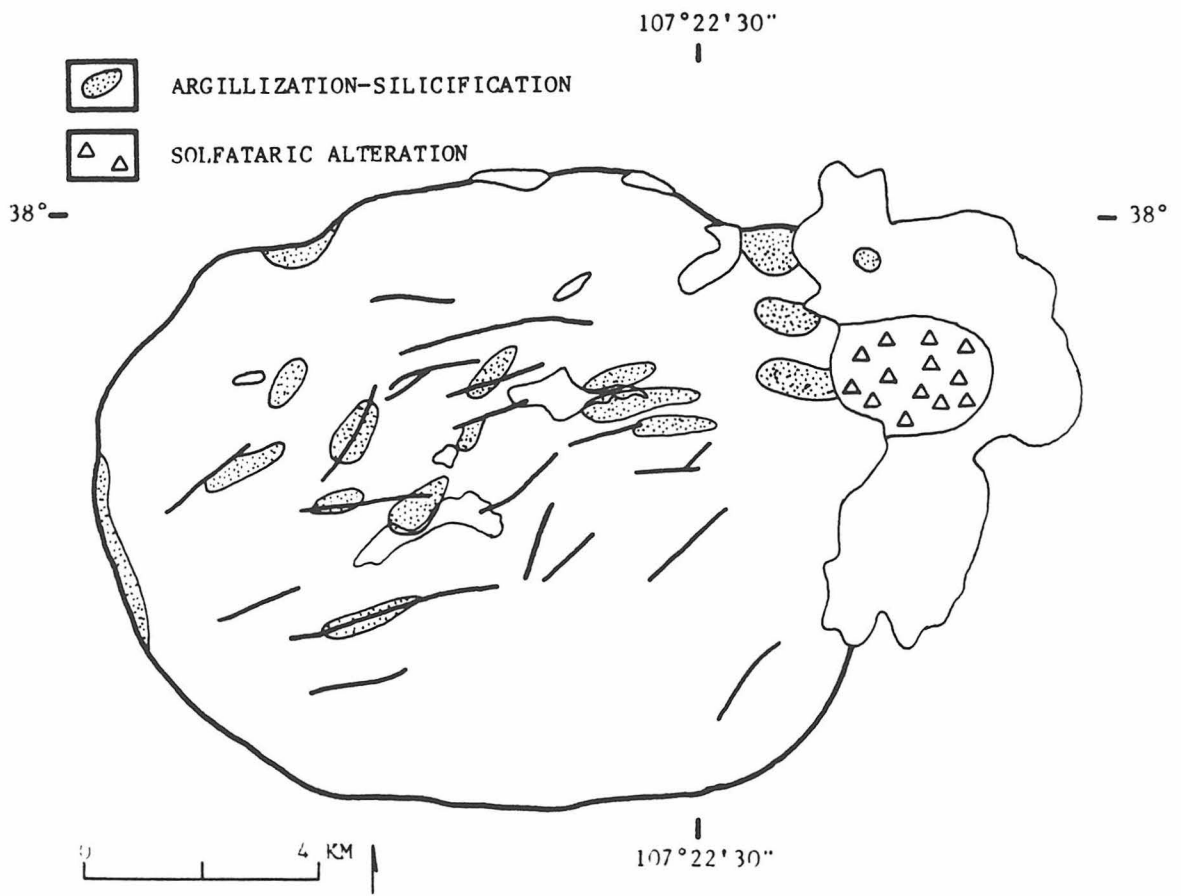
K-Ar age determinations for biotite and sanidine have shown that the lower and upper Sunshine Peak Tuff, the quartz latite lava domes, and the resurgent intrusions are all concordant at 23 m.y. (Hon et al, 1983). North of the Lake City caldera, in the moat of the older Uncompahgre caldera (Fig. 2.4c), an east-northeast trending line of rhyolite intrusions mineralogically similar to the Sunshine Peak Tuff was emplaced at about 18 m.y. (Steven and Lipman, 1976). These intrusive rocks are fluorine-rich, topaz-bearing rhyolites, similar to other Cenozoic topaz-bearing rhyolites in the western United States (Burt et al, 1982).

2.3.2 Hydrothermal Alteration in the Lake City Caldera

A hydrothermal system was established in the Lake City caldera shortly after collapse. Rocks mineralogically altered during this hydrothermal episode are exposed throughout the caldera (Fig. 2.7). The most intensely altered rocks within the resurgent dome occur around or above the resurgent intrusions (Steven and Lipman, 1976), suggesting a close genetic relationship. In this area, irregular zones of pervasive argillization and silicification, with minor pyrite, are centered on meter-wide quartz veins that fill resurgence-related fractures. Locally, the veins contain base-metal sulfides and pyrite. The altered zones extend from ten to several hundred meters away from the central veins. The abundance of alteration products in the rock decreases away from the veins, passing through a zone developed in the tuff where sericite replaces biotite, and eventually grading into a pervasive, caldera-wide, weak alteration characterized by spotted development of clay in the sanidine. Locally, calcite is an important alteration product in the tuff in the weakly altered areas. Sunshine Peak Tuff within several hundred meters of the resurgent intrusions has been hornfelsed, such that the initially fine-grained, devitrified groundmass is recrystallized to a coarser, even-grained, aggregate of quartz and potassium feldspar. In the hornfelsed tuff, the sanidine has unmixing to perthite. Surface oxidation of hypogene disseminated pyrite in the most intensely altered rocks imparts a bright red hematitic color to those exposures.

In Burrows Park, in the southwestern corner of the collapsed block, and in the lower Cooper Creek drainage adjacent to this area, quartz veins containing concentrations of pyrite, chalcopyrite, sphalerite,

Figure 2.7 Schematic distribution of intensely altered areas within the Lake City caldera (modified after Lipman, 1976a). The geology is taken from Figure 2.6. Outlines of outcrops of intrusive rocks are shown. Note the correspondence between the areas of resurgent intrusive rocks and argillized-silicified rocks within the caldera. The brecciated, solfatarically altered area in the Red Mountain quartz latite ring dome is also shown.



galena, and tetrahedrite have been mined (Woolsey, 1907; Krasowski, 1976). Alteration extends on an average 3 to 8 meters away from these veins, and consists of the development of quartz, sericite, and pyrite. Andesitic megabreccia in this area has been propylitically altered; it now contains albite, epidote, chlorite, sericite, pyrite, carbonates, and clays as alteration minerals (Krasowski, 1976).

Solfataric, acid-sulfate, hot spring alteration, centered on a brecciated area, occurs in the Red Mountain quartz latite (Larsen, 1913; Burbank, 1950). Mineralogically, the alteration consists of the pseudomorphic replacement of potassium feldspar phenocrysts by alunite and quartz, or by kaolinite and illite, with the groundmass completely altered to quartz and scattered grains of alunite or kaolinite/illite. Fine-grained disseminated pyrite initially made up several percent of the altered rock, but surface samples are oxidized to red iron oxides. The alteration grades outward through several hundred meters of pyritized and weakly argillized quartz latite to fresh rock. Hall (1978) estimates that 250 million metric tons of alunite, a potential aluminum resource, are contained in the Red Mountain deposit.

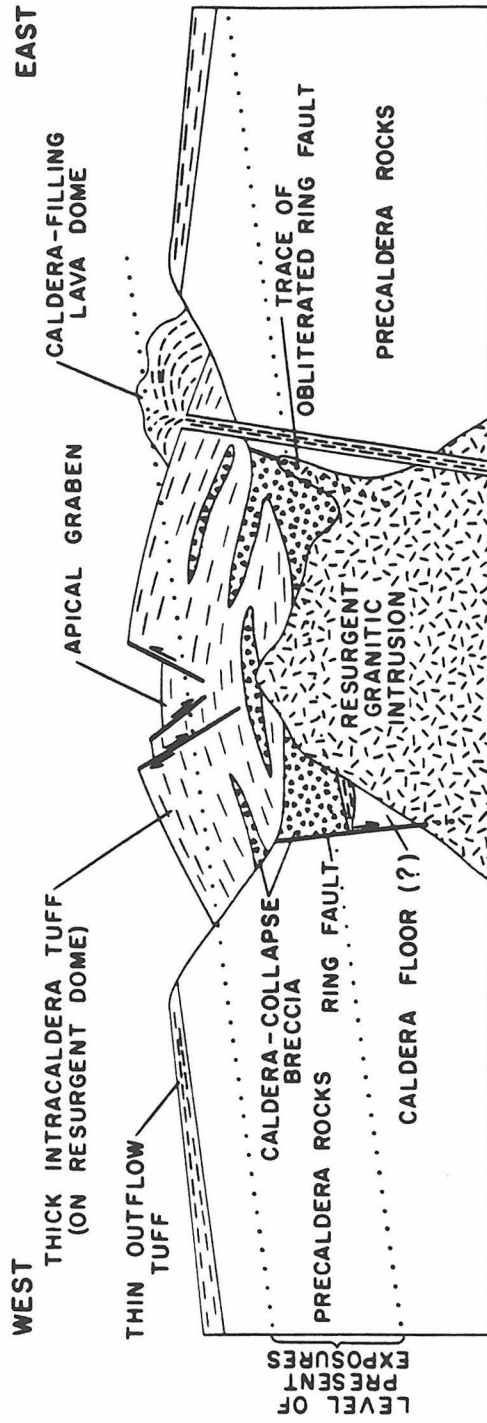
An 840 m deep diamond drill hole, collared at an elevation of 3780 m on the west flank of Red Mountain, was drilled by AMOCO in the summer of 1981. This hole penetrated locally-brecciated Red Mountain quartz latite throughout its extent. Above about 200 m, alteration in the drill hole remains similar to that exposed on the surface of the solfatarically altered zone. Below 200 m, alteration consists of variable amounts of kaolinite, illite, montmorillonite, quartz, and minor (< 3 percent) pyrite (Ken Hon and Dana Bove, personal

communication, 1983). The lower-elevation alteration mineralogically and texturally resembles the alteration surrounding quartz veins above the resurgent intrusion in the central part of the caldera.

Two samples of alunite from Red Mountain have been radiometrically dated using K-Ar (Mehnert et al, 1980). The two dates of 22.9 and 23.3 m.y. are virtually identical to the age of the Sunshine Peak Tuff, the Lake City caldera resurgent intrusions, and the ring dome quartz latites (Hon et al, 1983).

On the west side of Alpine Gulch, within the caldera 3 km northwest of the summit of Red Mountain (3909 m), several abandoned mines have exploited quartz veins bearing base-metal sulfides and pyrite. These veins are enclosed in pervasively altered caldera-fill tuff and megabreccia. This alteration is continuous with, although lower than (2990 to 3320 m elevation), the solfataric zone at Red Mountain. These relationships suggest that erosion has exposed different levels of the same hydrothermal system. It is also clear that erosion within the central and western parts of the caldera, where the resurgent intrusion and the lower units of the Sunshine Peak Tuff are exposed, has cut deeper into the stratigraphy than along the eastern caldera margin (Fig. 2.8), where the eruptive ring domes overlie the original top of the youngest Sunshine Peak Tuff unit. The top of this unit forms a dip slope away from the domed caldera core on the southeastern side of the caldera. Erosion within the central and eastern parts of the caldera has thus exposed deeper, hotter levels of the caldera's hydrothermal system than that exposed at Red Mountain. The mineralized veins in the Burrows Park area are also in a deeply eroded area, but both the sulfide mineral zonation

Figure 2.8 Diagrammatic E-W cross section through the Lake City caldera (from Lipman, 1976b). The present level of exposure within the caldera varies from east to west. On the eastern margin, the initial top of the caldera-fill Sunshine Peak Tuff is preserved beneath the quartz latite ring dome. Erosion in the central and western parts of the caldera has cut deeply into the resurgent dome, exposing the resurgent granitic intrusion. A section up to two km thick has been removed by erosion in the central and western part of the caldera.



and the proximity of these veins to the mineralized structures of the Eureka graben suggest a source in that direction (Krasowski, 1976). Some of the mineralization in the Eureka graben is as young as 10 to 17 m.y. old (Casadevall and Ohmoto, 1977; Lipman et al, 1976).

CHAPTER 3

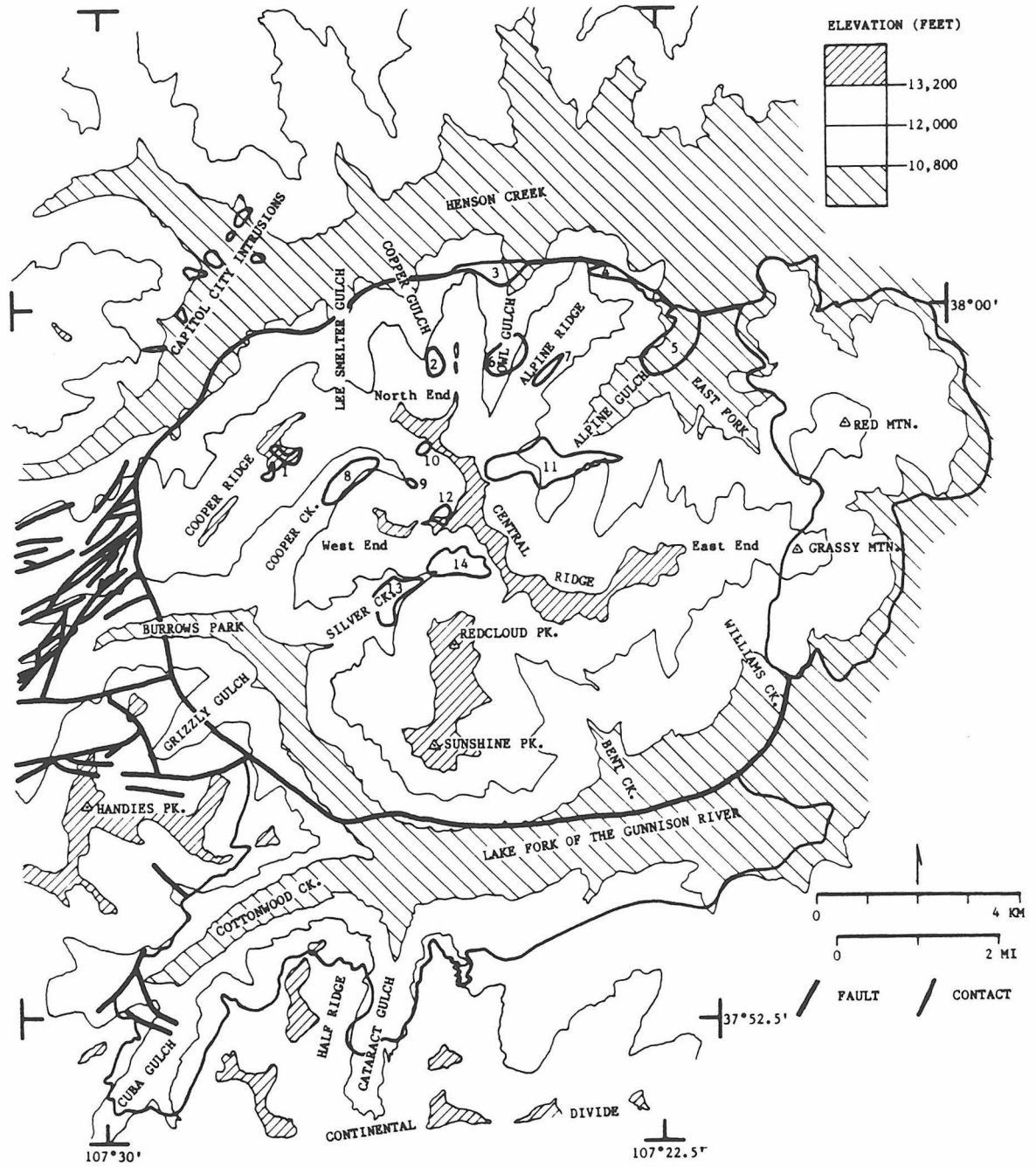
OXYGEN ISOTOPIC ANALYSES OF ROCKS FROM THE LAKE CITY CALDERA

3.1 Sampling Program and Sample Preparation

Three months were spent during the summers of 1981 and 1982 collecting samples from within and adjacent to the Lake City caldera. The extremely rugged terrain (2620 to 4273 m elevation; Fig. 3.1) and limited vehicular access within the caldera required that sampling be conducted almost entirely on foot. During the course of the field work, over 70,000 vertical feet (21 km) and 100 horizontal miles (160 km) were traversed. Samples were collected at approximately 400 meter intervals along the traverses, unless visual indications of varying alteration intensity necessitated shorter intervals. All quartz veins were sampled when encountered. All samples consist of single hand samples, approximately 1 kg in size, and care was taken to avoid oxidized or weathered rocks. More than 500 samples were collected, about half of which have been isotopically analyzed. 23 additional surface samples were provided by Ken Hon of the U. S. Geological Survey, and 16 samples of drill core from the Red Mountain area were provided by Ken Hon and Dana Bove of the U. S. Geological Survey. An additional 31 samples were collected at other solfatarically altered areas within the San Juan Mountains, including the Red Mountain district near Silverton, the Summitville district, and Calico Peak near Rico.

Standard 2 by 3 cm petrographic thin sections were prepared for nearly all the isotopically analyzed samples. Two to five grams of chips from the samples were ground by hand for the whole-rock isotopic

Figure 3.1 Map of the Lake City caldera showing topography. Place names as used in the text are shown. For convenient reference the exposures of the ring fracture and resurgent intrusion are numbered (from 1 to 14). See Plate 1 (in pocket) or Figure 2.6 for a lithologic explanation.



analyses, with care being taken to avoid oxidized or weathered rinds on the rocks. Coarser-grained samples, such as those from the Precambrian granite of Cataract Gulch and the Lake City resurgent intrusion, required larger ground samples in order to insure a representative analysis. Mineral separates were prepared by hand-picking 20 to 40 mg of clean mineral from 15 to 30 gm of crushed sample. Quartz phenocrysts from the rocks were routinely treated with concentrated HF to dissolve any matrix or other minerals adhering to them. Hand-picked feldspar and mica separates were generally greater than 95 percent pure. Quartz from quartz veins was also hand-picked from crushed vein material in order to remove fragments containing sulfides or their oxidation products. Hydrothermal quartz from the solfatarically altered areas was prepared by hand-picking clean quartz fragments from crushed rock that had been treated with concentrated HF. The HF treatment dissolved any alunite or kaolinite in the rock. Pure ground alunite, donated from the Caltech collection by Dr. George Rossman, was treated with concentrated HF in order to determine if it would dissolve in the cold acid, which it did.

3.2 Analytical Procedures

The technique used for $^{18}\text{O}/^{16}\text{O}$ determinations is essentially the same as that described by Taylor and Epstein (1962a). This involves the reaction of silicate minerals with excess fluorine gas, purification of the oxygen released by this reaction, reaction of the oxygen with a resistance-heated carbon rod to produce CO_2 , and analysis of the CO_2 with a McKinney-Nier double collecting mass spectrometer.

All results are reported in the familiar δ notation in parts per mil. Precision is better than 0.2 per mil. Raw δ values are corrected to the SMOW scale using the Caltech rose quartz δ value of 8.45. NBS-28 has a δ value of +9.60 on this scale.

3.3 Data from the Lake City Caldera

Oxygen isotopic data for rocks from the Lake City caldera area and for selected solfatarically altered areas in the San Juan Mountains are presented in Table 3.1. These data are listed by lithology. Included in Table 3.1 are mineralogical alteration data for nearly all the isotopically analyzed rocks. The mineralogical data are based on petrographic examination of thin sections prepared from the same hand samples from which the isotopic analyses were made. All sample locations and data from the Lake City caldera area are shown on Plate 1 (in pocket), which also includes the geology of the Lake City caldera area, together with the locations of the cross sections shown in Plate 4 (in pocket). Figure 3.1 is a condensed map of the caldera that shows topography, place names as used in this text, and the distribution of the resurgent and ring fracture intrusions that have been mapped within the caldera.

Table 3.1 Oxygen Isotopic Analyses of Rocks from the Lake City Caldera and Solfatarically Altered Areas, San Juan Mountains, Colorado

The data are listed according to lithology, beginning with the Precambrian granite of Cataract Gulch, and followed by the Sunshine Peak Tuff, the Lake City caldera resurgent intrusive rocks, the quartz latites of Grassy and Red Mountains, the Red Mountain quartz latite from the AMOCO drill hole on Red Mountain, vein quartz, the Sunshine Peak Tuff megabreccia, other volcanic rocks outside the caldera, and the solfatarically altered rocks from Red Mountain at Lake City, Carson Camp, Engineer Mountain, the National Belle Mine in the Red Mountain district, Calico Peak, and the Summitville district.

The following explanatory notes refer to the various columns, as are enumerated on the first page of each lithologic listing:

- 1) Latitude and longitude are N and W, respectively. Elevations are given in meters.
 Quadrangle abbreviations are as follows:

BH	Bristol Head	PCM	Pole Creek Mountain
FM	Finger Mesa	R	Rico
HP	Handies Peak	RP	Redcloud Peak
I	Ironton	S	Summitville
LC	Lake City	UP	Uncompahgre Peak
LSC	Lake San Cristobal	WP	Wetterhorn Peak

- 2) All data are per mil relative to SMOW. (*) denotes replicate analyses, the standard deviation is given as \pm , and the number of analyses is listed in parentheses.
 Mineral and other abbreviations are as follows:

A	Clay	F	Fluorite	Py	Pyrite
Al	Alunite	Gal	Galena	Q	Quartz
Ba	Barite	K	Alkali Feldspar	S	Sericite
C	Chlorite	M	Muscovite	Sp	Sphalerite
CC	Calcite	Ma	Marcasite	Su	Sulfur
Cpy	Chalcopyrite	Mo	Molybdenite	Tet	Tetrahedrite
E	Epidote	P	Plagioclase	WR	Whole Rock
En	Enargite				

- 3) The percentage listed under alteration is the volume of the designated phase that has been altered, followed by the major alteration products. Mineral abbreviations are the same as listed under (2). Where noted, the relative proportions of alteration products are shown as: >, greater than; >>, much greater than; or =, equal.
- 4) This column includes the alteration facies observed in thin section for the Sunshine Peak Tuff samples (see Chapter 6).
- 5) Abbreviations for lithologic units were taken directly from published maps of areas from which the samples were collected. The abbreviations are listed below, together with the references for the maps:
- | | |
|------|--|
| Tbb | Silverton volcanics, Burns member, biotite quartz latite (Lipman, 1976a) |
| Tca | Calico Peak porphyry (Pratt et al, 1969) |
| Tcr | Carpenter Ridge Tuff (Lipman, 1976a) |
| Tef | Intermediate lava flows related to the Carson volcano (Lipman, 1976a) |
| Tir | Rhyolite intrusive rock (Lipman, 1976a) |
| Tm | Monzonite intrusive rock, related to the Uncompahgre caldera (Lipman, 1976a) |
| Tmp | Monzonite porphyry intrusive rock, Uncompahgre caldera cycle (Lipman, 1976a) |
| Tqr | Quartz latite of Red Mountain (Lipman, 1976a) |
| Tsb | Burns Formation, intermediate volcanic rocks (Burbank and Luedke, 1964) |
| Tse | Eureka member, Sapinero Mesa Tuff (Lipman, 1976a) |
| Tsl | Landslide breccia member, Sapinero Mesa Tuff (Lipman, 1976a) |
| Tsm | Picayune megabreccia member, Sapinero Mesa Tuff (Lipman, 1976a) |
| Tspm | Megabreccia member, Sunshine Peak Tuff (Lipman, 1976a) |
| Tsq | Quartz latite of South Mountain (Lipman, 1974) |

Precambrian Granite of Cataract Gulch

Field#:	Location (1):		Elev	$\delta^{18}O$ Analyses (2):			Alteration (3):		Remarks:
	Lat/Long	Quad		WR	Q	K	Other	Biotite	
SC-75	37°57.50'	RP	3908	3.6				100% S	
	107°29.58'								
SC-84	37°54.60'	RP	2917	7.9				100% S	
	107°22.99'								
SC-85	37°54.46'	RP	2874	5.8				40% S=C	
	107°23.40'								
SC-86	37°54.24'	RP	2886	4.6	9.9	4.0	6.6 M	90% S=C	
	107°24.16'								
SC-90	37°56.57'	RP	3277	2.6				100% S	
	107°29.35'								
SC-95	37°56.67'	RP	3322	4.0	9.8	2.3		90% C>S	
	107°29.99'								
SC-97	37°56.60'	RP	3301	0.7				90% C,A	Plagioclase entirely argillized; collected 1 m from sulfide- bearing quartz vein.
	107°30.01'								
SC-102	37°53.47'	RP	3200	4.9				50% C>S	
	107°25.95'								
SC-103	37°53.14'	RP	3280	3.4				80% C>>S	
	107°26.04'								

Field#:	Location:		Elev	$\delta^{18}O$ Analyses:				Alteration:	Remarks:
	Lat/Long	Quad		WR	Q	K	Other		
SC-105	37°52.85' 107°26.10'	RP	3392	6.4			5% C		
SC-106	37°52.68' 107°26.11'	RP	3444	5.0			70% C		
SC-107	37°52.41' 107°26.24'	PCM	3520	6.2				No thin section	
SC-109	37°53.29' 107°27.19'	RP	4023	6.2			90% C		
SC-110	37°53.17' 107°27.63'	RP	3889	7.3			10% C		
SC-111	37°53.04' 107°27.97'	RP	3719	7.8				No thin section	
SC-112	37°53.08' 107°28.14'	RP	3560	7.5			10% C		
SC-114	37°54.35' 107°26.81'	RP	3609	3.2			90% C>>S		
SC-116	37°54.30' 107°26.60'	RP	3475	4.9			60% C>>S		
SC-117	37°54.18' 107°26.35'	RP	3277	5.6			40% S		
SR-17	37°54.40' 107°23.76'	RP	3082	4.1	10.0	5.5	100% C=S		

Field#:	Location:		Elev	$\delta^{18}O$ Analyses:				Alteration:	Remarks:
	Lat/Long	Quad		WR	Q	K	Other		
HP-16	37°53.98' 107°26.25'	RP	2969	4.9			100% S		
CG-6	37°54.35' 107°20.65'	LSC	2880	8.5			100% S,A	Feldspars and micas entirely altered to clays, sericite, and quartz	
CG-11	37°53.81' 107°21.84'	LSC	3072	9.2	10.5	8.6	25% S		
CG-33	37°54.48' 107°22.32'	LSC	2862	8.4			Fresh		
CG-35	37°54.37' 107°21.38'	LSC	2847	8.2			70% C		
CG-36	37°54.62' 107°20.31'	LSC	2832	7.4	9.7		90% S>>A		
LC-17	37°56.36' 107°30.51'	HP	3377	3.3	10.4	1.9	95% C>>S	Dump sample, Bon Homme mine, plagioclase 30% to clay and sericite.	

Sunshine Peak Tuff

Field#:	Location (1):		Elev	δ ¹⁸ O WR	Analyses (2):		Alteration (3):		Remarks (4):
	Lat/Long	Quad			Other	Sanidine	Biotite		
SC-1	37°56.48'	RP	3719	0.8	15% A	90% S		IV	
	107°26.35'								
SC-4	37°56.34'	RP	3783	4.5	100% A, Q	100% A		II	
	107°26.31'								
SC-6	37°56.30'	RP	3792	2.1	100% Q	100% Q		I	
	107°26.30'								
SC-11	37°55.93'	RP	4094	3.5	50% A, Q	100% S		III	
	107°26.28'								
SC-12	37°56.29'	RP	3728	1.3	100% A, Q	100% A, Q		II	
	107°26.24'								
SC-14	37°56.23'	RP	3685	1.7				No thin section	
	107°26.00'								
SC-19	37°56.43'	RP	4278	5.3	10% A	100% A	8.1 Q 4.3 K	V	
	107°25.26'								
SC-21	37°56.62'	RP	4221	5.9	Turbid	Fresh		V	
	107°25.24'								
SC-26	37°56.67'	RP	3920	4.6	15% A	Fresh		IV	
	107°27.40'								
SC-27	37°56.96'	RP	3840	2.9	40% A	100% S		IV	
	107°27.43'								

Field#:	Location:		Elev	$\delta^{18}O$ Analyses:		Alteration:		Remarks:
	Lat/Long	Quad		WR	Other	Sanidine	Biotite	
SC-28	37°57.18' 107°25.67'	RP	3658	2.9		75% A,Q	100% S	III, quartz micro- veinlets
SC-33	37°56.98' 107°27.29'	RP	3731	2.0		30% A	100% S	IV
SC-35	37°57.24' 107°26.94'	RP	3975	1.3		10% A	90% S	Hornfelsed
SC-38	37°57.47' 107°26.60'	RP	3999	1.3		40% A	100% S	Hornfelsed
SC-39	37°57.54' 107°26.35'	RP	3950	10.4		100% Q	100% Q	I, with relict zircons
SC-40	37°57.31' 107°26.19'	RP	3706	2.2		10% A,Q	Fresh	Hornfelsed
SC-41	37°57.16' 107°26.07'	RP	3597	8.5		100% Q	100% Q	I, with relict zircons
SC-45	37°56.96' 107°25.93'	RP	3658	3.0		5% A	Fresh	Hornfelsed
SC-50	37°57.33' 107°25.69'	RP	3795	3.3		15% A	100% S	IV
SC-64	37°57.60' 107°27.82'	RP	3536	3.4		90% A,Q	100% S	III
SC-68	37°57.66' 107°29.43'	RP	3926	-0.9		40% CC	100% S	chlorite/calcite

Field#:	Location:			$\delta^{18}O$ Analyses:		Alteration:		Remarks:
	Lat/Long	Quad	Elev	WR	Other	Sanidine	Biotite	
SC-69	37°57.68' 107°29.28'	RP	3901	0.7		10% A,Q	50% S	III
SC-71	37°57.54' 107°28.61'	RP	4039	0.4		20% CC	100% S,Q	chlorite/calcite
SC-72	37°58.00' 107°28.17'	RP	4057	1.6		50% A,Q	80% Q	III
SC-81	37°55.15' 107°23.10'	RP	3097	3.8	8.1 Q	10% A Turbid	Fresh	IV
SC-83	37°54.65' 107°23.00'	RP	2926	1.8		10% A Turbid	Fresh	IV
SC-121	37°56.95' 107°23.20'	RP	4051	6.5		Turbid	Fresh	V
SC-122	37°57.28' 107°22.67'	RP	4210	6.9		Turbid	Fresh	V
SC-123	37°56.93' 107°22.69'	RP	3962	7.5		Turbid	Fresh	V
SC-124	37°56.64' 107°22.32'	LSC	3805	6.9		Turbid Chatoyant	Fresh	V
SC-129	37°55.21' 107°22.18'	LSC	3170	7.3±0.1* (4)		Fresh	Fresh	V
SC-135	37°56.19' 107°25.31'	RP	4246	4.4		5% A Turbid	Fresh	IV

Field#:	Location:		Quad	Elev	δ^{18} Analyses:		Alteration:		Remarks:
	Lat/Long	RP			WR	Other	Sanidine	Biotite	
SC-136	37°55.88'	RP	RP	4219	4.8		20% A	100% A	IV
	107°28.61'								
SC-137	37°55.59'	RP	RP	4228	4.9		30% A	Fresh	IV
	107°25.47'								
SC-138	37°55.37'	RP	RP	4268	5.3		Turbid	Fresh	V
	107°25.36'								
SC-139	37°55.33'	RP	RP	4084	5.5		30% A	50% S,A	IV
	107°25.77'								
SC-140	37°55.61'	RP	RP	3993	3.4				No thin section
	107°26.00'								
SC-141	37°55.57'	RP	RP	3901	4.1		5% A	Fresh	V
	107°26.18'						Turbid		
SC-142	37°55.40'	RP	RP	3627	2.1		20% A,C,CC	100% S	chlorite/calcite
	107°26.47'								
SC-144	37°55.29'	RP	RP	3267	1.5		60% CC,C	100% C	chlorite/calcite
	107°26.79'								
SC-151	37°58.12'	RP	RP	4127	3.0		60% A,Q	100% A	III
	107°24.93'								
SC-155	37°57.71'	RP	RP	4008	1.6		100% A,Q	100% A,Q	II, Entirely altered to quartz and clay
	107°25.65'								
SC-159	37°57.70'	RP	RP	4081	2.3		30% A,Q	100% S	III
	107°26.15'								

Field#:	Location:		Elev	$\delta^{18}O$ Analyses:		Alteration:		Remarks:
	Lat/Long	Quad		WR	Other	Sanidine	Biotite	
SC-160	37°58.57' 107°27.13'	RP	3932	1.4		50% A,Q	100% S,Q	III
SC-168	37°57.92' 107°27.89'	RP	3810	2.1		25% A	100% S,Q	III
SC-169	37°57.73' 107°27.86'	RP	3679	2.4		50% CC,C	100% S	chlorite/calcite
SR-4	37°55.63' 107°24.85'	RP	3146	0.5		20% CC,C,A	100% S,C	chlorite/calcite
SR-26	37°56.63' 107°28.49'	RP	3240	-0.5		15% A	100% S	Hornfelsed
AG-1	37°56.15' 107°23.63'	RP	3304	0.1	8.1 Q	10% A	100% S,C	IV
AG-3	37°56.01' 107°23.82'	RP	3389	2.3	4.8 K	15% A	100% C	Hornfelsed
AG-9	37°57.04' 107°21.89'	LSC	2963	-0.1		5% A	100% C	Hornfelsed
AG-11	37°59.86' 107°21.71'	LSC	2874	-1.6	-1.9 K	5% A	100% C	Hornfelsed
RM-40	37°57.58' 107°21.10'	LSC	3880	6.3		15% A	Fresh	IV
RM-41	37°57.58' 107°21.50'	LSC	3917	6.7		10% A	Fresh	IV

Field#:	Location:		Quad	Elev	$\delta^{18}O$ Analyses:		Alteration:		Remarks:
	Lat/Long	Lat/Long			WR	Other	Sanidine	Biotite	
RM-42	37°57.43'	107°21.57'	LSC	3920	5.9		10% A,Q	Fresh	IV
RM-43	37°57.10'	107°21.38'	LSC	3719	6.6		5% A Turbid	Fresh	V
RM-44	37°56.89'	107°21.21'	LSC	3612	6.5		5% A Turbid	Fresh	V
RM-46	37°56.39'	107°21.36'	LSC	3292	6.6±0.1* (2)		Turbid	Fresh	V
RM-48	37°55.85'	107°20.93'	LSC	3048	7.1		10% A	Fresh	IV
RM-57	37°59.21'	107°21.41'	LSC	3368	6.6		100% A,Q,S	100% A	II
RM-60	37°58.86'	107°21.53'	LSC	3139	2.6		75% A,CC	100% S,C	chlorite/calcite
HC-48	37°59.36'	107°27.11'	RP	3709	2.9		5% A	100% S	IV
HC-49	37°59.19'	107°27.24'	RP	3770	3.7		100% Q	100% Q	I
HC-53	37°59.41'	107°26.47'	RP	3542	0.5		10% A	20% S	IV
HC-60	38°00.37'	107°22.45'	LC	3341	6.2		10% A,Q	Fresh	IV

Field#:	Location:		Elev	$\delta^{18}O$ Analyses:		Alteration:		Remarks:
	Lat/Long	Quad		WR	Other	Sanidine	Biotite	
HC-64	37°59.93' 107°23.14'	RP	3792	2.3		95% A	100% S	III
HC-65	37°59.88'	RP	3988	3.3		70% S,Q,A	100% S	III
HC-66	37°59.70' 107°23.88'	RP	3999	3.1±0.0* (2)		40% A	100% S	IV
HC-67	37°59.51' 107°24.04'	RP	3962	2.7		15% A	60% A	IV
HC-69	37°59.11' 107°24.38'	RP	3865	3.3		10% A	100% S	Hornfelsed
HC-76	37°58.56' 107°23.13'	RP	3475	1.8		5% A	100% C	Hornfelsed
HC-78	37°58.36' 107°23.19'	RP	3658	1.4		10% A	100% A,Q	Hornfelsed
HC-83	37°57.80' 107°23.60'	RP	3920	2.1		15% A	100% S	III
HC-85	37°57.52' 107°23.68'	RP	3926	3.6		70% A	100% A	III
HC-86	37°57.43' 107°23.75'	RP	3908	4.1		80% CC,A	100% S	chlorite/calcite
HC-87	37°57.42' 107°23.77'	RP	3908	4.0		30% A	100% S	III

Field#:	Location:		Quad	Elev	$\delta^{18}O$ Analyses:		Alteration:		Remarks:
	Lat/Long				WR	Other	Sanidine	Biotite	
HC-89	37°57.57'	107°23.29'	RP	3652	3.1		10% A	100% A	III
HC-96	37°58.96'	107°28.34'	RP	3444	0.2		15% CC,A	100% S,C	chlorite/calcite
2-6-14A	38°00.07'	107°25.10'	UP	3825	2.2				From Ken Hon, no thin section
2-6-28A	38°00.38'	107°23.46'	UP	3731	6.3				From Ken Hon, no thin section
5-2C-122E	37°57.10'	107°24.42'	RP	4118	7.5				From Ken Hon, no thin section
RC4-55A	37°57.49'	107°22.86'	RP	3990	6.7				From Ken Hon, no thin section
RC4-30A	37°57.09'	107°24.15'	RP	4121	6.9				From Ken Hon, no thin section
RC4-12A	37°57.44'	107°22.45'	RP	4090	7.1				From Ken Hon, no thin section
RC4-27A	37°56.94'	107°23.98'	RP	4161	6.4				From Ken Hon, no thin section
RC4-28A	37°57.00'	107°24.05'	RP	4161	7.1				From Ken Hon, no thin section
RC4-30C	37°57.09'	107°24.15'	RP	4121	6.8				From Ken Hon, no thin section

Field#:	Location:		Elev	δ ¹⁸ O WR	Analyses:		Alteration:		Remarks:
	Lat/Long	Quad			Other	Sanidine	Biotite		
RC4-22A	37°56.90' 107°23.57'	RP	4115	5.6					From Ken Hon, no thin section
RC4-24A	37°56.83' 107°23.84'	RP	4206	6.5					From Ken Hon, no thin section
RC4-2A	37°57.33' 107°22.80'	RP	4182	6.5					From Ken Hon, no thin section
RC2-64A	37°59.23' 107°24.28'	RP	3908	3.1					From Ken Hon, no thin section
RC2-3A	37°58.51' 107°24.09'	RP	3536	2.6±0.1* (2)					From Ken Hon, no thin section
					<u>Outflow Facies Samples</u>				
CC-7	37°55.72' 107°09.80'	BH	3289	8.2	8.1 Q 7.0 K	Fresh	Fresh		Not altered
CC-8	37°55.22' 107°09.69'	BH	3286		8.1 Q 6.8 K	Fresh	Fresh		Not altered
BHS-1A	location unknown, outside caldera			7.8					From Ken Hon, no thin section, listed only as outflow facies

Resurgent Intrusive Rocks of the Lake City Caldera

Field#:	Location (1):		Elev	$\delta^{18}O$ Analyses (2):		Alteration (3):		Remarks:
	Lat/Long	Quad		WR	Other	Sanidine	Biotite	
<u>Medium Grained Porphyritic Granite</u>								
SC-43	37°57.07'	RP	3536	0.5	2.9 K	20% S,A	95% C,S	
	107°26.07'							
SC-44	37°57.00'	RP	3499	2.9		10% A	30% C,S	Minor calcite in matrix
	107°26.15'							
SC-46	37°56.98'	RP	3627	4.8		30% A	30% C	
	107°25.95'							
SC-51	37°57.10'	RP	3612	4.3		30% A	90% C,S	
	107°25.71'							
SC-52	37°58.12'	RP	3694	-1.6	-4.0 K	15% A	100% S	Trace disseminated pyrite
	107°25.82'							
SC-57	37°58.28'	RP	3658	-1.8		50% A	100% C,S	Trace disseminated pyrite
	107°26.44'							
SC-152	37°57.72'	RP	4106	4.1				No thin section
	107°25.31'							
AG-4	37°55.82'	RP	3475	-0.7	1.6 K	30% A	70% C,CC	
	107°23.94'							
HC-73	37°58.51'	RP	3639	-1.0		20% A	90% C,S	
	107°24.06'							

Field#:	Location:		Quad	Elev	$\delta^{18}O$ Analyses:		Alteration:		Remarks:
	Lat/Long	Lat/Long			WR	Other	Sanidine	Biotite	
HC-77	37°58.43'	107°23.18'	RP	3597	1.1		10% A	40% C	Minor calcite in matrix
HC-91	37°59.75'	107°22.14'	LSC	3124	2.9		Fresh	10% S	5% pyroxene phenocrysts
2-6-28B	38°00.38'	107°23.46'	UP	3731	4.6				From Ken Hon, no thin section
2-6-13A	38°00.17'	107°22.70'	UP	3597	3.8				From Ken Hon, no thin section
6-1-12A	37°59.86'	107°22.18'	LSC	3219	2.4				From Ken Hon, no thin section
RC-2-7B	37°59.32'	107°24.03'	RP	3840	2.4				From Ken Hon, no thin section
RC-2-8A	37°59.27'	107°24.13'	RP	3853	1.1				From Ken Hon, no thin section
2-6-2A	38°00.14'	107°25.00'	UP	3719	0.1±0.1* (2)				From Ken Hon, no thin section
<u>Rhyolite Porphyry</u>									
SC-79	37°57.30'	107°30.54'	HP	4029	1.0		80% A,CC	100% S	Rhyolite dike west of caldera margin
SC-161	37°58.53'	107°27.23'	RP	3975	1.2	-1.1 K 7.9 Q	20% A	80% S	

Field#:	Location:		Elev	$\delta^{18}O$ Analyses:		Alteration:		Remarks:
	Lat/Long	Quad		WR	Other	Sanidine	Biotite	
SC-164	37°58.51'	RP	4127	2.2		10% A	Fresh	
	107°27.68'							
SC-166	37°58.20'	RP	3973	2.4		100% A,Q	100% A,Q	Quartz microveinlets
	107°27.81'							
2-5-9A	38°00.22'	UP	3371	4.8				From Ken Hon, no thin section
	107°26.97'							
RC-4-31D	37°57.16'	RP	4023	7.0				From Ken Hon, no thin section
	107°24.04'							

Quartz Latites of Grassy and Red Mountain

Field#:	Location (1):		Elev	$\delta^{18}O$ Analyses (2);			Alteration:	Remarks:
	Lat/Long	Quad		Feldspar	Biotite	Other		
SC-125	37°56.64' 107°22.36'	RP	3717			7.4 WR		
RM-1	37°59.70' 107°19.21'	LSC	3597	6.7	5.2	8.3 WR 7.8 Q		
RM-2	37°59.56' 107°19.35'	LSC	3566	6.6				
RM-3	37°59.50' 107°19.53'	LSC	3499	6.6				
RM-4	37°59.58' 107°19.67'	LSC	3438	6.8		5.7 WR 7.3 Q		
RM-5	37°59.69' 107°19.59'	LSC	3365	7.0			Minor plagioclase to calcite	
RM-6	37°59.76' 107°19.54'	LSC	3359	6.6	4.5	5.8 WR 8.4 Q	Minor plagioclase to calcite	
RM-7	38°00.01' 107°19.44'	LC	3304	6.6	5.5		Minor plagioclase to calcite	
RM-8	38°00.01' 107°19.44'	LC	3304	6.6			Minor plagioclase to calcite	Same location as RM-7
RM-18	37°58.86' 107°19.48'	LSC	3627	6.2		5.2 WR		

Field#:	Location:		Elev	δ ¹⁸ O Analyses:			Alteration:	Remarks:
	Lat/Long	Quad		Feldspar	Biotite	Other		
RM-20	37°59.19 107°19.25'	LSC	3542	6.7				
RM-21	37°59.22' 107°18.90'	LSC	3514	6.5	5.4			
RM-29	37°58.66' 107°21.64	LSC	3620	6.4		6.2 WR		
RM-30	37°58.44' 107°21.39'	LSC	3542	6.1	4.8	8.3 WR 7.0 Q		
RM-31	37°58.69' 107°21.16'	LSC	3566	6.2			Spotty calcite in matrix	
RM-32	37°58.75' 107°21.63'	LSC	3572	6.2			Minor plagioclase to clay	80
RM-33	37°58.81' 107°21.71'	LSC	3572	6.6			Plagioclase 30% to calcite and clay	Dump sample
RM-35	37°57.23' 107°19.93'	LSC	3578			3.1 WR	No thin section	
RM-34	37°58.81' 107°21.71'	LSC	3572	6.4			Plagioclase 15% to calcite	Outcrop adjacent to RM-33
RM-36	37°57.42' 107°20.86'	LSC	3889			4.2 WR	Plagioclase and sanidine 25% to calcite and clay	

Field#:	Location:		δ ¹⁸ O Analyses:			Alteration:	Remarks:
	Lat/Long	Quad	Elev	Feldspar	Biotite		
RM-38	37°57.44'	LSC	3847			6.8 WR	
	107°20.73'						
RM-53	37°59.69'	LSC	3490			5.9 WR	Feldspars 80% to clay and quartz, biotite 10% to sericite
	107°20.57'						
6-1-1D	37°59.57'	LSC	3438			7.2 WR	From Ken Hon, no thin section
	107°19.66'						

Red Mountain Quartz Latite, AMOCO Drill Hole

Collar at about 3749 m elevation, 37°58.64' N, 107°20.10 W

Meters below collar:	Elevation: meters	$\delta^{18}O$ Analyses: Whole Rock	Alteration(3):	Remarks:
52.4	3696.6	8.1	Q, A, Py, Al(?)	
106.7	3642.3	6.7	Q, A, Py	
171.6	3577.4	6.6	Q, A, Py	
216.7	3532.3	8.2		No thin section, not intensely altered
283.8	3465.2	4.7	Q, A, Py	
428.5	3320.5	6.1	Q, A, Py	
507.8	3241.2	5.5	Q, A, Py	
551.1	3197.9	5.4	Q, A, Py	
734.3	3014.7	1.7	Q, A, Py, S	
832.1	2916.9	2.7	Q, A, Py, S	
837.0	2912.0	3.4		No thin section, not intensely altered

Vein Quartz

Field#:	Location (1): Lat/Long Quad Elev	$\delta^{18}O$ Analyses (2): Quartz	Associated Minerals (3):	Remarks:
SC-36	37°57.39' RP 3956 107°26.80'	4.7	Py	Oxidized
SC-58	37°57.82' RP 3560 107°27.49'	-2.0		1 cm barren quartz veinlet, same dump as SC-59
SC-59	37°57.82' RP 3560 107°27.49'	2.3	Py, Sp, Cpy	Dump sample
SC-62	37°57.64' RP 3554 107°27.74°	1.6	Py, Gal, Sp, Cpy	
SC-65	37°57.57' RP 3511 107°27.74'	1.3	Gal	Oxidized
SC-66	37°57.66' RP 3920 107°29.51'	0.7		Oxidized
SC-67	37°57.66' RP 3920 107°29.51'	1.8		Oxidized, same location as SC-66
RM-55	37°59.20' LSC 3368 107°21.41'	1.7	Py, Sp, Gal	Dump sample
RM-64	37°59.50' LSC 3048 107°21.69'	-0.1	Py, Sp, Gal	Dump sample
RM-65A	37°59.50' LSC 3048 107°21.69'	-1.4 ± 0.0* (2)	Py, Sp, Gal	Dump sample, same location as RM-64

Field#:	Location: Lat/Long	Quad	Elev	$\delta^{18}O$ Analyses: Quartz	Associated Minerals:	Remarks:
AG-16(I)	38°00.74' 107°21.52'	LC	2780	1.2	Py,Sp,Gal,Cpy	Dump sample, interior of 5 cm vein
AG-16(E)	38°00.74' 107°21.52'	LC	2780	1.3	Py,Sp,Gal,Cpy	Dump sample, exterior of 5 cm vein, same sample as AG-16(I)
SR-1	37°56.33' 107°27.72'	RP	3185	4.6	Py,Tet,Sp,Cpy	Dump sample, Ohio mine
SR-2	37°56.33' 107°27.72'	RP	3185	5.7	Py,Tet,Sp,Cpy	Dump sample, same location as SR-1
SR-13	37°54.58' 107°26.37'	RP	3100	-3.4	CC	Interior of quartz- carbonate-fluorite vein, same vein as SR-16
SR-16	37°54.58' 107°26.37'	RP	3100	-2.5	F	Exterior of quartz- carbonate-fluorite vein, same vein as SR-13
SR-27	37°54.56' 107°25.98'	RP	3054	-3.4	CC,F,Py	
SR-28(I)	37°54.56' 107°25.98'	RP	3054	-4.5	CC,F	Interior of 10 cm vein, same sample as SR-28(E)
SR-28(E)	37°54.56' 107°25.98'	RP	3054	-4.4	CC,F	Exterior of 10 cm vein, same sample as SR-28(I)

Sunshine Peak Tuff Megabreccia

Field#:	Location(1):		$\delta^{18}O$ Analyses(2):		Lithologic Unit(5):	Alteration Phases(3):	Remarks:
	Lat/Long	Quad	Elev	WR			
SC-17	37°56.39'	RP	3728	-0.3	Tspm	C,S,Q	
	107°27.31'						
SC-29	37°56.73'	RP	3408	2.4	Tspm	A,Q	
	107°27.77'						
SC-63	37°57.62'	RP	3536	-1.7	Tspm	A,S,CC,Q	
	107°27.84'						
SC-127	37°55.75'	RP	3402	8.9	Tspm	Fresh	
	107°22.04'						
SC-147	37°57.44'	RP	4133	5.4	Tspm	A,Q	
	107°24.68'						
SC-149	37°57.74'	RP	4093	4.7	Tspm	A	
	107°24.93'						
SC-154	37°57.73'	RP	4066	-0.9	Tspm	CC,A,Q	
	107°25.55'						
SR-9	37°54.79'	RP	3103	-2.5	Tspm	CC,C,Q,E	
	107°24.07'						
SR-24	37°56.36'	RP	3194	-2.1	Tspm	CC,A,Q	
	107°27.80'						
AG-8	37°59.15'	RP	3106	3.6	Tspm	A,Q,Py	
	107°22.76'						

Field#:	Location:		Elev		$\delta^{18}O$ Analyses:		Lithologic Unit:	Alteration Phases:	Remarks:
	Lat/Long	Quad	WR	Other	WR	Other			
HP-3	37°55.75'	RP	3505		-1.7		Tspm	CC, A, Q, C	
	107°28.47'								
RM-61	37°59.08'	LSC	3060		3.4		Tspm	Q, S, A, CC, Py	
	107°21.78'								
RM-63	37°59.23'	LSC	3002		1.6		Tspm	Q, S, A, Py	
	107°21.89'								
HC-44	37°59.75'	RP	3481		3.6		Tspm	A, S, E, Q	
	107°27.10'								
HC-45	37°59.74'	RP	3481		7.5 ± 0.1*		Tspm	Q, Al	Entirely altered
	107°27.11'				(2)				
HC-46	37°59.73'	RP	3481		10.0		Tspm	Q	Entirely silicified
	107°27.11'								
HC-50	37°58.85'	RP	3962		0.0		Tspm	S, CC	
	107°27.14'								
HC-71	37°58.81'	RP	3767		-0.1		Tspm	CC, S	
	107°24.28'								
HC-82	37°58.05'	RP	3868		-0.2		Tspm	A, S, Q	
	107°23.46'								
HC-90	37°58.28'	RP	3399		-1.4		Tspm	A, S, Q, Py	
	107°22.90'								

Field#:	Location:		$\delta^{18}O$ Analyses:		Lithologic Unit:	Alteration Phases:	Remarks:
	Lat/Long	Quad	Elev	WR			
HC-95	37°59.22'	RP	3280	3.2	Tspm	C, CC, A, Q	
	107°28.23'						
HC-97	37°58.96'	RP	3353	-1.9 ± 0.5*	Tspm	A, CC, C, Q, S	
	107°28.34'			(2)			

Other Volcanic and Intrusive Rocks Outside the Caldera

Field#:	Location(1):	$\delta^{18}O$	Analyses(2):	Lithologic	Alteration	Remarks:
	Lat/Long Quad Elev	WR	Other	Unit(5):	Phases(3):	
SC-76	37°57.50' RP 107°29.91'	1.2		Tse	A,Q	Eureka Graben group
SC-101	37°55.96' HP 107°30.88'	-3.1		Tsm	A,C,Q,Py	Eureka Graben group
AG-12	38°00.14' LC 107°21.78'	1.6		Tse	Q,A	Alpine Gulch group
AG-14	38°00.47' LC 107°21.75'	1.1		Tse	CC,A,C,Q,Py	Alpine Gulch group
AG-19	38°01.24' LC 107°21.49'	0.4		Tse	A,S,Q	Alpine Gulch group
RM-10	38°00.37' LC 107°19.40'	5.8		Tcr	Q,A	Alpine Gulch group
RM-50	37°55.76' LSC 107°20.80'	6.2		Tbb	CC,A,Q,S,C	Southeast group
RM-51	37°55.67' LSC 107°20.61'	6.8		Tbb	CC,A,S,Q	Southeast group
RM-64U	37°55.26' LSC 107°20.05'	6.9		Tm	Fresh	Southeast group
HC-7	37°59.13' RP 107°29.01'	-2.4		Tse	A,C,Q	Capitol City group

Field#:	Location:	$\delta^{18}O$ Analyses:			Lithologic Unit:	Alteration Phases:	Remarks:
		Lat/Long	Quad	Elev			
HC-17	38°00.54' UP 107°26.88'	UP	2935	0.4	Tsm	C,A,Q	Capitol City group
HC-18	38°00.71' UP 107°26.30'	UP	2923	-0.7	Tsm	CC,E,C,Q	Capitol City group
HC-22	38°01.00' UP 107°25.65'	UP	2896	2.9	Tsm	S,E,CC,Q	Owl Gulch group
HC-29	38°01.28' UP 107°24.46'	UP	2914	0.2	Tsm	A,C,CC	Owl Gulch group
HC-31	38°01.29' UP 107°23.74'	UP	2829	-0.7	Ts1	CC,Q,S	Owl Gulch group
HC-34	38°01.23' LC 107°22.03'	LC	2792	4.2	Tse		No thin section Alpine Gulch group
HC-37	38°01.11' LC 107°20.65'	LC	2691	3.7	Tsm	CC,Q,S	Alpine Gulch group
HC-38	37°01.11' LC 107°20.65'	LC	2691	2.4	Tsm	CC,Q,S,E	Alpine Gulch group
HC-40	38°01.31' LC 107°19.72'	LC	2661	3.8	Tse	CC,S	Alpine Gulch group
HC-54	38°00.20' UP 107°26.73'	UP	3097	-2.1	Tse	A,C,S,Q	Capitol City group

Field#:	Location:		$\delta^{18}O$ Analyses:		Lithologic Unit:	Alteration Phases:	Remarks:
	Lat/Long	Quad	Elev	WR			
HC-56	38°00.64' 107°25.36'	UP	3319	1.7		Tse	No thin section Owl Gulch group
HC-57	38°00.71' 107°25.57'	UP	3139	3.1		Tse	No thin section Owl Gulch group
HC-94	37°59.40' 107°28.47'	RP	3088	-1.3		Tse	Capitol City group
HC-98	37°59.00' 107°28.72'	RP	3231	1.5		Tse	Capitol City group
HC-99	38°02.95' 107°25.12'	UP	3414		6.0 B 6.9 K 8.6 Q	Tir	Topaz in cavities
HC-100	38°03.00' 107°24.68'	UP	3298	8.2		Tsm	Very weakly altered, Owl Gulch group
HC-101	38°02.57' 107°24.25'	UP	3176	6.3		Tsm	Owl Gulch group
HC-102	38°00.51' 107°27.93'	UP	2975	-1.2		Tmp	Capitol City group
HC-103	38°01.24 107°30.55'	WP	3261		7.3 K 9.2 Q	Tir	

Solfatarically Altered Areas

Field#:	Location(1):	$\delta^{18}O$ Analyses(2):			Lithologic Unit(5):	Alteration Phases(3):	Remarks(3):
		Quartz	WR	Other			
	Lat/Long	Quad	Elev				
<u>Lake City Caldera-Red Mountain</u>							
RM-13	37°58.82' 107°19.64'	LSC	3686	4.9	Tqr	Q,Al,Py	
RM-15	37°58.70' 107°19.99'	LSC	3909	6.6	Tqr	Q,Al,Py	
RM-16	37°58.73' 107°19.95'	LSC	3896	6.1	Tqr	Q,A,Py	
RM-17	37°58.75' 107°19.93'	LSC	3878	11.2	Tqr	Q	
RM-22	37°58.49' 107°19.93'	LSC	3805	7.3	Tqr	Q,Al,Py	
RM-23	37°58.59' 107°19.99'	LSC	3841	5.7	Tqr	Q,Al,Py	
RM-24	37°58.53' 107°19.95'	LSC	3811	7.4	10.9 A	Q,A	
RM-25	37°58.59' 107°19.99'	LSC	3841	9.2	Tqr	Q,E	
RM-26	37°58.41' 107°20.47'	LSC	3842	11.2	Tqr	Q,Py	

Field#:	Location:	δ ¹⁸ O Analyses:				Lithologic Unit:	Alteration Phases:	Remarks:
		Lat/Long	Quad	Elev	Quartz WR			
RM-27	37°58.53' 107°20.32'	LSC	3762	6.8		Tqr	Q,Al,Py	
RM-28	37°58.56' 107°20.28'	LSC	3741	6.3		Tqr	Q,Al,Py	
<u>Carson Camp</u>								
CG-17	37°51.30' 107°21.85'	FM	3743	13.6		Tef	Q,Py	Dump sample, with Ba, A, Sp, Gal
CG-27	37°51.06' 107°22.09'	FM	3706	12.7		Tef	Q,Py	Dump sample, with Ba, A, En, Al
CG-28	37°51.06' 107°22.09'	FM	3706	11.9		Tef	Q,Py,En,Ba	Dump sample, same location as CG-27
CG-30	37°52.06' 107°21.77'	FM	3523	12.2		Tef	Q	Dump sample, with Py, Sp, Gal
<u>Engineer Mountain</u>								
EK-25	37°59.04' 107°35.29'	HP	4026	6.4		Tir	Q	
EK-26	37°58.94' 107°35.23'	HP	4017	1.9		Tir	S,A	
EK-27	37°58.86' 107°35.19'	HP	3987	3.4		Tir	CC,Q,S	

Field#:	Location:	δ ¹⁸ O Analyses:			Lithologic Unit:	Alteration Phases:	Remarks:
		Lat/Long	Quad	Elev			
<u>Red Mountain District-National Belle Mine</u>							
SRM-1	37°54.32' 107°42.26'	I	3380	11.1	Tsb	Q	
SRM-2	37°54.30' 107°42.26'	I	3385	12.0	Tsb	Q	
SRM-3	37°54.29' 107°42.25'	I	3353	12.3	Tsb	Q	
SRM-4	37°54.29' 107°42.25'	I	3353	10.0	Tsb	Q, Py, En	Dump sample
SRM-5	37°54.27' 107°42.25'	I	3322	10.7	Tsb	Q, Py	Dump sample
SRM-6	37°54.27' 107°42.25'	I	3322	11.5	Tsb	Q, Py	Dump sample
<u>Calico Peak</u>							
CP-1	37°42.75' 108°05.30'	R	3532	9.0±0.1* (2)	6.5	Tca	Q, Py, Mo vein- lets in Q, A Quartz sample from Q, Py, Mo veinlet
CP-3	37°42.80' 108°05.41'	R	3566	6.9	Tca	Q, A	
CP-5	37°42.70' 108°05.39'	R	3606	6.4	Tca	Q, A, Py	

Field#:	Location:	δ ¹⁸ O Analyses:			Lithologic Unit:	Alteration Phases:	Remarks:
		Lat/Long	Quad	Elev			
CP-8	37°42.59 108°05.43'	R	3636	6.9	Tca	Q,Al	
CP-10	37°42.62' 108°05.33'	R	3642	6.1	Tca	Q,A,S	
CP-11	37°42.61' 108°05.30'	R	3584	8.7	Tca	Q,Al	Brecciated
CP-14	37°45.52' 108°05.50'	R	3587	4.7	Tca	Q,A	
<u>Summitville District</u>							
SM-2	37°25.17' 106°35.82'	S	3719	15.2	Tsq	Q	Southeastern Tewksbury zone
SM-4	37°25.21' 106°35.90'	S	3746	13.8	Tsq	Q,Al	Dump sample, Aztec glory hole
SM-5	37°25.40' 106°35.85'	S	3642	13.5	Tsq	Q,Al	Copper Hill Knob
SM-6	37°25.40' 106°35.85'	S	3642	13.0	Tsq	Q	Copper Hill Knob
SM-7	37°25.28' 106°35.77'	S	3621	15.5	Tsq	Q,Al,A,Su,Py,En	Dump sample, Science adit
SM-8	37°25.77' 106°35.62'	S	3450	13.4	Tsq	Q,Al,A,Su,Py,En,Ba	Dump sample, Missionary mine

CHAPTER 4

OXYGEN ISOTOPE RELATIONSHIPS IN METEORIC WATERS AND ROCKS
IN THE VICINITY OF THE LAKE CITY CALDERA4.1 Meteoric Water as a Hydrothermal Fluid4.1.1 Oxygen Isotope Relationships in Meteoric-Hydrothermal Systems

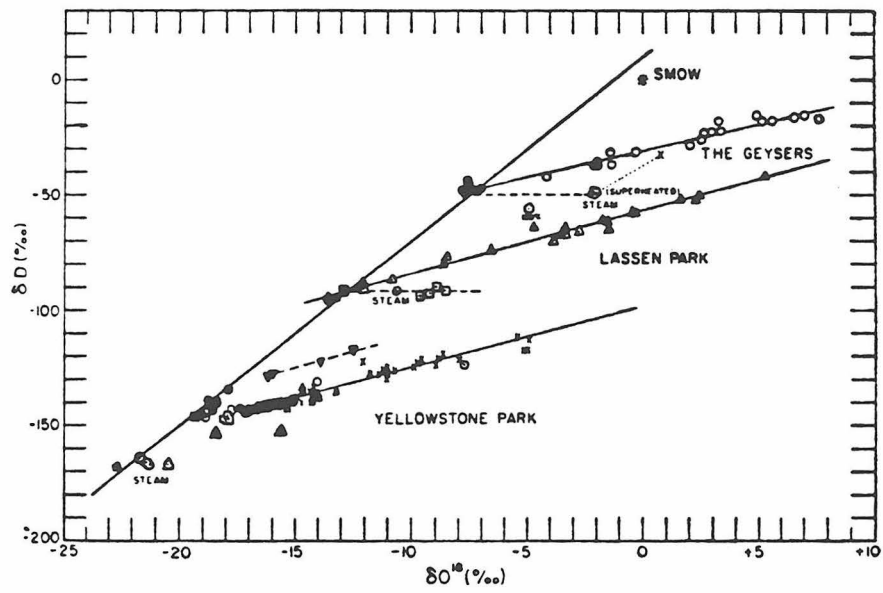
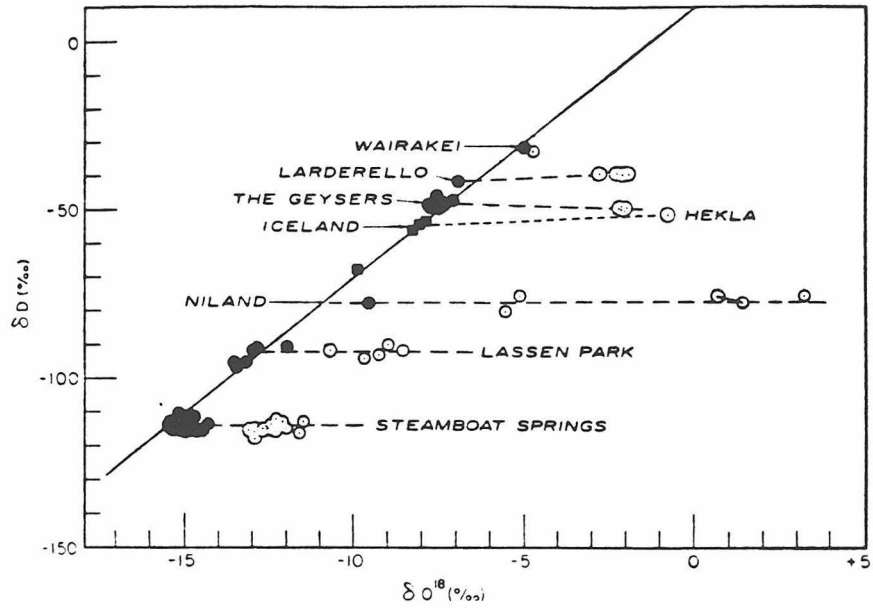
The discovery that fossil hydrothermal systems were very common around epizonal and deeper plutons was made through systematic $^{18}\text{O}/^{16}\text{O}$ and D/H studies which showed that large volumes of rocks centered on such intrusions are depleted in deuterium and ^{18}O . These low- ^{18}O areas include the Tertiary volcanic centers of Skye, Mull, and Ardnamurchan in western Scotland (Taylor, 1968; Taylor and Forester, 1971), the Western Cascade Range, Oregon (Taylor, 1971), the Skaergaard intrusion, Greenland (Taylor and Forester, 1979), the Silverton caldera and associated volcanic and intrusive rocks in the western San Juan Mountains, Colorado (Taylor, 1974a; Jackson et al, 1980; Ringrose et al, 1981), the Boulder Batholith, Montana (Sheppard and Taylor, 1974), the Stony Mountain intrusive complex, western San Juan Mountains, Colorado (Forester and Taylor, 1980), and the Idaho Batholith (Taylor and Magaritz, 1978; Criss and Taylor, 1983).

The rocks affected by these fossil hydrothermal systems were depleted in deuterium and ^{18}O by interaction with large quantities of convectively-driven meteoric-hydrothermal fluids (Taylor, 1977, 1979). Meteoric groundwater is the only substantial reservoir for the low- ^{18}O , low-D, fluids required to produce such depletions. The most intense ^{18}O depletions occur in intrusive rocks emplaced into young, highly

jointed, permeable, volcanic rocks. Propylitization, characterized by the development of chlorite, albite, calcite, and epidote, also generally accompanies the deuterium and ^{18}O effects. Feldspars in these rocks are typically depleted in ^{18}O to a greater extent than other coexisting igneous minerals, and such feldspars commonly exhibit turbidity as a result of the production of fine-grained hydrothermal alteration products. Water/rock ratios, integrated over the lifetime of the hydrothermal systems, are at least 1, and are probably significantly greater, which is not surprising considering the extent of mineralogical alteration in the rocks.

The $\delta^{18}\text{O}$ values of hydrothermal waters in equilibrium with minerals produced in these systems are generally shifted to several per mil higher values, away from the meteoric water line (Fig. 4.1). This results from isotopic exchange between the deeply-circulating, heated meteoric waters and silicate or carbonate country rocks. Such rocks characteristically have initial $\delta^{18}\text{O}$ values greater than +5.5 prior to alteration. As expected, the δD values of the hydrous minerals indicate no significant complementary shift in D/H ratios in the fluid, because of the very low initial hydrogen contents of the rocks as compared with the waters. Such effects are observed in a number of epithermal vein systems, including the ore districts at Tonopah, Goldfield, and Comstock Lode, Nevada (Taylor, 1973), the Bodie district, California (O'Neil et al, 1973), and in the Sunnyside and other vein systems in the western San Juan Mountains, Colorado (Casadevall and Ohmoto, 1977; Taylor, 1974a; Forester and Taylor, 1980). D/H analyses of inclusion fluids from the Bodie district veins, and from veins in a number of similar districts in

Figure 4.1 Oxygen and hydrogen isotopic analyses of fluids discharging in active geothermal areas (from Craig, 1963). The characteristic O-shift in these systems is indicated by the sub-parallel horizontal trajectories in the upper diagram, toward heavier $\delta^{18}\text{O}$ values and away from the meteoric water line. This results from oxygen isotopic exchange between the heated meteoric-hydrothermal fluid and the rocks through which it is flowing. The δD of the water does not show a measurable shift because only small quantities of hydrogen are initially available for exchange in the rocks. Although fluids showing δD shifts do occur, they are typically found only in hot springs that show evidence of boiling (lower diagram). The parallel trajectories with slopes of about 3 that are shown in the lower diagram are the result of kinetic fractionation effects in the boiling fluid (Craig, 1963).



the Great Basin of Nevada, have shown that the δD values of these meteoric-hydrothermal fluids were not measurably shifted away from those of the local meteoric waters (O'Neil et al, 1973; O'Neil and Silberman, 1974).

Oxygen and hydrogen isotopic analyses of meteoric-hydrothermal fluids discharging from hot springs in modern hydrothermal systems also exhibit the characteristic ^{18}O shift (Fig. 4.1) (Craig, 1963). Wairakei, New Zealand, however, shows only a small ^{18}O shift, either because the rocks have been previously altered or because of a high water/rock ratio. Also, geothermal fluids that have experienced boiling (e.g. Geysers, Lassen, Yellowstone) are systematically enriched in deuterium and ^{18}O along linear, parallel, trends having slopes of about 3 (Fig. 4.1). This is due to nonequilibrium evaporation and is a kinetic effect (Craig, 1963).

4.1.2 Isotopic Composition of Tertiary Meteoric Water in the Western San Juan Mountains

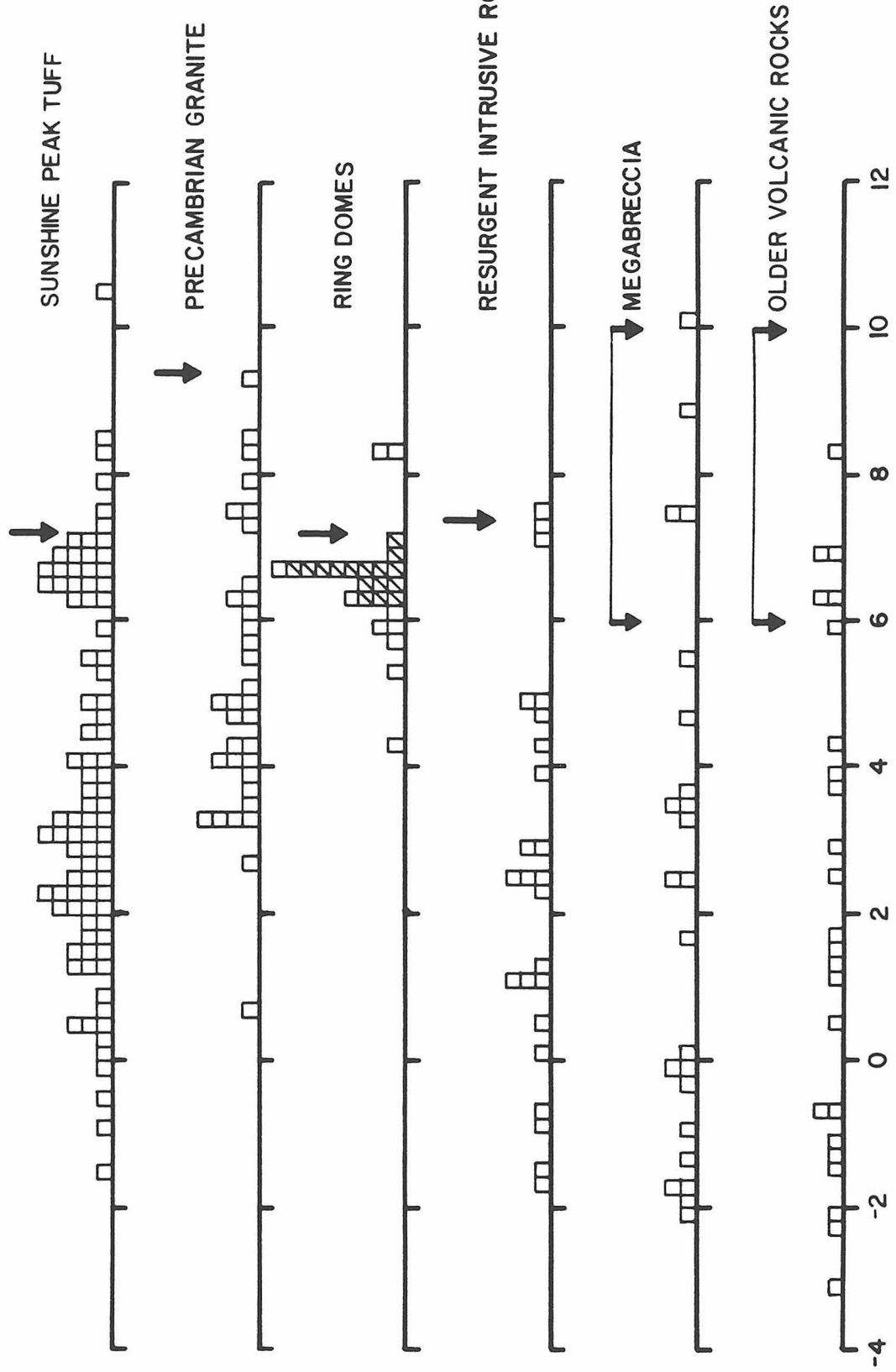
Much of the alteration and mineralization in the western San Juan Mountains took place in mid to late Tertiary time (Lipman et al, 1976). Isotopic analyses of minerals formed in these meteoric-hydrothermal environments can be used to calculate the initial isotopic composition of the meteoric water involved in these systems. Taylor (1974a) noted that ^{18}O -depleted, altered rocks from the Silverton caldera in the western San Juans exhibit uniformly low δD values of -137 to -150 per mil, from which he calculated a δD range of about -100 to -120 per mil for the hydrothermal fluid. Applying the meteoric water equation (Craig,

1961) to this range of δD implies an initial $\delta^{18}O$ of -14 to -16 per mil for pristine meteoric water. Deuterium analyses of hydrous alteration minerals at the Stony Mountain complex suggest a similar initial meteoric water $\delta^{18}O$ of -14 to -15 and δD of about -110 per mil (Forester and Taylor, 1980). Sheppard et al (1969) analyzed a hydrothermal dickite from the Koehler tunnel north of Silverton ($\delta D = -141$ per mil; $\delta^{18}O = -6.2$ per mil) that must have been deposited from a similar type of meteoric-hydrothermal fluid. Deuterium analyses of inclusion fluids from the Sunnyside vein system range from -96 to -135 per mil (Casadevall and Ohmoto, 1977), which imply a $\delta^{18}O$ range of about -13 to -18 per mil, using the meteoric water equation (Craig, 1961). The $\delta^{18}O$ of pristine mid to late Tertiary meteoric water in the western San Juans thus appears to have been in the range -13 to -18 per mil, roughly similar to the present-day values (Friedman et al, 1964). For purposes of subsequent discussion, a value of -15 per mil is considered to be appropriate for these waters.

4.1.3 Meteoric Water as a Fluid Reservoir for the Lake City Caldera Hydrothermal System

Fluids in meteoric-hydrothermal convection systems around epizonal plutons exchange oxygen isotopes with the wall rocks, and these rocks thereby become depleted in ^{18}O . A histogram of whole-rock or feldspar oxygen isotope compositions from lithologic units associated with the Lake City caldera (Fig. 4.2) shows that nearly all the samples analyzed in this study are depleted in ^{18}O relative to the original whole-rock isotopic compositions. The measured ^{18}O depletions in these various lithologic units form the basis for mapping the hydrothermal

Figure 4.2 Histogram showing all whole-rock oxygen isotopic analyses made in this study from outcrop samples in the Lake City caldera area. The data are grouped by lithology. All of the data shown are whole-rock values except those denoted with a slash, which represent feldspar separates from the ring domes. The downward pointing arrows indicate our best estimates of the initial $\delta^{18}\text{O}$ value of that particular rock unit prior to hydrothermal alteration (see text). However, the initial $\delta^{18}\text{O}$ values of the megabreccias and older volcanic rocks are only approximately known ($\delta^{18}\text{O}$ in the range +6 to +10).



$\delta^{18}\text{O}$, whole rock

systems associated with the Lake City caldera (to be discussed in Chapter 7). Within each lithologic unit shown on Figure 4.2, almost all of the samples show varying degrees of depletion in ^{18}O , from 1 to 10 per mil, except for the ring domes. These domes were extruded during the later stages of volcanism, were emplaced at the surface, and are peripheral to the major ^{18}O -depleted zones within the caldera; thus the outcrop samples from the ring domes were in general not subjected to intense hydrothermal activity. However, deeper samples from a 1000-meter drill core (not plotted in Figure 4.2) do show marked ^{18}O depletions, down to $\delta^{18}\text{O} = +1.8$ (see Chapter 5).

Meteoric water and magmatic water represent the only plausible sources for the hydrothermal fluids involved in a rhyolitic caldera-type environment such as Lake City. At temperatures near the granite solidus, waters in equilibrium with isotopically normal magmatic rocks would have about the same oxygen isotopic composition as the rocks themselves, because the mineral-water isotopic fractionations at these high temperatures are generally quite small (Taylor, 1974b, 1979). Thus, magmatic waters in equilibrium with isotopically normal magmatic rocks would have a $\delta^{18}\text{O}$ range of about +5 to +10 per mil (Taylor, 1974b, 1979). At temperatures typical of caldera-type hydrothermal systems (less than about 500°C), such magmatic fluids would shift whole-rock oxygen isotopic compositions to heavier, not lighter, $\delta^{18}\text{O}$ values. Magmatic water thus can be virtually eliminated as a possible major component in the hydrothermal fluids of the Lake City caldera, and a low- ^{18}O fluid of meteoric origin is required to produce the ^{18}O depletions observed in the Lake City caldera rocks. This is consistent with fluid sources defined for

the other hydrothermal systems that have been studied in the the western San Juan Mountains (Sheppard et al, 1969; Taylor, 1974a; Casadevall and Ohmoto, 1977; Forester and Taylor, 1972, 1980; Jackson et al, 1980; Ringrose et al, 1981).

4.2 $\delta^{18}\text{O}$ Variations in the Precambrian Granite of Cataract Gulch

4.2.1 Initial Magmatic Isotopic Composition

Although unaltered specimens of the Precambrian granite of Cataract Gulch are rare, the original rock is readily inferred to have contained about 35 percent tabular, subhedral, perthitic orthoclase; 35 percent anhedral, interstitial quartz; 25 percent tabular, subhedral calcic oligoclase-sodic andesine; and a total of 5 percent subhedral biotite and anhedral muscovite. The granite ranges from hypidiomorphic granular (2 to 8 mm in grain size) to porphyritic, with up to 20 percent tabular, euhedral orthoclase phenocrysts to 1.5 cm in length. Magnetite, apatite, garnet, fluorite, and allanite occur as accessories. The proportions of the primary mineral phases in the granite are approximately uniform throughout the area of exposure. All isotopically analyzed samples of the granite are, however, either depleted in ^{18}O or mineralogically altered, or both. A number of isotopic, petrographic, and location data for the samples of granite analyzed in this study are compiled in Table 4.1.

Analyzed quartz from the Cataract Gulch granite has $\delta^{18}\text{O} = +9.5$ to $+10.5$, and averages $+10.0$. Analyzed orthoclase ranges from $+1.5$ to $+8.6$, and averages $+4.0$. Quartz-orthoclase ^{18}O fractionations range from 1.9 to 8.5 per mil, compared to the "normal" quartz-orthoclase

Table 4.1. Isotopic, petrographic, and location data for samples of the Precambrian granite of Cataract Gulch. Isotopic data are per ml, relative to SMOW. Abbreviations are: OTZ, quartz; ORTH, orthoclase; S, sericite; C, chlorite; A, clays; t, turbid. * for $\delta^{18}O_{\text{Orth}}$ denotes values calculated from the whole-rock values, assuming an ORTH/OTZ ratio of 7:3 in the granite, and using the regression equation: $\delta^{18}O_{\text{Orth}} = 8.75 \delta^{18}O_{\text{OTZ}} - 83$ (see Fig. 4.3).

Sample Number	Distance From Ring Fault (m)	Elevation (m)	Distance From Graben Axis (km)	$\delta^{18}O$ Whole Rock	$\delta^{18}O$ Orthoclase	Δ (OTZ-ORTH)	Average Grain Size (mm)	Orthoclase Megacryst Size (mm)	Biotite % Altered	Biotite Alteration Products	Plagioclase % Altered	
GRAHEN GROUP												
SC-75	100	3908	1.2	3.6	1.1*		2		100	S	20	
SC-90	200	3277	0.4	2.6	-0.3*		4		100	S	15	
SC-95	1150	3322	0.3	4.0	2.3, 1.7*	7.5	4	12	90	C>S	10	
SC-97	1200	3301	0.3	0.7	-2.9*		5	10	90	C, A	7.5	
HP-1	700	3551	2.2	3.9	4.4, 1.6*	5.7	5		95	C>S	20	
LC-17	2100	3377	0.0	3.3	1.9, 0.7*	8.5	2.5		95	C>S	20	
5.5 to 9.0 km GROUP												
LOW-ELEVATION SUB-GROUP												
SC-86	500	2886	8.7	4.6	4.0, 2.5*	5.9	5	10	90	S=C	10	
SC-102	2100	3200	7.9	4.9	2.8*		3	10	50	C>S	10	
SC-105	3300	3392	8.6	6.4	4.8*		4	12	5	C	t	
SC-112	3400	3560	6.3	7.5	6.3*		2	8	10	C	t	
SC-117	700	3277	6.6	5.6	3.7*		4		40	S	10	
SR-17	100	3082	6.2	4.1	5.5, 1.8*	4.5	4	14	100	S=C	20	
SR-19	600	3033	7.1	4.1	5.0, 1.8*	4.5	2	6	80	C>S	10	
SR-21	450	2986	7.5	4.4	2.1*		3	7	Thin Section Not Available			
SR-23	450	2950	7.9	2.3	-0.8*		3		50	C	t	
HP-9	4700	3359	6.0	4.700	4.3*		2	15	90	C>S	15	
HP-11	4200	3267	5.4	5.5	4.3, 3.8*	5.9	4		90	C+S	10	
HP-13	2800	3188	5.5	4.3	2.0*		5		90	C>S	t	
HP-15	1000	3011	6.3	4.3	2.0*		3		10	C>S	t	
HP-16	1100	2969	7.0	4.9	2.8*		7		100	S	t	
HIGH-ELEVATION SUB-GROUP												
SC-103	2750	3280	8.3	3.4	0.7*		6	15	80	C>S	10	
SC-106	3550	3444	8.8	5.0	2.9*		4	15	70	C	10	
SC-107	4100	3520	9.0	6.2	4.6*		8	12	Thin Section Not Available			
SC-109	2400	4023	6.9	6.2	4.6*		8	12	90	C	t	
SC-110	2900	3889	6.7	7.3	6.0*		1		10	C	<t	
SC-111	3400	3719	6.5	7.8	6.7*		2	8	Thin Section Not Available			
SC-114	450	3609	5.9	3.2	0.5*		3		90	C>S	t	
SC-116	500	3475	6.2	4.9	2.8*		4	10	60	C>S	t	
HP-5	6600	3493	6.5	3.3	1.5, 0.7*	8.2	3	8	100	S	10	
HP-6	5700	3429	6.3	4.7	2.5*		3	14	90	S>>C	10	
>9.0 km GROUP												
SC-84	50	2917	9.5	7.9	6.9*		3		100	S	10	
SC-85	200	2874	9.3	5.8	4.0*		3		40	S=C	t	
CG-6	1700	2880	12.1	8.5	7.7*		3		100	S, A	100	
CG-11	1750	3072	11.6	9.2	8.6, 9.0*	1.9	4		25	S	t	
CG-33	450	2862	10.3	8.4	7.5*		5		Fresh		t	
CG-35	1100	2847	11.3	8.2	7.3*		5		70	C	t	
CG-36	1700	2832	12.1	7.4	6.2*		4		90	S>>A	t	

fractionation of about 1.5 per mil in unaltered plutonic rocks (Taylor and Epstein, 1962b; Taylor, 1968; Blattner and Bird, 1974; Criss and Taylor, 1983). Isotopic analyses of quartz-orthoclase pairs from the Cataract Gulch granite exhibit systematics (Fig. 4.3) similar to those observed by Criss and Taylor (1983) in the meteoric-hydrothermally altered rocks of the Idaho Batholith (Fig. 4.4). The points in Figure 4.3 that lie below the primary magmatic fractionation line all have anomalous quartz-orthoclase fractionations, clearly indicative of exchange with hot, low- ^{18}O fluids. Compared to the orthoclase, the quartz exchanged very slowly with the meteoric-hydrothermal fluids.

Only one sample of the granite, CG-11, exhibits a very small quartz-orthoclase fractionation (1.9 per mil), compatible with little or no hydrothermal exchange. The whole rock $\delta^{18}\text{O}$ analysis of this sample, +9.2, is within the range of normal granitic plutonic rocks (Taylor, 1968). Note, however, that the biotite, which makes up less than 5 volume percent of this sample, is about 25 percent altered to sericite, indicating at least some hydrothermal alteration. Based upon the quartz $\delta^{18}\text{O}$ value of +10.5, The initial $\delta^{18}\text{O}$ of this rock was probably slightly greater than +9.2, perhaps as high as +9.4 to +9.8 per mil.

4.2.2 Mineral-Mineral Isotopic Relationships

Thirty-five whole-rock samples of the Precambrian granite of Cataract Gulch were analyzed for $\delta^{18}\text{O}$, representing most known outcrops outside the southern and western margins of the Lake City caldera. The results range from +0.7 to +9.2 (Fig. 4.2). A number of mineral sepa-

Figure 4.3 Oxygen isotopic analyses of quartz-orthoclase pairs from the Precambrian granite of Cataract Gulch. Also shown is the diagonal, 45° quartz-orthoclase fractionation line at 2 per mil; values of 1 to 2 per mil are typical of unaltered plutonic rocks, and all known samples with $\Delta^{18}\text{O}_{\text{O-F}} > 2.0$ have undergone subsolidus isotopic exchange (Taylor, 1968). The $\delta^{18}\text{O}$ values in the Cataract Gulch granite all indicate marked isotopic disequilibrium, except CG-11, the sample that plots on the unaltered plutonic curve; similar relationships were found for mineral pairs from the Idaho batholith by Criss and Taylor (1983) (see Fig. 4.4). Seven of the nine samples of Cataract Gulch granite define a (dashed) ^{18}O exchange line with a very steep slope ($\delta^{18}\text{O}_{\text{KSPAR}} = 8.75\delta^{18}\text{O}_{\text{OTZ}} - 83$). Two samples plot slightly off this dashed line, SR-19 and LC-17; their slightly anomalous $\delta^{18}\text{O}$ values are readily explained by grain-size effects (Section 4.2.5), because relative to the other samples on the main trend line, SR-19 is a fine-grained sample and LC-17 is a very coarse-grained sample. The quartz in these samples thus would be, respectively, much less resistant and much more resistant to hydrothermal ^{18}O exchange than the average granite sample.

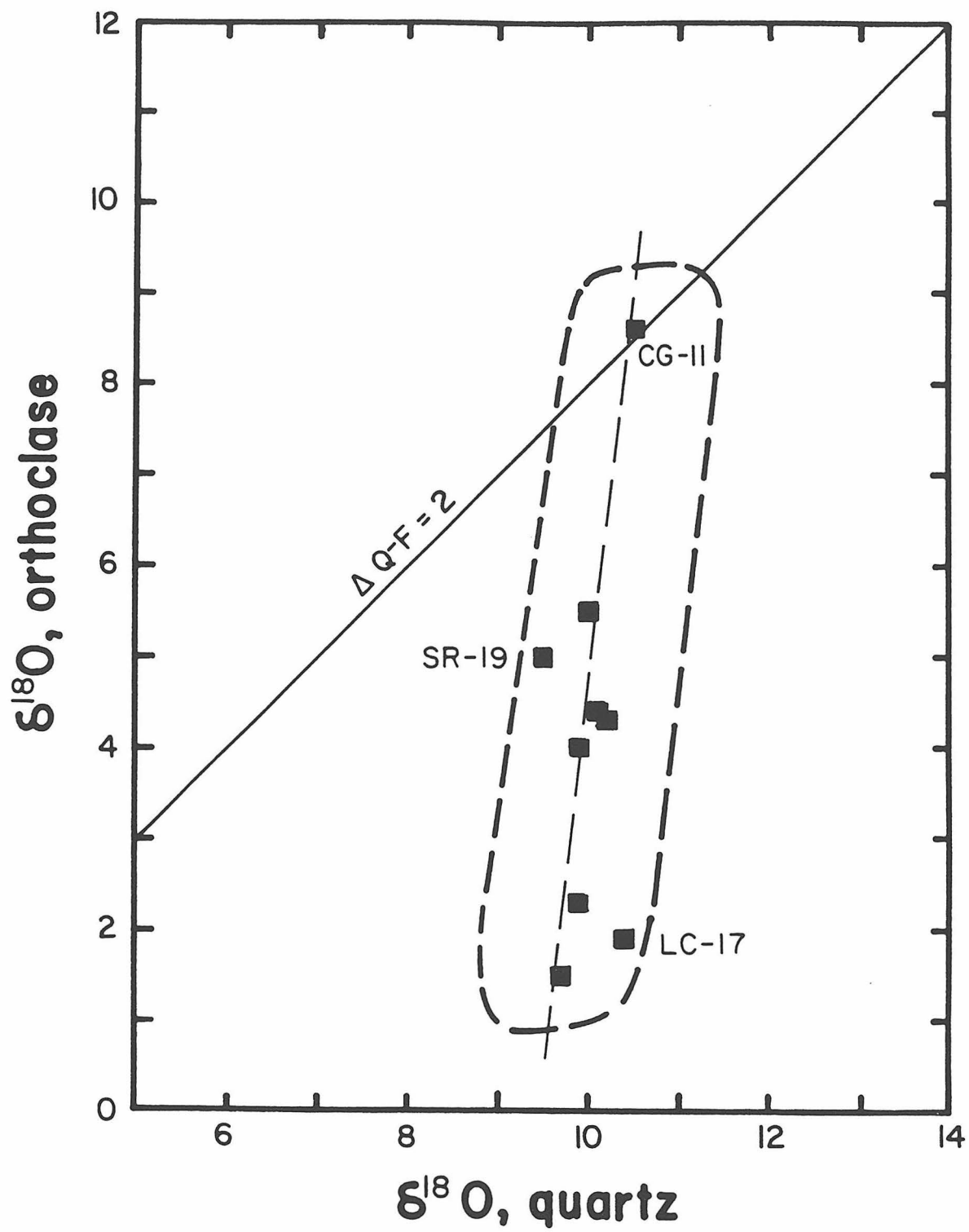
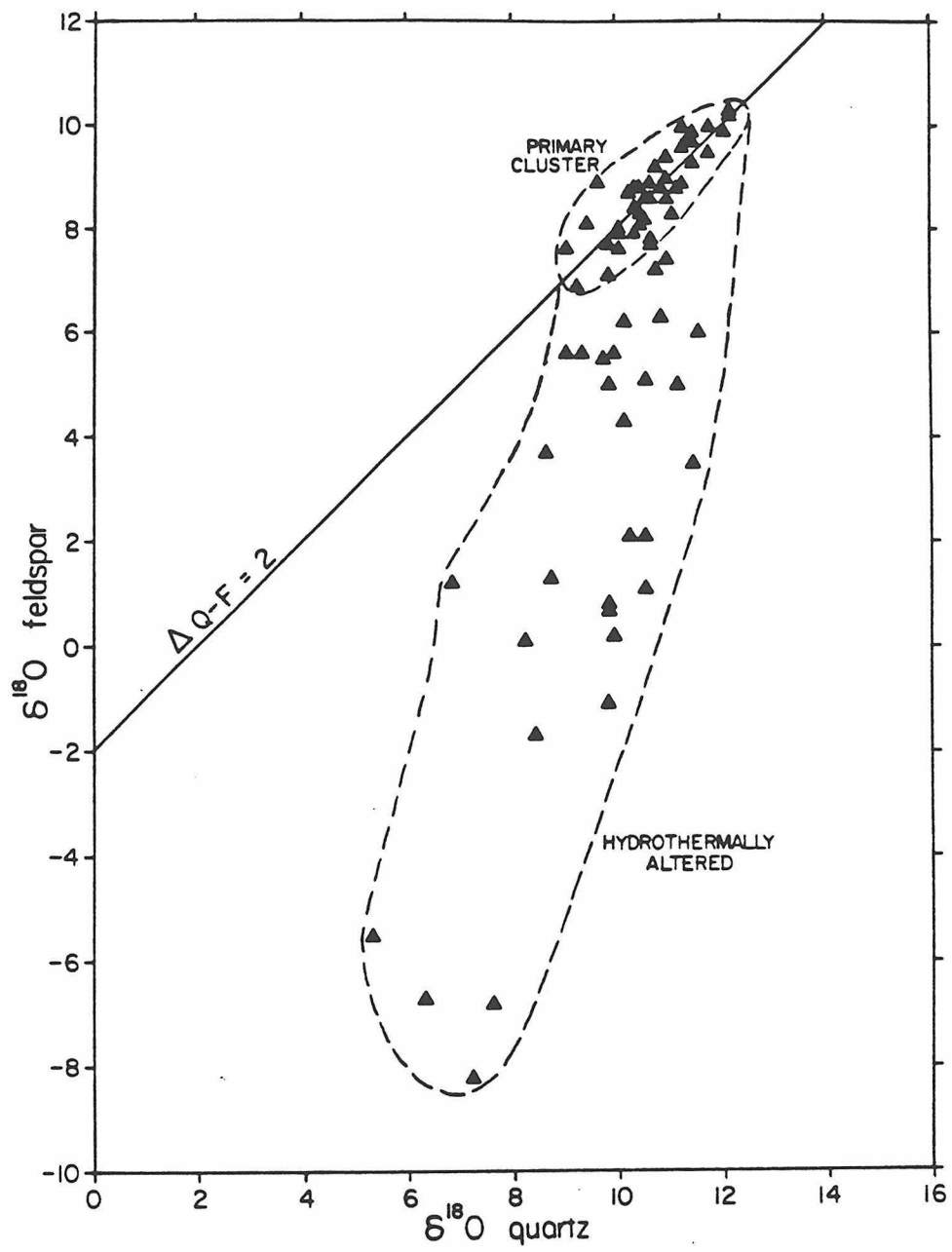


Figure 4.4 Oxygen isotopic analyses of quartz-feldspar pairs from the Idaho batholith (from Criss and Taylor, 1983). Data from the Precambrian granite of Cataract Gulch define a nearly identical relationship (Fig. 4.3), although the Idaho batholith data show a more pronounced decrease in quartz $\delta^{18}\text{O}$ values with decreasing feldspar values (because of the shallower level and lower temperature of hydrothermal activity at Lake City?).



rates from these samples were also analyzed; the quartz-orthoclase fractionations are discussed above (Fig. 4.3). Although the orthoclase was thoroughly isotopically altered as a result of exchange with the meteoric-hydrothermal fluids, it is mineralogically unaltered in nearly all the samples. Minor turbidity is only rarely developed in the orthoclase. In contrast, the plagioclase in all samples displays variable degrees of turbidity, due to the development of alteration products (minute flakes of clay?) throughout the grains. Although the alteration minerals were not positively identified, they display a high birefringence similar to that of sericite.

Biotite exhibits the widest variation in mineralogic alteration, and ranges from fresh to totally altered. Common biotite alteration products are sericite, chlorite, and very fine-grained opaque minerals. Quartz and clay are less common alteration products. Sericite and chlorite occur in variable proportions replacing the biotite along cleavage planes and along rims.

Isotopic data for the mineral separates are plotted in Figure 4.5 versus the whole-rock $\delta^{18}\text{O}$ values of the respective samples. All mineral phases except quartz, and perhaps muscovite, exhibit depletions in ^{18}O , the magnitudes of which correlate positively with the magnitudes of the whole-rock ^{18}O depletions.

The isotopic fractionations among the coexisting phases can be used to evaluate the relative isotopic exchange rates between the minerals and the hydrothermal fluids, assuming the appropriate fractionation factors are known. Equilibrium fractionation curves utilized in the following discussion are shown graphically in Figure 4.6. Mineral-

Figure 4.5 Oxygen isotopic compositions of minerals from the Precambrian granite of Cataract Gulch, plotted as a function of whole-rock $\delta^{18}\text{O}$ of the granite. Quartz and muscovite show only minor ^{18}O variations, but the $\delta^{18}\text{O}$ of orthoclase decreases systematically with whole-rock $\delta^{18}\text{O}$ value. Thus the $\delta^{18}\text{O}$ variations in the rocks are mostly attributable to effects in the alkali feldspar, which is the most abundant mineral in the rock. Limited data for plagioclase and chlorite (an alteration product of the biotite) indicate ^{18}O effects similar to that observed for the orthoclase.

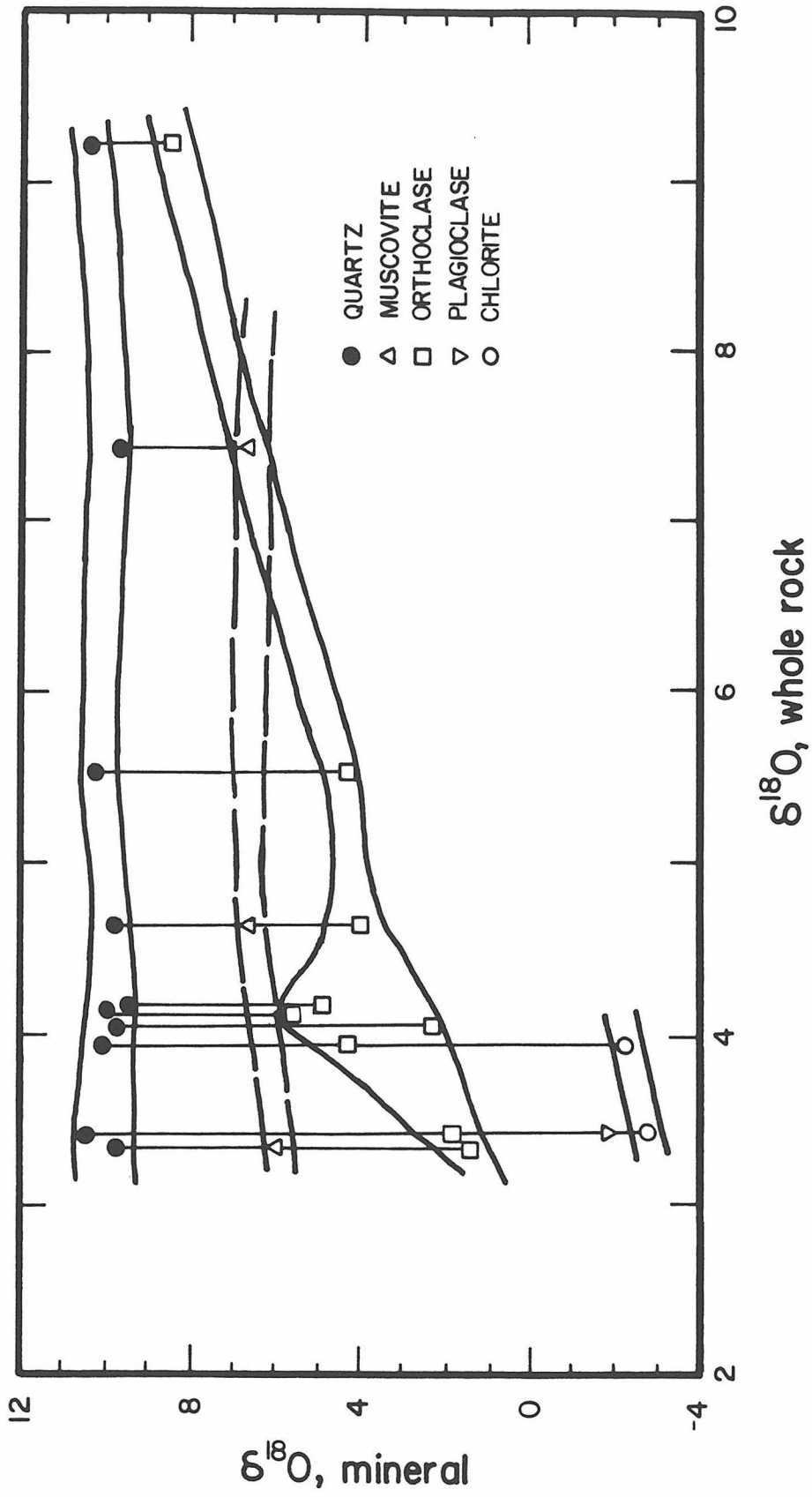
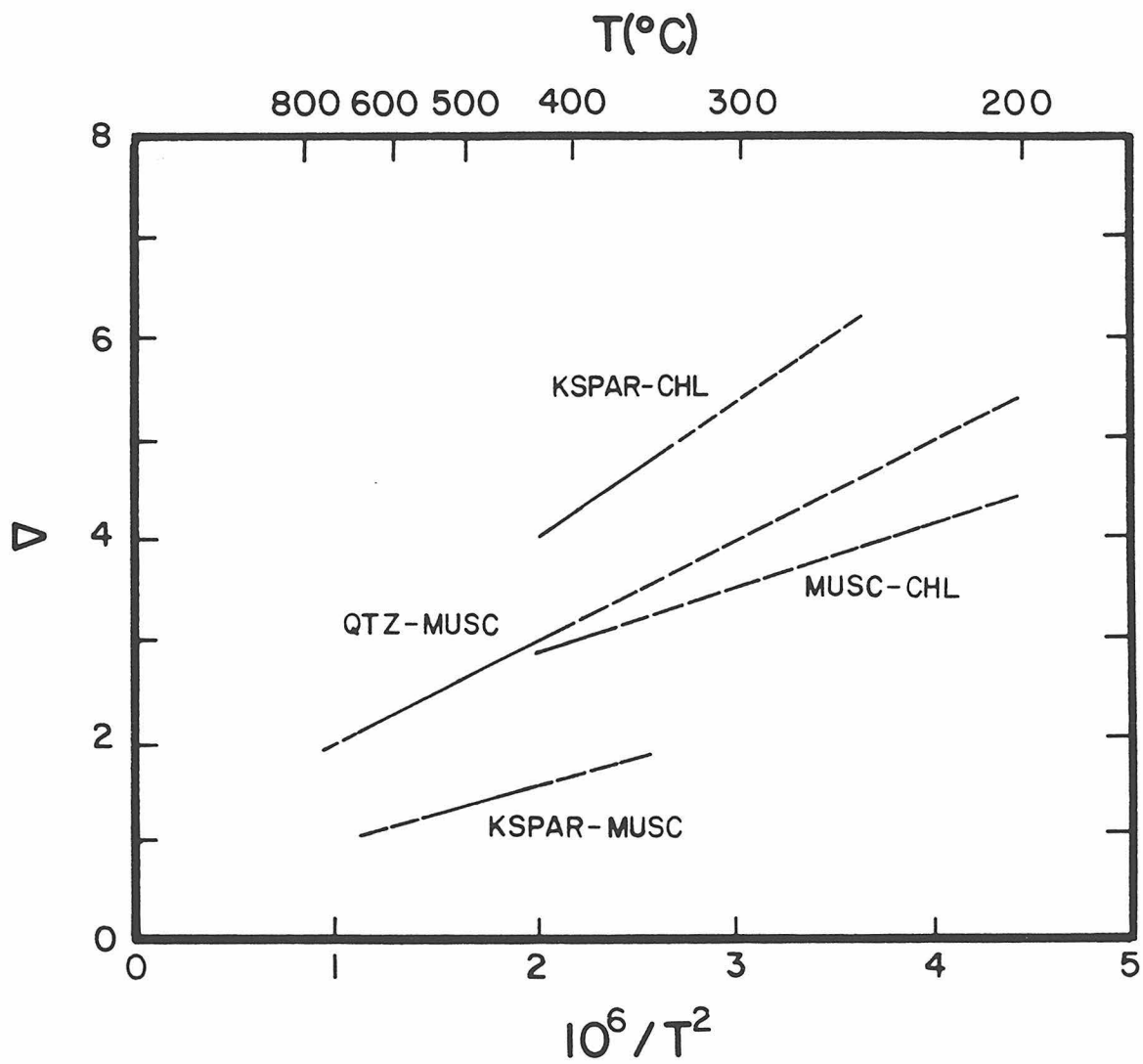


Figure 4.6 Mineral-mineral fractionation factors used in discussion of the mineral isotopic analyses. Data sources are listed in the text. Abbreviations used in the figure are: KSPAR, alkali feldspar; CHL, chlorite; MUSC, muscovite; QTZ, quartz.



mineral fractionation curves were derived by combining the appropriate mineral-water fractionation curves, first assuming that the fractionation, Δ , between phases A and B can be approximated by:

$$\Delta_{A-B} = \delta_A - \delta_B \approx 10^3 \ln \alpha,$$

where α is the ratio of $^{18}\text{O}/^{16}\text{O}$ in mineral A to that in mineral B. The experimentally determined fractionation curves of O'Neil and Taylor (1969) for muscovite-water, of O'Neil and Taylor (1967) for alkali feldspar-water, and of Clayton et al (1972) for quartz-water were used, together with the empirically determined chlorite-water curve of Wenner and Taylor (1971). Calculated equilibrium fractionation temperatures for mineral pairs from the Precambrian granite are shown in Table 4.2.

Muscovite-orthoclase fractionations of 2.6 and 4.5 per mil are observed in samples SC-86 and HP-5, respectively. These data clearly represent isotopic disequilibrium between these phases, as the alkali feldspar should have a higher $^{18}\text{O}/^{16}\text{O}$ ratio than that of the muscovite (Fig. 4.6). Also, unlike the orthoclase, the muscovite does not show a progressive ^{18}O depletion correlative with the whole-rock ^{18}O depletion (Fig. 4.5). It appears that the muscovite exchanged oxygen with the hydrothermal fluids very slowly, as did quartz (Fig. 4.3). However, the muscovite did not perfectly preserve its initial magmatic $\delta^{18}\text{O}$ value throughout the duration of the hydrothermal event, because the quartz-muscovite fractionations of 3.3, 3.7, and 2.9 per mil measured for samples SC-86, HP-5, and CG-36, respectively, yield equilibrium fractionation temperatures of about 335° to 450°C (Fig. 4.6), clearly lower

Table 4.2 Oxygen isotopic fractionation temperatures for mineral pairs from the Precambrian granite of Cataract Gulch (assuming isotopic equilibrium). Minerals are abbreviated as: QTZ, quartz; MUSC, muscovite; ORTH, orthoclase; CHL, chlorite. Fractionation curves used for these calculations are plotted on Figure 4.6.

Field #	Δ QTZ-MUSC	Δ ORTH-CHL	$T_{\text{QTZ-MUSC}}$	$T_{\text{ORTH-CHL}}$
SC-86	3.3		385° C	
HP-1		6.6		230° C
HP-5	3.7		335° C	
CG-36	2.9		450° C	
LC-17		4.7		355° C

than granite solidus temperatures. This conceivably could be in part due to subsolidus oxygen isotopic exchange during cooling of the granite in Precambrian time, as has been demonstrated for a number of intrusive rocks by Taylor (1968). However, Taylor's (1968) compilation of oxygen isotopic fractionation temperatures for typical intrusive rocks shows that such exchange does not appreciably occur below about 500°C, so these muscovites have apparently exchanged with the mid-Tertiary hydrothermal fluids (at a rate faster than quartz and slower than orthoclase).

Chloritized biotites from two samples, HP-1 and LC-17, exhibit $\delta^{18}\text{O}$ values of -2.2 and -2.8, respectively. The biotite in both these rocks is 90 to 95 percent altered to chlorite, with less than 10 percent sericite. Because of the very fine-grained nature of the chlorite-biotite-sericite intergrowth, pure chlorite cannot be separated from the samples. However, based on numerous isotopic and chemical analyses of altered biotites from the Idaho Batholith, the oxygen isotopic fractionation between igneous biotite and hydrothermal chlorite was shown to be on the order of 5 to 10 per mil for meteoric-hydrothermal alteration at 150° to 400°C (Criss and Taylor, 1983). Also, Figure 4.6 shows that, at equilibrium, muscovite (sericite) is always richer in ^{18}O than coexisting chlorite over this temperature range. Thus, contamination of the chlorite separate by biotite and sericite produces higher $\delta^{18}\text{O}$ values than we would observe in pure chlorite, implying that the measured orthoclase-chlorite equilibrium fractionations are, if anything, too small in HP-1 and LC-17. The temperatures of 230° and 355°C would therefore be maximum alteration temperatures, if equilibrium was attained and if the calibration curves utilized in Figure 4.6 are correct.

From sulfur isotope fractionation data among pyrite, chalcopyrite, and galena, Krasowski (1976) estimates the temperature of vein formation at the Bon Homme mine, within the Eureka graben, to be about 250° to 335°C. Sample LC-17, which yields an orthoclase-chlorite temperature of 355°C, was collected from the dump at this mine.

Assuming an alteration temperature of 300°C, which is consistent with both the sulfur and oxygen isotopic data, water in isotopic equilibrium with the ¹⁸O-depleted orthoclase in LC-17 would have a $\delta^{18}\text{O} = -3.6$ using the alkali feldspar-water fractionation curve of O'Neil and Taylor (1967). At 250° and 350°C, this water would have $\delta^{18}\text{O} = -5.4$ and -2.2 , respectively. The hydrothermal fluids, therefore, clearly experienced an ¹⁸O shift from the pristine meteoric $\delta^{18}\text{O}$ value of -15 , as a result of prior interaction with rocks elsewhere in the hydrothermal system.

4.2.3 Water/Rock Ratios and Mineral Alteration

Ideally, if equilibrium is attained in a closed hydrothermal system, it is possible to calculate the total amount of water in the system using the mass balance of oxygen isotopes distributed between the fluid and the rock. This is a function of the temperature of the interaction, and the initial isotopic compositions of the fluid (δi_w) and rock (δi_r). For a closed system that undergoes cyclic convection with no loss of H₂O, the conservation relation can be written (Taylor, 1977):

$$W/R_{\text{CLOSED}} = \frac{\delta f_r - \delta i_r}{\delta i_w - (\delta f_r - \Delta)}$$

where W/R is the ratio of water to rock in the system on the basis of the ratio of atomic oxygen, δf_r is the isotopic composition of the altered rock, and Δ is the fractionation factor between the water and the rock at the temperature of interest. For an open system, where each packet of fluid equilibrates with the rock and then leaves the system forever, this equation becomes, by integration (Taylor, 1977):

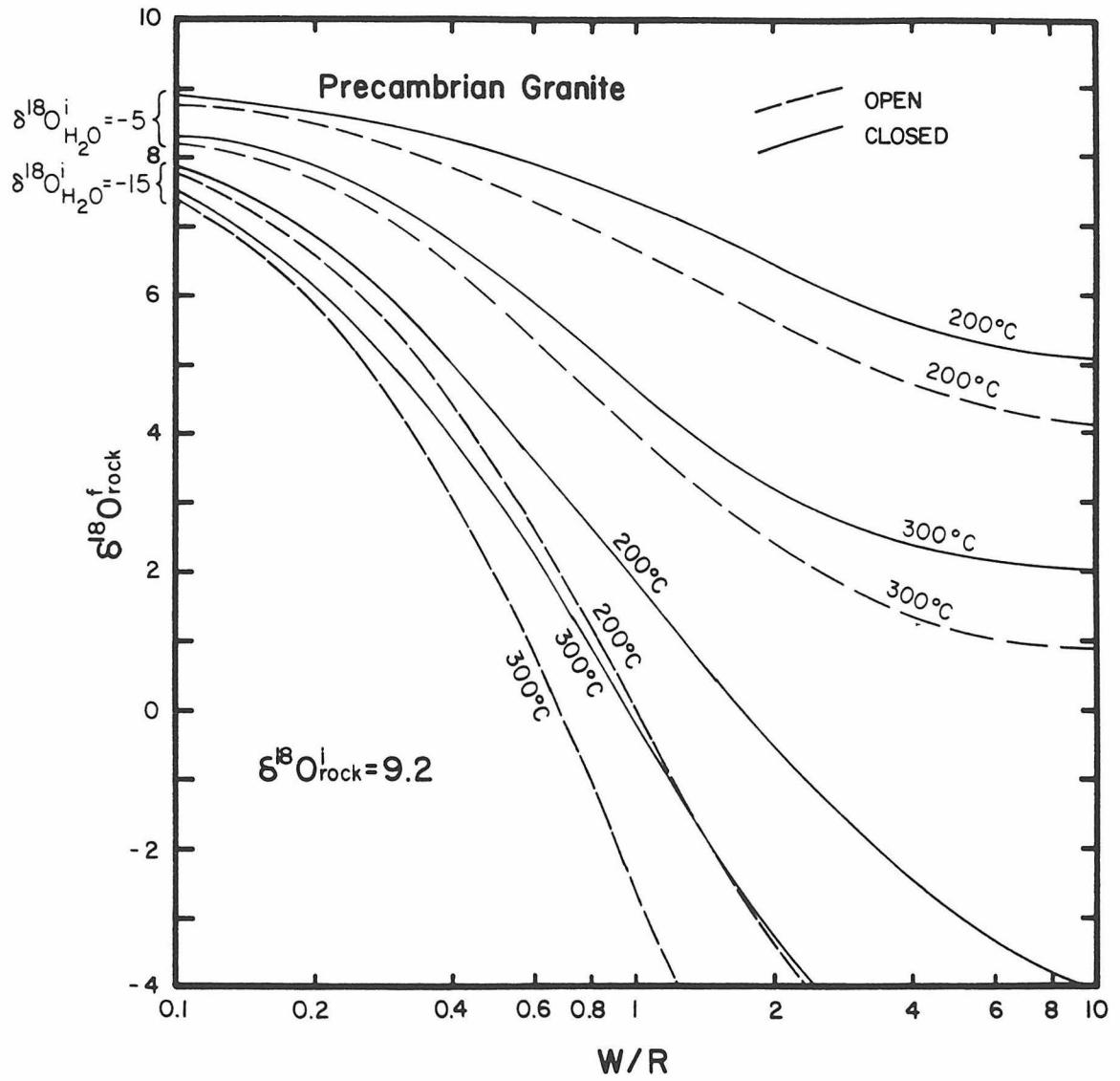
$$W/R_{\text{OPEN}} = \ln \left[\frac{\delta i_w + \Delta - \delta i_r}{\delta i_w - (\delta f_r - \Delta)} \right]$$

or:

$$W/R_{\text{OPEN}} = \ln (W/R_{\text{CLOSED}} + 1).$$

Plots of W/R versus δf_r for the Precambrian granite at temperatures of 200° and 300°C are shown in Figure 4.7. δi_r was taken as 9.2 per mil, the isotopic analysis of that sample of the granite which gave a magmatic quartz-orthoclase fractionation, CG-11. Two values of δi_w were used: -15 per mil, pristine mid-Tertiary western San Juan meteoric water; and -5 per mil, representative of a plausible ^{18}O shifted meteoric-hydrothermal fluid, as described in the previous section. Δ was assumed to be that of the alkali feldspar-water fractionation for the appropriate temperature (O'Neil and Taylor, 1967). If equilibrium is not achieved between the rock and water, the ^{18}O depletion in the rock would not be as large as indicated. The W/R plots are thus minimum estimates of the actual W/R ratios in the hydrothermal system.

Figure 4.7 Idealized $\delta^{18}\text{O}$ versus W/R ratio plot for the Precambrian granite of Cataract Gulch. Initial water $\delta^{18}\text{O}$ values of -15 and -5 per mil, and an initial rock composition of +9.2 per mil, were used. Rock-water fractionation is assumed to be that of orthoclase-water (O'Neil and Taylor, 1967).



The most pertinent aspects displayed in Figure 4.7 are: (1) For a given initial δ_{i_w} , higher temperature water/rock interaction produces significantly lower final rock $\delta^{18}O$ values than does a lower temperature interaction. (2) At a given temperature, higher W/R ratios produce lower whole-rock $\delta^{18}O$ values. (3) Obviously, higher δ_{i_w} also produces higher δ_{f_r} , holding temperature and W/R constant. The progression of ^{18}O depletions in whole-rock and feldspar data from right to left in Figure 4.5 must therefore result from a systematically increasing temperature of hydrothermal alteration, a systematically increasing W/R ratio, or influx of a different water with a lower δ_{i_w} (or some combination of all three effects).

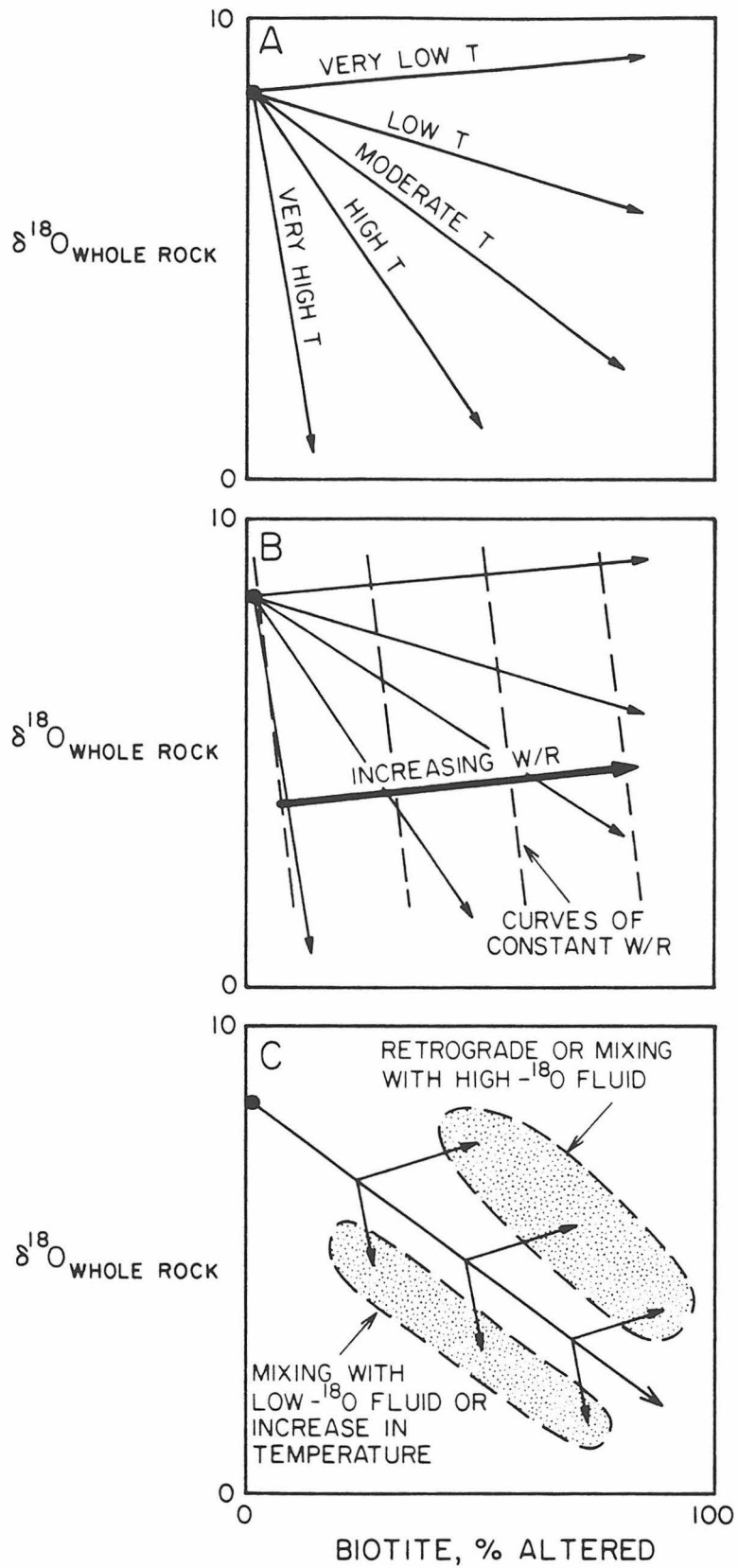
The $\delta^{18}O$ value of an altered rock reflects the cumulative effects of water/rock interaction integrated over the lifetime of a hydrothermal system. Another measure of water/rock interaction, the degree of mineral alteration of the biotite (to chlorite or sericite), has been estimated from petrographic examination of thin sections of the Cataract Gulch granite (Table 4.1). The degree of mineralogical alteration of the biotite in the granite is a function of temperature, water/rock ratio, and chemical composition of the hydrothermal fluids, and is thus a somewhat more complex indication of the water/rock interaction than the whole-rock $\delta^{18}O$ value, which is a function just of temperature and water/rock ratio (assuming that the initial $\delta^{18}O$ value of the fluid remains constant).

Using the two parameters of whole-rock $\delta^{18}O$ and volume percent of alteration products in the biotite, a plot analogous to Figure 4.7 can be constructed. The interpretation of such a diagram is aided by first

considering several theoretical $\delta^{18}\text{O}$ -mineral alteration trajectories (Fig. 4.8abc). For a constant initial fluid $\delta^{18}\text{O}$, isothermal water/rock interaction would define a single trajectory on Figure 4.8a away from the initial whole-rock composition. Several such hypothetical isothermal trajectories are shown on Figure 4.8a; note that the actual shapes of the trajectories are not known, and they are shown as straight lines only for purposes of discussion. (If mineralogical alteration of the biotite occurs much faster than ^{18}O exchange with the whole-rock, the curves with negative slopes would all be convex upward, and vice versa). The water-mineral $^{18}\text{O}/^{16}\text{O}$ fractionations at low temperatures are very large, whereas at high temperatures the fractionations are very small. Therefore, although biotite can be altered to chlorite over a wide range of temperatures, the $\delta^{18}\text{O}$ of the whole-rock will change along drastically different paths that depend strongly upon the temperature. Slopes of the lines would thus decrease from shallow positive slopes for very low temperature alteration to very steep negative slopes for extremely high temperature alteration (at high temperatures the ^{18}O changes would still be very dramatic, even though biotite would be stable and there might be little or no chloritic alteration products).

The water/rock ratio increases to the right along each isothermal trajectory in Figure 4.8a. However, because the kinetics of mineral-water reactions are enhanced by increasing temperature, contours of equal water/rock ratios will not be vertical lines on such a diagram. At temperatures below the stability of biotite, higher-temperature interaction would convert more biotite to chlorite than would lower-

Figure 4.8 Hypothetical whole-rock $\delta^{18}\text{O}$ variations as a function of the degree of mineralogic alteration of biotite in the Cataract Gulch granite. (a) Generalized isothermal alteration trajectories are shown for several alteration temperatures. The actual shapes of the curves are unknown, but the systematic change in slope from very low to very high temperature alteration is correct. Time increases in the direction of the arrows. (b) Constant W/R ratio curves superimposed on the isothermal trajectories of Figure 4.8a. Along a single isothermal trajectory, the W/R ratio must increase monotonically with the amount of biotite that has been destroyed as long as the temperature and chemical composition of the fluid lie outside the stability field of biotite. The higher the temperature of alteration, the lower is the W/R ratio required to produce a given degree of mineralogical alteration of the biotite. Thus the constant W/R curves will not be vertical, but they will have steeper slopes than the isothermal trajectories. (c) A generalized two-stage hydrothermal event is shown in which fluids that have evolved to variable degrees in an isothermal environment are (1) uniformly heated so that they evolve along parallel trajectories (downward arrows) to lower $\delta^{18}\text{O}$ values or (2) they are uniformly cooled so that they evolve along near-horizontal trajectories toward greater degrees of chloritic alteration of the biotite (upward arrows). The locus of rocks altered in these two hypothetical environments are shown as oval-shaped fields in Figure 4.8c. Note that process (1) might equally well represent mixing with either lower- ^{18}O waters or hotter waters, whereas process (2) could also represent mixing with either higher- ^{18}O waters or cooler waters.

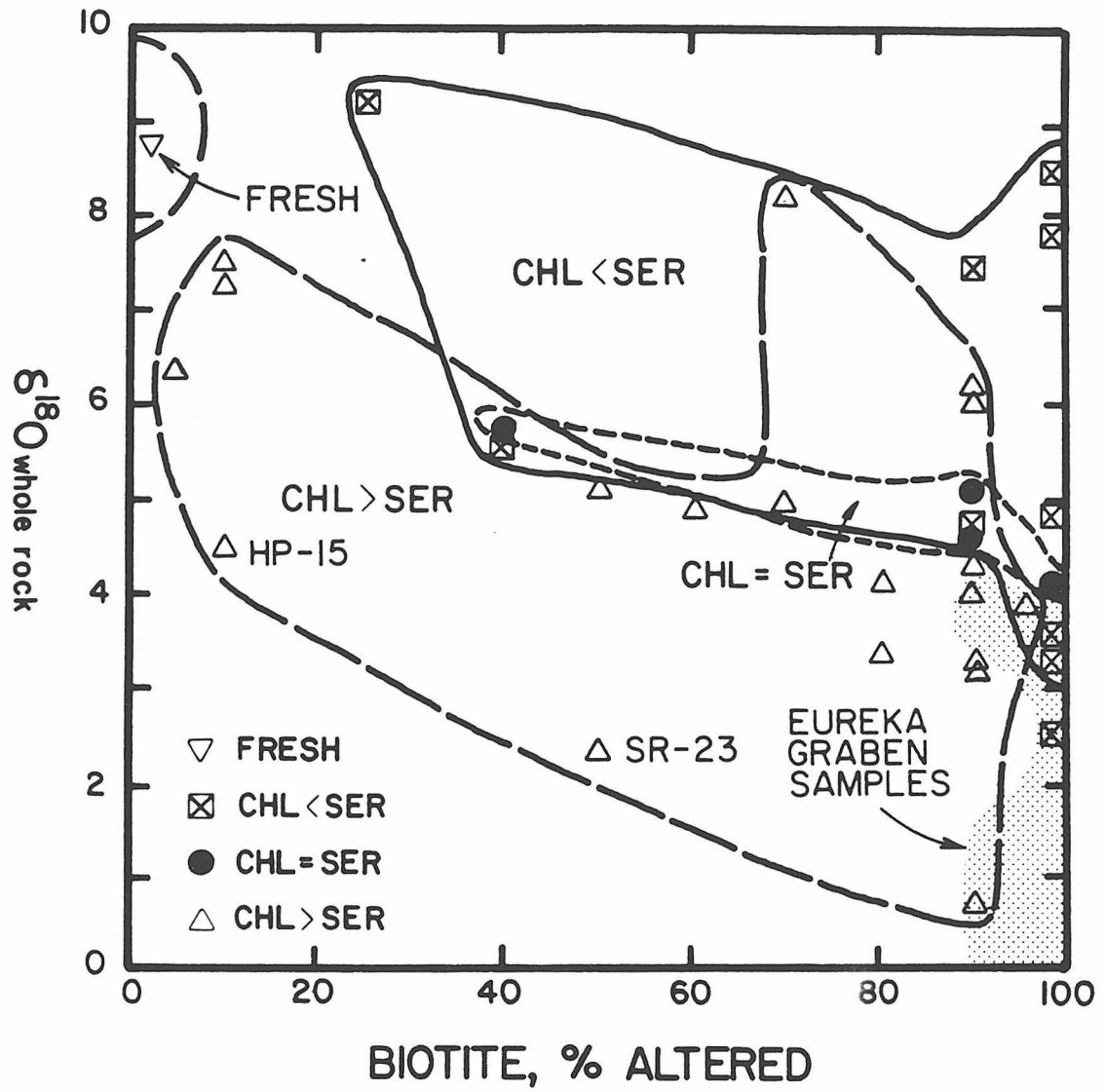


temperature interaction at the same water/rock ratio. A series of hypothetical W/R ratio curves are shown in Figure 4.8b; the lines of equal water/rock ratio would have steep negative slopes, steeper than the isothermal trajectories (they would also probably be curved lines, possibly convex upward).

Finally, we can examine more complex scenarios involving mixing of fluids or changes in the temperature of interaction in a hydrothermal system with time. The paths of fluids that evolved along a single, isothermal trajectory on Figure 4.8c could abruptly move downward along steeper, secondary trajectories to lower $\delta^{18}O$ values if the alteration temperature was instantaneously increased, or they could move to the right along near-horizontal trajectories if retrograde alteration occurred. However, retrograde phenomena of that type are probably uncommon in most hydrothermal systems because of self-sealing by mineral deposition in veins and fractures.

Figure 4.9 plots the whole-rock $\delta^{18}O$ values in the granite against the percent of mineralogical alteration products in the biotite. Thus, Figure 4.9 can in a sense be considered as a plot of δf_r versus W/R ratio, analogous to Figures 4.7 and 4.8. The approximate chlorite/sericite ratio in the altered biotite is also indicated on Figure 4.9. A comparison of Figures 4.7, 4.8 and 4.9 suggests that the granite was altered over a wide range of W/R ratios in two distinct regimes, one at relatively low temperature that produced a dominantly sericitic alteration of biotite, and one at higher temperature that produced a dominantly chloritic alteration. Or, conversely, the sericitic biotite alteration could have been produced by more evolved (more ^{18}O -shifted)

Figure 4.9 Whole rock isotopic compositions of the Precambrian granite of Cataract Gulch as a function of the degree of mineralogic alteration of the biotite. This plot is analogous to the W/R plot shown in Figure 4.7, as well as to the various models shown in Figure 4.8. The percent of altered biotite in each sample is a complex function of temperature, water/rock ratio, and chemical composition of the hydrothermal fluids. Assuming a constant initial $\delta^{18}\text{O}$ of the fluid, the whole-rock $\delta^{18}\text{O}$ value is a somewhat simpler function just of temperature and water/rock ratio. A plausible interpretation of the relationships shown above (i.e. that the chlorite-rich samples have lower $\delta^{18}\text{O}$ than the sericite-rich samples) is that the samples with chlorite-rich biotite alteration products underwent higher temperature water-rock interaction than samples in which sericite is predominant over chlorite. Within each grouping, the decrease in $\delta^{18}\text{O}$ with increase in degree of mineralogic alteration of the biotite is best ascribed to increasing water/rock ratio. CHL = chlorite; SER = sericite.



fluids than those that produced the chloritic biotite alteration. The Eureka graben samples obviously indicate the highest water/rock ratios (and highest temperatures?) of the samples shown in Figure 4.9, compatible with the geologic evidence outlined below.

4.2.4 Effects of Fractures and Faults on Fluid Flow

The northwestern-most exposure of Precambrian granite in the Lake City area is extensively faulted and fractured in the area of the Eureka graben. Starting in the northeast, where the graben is truncated by the Lake City ring fault, structures in the graben are vein-filled and locally mineralized all the way to the termination of the graben in the Silverton caldera. Here, the structures host the economic mineralization at the Sunnyside mine (Casadevall and Ohmoto, 1977). Thus it is obvious, simply from the field evidence that the structures exerted a strong influence on the hydrothermal fluid flow patterns. This is backed up strongly by the geographic patterns of $\delta^{18}O$ and mineralogic alteration in the Cataract Gulch granite, as shown on Figures 4.10, 4.11, and 4.12. For example, note that the lowest- ^{18}O rock analyzed in this entire study ($\delta^{18}O = -3.1$) is an altered volcanic rock from the Eureka graben (Plate 1, Fig. 4.20).

Mineralization in the Sunnyside mine occurred between 13.0 and 16.6 m.y. ago (Casadevall and Ohmoto, 1977). Several other ore-forming magmatic and hydrothermal events in the western San Juans occurred between 10 and 22.5 m.y. ago (Lipman et al, 1976). The hydrothermal systems in the Lake City caldera were initiated shortly after collapse of this caldera about 23 m.y. ago. Thus, the alteration in the Eureka graben is

Figure 4.10 Map of the Precambrian granite showing sample locations, structure, and composite mineralogic alteration effects. The extensive fracturing in the northwestern granite exposure is the Eureka graben, which is truncated by the Lake City caldera ring fault. Note that intense alteration of the plagioclase is confined to the Eureka graben, and that the least-altered granite samples are located farthest from the Eureka graben and/or farthest from the caldera ring fault.

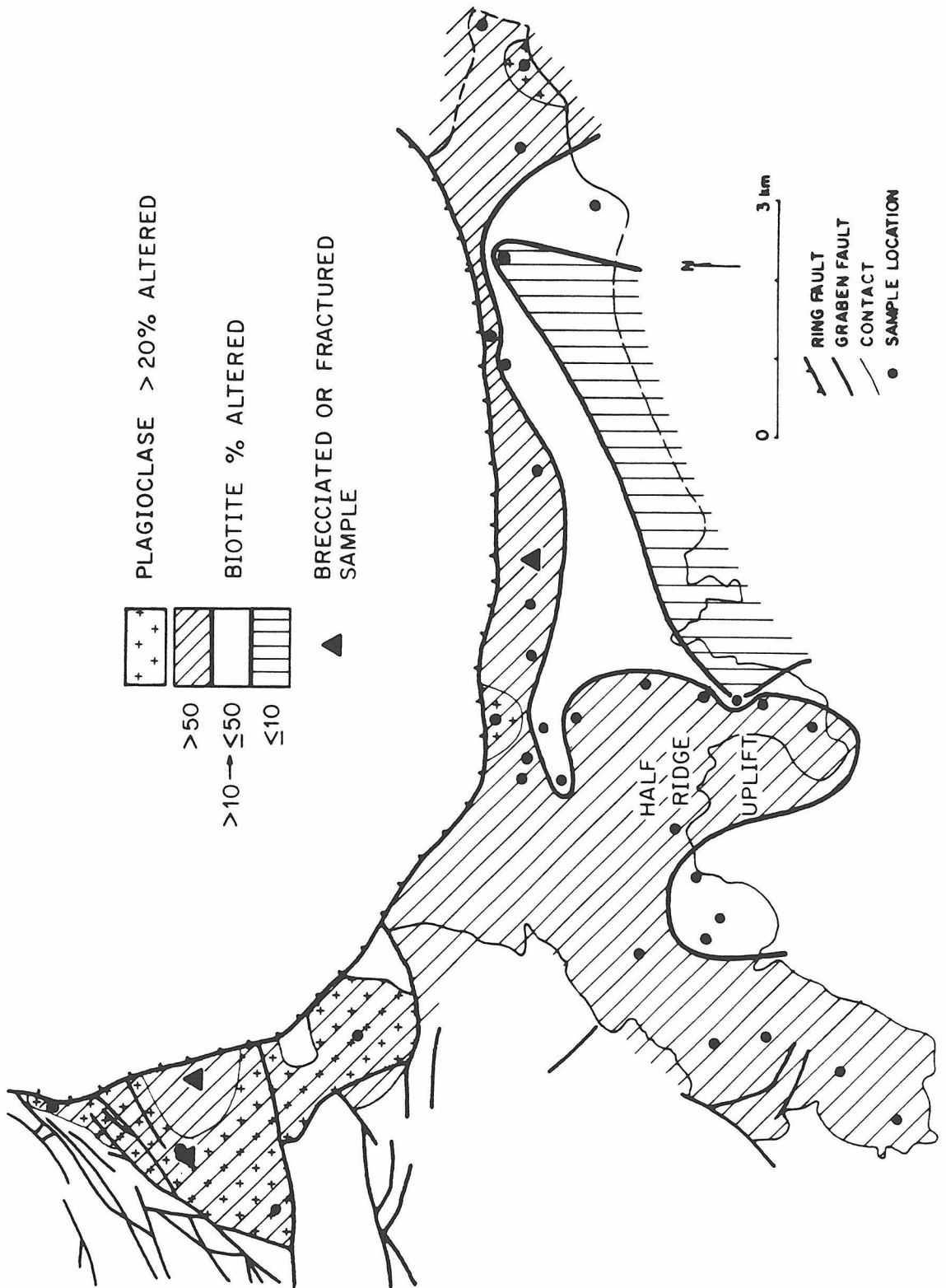


Figure 4.11 Map of the Precambrian granite showing contours of whole-rock $\delta^{18}O$ values. As distance from the Eureka graben increases, the whole-rock $\delta^{18}O$ values in the granite also increase. The $\delta^{18}O$ contours in areas away from the graben are basically sub-parallel to the graben axis, although they also seem to be influenced slightly by proximity to the Lake City caldera ring fault. The graben was a major recharge channel for the Lake City meteoric-hydrothermal system and also was a conduit for flow in younger systems centered to the west of the Lake City caldera. The contour pattern reflects (1) the dominant influence that the highly-fractured area of the graben and the less highly-fractured caldera ring fault have exerted over fluid flow in these systems; and (2) a decrease in temperature of alteration of the granite eastward away from the graben axis (see text).

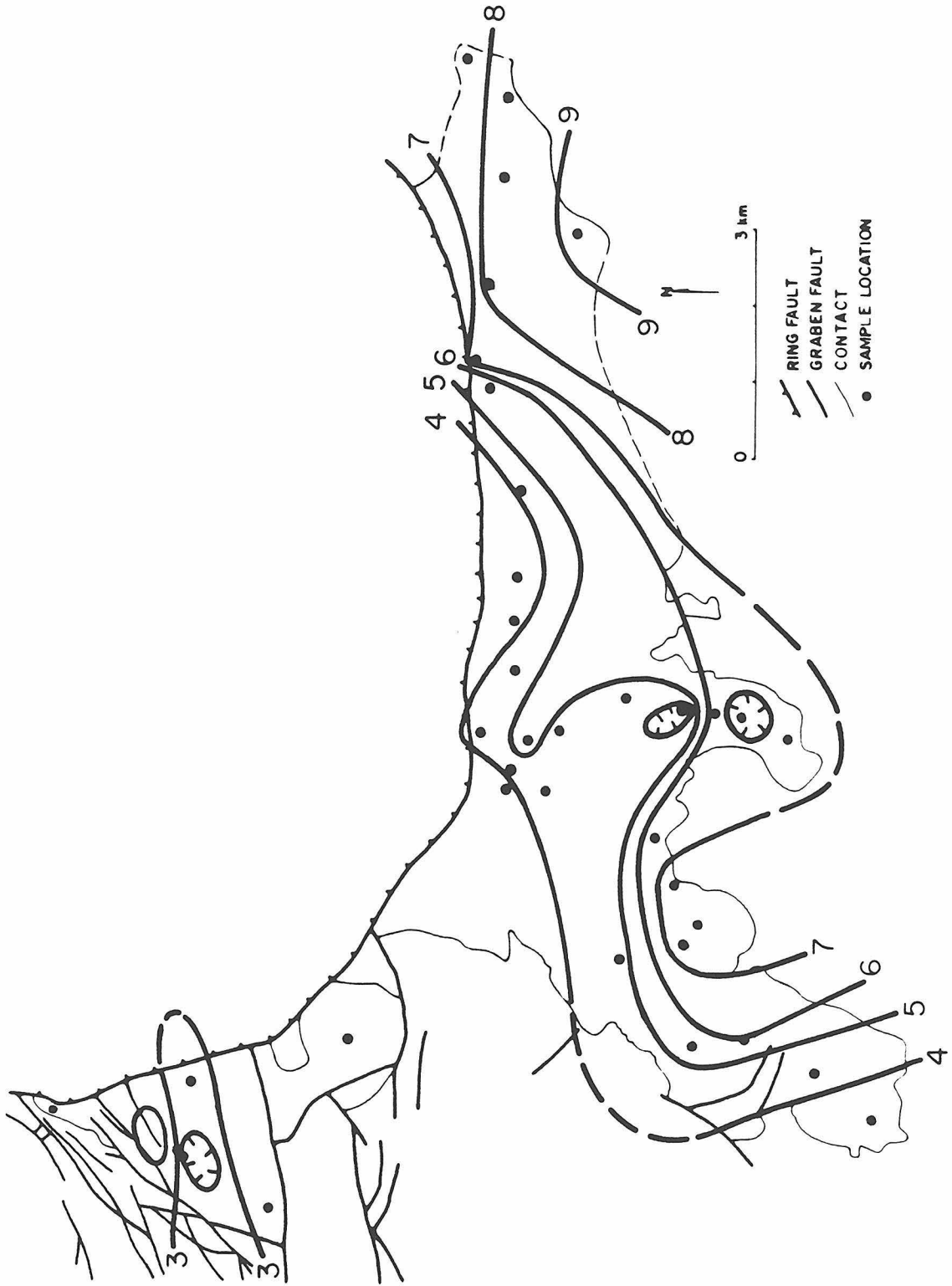
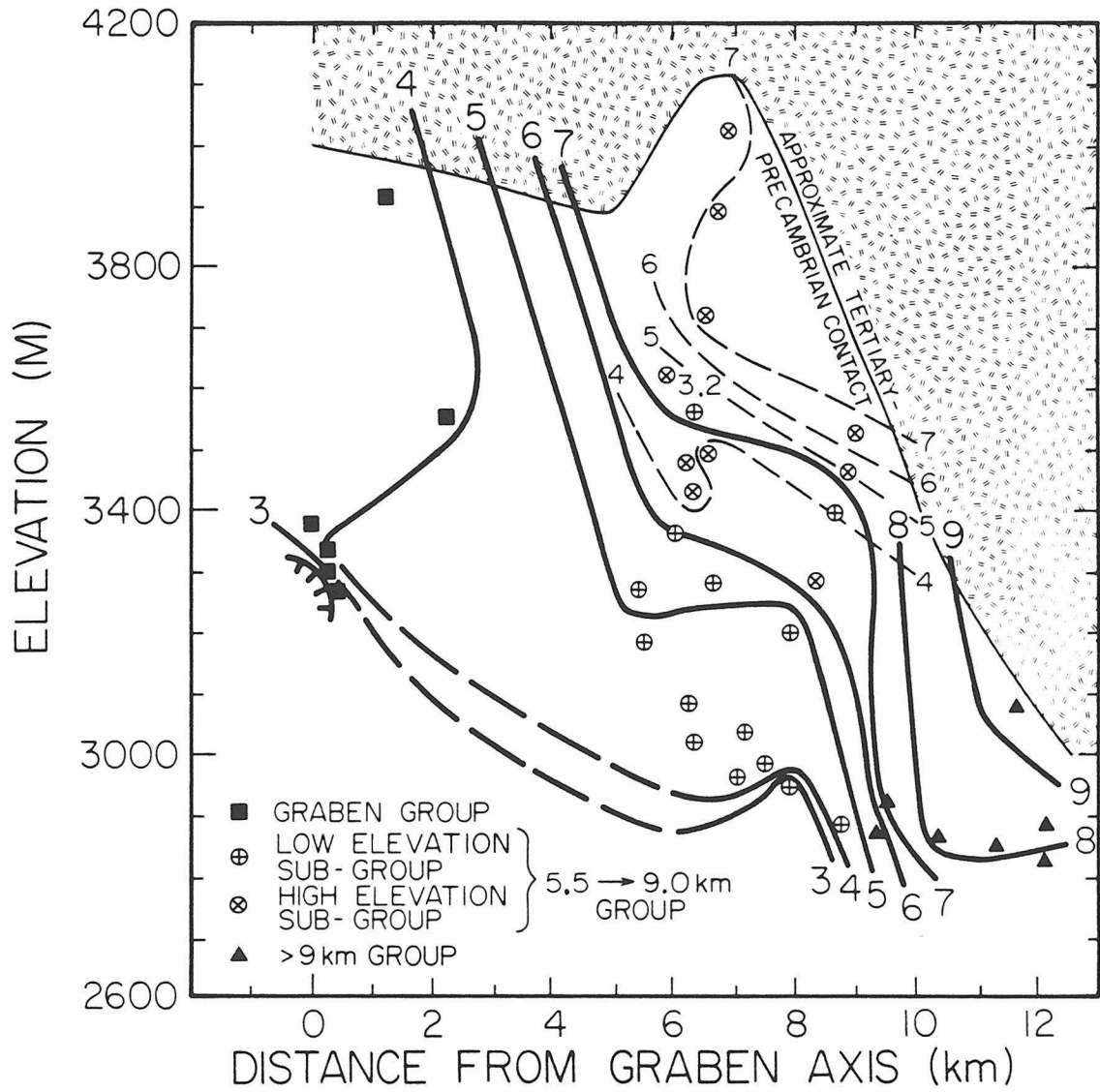


Figure 4.12 Variations in whole-rock $\delta^{18}\text{O}$ values of the Precambrian granite as a function of sample elevation and distance from the graben axis. Distance from the graben was measured on lines projected perpendicularly from the sample locations to a line trending N47°E (parallel to graben structures in the Lake City area) drawn through location LC-17 (centrally located within the graben). The major control on $\delta^{18}\text{O}$ is clearly the distance from the graben axis. However, elevation also exerts some control on the $\delta^{18}\text{O}$ values (e.g. see Fig. 4.15). The heavy contours indicate the variations in whole-rock $\delta^{18}\text{O}$ for all granite samples except those from the high-elevation sub-group of the 5.5 to 9.0 km group (defined in Figure 4.14). The $\delta^{18}\text{O}$ variation in the high-elevation sub-group (excluding a single sample associated with fluorite veins, $\delta^{18}\text{O} = +3.2$) is shown separately by light dashed contours; these contours are all offset to higher elevations than the equivalent $\delta^{18}\text{O}$ contours for the rest of the samples. This offset also appears in the position of the Precambrian-Tertiary unconformity, suggesting that the high-elevation subgroup was uplifted relative to nearby samples (see text).



the cumulative, integrated effect of at least two hydrothermal events (Lake City age and Sunnyside age), and probably several others as well.

$\delta^{18}\text{O}$ values and alteration mineralogy within the Precambrian granite vary systematically with distance away from the highly altered Eureka graben, and, to a lesser extent, with proximity to the Lake City ring fault. A number of parameters that vary spatially relative to these two major structural features are shown in Figures 4.10 and 4.11, and are summarized below: (1) Whole-rock $\delta^{18}\text{O}$ values of the granite increase gradationally away from the area of the graben, indicating that the granite in the graben interacted with a larger volume of meteoric-hydrothermal fluid than did the rocks away from the graben (Fig. 4.11). Also, Figure 4.12 shows that the whole-rock $\delta^{18}\text{O}$ values are more strongly dependent on the distance from the axis of the graben at which the sample was collected than on the sample elevation. (2) The degree of alteration of the plagioclase is consistently greater than 20 percent for samples collected within the graben, and less than 20 percent for most samples collected outside the graben (Fig. 4.10). (3) The degree of mineralogic alteration of the biotite is greatest in samples collected closer to and within the graben than for samples away from the graben (Fig. 4.10). Samples collected in the vicinity of the Lake City ring fault also contain highly altered biotite. (4) Hand specimens of granite that are fractured or brecciated tend to be the most ^{18}O -depleted granite samples in a given area (Figs. 4.10 and 4.11).

Three samples of granite collected in the vicinity of the Lake City caldera ring fault show major discrepancies between the calculated $\delta^{18}\text{O}$ of the feldspar (Table 4.1) and the measured $\delta^{18}\text{O}$ of the orthoclase

(SR-17, SR-19, and HP-1). In each of these 3 examples, the calculated $\delta^{18}\text{O}$ of the feldspar is 3 to 4 per mil lower in ^{18}O than the measured value. This might in part be due to the fact that the measured values are all on hand-picked orthoclase, whereas the calculated value includes a considerable amount of plagioclase that is 10 to 20 percent altered to sericite and clays. However, none of the other analyzed samples more distant from the ring fault exhibit such a discrepancy (SC-86, SC-95, LC-17, HP-5, HP-11, and CG-11), and most of these also contain altered plagioclase. The orthoclase megacrysts in SR-17 and SR-19 have a grain size of 6 to 14 mm, and were apparently more resistant to ^{18}O exchange than the associated finer-grained feldspars in the groundmass; however, there is no other evidence that the grain size of the feldspar played a significant role in the hydrothermal $\delta^{18}\text{O}$ patterns in the granite (see Section 4.2.5).

The above data imply a lack of $^{18}\text{O}/^{16}\text{O}$ homogeneity in the feldspars of these three samples. The most plausible explanation of this isotopic heterogeneity is that these samples underwent a two-stage (or multiple-stage) hydrothermal history that imprinted a complex ^{18}O pattern in the rocks. For example, one possible scenario could involve periodic or renewed displacement on the ring-fault during the period of hydrothermal activity. Such displacements could drastically affect the local temperature gradients and/or flow regimes.

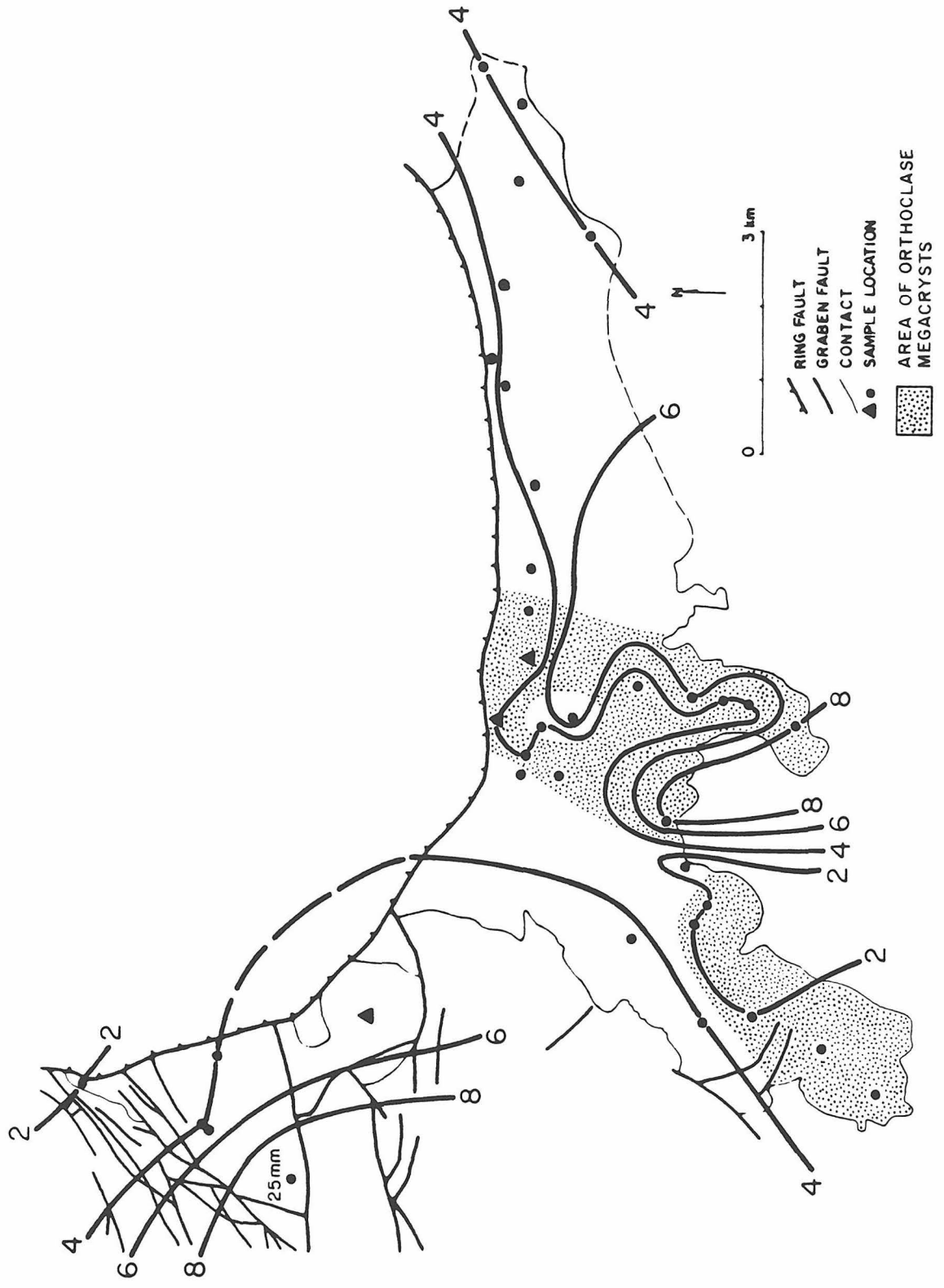
The samples collected from within the Eureka graben are coded in Figure 4.9. By analogy to Figure 4.7, and considering the patterns in Figures 4.10 and 4.11, it is clear that the graben fractures controlled meteoric-hydrothermal fluid flow within the granite, such that the

granite now exposed in the graben experienced much higher W/R ratios and/or higher temperatures than granite away from the graben. In part, this may be because of the more pronounced uplift that has occurred on the southwestern edge of the caldera; thus erosion has been more extensive here, so we are looking into a deeper part of the hydrothermal system (see Fig. 4.17 and Chapter 6). In any event, there is little doubt that these graben structures acted as significant recharge channels during the life of the Lake City hydrothermal system.

4.2.5 Effect of Grain Size

Because the minerals of finer-grained rocks present a higher surface area in which intimate grain-fluid contact can occur, it is instructive to examine whether the grain-size variations in the Cataract Gulch granite played any role in fixing the $\delta^{18}\text{O}$ distribution in the granite. Although we will show below in Chapter 6 that the very fine-grained Sunshine Peak Tuff was definitely more susceptible to hydrothermal ^{18}O exchange than the granite, comparison of the grain size data in Figure 4.13 with the pattern of $\delta^{18}\text{O}$ values in Figure 4.11 shows clearly that grain size was not important in determining the whole-rock $\delta^{18}\text{O}$ values in the granite. Moreover, grain size shows no correlation with any of the parameters plotted in Figure 4.12. For example, SC-110, 1 mm grains, and SC-109, 8 mm grains, have widely different grain sizes, but both have high $\delta^{18}\text{O}$ values and they were collected close together at similar elevations. Also, neither the two highest- ^{18}O samples, nor the lowest- ^{18}O sample of granite display unusual grain size; in fact, one of the lowest ^{18}O samples (LC-17,

Figure 4.13 Map of the Precambrian granite showing contours of average grain size of the samples (in mm). Also shown is that area of the granite that contains orthoclase megacrysts. The three localities near the ring fault that are shown as triangles represent samples with isotopically heterogeneous feldspars (the finer-grained plagioclase and orthoclase in the groundmass is lower in ^{18}O than the coexisting megacrysts). However, comparison of this figure with Figure 4.10 shows that grain size was not an important factor in determining the hydrothermal ^{18}O -depletions observed in the granite.



$\delta^{18}\text{O} = 3.3$) is a pegmatitic sample with a grain size an order of magnitude higher than most other samples of the granite. Two samples (SC-103 and SC-106) appear to have anomalously low $\delta^{18}\text{O}$ values for their geographic positions, in that they lie within the small, closed, hatched contours on the east flank of the Half Ridge uplift on Figure 4.11; however, if anything, these samples have higher than average grain size of 4 to 6 mm.

With the exception of the three anomalous samples near the ring fault (described above in Section 4.2.4 and Fig. 4.13), grain size did not markedly influence the $\delta^{18}\text{O}$ values of the feldspars in the granite. The calculated $\delta^{18}\text{O}$ values of the other feldspars shown in Table 4.1 are also lower than the measured $\delta^{18}\text{O}$ values, but only by 0.5 to 1.5 per mil. These differences are readily attributable to the fact that the whole-rock $\delta^{18}\text{O}$ values also include low- ^{18}O chloritized and/or sericitized biotite (80 to 100 percent altered) not taken into account in this idealized calculation. Calculated feldspar $\delta^{18}\text{O}$ for one sample (CG-11) is 0.4 per mil higher than the measured feldspar $\delta^{18}\text{O}$ value, and in this sample the biotite is only 25 percent altered. Note that the zone of orthoclase megacrysts on Figure 4.13 includes some of the lowest- ^{18}O samples observed in the 5.5 to 9.0 km group (defined below), and that 60 percent of the samples in the 5.5 to 9.0 km group have whole-rock $\delta^{18}\text{O}$ less than or equal to 5.0, irrespective of whether they contain megacrysts or not. Thus, most of the feldspars seem to have thoroughly exchanged oxygen with the hydrothermal fluids.

Examination of Figure 4.3 shows that grain size had a very slight effect on the degree of oxygen isotope exchange between the the granite quartz and the hydrothermal fluids. All of the samples that define the

steep, linear trend-line in Figure 4.3 exhibit a narrow range of grain size from 3 to 5 mm. Sample LC-17, a pegmatitic granite with 25 mm grains, has a quartz $\delta^{18}\text{O}$ value greater than would be predicted by the main trend. Sample SR-19, with 2 mm grains, has a quartz $\delta^{18}\text{O}$ value lower than would be predicted by the main trend. The coarse-grained quartz in LC-17 was apparently more resistant to hydrothermal ^{18}O exchange than the average granite quartz, whereas the fine-grained SR-19 quartz was slightly less resistant.

4.2.6 Effect of Elevation on the $^{18}\text{O}/^{16}\text{O}$ Ratio

The whole-rock $\delta^{18}\text{O}$ analyses of the granite samples have been contoured (Fig. 4.12) on a plot of the elevation of the sample location versus its distance from the Eureka graben. These distances were measured on a series of lines projected from the sample locations perpendicular to the N47°E-trending graben axis; the latter was drawn through sample location LC-17, which is centrally located within the graben structures.

Three groups of samples (those collected within the graben, those collected 5.5 to 9.0 km from the graben, and those collected >9.0 km from the graben) are defined in Figure 4.14; these groups separate out as three distinct fields when the $\delta^{18}\text{O}$ values of the samples are plotted as a function of elevation (Fig. 4.15). Although there is a slight indication of a correlation trend, the $\delta^{18}\text{O}$ values in the graben group appear to be essentially independent of elevation on Figure 4.15. Except for one ^{18}O -depleted sample, the samples from the >9.0 km group display a linear, positive correlation between $\delta^{18}\text{O}$ and elevation. The

Figure 4.14 Geographic subdivisions of sample locations within the Precambrian granite (see text). Samples from the three main groups, as well as the two sub-groups of the 5.5 to 9.0 km group are delineated on a plot of elevation vs. $\delta^{18}\text{O}$ on Figures 4.12 and 4.15.

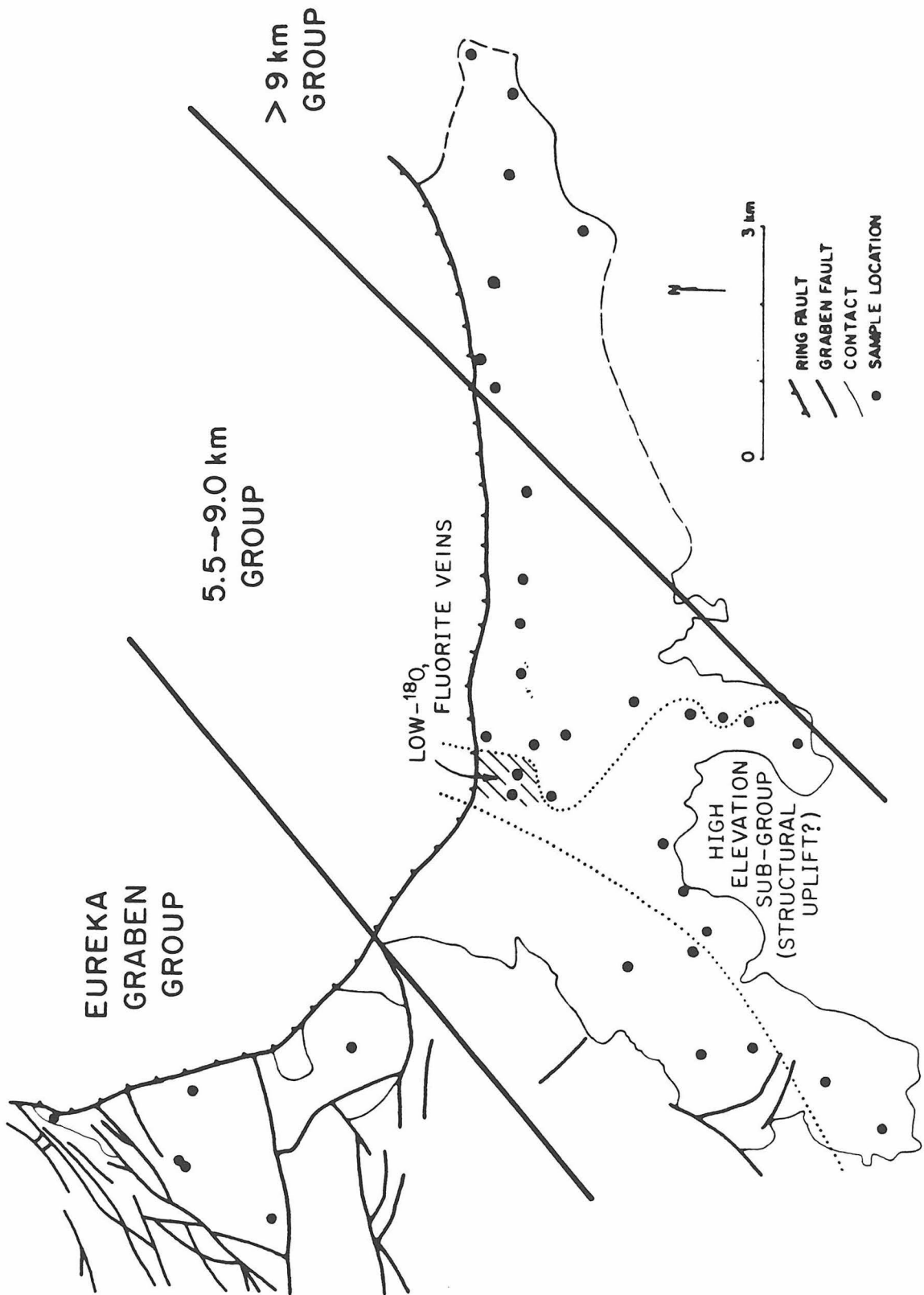
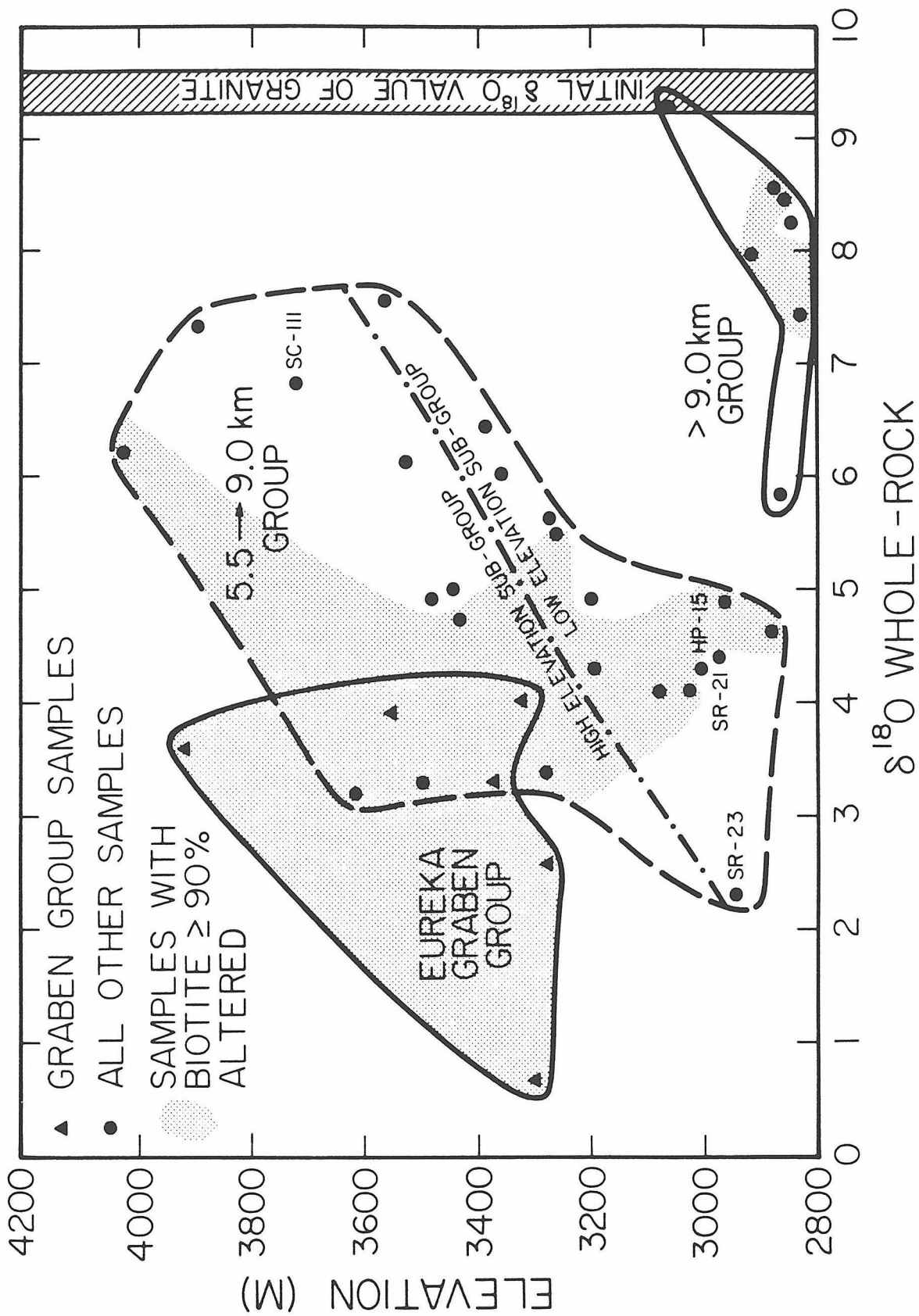


Figure 4.15 $\delta^{18}\text{O}$ values of the Precambrian granite plotted as a function of the sample elevation. The vertical band at $\delta^{18}\text{O} = +9.2$ to $+9.6$ indicates the initial isotopic composition of the granite, prior to hydrothermal alteration. Three groups of samples defined by distance of the sample from the Eureka graben are shown (see Fig. 4.14): samples collected within the graben; samples collected 5.5 to 9.0 km from the graben; and samples collected > 9.0 km from the graben. Although there is appreciable scatter in the data, within each of the 3 groups there is a tendency for the lower elevation samples to have lower $\delta^{18}\text{O}$ values than the higher elevation samples. A "high-elevation" sub-group within the 5.5 to 9.0 km group can be separated out based on the $\delta^{18}\text{O}$ -elevation plot and the geographic distribution of the sample localities (see Fig. 4.14). Both this sub-group and the adjoining low-elevation sub-group show strong positive correlations between $\delta^{18}\text{O}$ and elevation. The two northernmost samples within the "high-elevation" sub-group are associated with fluorite-bearing veins, and may have been altered by a lower $\delta^{18}\text{O}$ fluid (see text).



5.5 to 9.0 km group defines an even more pronounced correlation trend with a positive slope. Note that relative to the >9.0 km group, the 5.5 to 9.0 km correlation trend is offset to overall lower $\delta^{18}\text{O}$ values, perhaps because of greater proximity to the Eureka graben.

The $\delta^{18}\text{O}$ -elevation correlations in Figure 4.15 become much better defined if we separate out a geographic sub-group, arbitrarily termed the "high-elevation" sub-group. This sub-group was initially delineated simply by inspection of the $\delta^{18}\text{O}$ plot of Figure 4.15, but the samples within this sub-group are also vertically and geographically separated from the other samples of the 5.5 to 9.0 km group (Fig. 4.14). To partially test the validity of these correlations between $\delta^{18}\text{O}$ and elevation, after the graph in Figure 4.15 was drawn up, two new samples, one from a high elevation and one from a low elevation, SC-111 and SR-21, respectively, were analyzed to see if they also fit the pattern. This test was an unqualified success; the two samples fit perfectly within the already established contours and groupings in Figures 4.11, 4.12, and 4.15. The high-elevation sub-group of samples is geographically confined to an area that has been domed or structurally uplifted, here termed the Half Ridge uplift (see Section 4.2.7). One plausible explanation for the isotopic systematics shown in Figure 4.15 is that the high-elevation sub-group trend line at one time correlated with that of the main part of the 5.5 to 9.0 km group, but subsequent to, or coincident with, the period of hydrothermal alteration the area of the high-elevation sub-group was uplifted. Such an interpretation is compatible with the positions of the dashed $\delta^{18}\text{O}$ contours and the Precambrian-Tertiary contact on Figure 4.12, as well as with geographic proximity

of these samples to the Half Ridge uplift (Fig. 4.11).

Two low- ^{18}O samples collected close together at the northern edge of the high-elevation sub-group (SC-114 and SC-116) came from an area that contains distinctive quartz-carbonate-fluorite veins not found elsewhere within the granite; the anomalous characteristics of these two samples were noted during field sampling long before any $\delta^{18}\text{O}$ analyses were carried out. As will be discussed in Chapter 5, $\delta^{18}\text{O}$ values of quartz from these fluorite-bearing veins are much lower than quartz $\delta^{18}\text{O}$ values from typical graben or Lake City caldera veins, suggesting that the fluids which formed the quartz-carbonate-fluorite veins had a significantly lower $\delta^{18}\text{O}$ value than the typical graben or caldera vein fluids. Interactions between the granite and these lower- ^{18}O fluids would have produced lower whole-rock $\delta^{18}\text{O}$ values than in the granite that had exchanged with typical higher- ^{18}O , ^{18}O -shifted, graben-type fluids. Thus these two samples at the north end of the "high-elevation" sub-group might a priori have been expected to be lower in ^{18}O than nearby, equivalent-elevation samples.

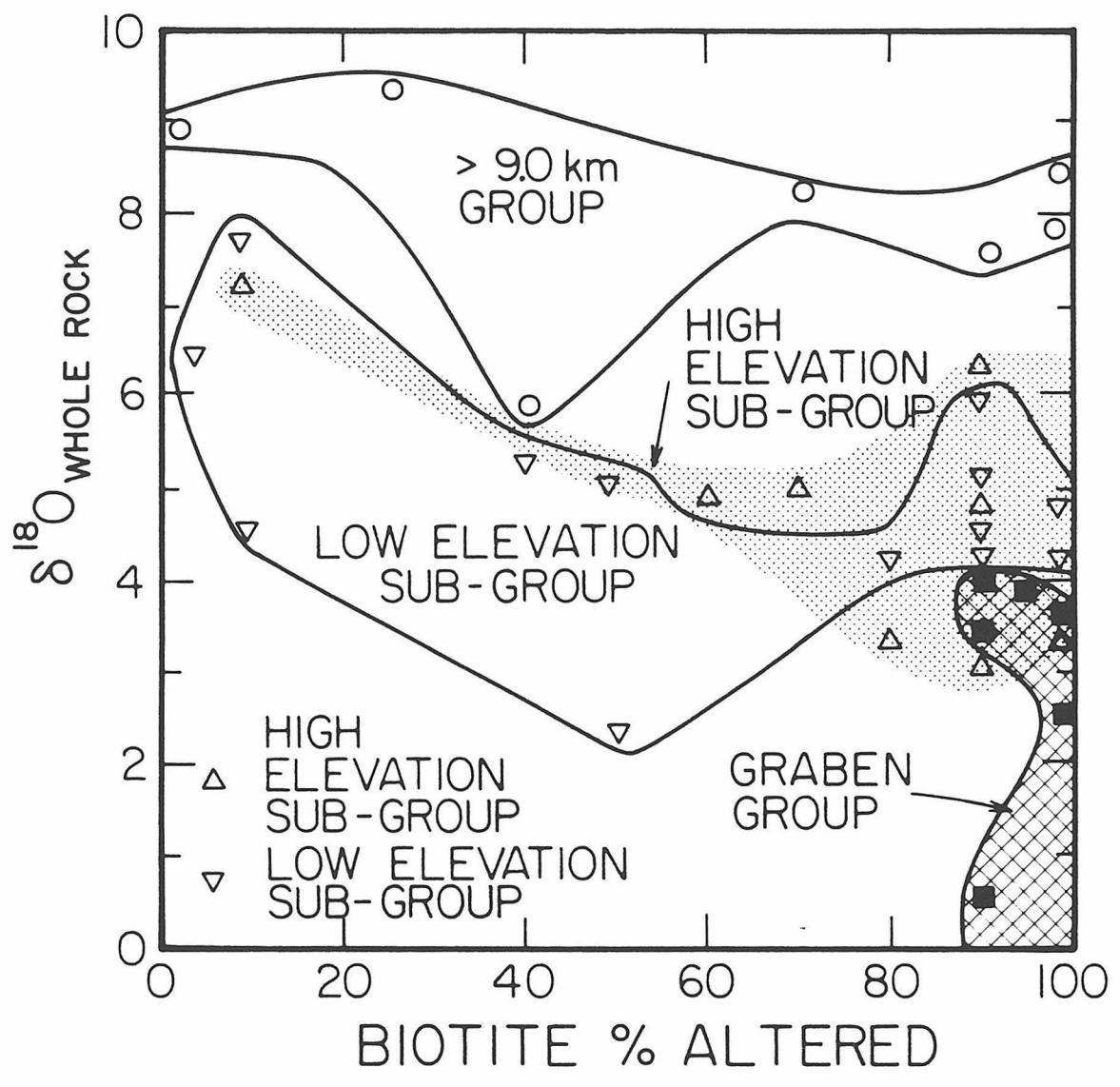
The distribution of those 5.5 to 9.0 km samples that contain highly altered (> 90 percent) biotite shows an interesting pattern on Figure 4.15. All samples with less than 90 percent alteration of the biotite plot in the upper right portion of the 5.5 to 9.0 km field, except two samples that lie at very low elevations (SR-23 and HP-15). These two low-elevation samples have very low $\delta^{18}\text{O}$ values, and thus plot on the correlation trend lines of Figure 4.15; they have clearly been altered at fairly high water/rock ratios, but their biotite is only 10 to 50 percent altered to chlorite. Why then should their biotite be so fresh?

Note that because of this small degree of mineralogic alteration, these two samples plot in unusual positions on Figure 4.9; however, there does not seem to be anything else unique about either sample, except that they were collected at very low elevations and SR-23 is highly brecciated and fractured. Based on the models of Figure 4.8, we can only conclude that these two samples were either altered at significantly higher temperatures than most of the Cataract Gulch granite, or the fluids which they encountered were chemically more compatible with biotite for some reason (f_{O_2} ? salinity?). Because both samples are from low elevations, the higher temperature explanation seems most likely.

A vertical thermal gradient during hydrothermal alteration is thus the most logical explanation of the positive correlation trends shown on Figure 4.15. This interpretation is examined more completely in the next section (4.2.7). Similar decreases in $\delta^{18}O$ with increasing depth have been observed in a number of active geothermal systems (Clayton et al, 1968; Eslinger and Savin, 1973; Lambert and Epstein, 1980). The decrease in $\delta^{18}O$ in all these samples is readily attributable to a decrease in the mineral-H₂O fractionation factors with depth because of the downward temperature increase.

The graph in Figure 4.16 is essentially identical to Figure 4.9, except that the various geographic groups and sub-groups are now delineated on Figure 4.16. Comparisons between Figure 4.16 and Figures 4.8, 4.9, and 4.12 suggest the following relationships between W/R, temperature, and elevation: (1) Because it is farthest from the main flow channels, the >9.0 km group experienced the lowest temperature alteration, and, locally, the smallest water/rock ratios; however the effects

Figure 4.16 Whole-rock $\delta^{18}O$ values of the Precambrian granite plotted as a function of the degree of mineralogic alteration of the biotite (see also Figs. 4.8 and 4.9). The samples are grouped according to the subdivisions in Figures 4.13 and 4.14. This plot is analogous in some respects to the W/R plot shown in Figure 4.7. The relationships shown in this figure can be plausibly interpreted to mean: (1) The granite exposed >9.0 km from the graben experienced lower-temperature hydrothermal alteration than granite closer to or within the graben, although W/R varied over a wide range. Note that the only overlap between the >9.0 km group and the others is with respect to sample SC-85, which lies near the western boundary of this group, closest to the graben. (2) Granite within the graben was altered at fairly high temperatures and consistently high W/R ratios. (3) The 5.5 to 9.0 km group is divided into a topographically higher sub-group (structurally uplifted?) and the topographically lower subgroup. Except for two samples, SR-23 and HP-15, the fields of both sub-groups are virtually coincident on this diagram, and both sub-groups indicate alteration over similar wide ranges of W/R ratios. Samples HP-15 and SR-23 are unique in that they have low $\delta^{18}O$ values but relatively unaltered biotite; inasmuch as they both were collected from very low elevations, they probably were altered in a relatively high-temperature hydrothermal regime where biotite was stable relative to chlorite.

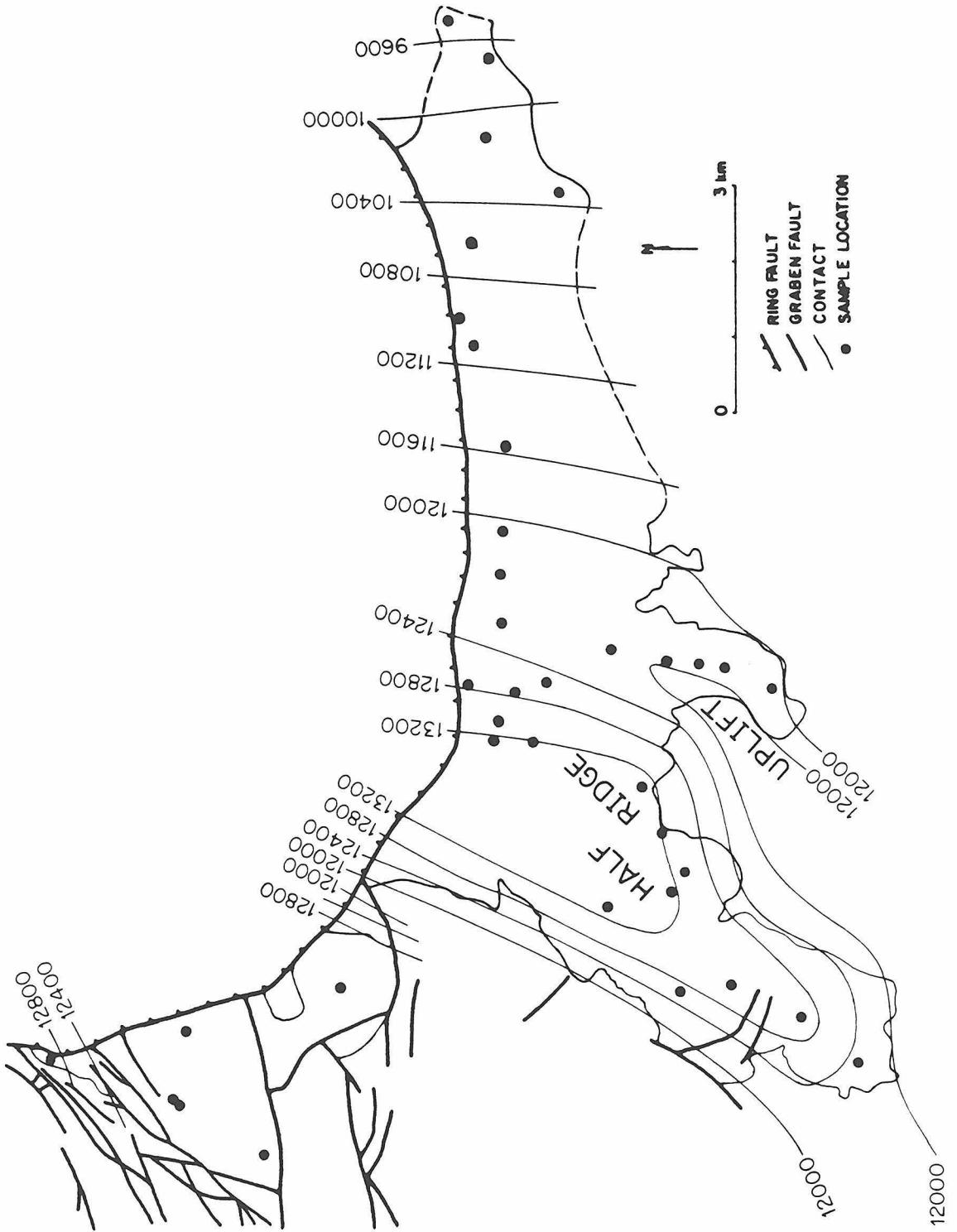


of a local thermal gradient are still evident in this area. These rocks characteristically have sericite > chlorite, particularly those that are most intensely altered. (2) The graben group experienced high temperatures, as well as by far the highest W/R; more sampling is required to establish the existence of a vertical thermal gradient in this structurally complex terrane. The graben samples show both dominantly chloritic and dominantly sericitic alteration, with the sericitic and argillic samples tending to have the lowest $\delta^{18}O$ values. (3) W/R for the 5.5 to 9.0 km sub-groups and the >9.0 group all span very wide ranges. Samples with thoroughly altered biotite (90 to 100 percent altered) are found in all of the groups and subgroups (Figs. 4.11, 4.15, and 4.16). Weakly altered biotite is also distributed in all groups except the graben group. Therefore a vertical thermal gradient probably existed in the hydrothermal system throughout the outcrop area of the granite; however, there also may have been a lateral gradient in temperature of alteration outward from the graben. The water/rock ratio varied dramatically from place to place, apparently independent of these temperature gradients, except within the graben where W/R was consistently very high. The W/R variations are probably related to local variations in fracture permeability within the granite.

4.2.7 Structural Interpretation of $\delta^{18}O$ Values

Isotopic and structural data both suggest that the topographically high granite exposures in the Half Ridge-Cottonwood Creek area were uplifted during or after alteration of the granite. Structural contours on the unconformity at the top of the granite (Fig. 4.17)

Figure 4.17 Structural contours on the upper contact of the Cataract Gulch granite. Also shown is the location of the Half Ridge uplift, a horst on the east side of the Eureka graben. See text for discussion.



define an elongate, north-northeast trending high area (the Half Ridge uplift) nearly parallel to and coincident with Cuba Gulch and Cottonwood Creek. A parallel, smaller, and lower arm of this uplift is exposed in Cataract Gulch. To the east of these highs the structural contours define a gently sloping surface dipping about 6° to the east away from the Eureka graben. Older San Juan volcanic rocks erupted on top of the granite do not thin to the west. Bedding in these rocks has the same 6° eastward dip as the granite-volcanic rock contact (Lipman, 1976a). It appears, therefore, that in this area the early Tertiary erosion surface on the granite was nearly flat prior to the San Juan volcanism, and in fact probably remained so through the early San Juan calc-alkaline volcanic episode.

Prior to formation of the Lake City caldera, resurgence of the San Juan-Uncompahgre-Silverton calderas developed symmetrically around the Eureka graben (Steven and Lipman, 1976). This uplift probably accounts for some of the eastward tilting of the Cataract Gulch granite. Resurgence of the Lake City caldera was asymmetric and was greater in the western than in the eastern part of the caldera. Resurgence within the caldera must also have been accompanied by uplift outside the ring fault; therefore this also accounts for some of the eastward tilting of the granite.

The Half Ridge uplift is an anomalously high area of granite exposure. It appears to be essentially a horst on the east side of the Eureka graben. Figure 4.17 shows that the flanks of this domical uplift are much steeper than the gently dipping granite-volcanic rock contact farther to the east. The steep western flank of the uplift formed as

part of the topographic wall of the San Juan caldera (Lipman, 1976a).

The uplift is located within the earlier-described 5.5 to 9.0 km sample group (Fig. 4.14), and the highest parts of the uplift coincide with the distribution of the "high-elevation" sub-group samples. Figure 4.12 shows that the "high-elevation" sub-group data can be contoured independently of all the other granite data, and that the $\delta^{18}\text{O}$ isopleths for this sub-group are displaced to higher elevations relative to the $\delta^{18}\text{O}$ isopleths for other parts of the granite.

One reasonable interpretation of these observations (the structural uplift and the displaced $\delta^{18}\text{O}$ contours) is that the rocks in the Half Ridge-Cottonwood Creek area were structurally domed during or after the major hydrothermal events that altered the granite. If the alteration effects in the granite were mostly developed during the older San Juan-Uncompahgre-Silverton caldera cycle, then the Half Ridge uplift could conceivably be related to resurgence of the Lake City caldera. Unfortunately, direct field evidence for this interpretation is lacking, because no younger intrusions or faults that might be related to such doming have been mapped in the area of the uplift (Lipman, 1976a).

If the "high-elevation" and "low-elevation" sub-groups have been differentially uplifted after they were altered, then whole-rock $\delta^{18}\text{O}$ values of the samples should vary relative to some pre-uplift elevation datum. The Tertiary-Precambrian unconformity is such a datum; therefore we have plotted the whole-rock $\delta^{18}\text{O}$ values of the granite as a function of sample depth below the unconformity in Figure 4.18. The granite samples from within the Eureka graben were not included in Figure 4.18 because it is not possible to accurately define the position of the

Figure 4.18 Variation of $\delta^{18}\text{O}$ values of the Cataract Gulch granite as a function of the depth of the sample location beneath the Tertiary-Precambrian unconformity. The initial $\delta^{18}\text{O}$ value of the granite is also shown. The horizontal lined pattern shows the distribution of samples in which sericite is the dominant alteration product of the igneous biotite. The vertical lined pattern shows the distribution of samples in which chlorite is the dominant alteration product of the biotite. Approximately equal amounts of sericite and chlorite are observed in the altered biotites of four samples that plot within the area of overlap of two lined patterns (Table 4.1). One sample from the >9.0 km group is fresh and unaltered (blank pattern). See text for discussion.

unconformity in those complexly eroded and fault-bounded blocks.

In Figure 4.18 the samples from both the 5.5 to 9.0 km group and the >9.0 km group lie along a single common trend with a positive slope. This provides strong support for the structural interpretation described above. In addition, the biotite alteration products in the granite vary systematically in Figure 4.18, with sericitic alteration predominating (1) deeper beneath the unconformity than the chloritic alteration for samples with $\delta^{18}\text{O} > +4.5$ and (2) at shallow levels in the >9.0 km group. These data indicate that the meteoric-hydrothermal system was continuous throughout the granite, and that the decrease in $\delta^{18}\text{O}$ with depth is mainly attributable to a systematic increase of temperature downward from the Precambrian-Tertiary unconformity. The scatter in the data points is due to local variations in the W/R ratio and/or to differences in the $\delta^{18}\text{O}$ of the hydrothermal fluids. The sericitic alteration was produced by either lower-temperature or higher- ^{18}O fluids than those involved in the chloritic alteration.

4.2.8 Comparison with $^{18}\text{O}/^{16}\text{O}$ Data from the Idaho Batholith

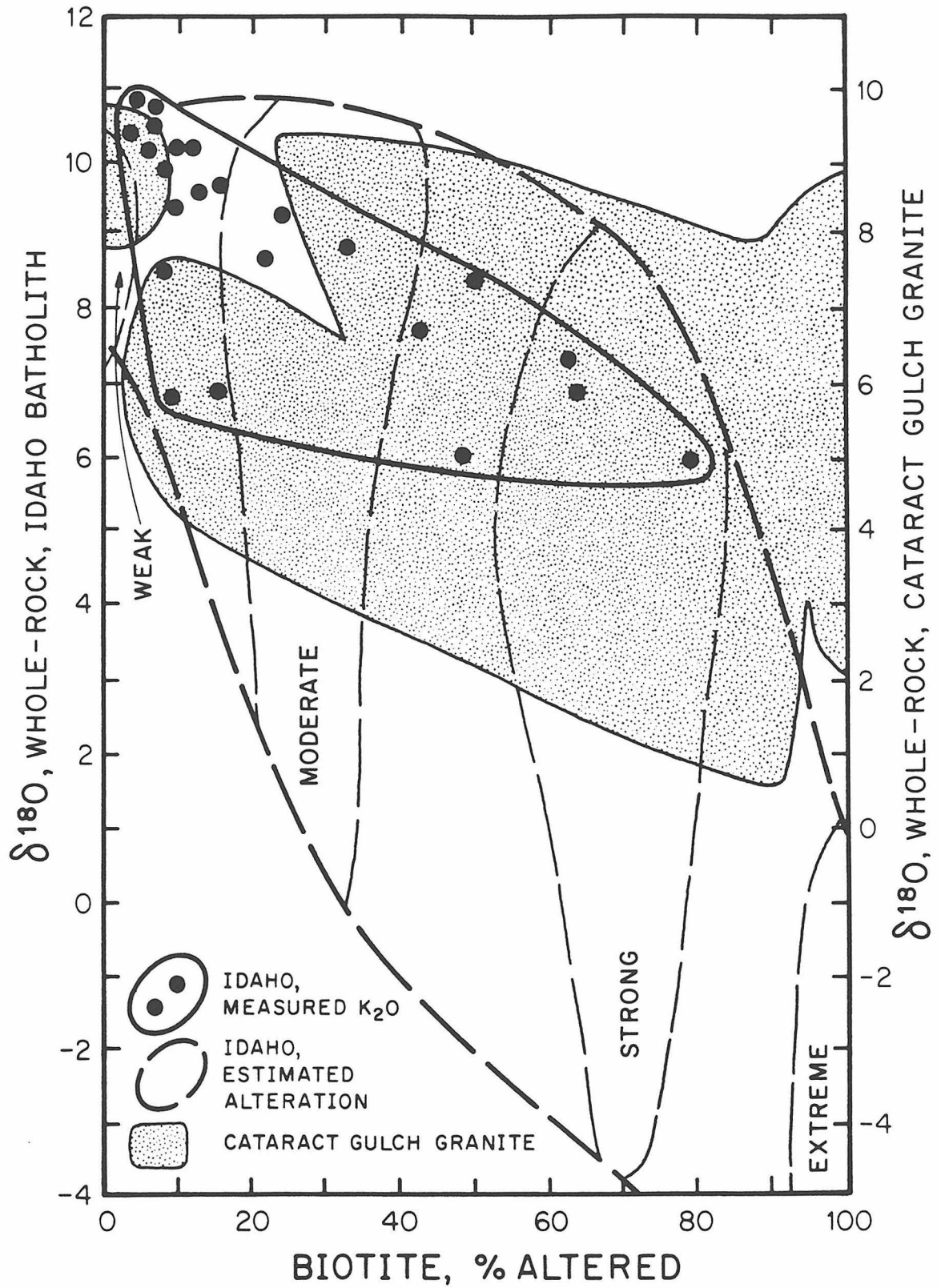
Criss et al (1982) and Criss and Taylor (1983) determined the isotopic composition of K feldspar and quartz and the K_2O content of biotite in granitic rocks altered by very large Eocene hydrothermal systems developed around epizonal plutons intruded into the Mesozoic Idaho batholith. The data from the Cataract Gulch granite are amenable to comparisons with the Idaho batholith data because: (1) The feldspar and quartz analyses (Criss and Taylor, 1983) exhibit similar features, as indicated on Figures 4.3 and 4.4; (2) The degree of alteration of

biotite to chlorite was quantitatively measured by Criss et al (1982) by K_2O analyses of the biotite/chlorite separates ($K_2O = 9.3$ percent represents no alteration of the biotite and $K_2O = 0.0$ percent indicates complete alteration of the biotite to chlorite); (3) Rocks from both areas are petrographically similar; (4) Pristine meteoric water from both areas had $\delta^{18}O \approx -15$ at the time of alteration; (5) Mineralogical alteration products are the same in both environments; (6) Water/rock ratios apparently varied over similar wide ranges in both areas; and (7) Hydrothermal systems in both areas were developed in and around calderas formed during rhyolitic ash-flow tuff eruptions.

Alteration in the granitic rocks from these two systems are compared on Figure 4.19. The fields of data for the Cataract Gulch granite in Figure 4.19 are taken directly from Figure 4.9, but because the unaltered whole-rock $\delta^{18}O$ values in the two areas are different (+8 to +11 for the Idaho batholith; about +9 for the Cataract Gulch granite), for comparison purposes the Cataract Gulch granite data-points were moved up by 1 per mil in Figure 4.19.

Idaho batholith samples for which biotite K_2O analyses and quartz-K feldspar $\delta^{18}O$ data are available are plotted individually and enclosed by the solid curve in Figure 4.19. Other Idaho batholith whole-rock $\delta^{18}O$ analyses are shown only as generalized fields in Figure 4.19 and are enclosed by the heavy dashed curve. For this latter data set, although quantitative measures of biotite alteration are not reported, Criss and Taylor (1983) assign an overall alteration grade to each sample; these four grades (weak, moderate, strong, and extreme) are plotted on Figure 4.19 as 0, 30, 70, and 100 percent altered biotite,

Figure 4.19 Comparison of hydrothermally altered rocks from the Cataract Gulch granite and the Idaho batholith. The Cataract Gulch fields (shaded) are taken directly from Figure 4.9 and have been raised by 1 per mil to account for differences in the initial $\delta^{18}\text{O}$ values in the two areas. The solid curve encloses data-points from the Idaho batholith for which both whole-rock $\delta^{18}\text{O}$ data (calculated from quartz and K feldspar analyses; Criss and Taylor, 1983) and the degree of biotite alteration (based on K_2O analyses of biotite/chlorite separates; Criss et al, 1982) are known. These samples of biotite are relatively unaltered because they are the ones selected for detailed K-Ar studies by Criss et al (1982). The dashed curve encloses a much larger set of batholith samples for which whole-rock $\delta^{18}\text{O}$ data, but no quantitative biotite alteration data, are available (Criss and Taylor, 1983). These samples were assigned to weak (biotite not altered), moderate (assumed to be about 30 percent altered biotite), strong (assumed to be about 70 percent altered biotite), and extreme (biotite totally altered) alteration grades by Criss and Taylor (1983).



respectively. This assignment is exact for the weak and extreme alteration grades (Criss and Taylor, 1983), and the shape of the dashed-curve field enclosing all these data in Figure 4.19 suggests that the moderate and strong alteration zones are also nearly correctly located.

Figure 4.19 indicates that samples from the Idaho batholith were altered at overall higher temperatures than samples from the Cataract Gulch granite (see Figs. 4.7 and 4.8). The pristine meteoric water $\delta^{18}\text{O}$ values were about the same in each environment and variations in this parameter cannot account for the overall lower $\delta^{18}\text{O}$ position of the batholith fields in Figure 4.19. Samples from both areas were altered under similar wide ranges of W/R ratio. The comparisons in Figure 4.19 are gratifying because it was expected a priori that alteration in the Idaho batholith should have occurred at generally higher temperatures; more extensive erosion has exposed deeper levels of the hydrothermal systems (5 km depth, Criss et al, 1982) in Idaho than we now observe in the Cataract Gulch granite (1 to 2 km depth).

4.3 $\delta^{18}\text{O}$ Variations in Older Volcanic Rocks Outside the Lake City Caldera

The Sapinero Mesa Tuff was erupted from the San Juan-Uncompahgre calderas well before formation of the Lake City caldera (Steven and Lipman, 1976). This tuff fills the Uncompahgre caldera and makes up the outer northern wall of the Lake City caldera (Lipman, 1976a). The Sapinero Mesa Tuff is crystal poor (< 10 percent 2 mm phenocrysts of feldspars and biotite) and is typically pervasively altered to chlorite, calcite, epidote, clays, sericite, quartz, and pyrite. A suite of

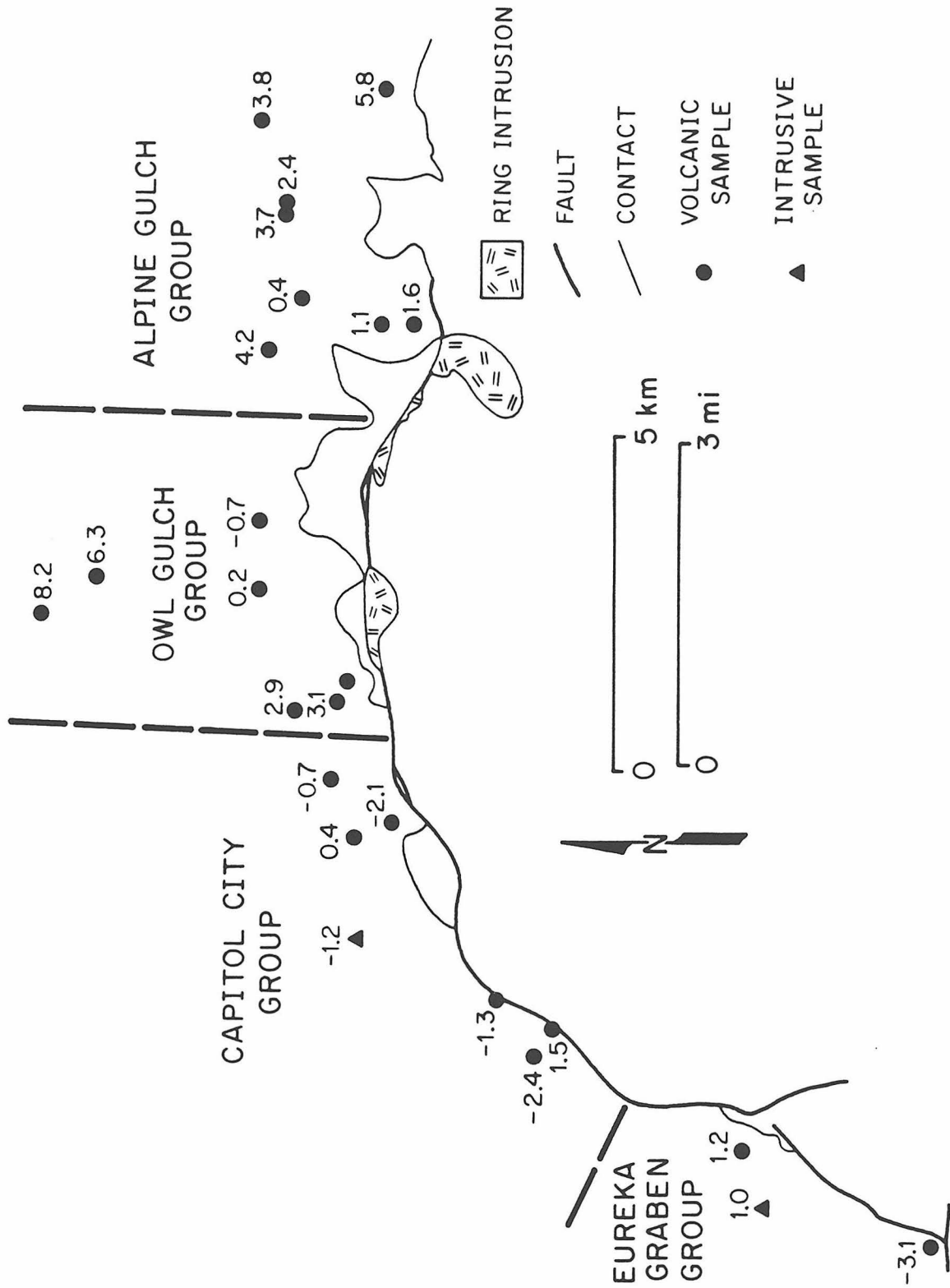
samples of this tuff from outside the northern Lake City ring fault has been analyzed (Fig. 4.20).

One sample from the Uncompahgre caldera-age Capitol City monzonite porphyry intrusions (HC-102, $\delta^{18}\text{O} = -1.2$) was also analyzed. This sample is partially altered to clays, sericite, quartz, and pyrite. Lipman et al (1976) noted altered fragments of this rock in the Sunshine Peak Tuff megabreccia inside the Lake City caldera south of the area of the Capitol City intrusions. Also, altered volcanic rocks in this area are truncated by the Lake City caldera ring fault. These relationships lead Lipman et al (1976) to conclude that the Capitol City hydrothermal system was established prior to formation of the Lake City caldera.

A northeast-trending line of small, 17 to 18 m.y.-old, topaz-bearing rhyolite intrusions lie about 5 km north of the Lake City caldera ring fault (Steven and Lipman, 1976; Burt et al, 1982). These rhyolite intrusions are mineralogically unaltered and have phenocryst mineral $\delta^{18}\text{O}$ values and fractionations typical of unaltered magmatic rocks (HC-99; quartz = +8.6, sanidine = +6.9, biotite = +6.0. HC-103; quartz = +9.2, sanidine = +7.3). These younger rhyolite intrusions clearly were not affected by any important hydrothermal systems.

Five geographic groups of older volcanic rocks have been arbitrarily defined for purposes of discussion. Three samples with $\delta^{18}\text{O} = +6.2$ to +6.9 (one from a monzonite intrusion) were collected from the Burns member of the Silverton volcanics in the Lake Fork of the Gunnison River just southeast of the caldera ring fault (Plate 1). These are termed the Southeast group. Another set of three samples (one a rhyolite porphyry dike) with $\delta^{18}\text{O} = -3.1$ to +1.2 was collected within the

Figure 4.20 Location of samples of the Sapinero Mesa Tuff collected north and west of the Lake City ring fault, showing whole-rock $\delta^{18}\text{O}$ values. Circles are tuff samples and the two triangles represent an intrusive monzonite porphyry and a rhyolite porphyry dike. The samples have been arbitrarily broken into four geographic groups for the purposes of discussion. Contacts between Lake City caldera rocks and Precambrian rocks and the older Tertiary volcanic rocks are shown, together with the Lake City caldera ring intrusions.

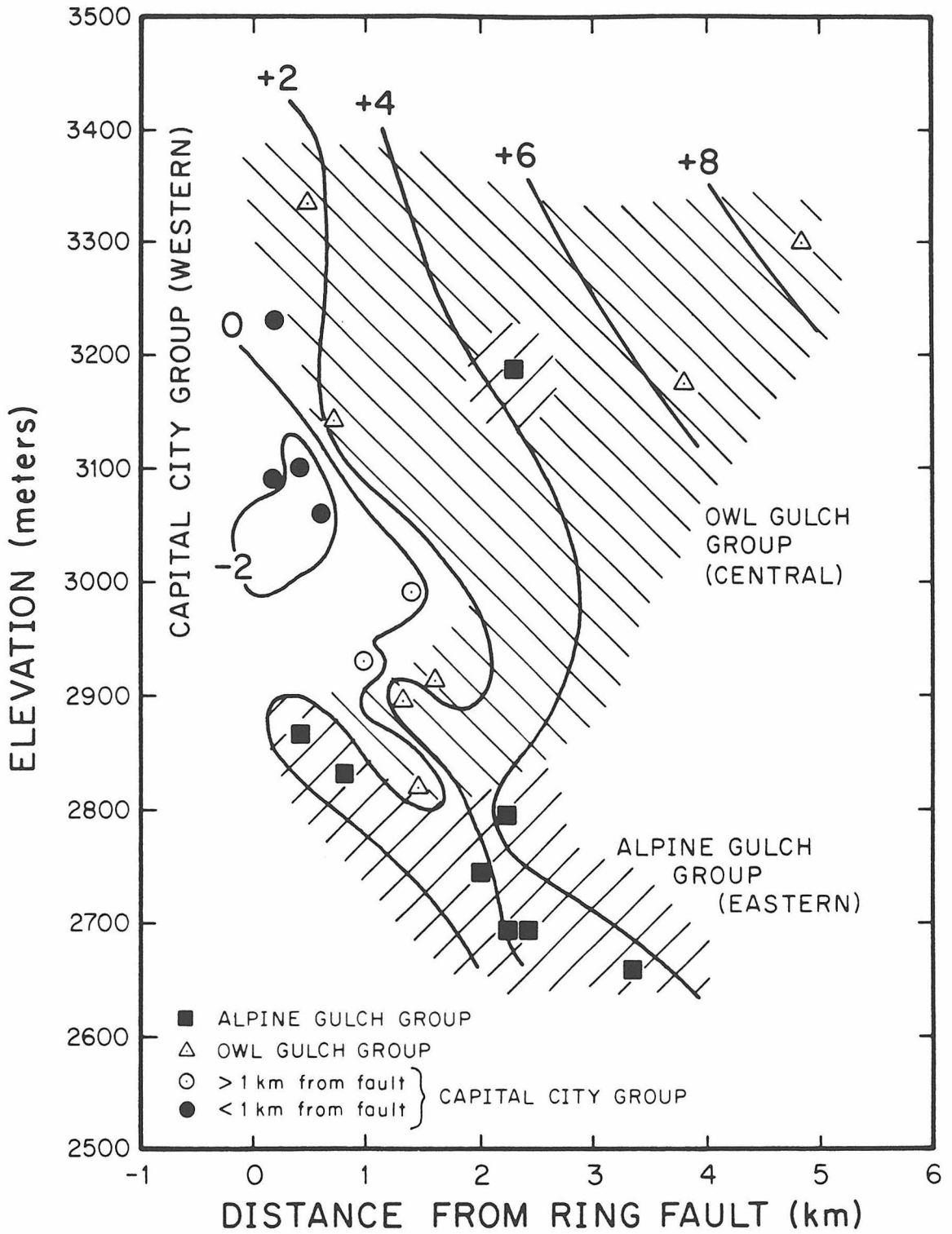


Eureka graben on the western margin of the caldera (Eureka Graben group). Along the northern margin of the caldera, an additional three groups within the Sapinero Mesa Tuff were also delineated (Fig. 4.20). The eastern or Alpine Gulch group contains all samples collected east of a north-south line drawn 1 km west of the junction of Alpine Gulch and Henson Creek. The central or Owl Gulch group contains all samples from the western boundary of the Alpine Gulch group to a north-south line drawn through the junction of Copper Gulch and Henson Creek. The western or Capitol City group contains all samples collected in the Henson Creek drainage west of the Owl Gulch group.

As might have a priori been expected from the discussion of the Precambrian granite in Section 4.2, of the five geographic groups of older volcanic rocks, the lowest- ^{18}O samples come from the Eureka Graben group, and the highest- ^{18}O samples come from the Southeast group. The latter group of samples was collected near the >9.0 km group of relatively unaltered, high- ^{18}O granite samples previously discussed. Except for this Southeast group, the $\delta^{18}\text{O}$ values of the volcanic rock samples are overall much lower than those of the Precambrian granite. This is probably mainly a function of the much finer grain size and more reactive volcanic glass shards in the Sapinero Mesa Tuff, but it might also be linked to the closer proximity of Lake City-age ring intrusions, which are abundant along the northern edge of the caldera (Chapter 6).

Data from the three northern groups are plotted on Figure 4.21 as functions of sample elevation and distance from the Lake City caldera ring fault. The $\delta^{18}\text{O}$ contours for all three groups are approximately parallel on Figure 4.21 and define $\delta^{18}\text{O}$ gradients that are clearly

Figure 4.21 Relationships between sample elevation and distance from the Lake City ring fault for samples of Sapinero Mesa Tuff collected outside the northern ring fault of the Lake City caldera. Three groups of samples have been spatially defined (see text).



related to distance from the Lake City caldera ring fault. However, the characteristic steep negative slopes of the $\delta^{18}\text{O}$ contours also imply a correlation between elevation and $\delta^{18}\text{O}$. In all three groups, the lowest ^{18}O rocks occur at the lowest elevations close to the ring fault. This suggests that the areas closer to and deeper along the ring fault were altered either at higher temperatures and/or higher W/R ratios. Because the northern caldera ring fault hosts a number of Lake City-age ring intrusions (Chapter 6), we perhaps should have expected to encounter significant meteoric-hydrothermal effects approaching this portion of the ring fault. The hydrothermal effects here are indeed stronger near the ring fault than they are at the southern edge of the caldera, where there are no ring intrusions (Section 4.2). Note that all of the high- ^{18}O samples were collected at elevations above 3100 m and at distances of at least 2 km from the ring fault. Starting 5 km away, these high-elevation samples decrease in $\delta^{18}\text{O}$ toward the ring fault in the sequence $8.2 \rightarrow 6.3 \rightarrow 5.8 \rightarrow 3.1 \rightarrow 1.7 \rightarrow 1.5$; the sample with $\delta^{18}\text{O} = +1.5$ occurs only 0.2 km from the ring fault (Fig. 4.21). Below 3100 m, the average $\delta^{18}\text{O}$ of 12 samples collected within 2 km of the ring fault is less than +0.1, and the values go down as low as -2.4.

Progressing from east to west, the $\delta^{18}\text{O}$ contours on Figure 4.21 shift to higher elevations. This is shown most clearly by the abrupt bends in the $\delta^{18}\text{O}$ contours in going west from the Alpine Gulch samples to the Owl Gulch suite. Also, each group exhibits a positive correlation between sample elevation and whole-rock $\delta^{18}\text{O}$ value (Fig. 4.22), particularly at a given distance from the ring fault. The groups are

Figure 4.22 Plot of $\delta^{18}\text{O}$ versus elevation for samples of volcanic rocks older than the Sunshine Peak Tuff. The data-points are subdivided into five geographic groups (SE, NE, N, NW, and W) scattered around the perimeter of the ring fault (see text). The different groups characteristically exhibit a positive correlation between sample elevation and whole-rock $\delta^{18}\text{O}$. Also, the individual groups are shifted to successively higher elevations and lower $\delta^{18}\text{O}$ as one proceeds counterclockwise from east to west around the northern edge of the ring fault. At a given elevation within each group the samples within 1 km of the ring fault or within 1 km of the Eureka graben have the lowest $\delta^{18}\text{O}$ values (+'s).

offset to successively higher elevations and lower $\delta^{18}\text{O}$ values as one proceeds west (Fig. 4.22). This could result either from (1) steeper thermal gradients to the west, (2) superimposed $\delta^{18}\text{O}$ effects of multiple meteoric-hydrothermal events in the west, or (3) a post-alteration tilting to the east. The latter is consistent with the asymmetric resurgent doming within the caldera (which resurged higher to the west) and with the eastward tilting observed in the Precambrian granite along the southern caldera margin (Section 4.2.7). However, it is also possible that the older hydrothermal systems associated with the Capitol City intrusions played a role in determining the final $\delta^{18}\text{O}$ patterns; for example, we might expect steeper thermal gradients near the Capitol City intrusions.

A pre-Lake City age hydrothermal system almost certainly produced some low- ^{18}O rocks in a limited area around the small Capitol City intrusions, and the integrated effects of these events combined with the Lake City hydrothermal event may have contributed to the overall lower $\delta^{18}\text{O}$ values of the westernmost group of samples in Figure 4.22. Geologic evidence (truncation of altered zones around the Capitol City intrusions by the Lake City ring fault) shows that a significant hydrothermal system existed in this area prior to formation of the Lake City caldera. However, judging by the small size of the altered areas associated with the Capitol City intrusions, this hydrothermal system was probably quite small. Variations in the $\delta^{18}\text{O}$ values of the Sapinero Mesa Tuff are much more closely related to proximity to the Lake City caldera ring fault and to the Lake City-age ring and resurgent intrusions than to the Capitol City intrusions (Figs. 4.21 and 4.22). Also,

the Sapinero Mesa Tuff samples have $\delta^{18}\text{O}$ values similar to those of the altered Sunshine Peak Tuff within the caldera (see Chapter 6); the Lake City age hydrothermal activity was thus clearly intense enough to produce all the observed depletions in ^{18}O observed in the Sapinero Mesa Tuff. Nevertheless, inasmuch as the Capitol City hydrothermal event and the Lake City caldera event both involved similar low- ^{18}O meteoric ground waters, more detailed work would be required to sort out the exact contributions of each hydrothermal system to the final $\delta^{18}\text{O}$ pattern of Figure 4.20.

CHAPTER 5

ISOTOPIC STUDIES OF QUARTZ VEINS AND SOLFATARIC HYDROTHERMAL
ACTIVITY IN THE SAN JUAN MOUNTAINS5.1 Alteration and Vertical Isotopic Gradients in the Ring Domes of
the Lake City Caldera5.1.1 Initial Isotopic Composition

In the Lake City area, strong, near-surface, solfataric hydrothermal activity is found only in brecciated portions of the lava ring domes. However, because of a widespread, pervasive, weak hydrothermal alteration, none of the whole-rock $\delta^{18}\text{O}$ analyses of the quartz-latices of Grassy Mountain and Red Mountain are suitable for defining the initial $\delta^{18}\text{O}$ values of these units. All analyzed samples are either slightly ^{18}O depleted, with $\delta^{18}\text{O}$ as low as +4.2 (due to exchange with meteoric-hydrothermal fluids), or enriched in ^{18}O to values as high as +8.3 (presumably as a result of low-temperature exchange of the locally glassy, perlitic, matrix with near-surface meteoric water). On the other hand, phenocryst minerals separated from some of the samples can be used to estimate the original isotopic compositions of these units. Feldspars separated from six of the hydrothermally least altered samples have $\delta^{18}\text{O} = +6.4$ to +6.7, and average +6.6 per mil. These data imply an initial whole-rock $\delta^{18}\text{O}$ value of +6.8 to +7.0, which is 0.2 to 0.4 per mil lower than the $\delta^{18}\text{O}$ of the intracaldera Sunshine Peak Tuff (described below in Chapter 6).

Quartz does not occur as a phenocryst phase in these quartz latices. Samples from the interior of the lava domes have a finely

crystalline, nonglassy matrix containing quartz and sanidine. Finely ground samples from four such rocks were treated with concentrated HF in order to digest the aluminosilicate phases. The residues from these reactions, assumed to be 100 percent matrix quartz, were analyzed; the $\delta^{18}\text{O}$ values range from +7.0 to +8.4, giving a range of 0.5 to 1.8 per mil for the quartz-feldspar fractionations. Although these fractionations are consistent with those typically observed in igneous rocks, their wide range, together with the wide $\delta^{18}\text{O}$ variation in the quartz, indicate either that the initial whole-rock $\delta^{18}\text{O}$ value of the quartz latite was not uniform, or more likely, that some of the very fine-grained matrix quartz was hydrothermally depleted in ^{18}O .

5.1.2 Vertical Extent of the Red Mountain Alteration System

Solfataric alteration occupies a 2 km diameter circular area approximately centered on Red Mountain (elevation 3909 m), and occurs entirely within a locally brecciated portion of the Red Mountain quartz latite ring dome (Fig. 5.1). The alteration is characterized by thorough aluniteization of primary feldspars, and virtually complete silicification of the matrix and other phenocrysts. Small needles of alunite are also commonly scattered throughout the matrix. Locally, alunite occurs as thin veins and as breccia cement. In places, kaolinite/illite replaces the feldspars and alunite is not present. Fine-grained, disseminated pyrite originally made up 2 to 3 percent of the hydrothermal mineral assemblage, but in surface exposures it is nearly totally oxidized to bright red to orange iron oxides.

During the summer of 1981, AMOCO drilled a vertical, 837 m,

Figure 5.1 Map showing the geology, hydrothermal alteration, sample locations, and $\delta^{18}\text{O}$ data from the Red Mountain lava dome at the eastern edge of the Lake City caldera (modified in part from Lipman, 1976a). The diagonal pattern indicates quartz-alunite-pyrite (solfataric) alteration. The horizontal pattern indicates deeper argillic alteration. The small triangle is the location of the AMOCO drill hole. See Plate 1 for explanations of the lithologic abbreviations.

exploration core hole on the west side of Red Mountain, collared at an elevation of about 3749 m. The hole penetrated Red Mountain quartz latite throughout its length. Alteration similar to that in surface exposures persisted to a depth of about 200 m in the hole. Below that level, the quartz latite lacks alunite and is intensely altered to quartz, clays, and pyrite to the bottom of the hole (Ken Hon and Dana Bove, 1982, personal communication).

Inside the Lake City caldera, just west of Red Mountain, several square kilometers of Sunshine Peak tuff and megabreccia are also intensely hydrothermally altered (see Chapter 6). Although this area lies at a lower topographic level (2750 to 3350 m elevation), it is semicontinuous with the solfataric zone at Red Mountain. Above about 3050 m elevation, this alteration is identical to the zone I to V argillic alteration developed in the Sunshine Peak Tuff throughout the higher elevations within the caldera. Below 3050 m elevation, we observe the characteristic chlorite-carbonate alteration that typifies the stratigraphically deeper parts of the Sunshine Peak Tuff inside the caldera (Chapter 6). Quartz veins up to a meter wide, containing pyrite and base metal sulfides, are scattered throughout the altered area below about 3150 m elevation, and locally the adjacent tuff is entirely altered to quartz, sericite, and pyrite.

The above relationships suggest that the vertical gradations in alteration mineralogy in the Red Mountain area represent vertical variations in a single hydrothermal system. The fluids depositing quartz and base metal sulfides at depth were the same fluids which, upon rising through 1 km of permeable zones such as fractures or breccias, produced

the shallow solfataric alteration near the summit of Red Mountain. The Red Mountain system thus probably represents only the shallowest part of a much larger meteoric-hydrothermal system that affected rocks throughout the Lake City caldera; that system is described in detail in Chapters 6 and 7.

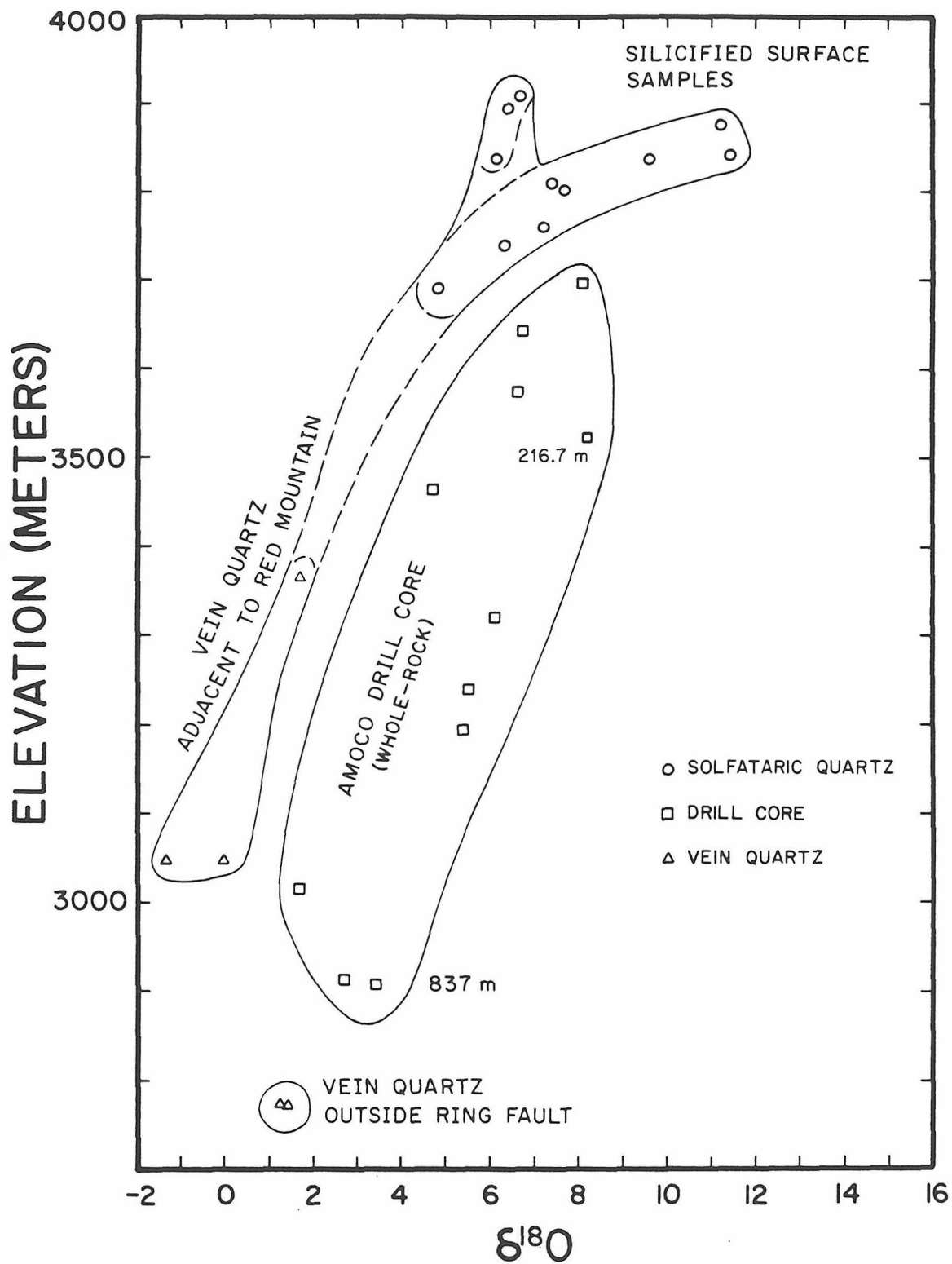
5.1.3 Vertical Variations in Oxygen Isotopic Compositions of Alteration Minerals

Hydrothermal quartz from the Red Mountain solfataric zone has $\delta^{18}\text{O} = +4.8$ to $+11.6$. The initial magmatic $\delta^{18}\text{O}$ of the quartz-latites was about $+6.8$ to $+7.0$. Thus, the hydrothermal quartz locally shows both enrichment and depletion in ^{18}O relative to unaltered quartz latite. The pervasive and complete conversion of the quartz latite to hydrothermal product minerals shows that the water/rock ratio for this part of the hydrothermal system was very large and that the hydrothermal fluids were drastically out of equilibrium with the igneous mineral assemblage.

When the quartz data are plotted versus the elevation of the sample locality (Fig. 5.2), some indication of a vertical control on the $\delta^{18}\text{O}$ data is evident. Two trends are apparent for the surface samples in Figure 5.2. First, a linear distribution of points ($\delta^{18}\text{O} = +4.9$ to $+11.2$) with a shallow positive slope defines a slightly curved (concave downward) trend. Second, a cluster of three points is offset above and to the left of the first trend; this cluster shows little vertical variation in isotopic composition. This set of three samples (RM-15, RM-16, and RM-23) was collected within a 150 m diameter area near the top of Red Mountain.

Analyses of 11 whole-rock samples from the AMOCO drill hole also

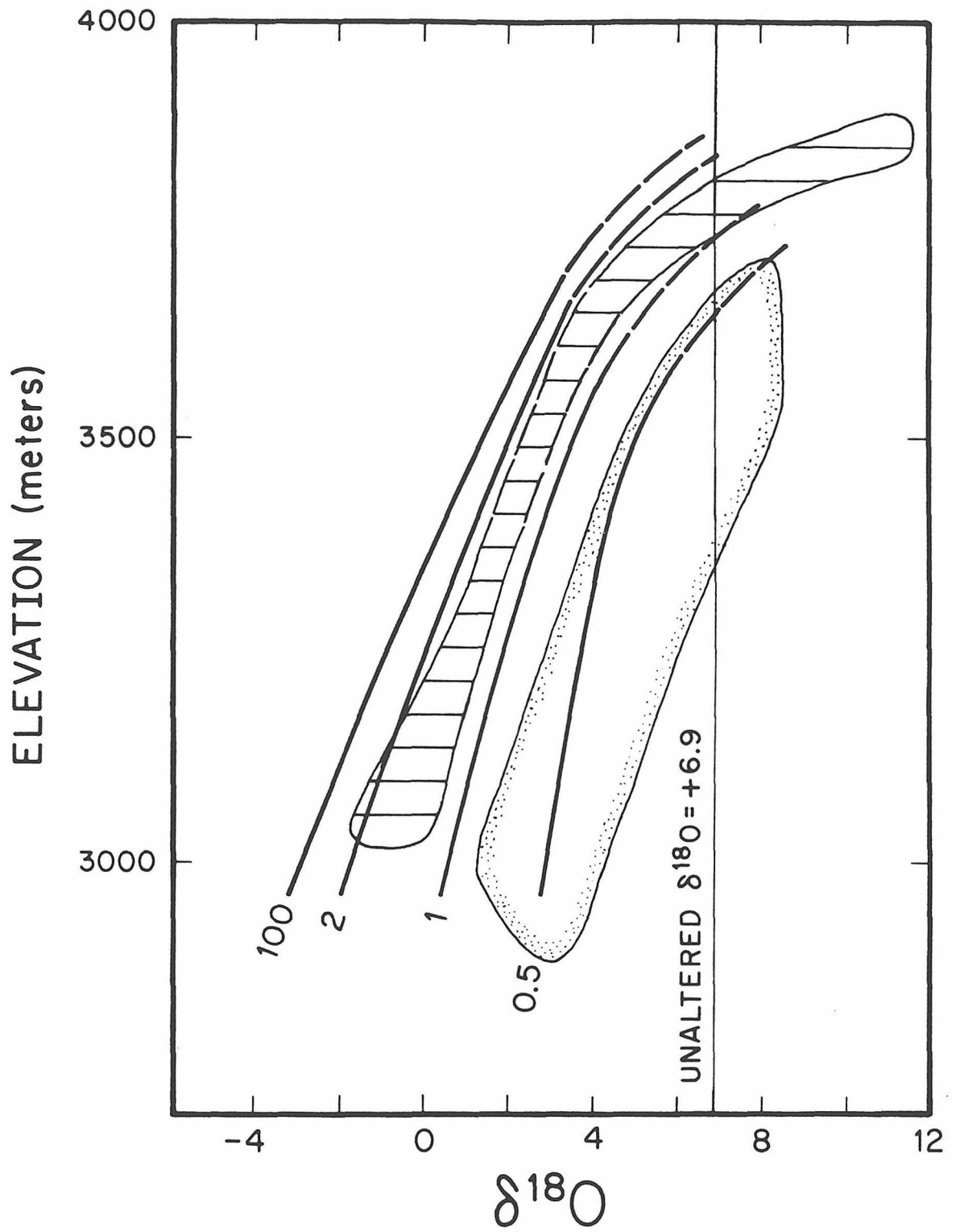
Figure 5.2 $^{18}\text{O}/^{16}\text{O}$ ratios in altered rocks and hydrothermal quartz from the Red Mountain fossil hydrothermal system, as a function of the elevation at which the samples were collected. Analyses of solfataric quartz collected on the surface at Red Mountain appear to define two trends, one with a shallow positive gradient in $\delta^{18}\text{O}$ as a function of elevation, and a subsidiary steeper trend to the left of the former trend defined by just three samples from a locality near the summit of Red Mountain. Whole-rock analyses of argillized core samples from the 837 m deep AMOCO drill hole also exhibit a steep positive vertical $\delta^{18}\text{O}$ gradient. Low-elevation vein quartz samples from the lower drainage of Alpine Gulch, northwest of the Red Mountain lava dome and inside the ring fault, show uniformly low $^{18}\text{O}/^{16}\text{O}$ ratios; these data lie on an extension of the solfataric quartz $\delta^{18}\text{O}$ trend. The $\delta^{18}\text{O}$ values of vein quartz collected outside the ring fault are also low, but do not lie on the above trend. Because the vein samples were collected from the dumps of old prospects and mines, their actual elevation is not known. However, inasmuch as none of these prospects or mines were large producers, it can be assumed with some confidence that the elevation of the dump is within 50 meters of the elevation at which the sample was collected.



show a decreasing ^{18}O content with depth (Fig. 5.2). These data-points lie within a 2 per mil wide band that exhibits a very steep slope. We observe a maximum $\delta^{18}\text{O}$ value of +8.2 at 3532.3 m elevation and a minimum of +1.7 at 2912 m elevation in the drill core. Two samples at 216.7 and 837 m depth, described as fresh Red Mountain quartz latite (Ken Hon, 1982, personal communication), are only weakly mineralogically altered. As might be expected a priori, these two samples lie on the heavy side of the $\delta^{18}\text{O}$ -elevation band in Figure 5.2. In general, samples on the low- ^{18}O side of the band exhibit more intense mineralogical alteration in thin section than those on the high- ^{18}O side. Thus, at any given elevation, increasing mineralogical alteration (= higher water/rock ratio?) in the samples tends to shift the quartz latite to lower $\delta^{18}\text{O}$ values.

Note in Figure 5.2 that the whole-rock samples from the AMOCO drill core are 2 to 4 per mil richer in ^{18}O than quartz vein samples from equivalent elevations just to the northwest of Red Mountain (see Section 5.2 below). Inasmuch as, at equilibrium, quartz is always richer in ^{18}O than coexisting feldspar, chlorite, and white mica, the data in Figure 5.2 mean that whole-rock samples are drastically out of $^{18}\text{O}/^{16}\text{O}$ equilibrium with the quartz veins and the solfataric quartz. A new diagram analogous to Figure 5.2 was constructed to quantify these relationships (Fig. 5.3). If we assume that the quartz veins and the hydrothermal alteration of the rocks were all produced by the same aqueous fluids, and if we assume that the W/R ratio in the veins was very large (>100), then we can plot contours of the W/R ratio in the rocks on Figure 5.3. Based on the discussion below in Section 5.3, it indeed

Figure 5.3 A $\delta^{18}\text{O}$ -elevation plot for the Red Mountain lava ring dome, showing water/rock ratios for the hydrothermal system that altered the quartz latite, contoured at $W/R = 100, 2, 1,$ and 0.5 . The field bounded by the stippled pattern shows the distribution of $\delta^{18}\text{O}$ values of whole-rock samples from the AMOCO drill hole, and the horizontal ruled field shows the distribution of $\delta^{18}\text{O}$ values of hydrothermal quartz (see Fig. 5.2). See text for discussion.



seems likely that all these areas were altered by the same types of waters, and we can also closely estimate the temperature of alteration from the boiling point curve. This requires the bulk rocks in the AMOCO drill hole to have been altered at an overall W/R ratio of about 0.5 if the hydrothermal fluid flowed out of the system after interaction (open system behavior). The water/rock equations presented in Chapter 4 were used in these calculations, together with the following parameters: (1) initial whole-rock $\delta^{18}\text{O}$ is that of unaltered quartz latite (+6.9); and (2) initial water $\delta^{18}\text{O}$ is that for a fluid in equilibrium with a typical vein quartz at 300°C (-4.5, Table 5.1).

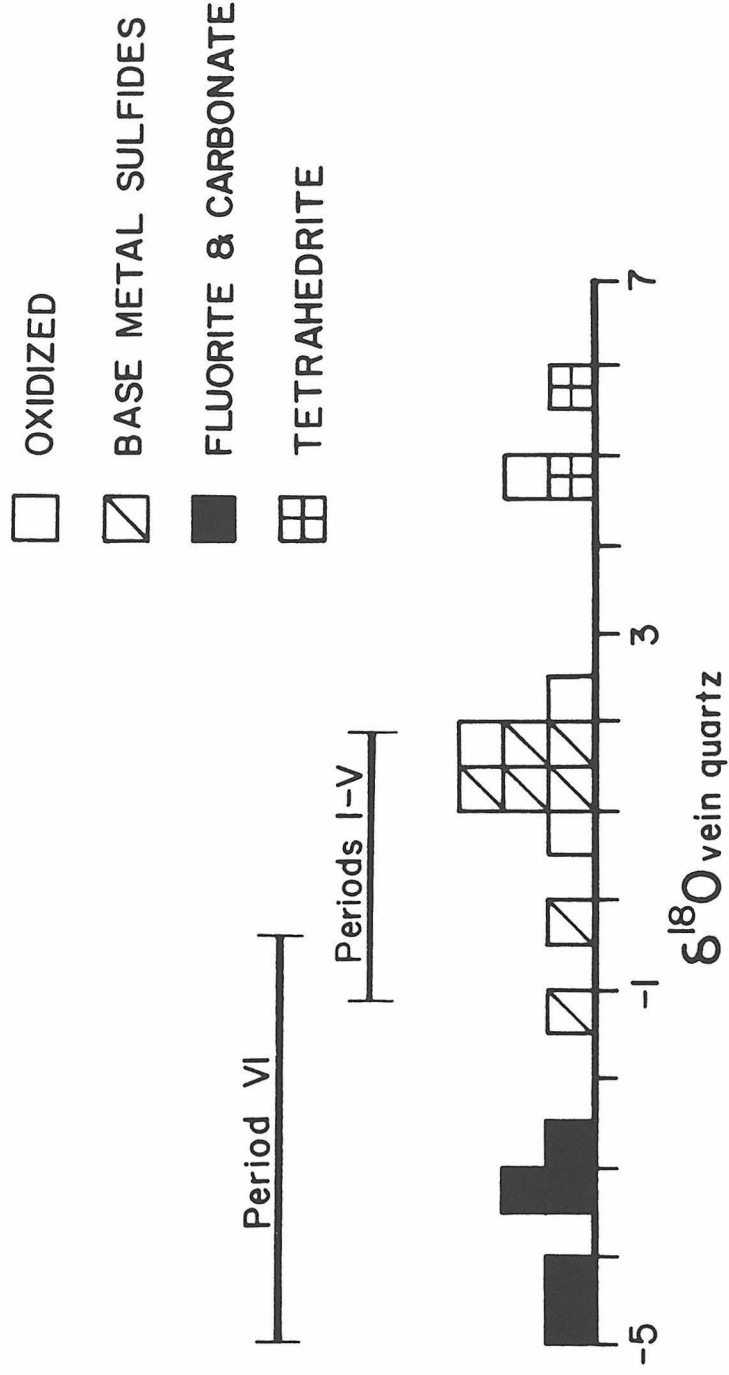
5.2 $^{18}\text{O}/^{16}\text{O}$ Variations in Vein Quartz

5.2.1 Data Obtained in the Present Study

Oxygen isotopic analyses of vein quartz from the deeper parts of the Red Mountain hydrothermal system (Fig. 5.2), collected within the caldera to the northwest of Red Mountain, are similar to quartz analyses from other base-metal sulfide veins throughout the caldera. All vein quartz analyses from the Lake City caldera area are plotted in Figure 5.4.

Three distinct groupings are evident in Figure 5.4. A low- ^{18}O group of veins containing quartz, fluorite, a carbonate mineral, and traces of pyrite lies just outside the caldera ring fault southeast of Burrows Park. These veins, which in this study were found only in the Precambrian granite of Cataract Gulch, contain quartz with $\delta^{18}\text{O} = -4.5$ to -2.5 per mil. The host rock here is the low-elevation subgroup granite defined in Chapter 4. Analyses of quartz from the interior and

Figure 5.4 Histogram of oxygen isotopic analyses of vein quartz from the Lake City caldera. Each of the three distinct vein assemblages exhibits a corresponding distinct range in $\delta^{18}\text{O}$ values. For comparison, the range of oxygen isotopic analyses of vein quartz 10 km farther west, from the Sunnyside mine, Eureka graben, are also shown (Casadevall and Ohmoto, 1977). Period VI from the Sunnyside mine corresponds mineralogically to the Lake City fluorite-carbonate veins. Periods I through V from the Sunnyside mine contain assemblages that correspond to the Lake City base metal sulfide veins.



Sunnyside Mine

exterior of one such vein, SR-28, are nearly identical at -4.5 and -4.4, respectively. Alteration selvages on these veins are negligible.

A second group with intermediate $\delta^{18}\text{O}$ values comprises quartz-base metal sulfide-pyrite (OBP) veins collected from throughout the Lake City caldera. This group includes the aforementioned veins in the deeper portions of the Red Mountain system, which are exposed in lower Alpine Gulch. Quartz from these veins has $\delta^{18}\text{O} = -1.4$ to $+2.1$, with most values clustering around $+1.5$ per mil. Analyses of quartz from the interior and exterior of one vein, AG-16, are nearly identical at $+1.2$ and $+1.3$, respectively.

A third group of veins, found within the caldera only in the Burrows Park area, has much higher $\delta^{18}\text{O}$ values. This group is distinguished by the presence of abundant tetrahedrite, as well as base metal sulfides. Quartz from these veins has $\delta^{18}\text{O} = +4.6$ to $+5.7$ per mil.

If the temperatures at which the quartz was precipitated in these veins can be estimated, then the oxygen isotopic composition of the vein-forming fluids can be calculated. This calculated isotopic composition will prove useful in further discussions of water-rock interactions throughout the caldera and in higher parts of the meteoric-hydrothermal systems, such as the solfataric zones.

5.2.2 Comparison with Fluid Inclusion Data

Measurement of fluid inclusion homogenization temperatures and freezing point depressions provide useful estimates of the temperatures of vein formation and fluid compositions. Such analyses have been published for a number of base-metal sulfide veins in the

western San Juan Mountains. Casadevall and Ohmoto (1977) studied fluid inclusions in vein quartz from the Sunnyside mine, which is developed in the Eureka graben 10 km west of the Lake City caldera. Filling temperatures of fluid inclusions in quartz for Period I through V mineralization (which includes quartz-base metal sulfide-pyrite ores) range from about 250° to 325°C. Period VI vein-filling material from the Sunnyside mine consists of quartz, fluorite, carbonates, and minor sulfates, and mineralogically resembles the quartz-fluorite-carbonate veins in the Precambrian granite south of the Lake City caldera. The bulk of period VI fluid inclusion filling temperatures lie between 175° and 250°C, although some samples filled as high as 320°C. Freezing point depression measurements of period I through VI samples from the Sunnyside mine show that the fluids in the inclusions generally contain less than 2 weight percent equivalent NaCl.

Casadevall and Ohmoto (1977) also measured the oxygen isotopic compositions of vein quartz for all periods of mineralization at the Sunnyside mine. Period I through V vein quartz $\delta^{18}\text{O}$ values range from -1.2 to +1.8. Period VI quartz $\delta^{18}\text{O}$ values range from -5.0 to -0.4, but $\delta^{18}\text{O}$ values are concentrated between -5.0 and -3.0. These ranges in isotopic composition are quite similar to the QBP and quartz-fluorite-carbonate veins associated with the Lake City caldera (see Fig. 5.4).

Fluid inclusion homogenization and freezing point depressions have also been determined for quartz and sphalerite from the quartz-base metal sulfide-pyrite vein assemblage in the Ute-Ulay mine, just north of the Lake City caldera in the Henson Creek drainage (Slack, 1980).

Homogenization temperatures range from about 200° to 280°C. Later fluorite in this vein yields filling temperatures between about 160° to 200°C. Freezing point depression measurements indicate salinities generally less than 3 equivalent weight percent NaCl, but locally as high as 7 equivalent weight percent NaCl.

5.2.3 Temperatures of Formation of Quartz Veins and $\delta^{18}\text{O}$ of Fluids, Lake City Caldera

Krasowski (1976) calculated sulfur isotopic equilibration temperatures for coexisting sulfides in QBP veins from Burrows Park, both inside and outside the southwestern margin of the Lake City caldera. These temperatures range from 250° to 370°C. Thus, based on fluid inclusion homogenization temperatures for mineralogically similar veins in the western San Juan Mountains, and on sulfur isotopic fractionations in veins in and adjacent to the western Lake City caldera margin, the QBP veins probably were deposited in the temperature range 250° to 350°C. The quartz-fluorite-carbonate veins probably precipitated at somewhat lower temperatures, in the range 150° to 250°C.

Using the quartz-water fractionation curve of Clayton et al (1972), fluids in equilibrium with the Lake City QBP vein samples are calculated (Table 5.1). Fluids from which the quartz-fluorite-carbonate veins precipitated had a $\delta^{18}\text{O} = -12$ to -17 , identical to the pristine western San Juan mid-Tertiary meteoric water (Chapter 4). This range is similar to that calculated by Casadevall and Ohmoto (1977) for fluids from which the Sunnyside period VI ores precipitated. Fluids from which the QBP veins precipitated could have ranged from -10 to -4 per mil. These

Table 5.1 Calculated fluid oxygen isotopic compositions for selected QBP and fluorite-carbonate veins associated with the Lake City caldera. The quartz-water fractionation curve of Clayton et al (1972) was used.

Field #	$\delta^{18}\text{O}_{\text{QUARTZ}}$	$\delta^{18}\text{O}_{\text{WATER}}$ @ Specified Temperature*			
		200°C	250°C	300°C	350°C
TEMPERATURE		200°C	250°C	300°C	350°C
$\Delta^{18}\text{O}_{\text{QUARTZ-WATER}}$		12.2	9.5	7.4	5.8
<u>QBP Veins</u>					
SC-66	0.7		-8.8	-6.7	-5.1
RM-55	1.7		-7.8	-5.7	-4.1
RM-65A	-1.4		-10.9	-8.8	-7.2
<u>Fluorite-Carbonate Veins</u>					
SR-16	-2.5	-14.7	-12.0		
SR-28(I)	-4.5	-16.7	-14.0		

* The QBP (quartz-base metal sulfide-pyrite) veins are assumed to have formed at 250° to 350°C. The fluorite-carbonate veins are assumed to have formed at 200° to 250°C.

fluids are evolved meteoric water, having undergone an ^{18}O shift resulting from previous interaction with wall rocks prior to entering the vein system. Similar water compositions have been calculated for the Sunnyside period I through V ores (Casadevall and Ohmoto, 1977). It is interesting to note that the $\delta^{18}\text{O}$ of inclusion fluids in vein quartz from the Creede mining district, 40 km to the southeast in the central San Juan Mountains, range from -5.9 to +1.8 (Bethke and Rye, 1979).

5.3 Boiling in an Upflowing Fluid as a Model for the Red Mountain Solfataric Alteration

5.3.1 Solfataric Alteration in Present-Day Hot Springs

The quartz-alunite-kaolinite alteration at Red Mountain is characteristic of a solfataric or acid-sulfate hot spring environment (Rose and Burt, 1979). The alteration is similar to that currently being produced at active acid-sulfate hot springs, such as at Yellowstone Park, Wyoming (Allen and Day, 1935), Lassen Peak, California (Day and Allen, 1925), and several areas in Japan (Ellis, 1979). In-hole temperature measurements of shallow drill holes in areas of active acid-sulfate hot spring activity show that the fluids in these hot springs are rising along hydrostatic boiling curves. Such drill hole temperature profiles have been published for Yellowstone Park (Fenner, 1936; White et al, 1975; White, 1978), and for the vapor-dominated geothermal system at the Geysers, California (White et al, 1971), among other areas. Temperature-depth profiles in active geothermal systems show that more deep-seated fluids lying at depths below the point of intersection with the hydrostatic boiling curve also tend to follow trajectories with very steep slopes.

5.3.2 Temperature-Depth Model of the Red Mountain Solfataric System

The relationships observed in active geothermal systems have been incorporated into a model which accounts for the steep $\delta^{18}\text{O}$ gradient in hydrothermal quartz from the solfataric zone in the Red Mountain system. The isotopic compositions of water in equilibrium with a typical quartz vein (RM-55, lower Red Mountain system, $\delta^{18}\text{O} = +1.7$, close to the mean value of QBP vein quartz in the Lake City area, see Fig. 5.4), are shown in Figure 5.5. This diagram considers three plausible temperatures of vein formation, 275°, 300°, and 325°C, as shown in Table 5.2. The evolution of three fluids with these temperatures was modelled (Fig. 5.5) by: (1) intersecting the boiling curve for pure water (Haas, 1971) at the respective temperature for each fluid; (2) moving the fluid up the boiling curve under hydrostatic pressure and generating a steam phase which remains in thermal and isotopic equilibrium with the liquid phase; (3) partitioning the oxygen isotopes between the vapor and liquid masses of the fluid; and (4) calculating the $\delta^{18}\text{O}$ of quartz in equilibrium with the liquid part of the system. Included in Figure 5.5 is the boiling curve for a 5 weight percent NaCl solution (Haas, 1971). Inclusion fluids in the western and central San Juan veins typically contain less than 3 equivalent weight percent NaCl equivalent (Casadevall and Ohmoto, 1977; Barton et al, 1977; Slack, 1980). As seen in Figure 5.5, using pure water as opposed to a saline solution introduces only minor errors into the model (boiling would occur at 100 to 150 m shallower depths in a 5 weight percent NaCl solution).

Truesdell et al (1977) used a similar model to evaluate the effects of subsurface boiling and mixing in hot springs at the Yellowstone

Figure 5.5 Model for boiling of meteoric-hydrothermal fluids rising along the hydrostatic boiling curve. The boiling curves are from Haas (1971). Three initial model fluids from Table 5.2 are shown. The isotopic compositions of these fluids are determined by calculating the composition of the water that would be in equilibrium with a quartz having $\delta^{18}\text{O} = +1.7$ at the respective temperatures. After intersecting the boiling curve at the appropriate temperature, the fluid rises along the hydrostatic boiling curve to the surface. The steam and liquid phases in the system are assumed to maintain both thermal and isotopic equilibrium in this model. Also shown is the approximate vertical extent of the solfataric alteration at Red Mountain.

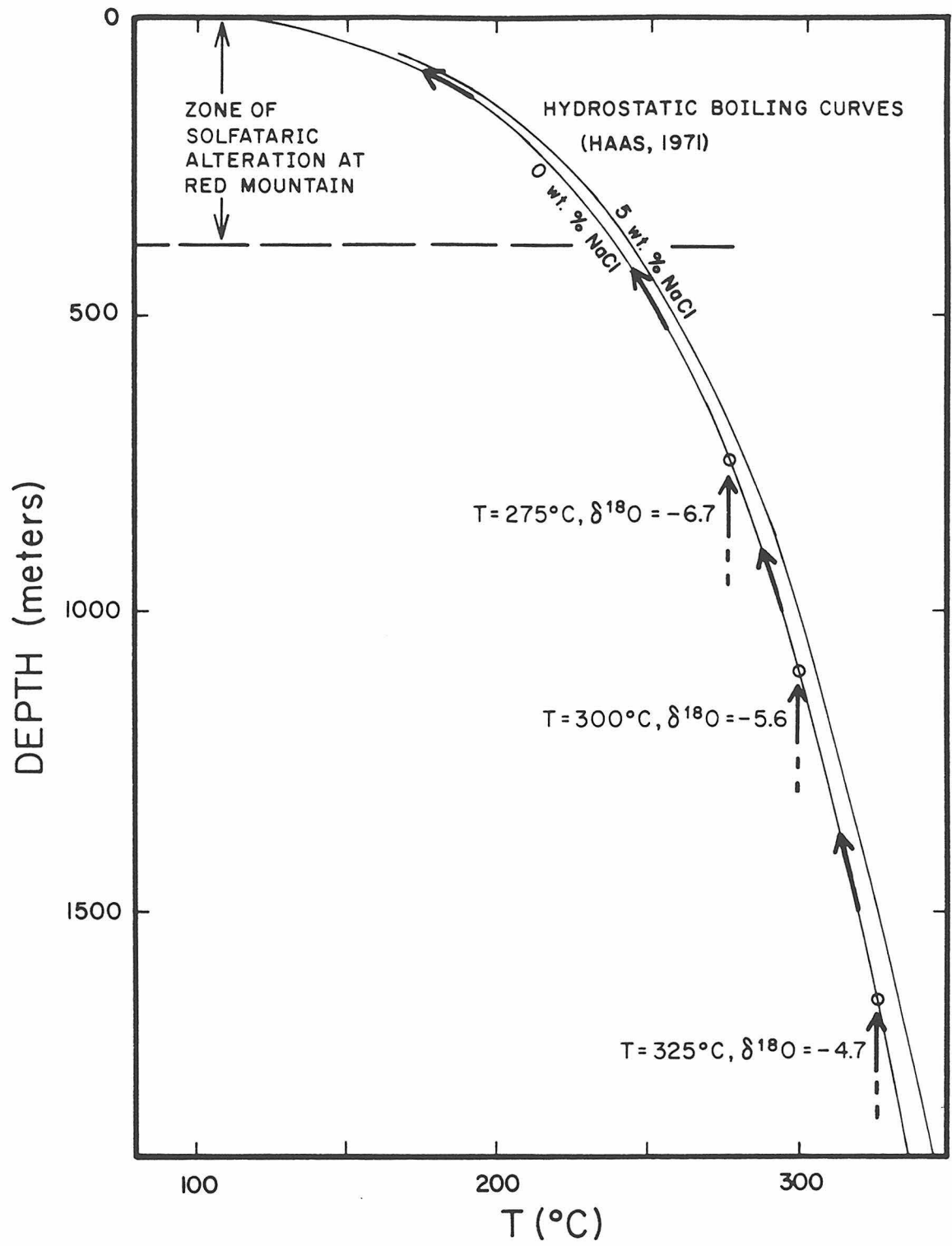


Table 5.2 Characteristics of three fluids used to model the solfataric alteration at Red Mountain. The initial fluid is that which is calculated to be in isotopic equilibrium with quartz having $\delta^{18}\text{O} = +1.7$.

	Initial Boiling Temperature		
	275°C	300°C	325°C
$\Delta^{18}\text{O}_{\text{QUARTZ-WATER}}^1$	8.4	7.4	6.5
$\delta^{18}\text{O}_{\text{WATER,initial}}$	-6.7	-5.6	-4.7
Depth of boiling curve intersection ²	723m	1088m	1609m
Steam/water ratio at surface	36:64	42:48	48:42
$\delta^{18}\text{O}_{\text{WATER,final}}$	-4.8	-3.5	-2.3

¹Clayton et al (1972)

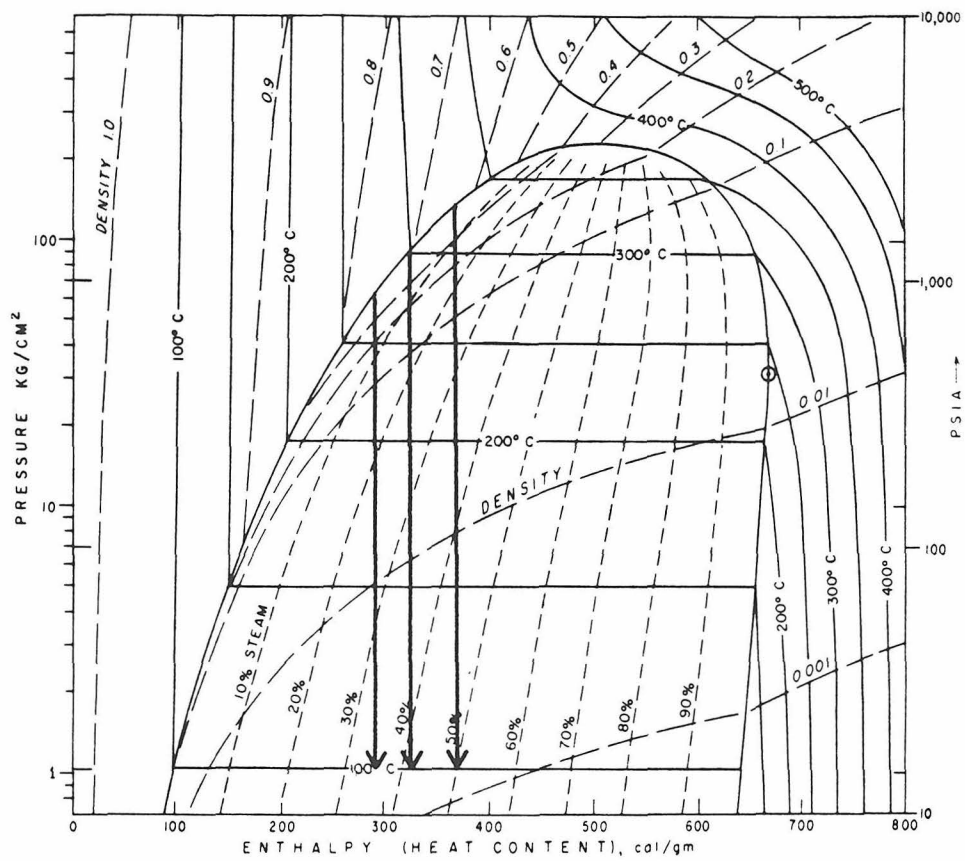
²Haas (1971)

geothermal system, Wyoming. They used two end member models, one of which corresponds to the model used for the Red Mountain system; Truesdell et al (1977) refer to this as single-stage. A second model was also considered, in which steam is separated from the liquid as it is formed; Truesdell et al (1977) refer to this as the continuous model. Truesdell et al (1977) conclude that a multiple-stage model, intermediate between the single-stage and continuous models, together with minor infiltration and mixing of pristine local meteoric water with the evolved hydrothermal fluid, best accounts for δD and chlorinity measurements of fluids presently discharging from the Yellowstone hot springs.

Upon intersecting the boiling curve, the rising fluid evolves into a two-phase system consisting of liquid water and vapor bubbles. As the fluid rises along the boiling curve the proportion of vapor bubbles in the system increases. The pressure-enthalpy diagram for pure water (Fig. 5.6) can be used to calculate the mass proportion of the fluid that is converted to steam (e.g. see White et al, 1971). Boiling in a rising hydrothermal fluid is an irreversible expansion, a constant enthalpy process (Barton and Toulmin, 1961). The model assumes that the vapor-liquid system remains in thermal equilibrium and is closed. In higher parts of the system, where large volumes of vapor are generated, bulk separation of the two phases must locally occur.

Assuming the two-phase system remains in isotopic equilibrium, mass balance and experimental steam-water isotope fractionation curves (Bottinga, 1968; Bottinga and Craig, 1968) can be used to distribute the oxygen isotopes between the two phases. The initial fluid isotopic compositions (100 percent liquid H_2O) are those that were calculated to

Figure 5.6 Pressure-enthalpy diagram for the system water-steam (from White et al, 1971). The proportions of steam to water in a closed-system fluid rising along the hydrostatic boiling curve were calculated for the three model fluids from this diagram, assuming constant-enthalpy paths (vertical arrows) and using the lever rule.



be in equilibrium with quartz ($\delta^{18}\text{O} = +1.7$) at the three assumed temperatures (Table 5.2). The steam-water isotope fractionation ($\Delta_{\text{L-V}}$) can be written:

$$\Delta_{\text{L-V}} = \delta^{18}\text{O}_{\text{Liquid}} - \delta^{18}\text{O}_{\text{Vapor}}.$$

Upon boiling, mass must be conserved between the liquid and vapor phases, and if X represents mole fraction, we have:

$$\delta^{18}\text{O}_i = X_L \cdot \delta^{18}\text{O}_L + X_V \cdot \delta^{18}\text{O}_V.$$

The subscripts i, L, and V denote the initial system, the liquid, and the vapor, respectively, and:

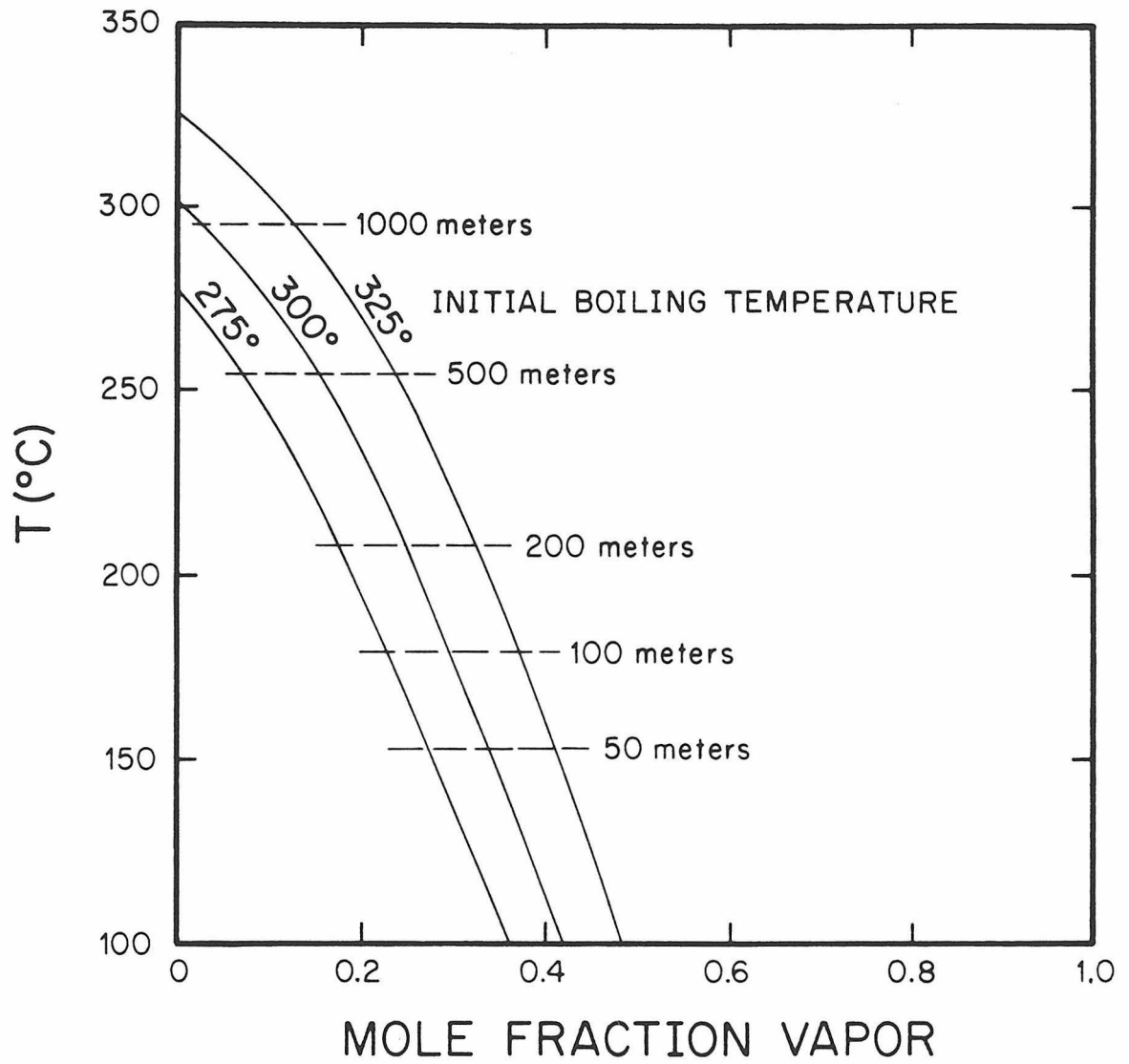
$$X_L + X_V = 1.$$

Combining the three above equations yields a simple relationship that defines the oxygen isotopic composition of the liquid in the two-phase system ($\delta^{18}\text{O}_L$) as a function of (1) the isotopic composition of the bulk system, which is identical to that of the initial fluid ($\delta^{18}\text{O}_i$); (2) the temperature-dependent liquid-vapor fractionation factor; and (3) the temperature-dependent mass fraction of the fluid that has been boiled to steam (X_V):

$$\delta^{18}\text{O} = \delta^{18}\text{O}_i + (\Delta_{\text{L-V}})(X_V).$$

The oxygen isotopic changes in the fluids for the three models were calculated using this equation. The proportions of steam and liquid water at each stage are shown in Figure 5.7. The calculations were conducted at 50°C intervals assuming closed-system behavior.

Figure 5.7 Plot of temperature ($^{\circ}\text{C}$) vs. mole fraction of vapor in the closed steam-water systems rising along the hydrostatic boiling curve. These ratios were calculated for initial liquids having the three model temperatures shown in Figure 5.6. As shown in Figure 5.5, the temperature of such a boiling system is a simple function of depth below the water table (hydrostatic pressure), and variations in depth are shown as contours on the three model curves.



In a hydrothermal system characterized by a high water/rock ratio, two factors control the final oxygen isotopic composition of the product phases: the isotopic composition of the liquid and the temperature of the reaction. Both of these variables exhibit vertical variations in the hot spring environment because of the cooling effect and formation of bubbles as the fluid rises along a boiling curve. If equilibrium is maintained between the fluid and the hydrothermal quartz, then a vertical gradient in the isotopic composition of the quartz is to be expected. $\delta^{18}\text{O}$ values of quartz in equilibrium with the model waters of Figure 5.7 are indicated by curved lines in Figure 5.8, together with the actual isotopic data from the Red Mountain solfataric zone. The quartz-water fractionation above 200°C was taken from Clayton et al (1972). Fractionations from 100° to 200°C were interpolated between the 200°C curve of Clayton et al (1972) and the 0°C fractionation (39 per mil) measured by Knauth and Epstein (1976), assuming that the fractionation factor varies linearly as $1/T^2$.

The curves in Figure 5.8 were visually fit to match the observed Red Mountain quartz trend. Each curve is constrained by the model to pass through a $\delta^{18}\text{O}$ quartz value of +1.7 at depth. Figure 5.8 also includes the estimated position of the water table as defined by projections of the model trajectories to 1 atm. The quartz $\delta^{18}\text{O}$ gradient is dominantly a function of increased quartz-water fractionation as a function of decreasing temperature, not liquid-vapor isotopic fractionation in the fluid (Fig. 5.9).

The close agreement between the calculated curves and the measured isotopic analyses from Red Mountain (Fig. 5.8) fits the geologic

Figure 5.8 Calculated hydrothermal quartz $^{18}\text{O}/^{16}\text{O}$ ratios for the three model fluids (curved lines), compared with the observed $\delta^{18}\text{O}$ variations in samples from the Red Mountain solfataric zone (dots). Also shown are isotherms along the $\delta^{18}\text{O}$ trajectories, as well as the projected water table for the three model fluids. The correspondence between the observed and calculated trends shows that the boiling model is applicable to the Red Mountain system. Moreover, this correspondence suggests that the same meteoric-hydrothermal fluid that deposited the deep quartz veins also produced the solfataric alteration in the near-surface environment.

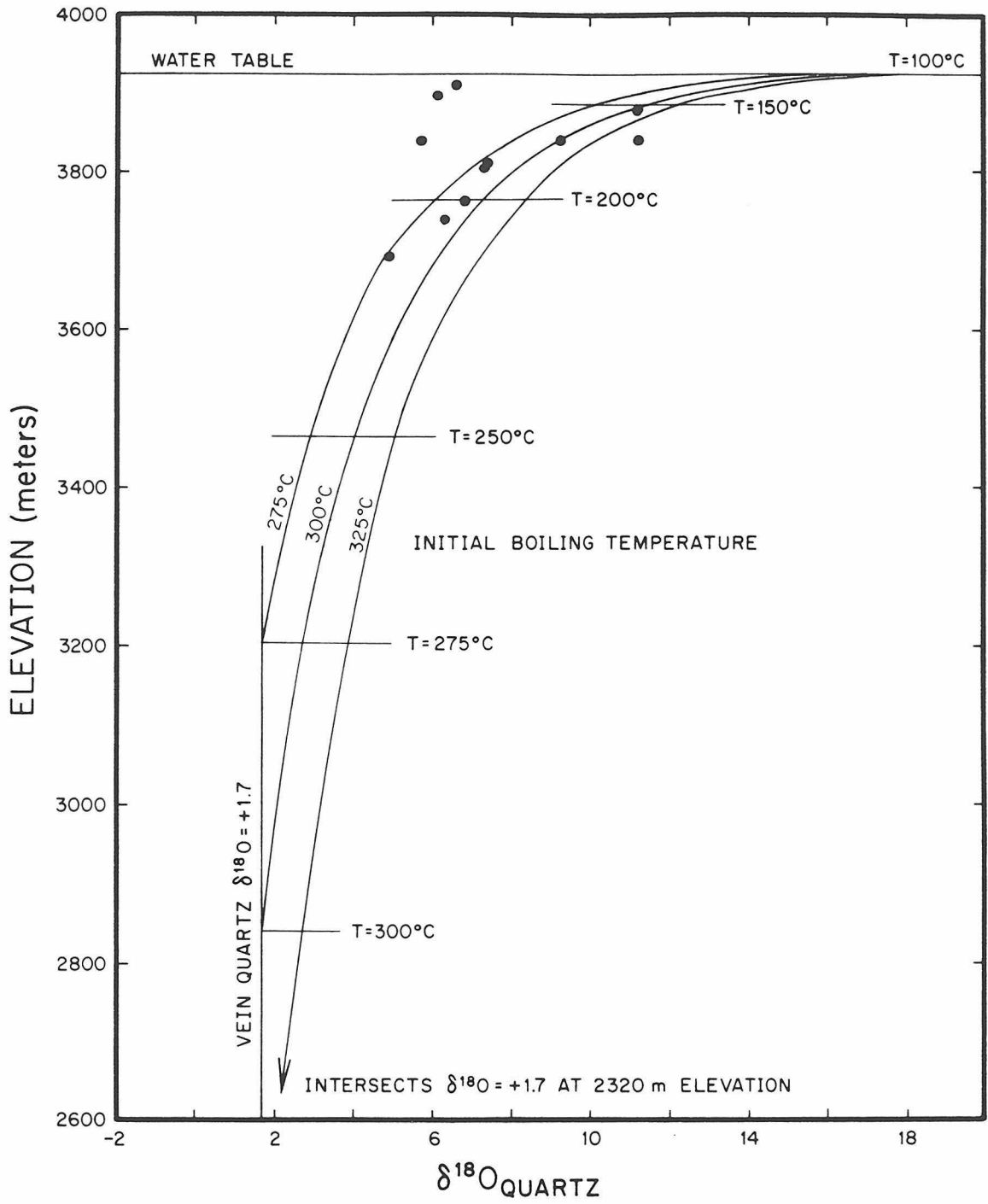
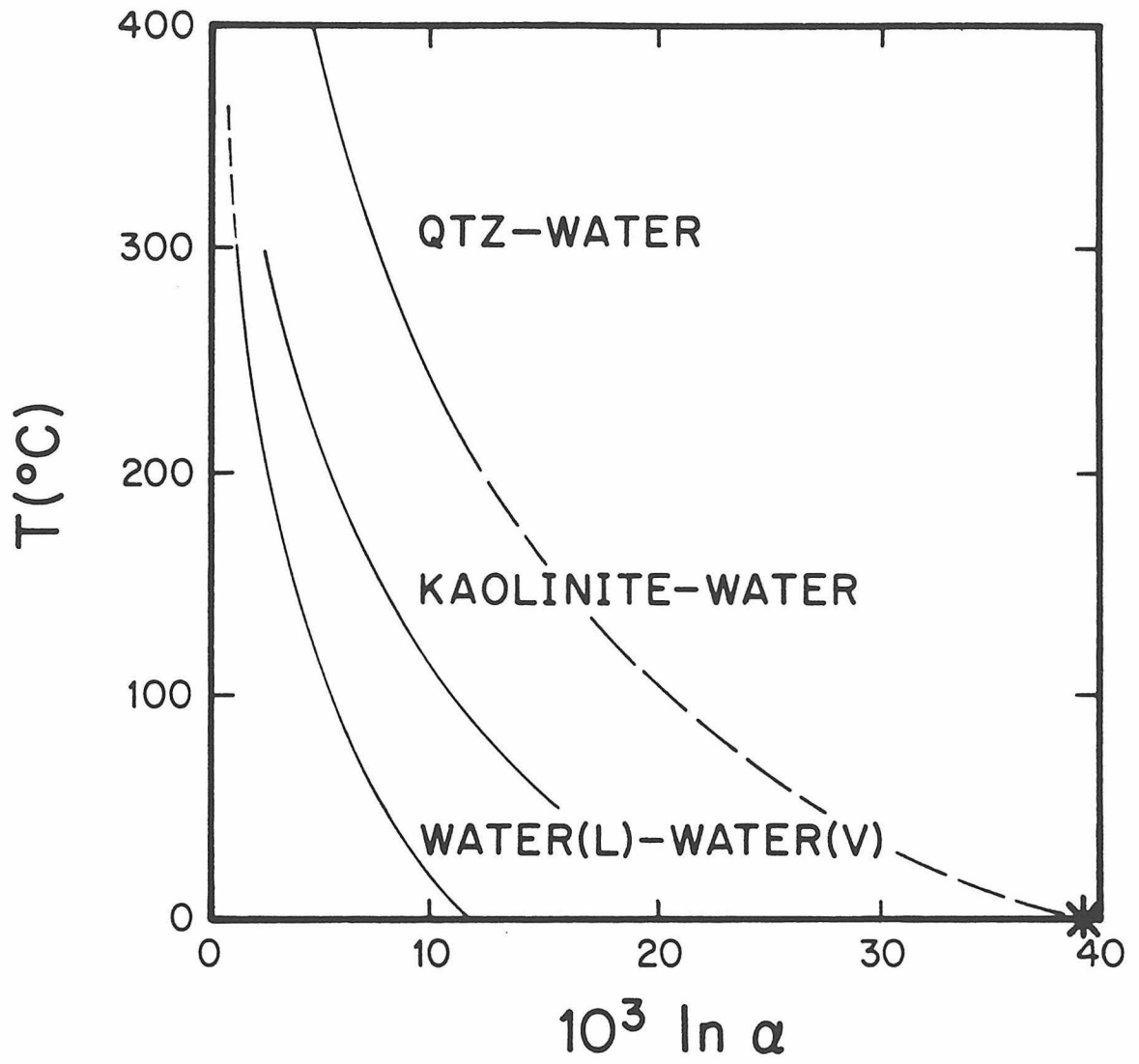


Figure 5.9 Oxygen isotopic fractionation curves used in the Red Mountain solfataric model. Data sources are listed in the text. Quartz-water fractionations between 100° and 200°C (dashed line) were interpolated between the >200°C curve and the data point at 0°C (asterisk), assuming a linear dependence of the fractionation on $1/T^2$. Comparison of the quartz-water and water(L)-water(V) curves shows that the high- $\delta^{18}O$ quartz values in the shallow solfataric environment are more a result of increasing quartz-water ^{18}O fractionations as a function of decreasing temperature, rather than the oxygen isotopic fractionation between the liquid and vapor phases.



evidence that the alteration at Red Mountain was produced in a shallow hot spring environment. Temperature conditions in the rising fluid were controlled by the hydrostatic boiling curve. Moreover, the fluid involved in the solfataric alteration was the same ^{18}O -shifted meteoric-hydrothermal fluid from which the QBP vein minerals were precipitating at depth. Three points lie off the model trend (RM-15, RM-16, and RM-23). These samples are readily interpreted to have formed (at equilibrium) from liquid H_2O condensed from a steam phase that originally separated at depth from the liquid phase and moved upward isothermally. The restricted location of these three samples, near the summit of Red Mountain, probably defines the location of a major steam vent.

Projecting the trend defined by these three points back to the boiling curve suggests that the steam-liquid separation occurred between about 150 and 200 m beneath the water table. Although conductive cooling of the fluid as it approached the surface or mixing with cool, near-surface meteoric water both probably occurred to some extent, neither process can account for these three data points. Both cooling and mixing would shift the equilibrium $\delta^{18}\text{O}$ value of the quartz to heavier values because of the significant increase in quartz-water fractionation with decreasing temperature (Fig. 5.9).

The vertical isotopic gradient observed in whole-rock samples of the AMOCO Red Mountain drill core (Fig. 5.2) also is consistent with hydrothermal alteration along a vertical thermal gradient, but extending to much greater depths, probably into an environment too deep for boiling to occur. Based on infrared absorption spectroscopy, the clays in the core sample from a depth of 283.8 m consist dominantly of

kaolinite with minor illite. Clays throughout the upper part of the drill hole petrographically resemble the clays in this sample. Alteration in all these samples is dominantly quartz and these clays. Both quartz and kaolinite exhibit increasing mineralwater fractionations as a function of decreasing temperature (Fig. 5.9), suggesting that the isotopically heavier samples from the upper portion of the drill hole were altered at a lower temperature than samples deeper in the hole. As discussed in Section 5.1.3, water/ rock ratios of about 0.5 are estimated for open system alteration of the most ^{18}O -depleted samples in the AMOCO drill core.

5.4 Solfataric Alteration Elsewhere in the San Juan Mountains

5.4.1 Localities Studied in this Work

Solfataric alteration similar to that at Red Mountain is developed in several other areas throughout the San Juan Mountains. Hydrothermal quartz samples from a number of such areas were analyzed in order to determine if their isotopic compositions can be explained using the Red Mountain model. None of these areas provides the degree of vertical control found at Red Mountain in the Lake City area, but if high $^{18}\text{O}/^{16}\text{O}$ ratios could be obtained from surface samples, it would strongly suggest that such a boiling system was operating. Additionally, economic mineralization occurs in a number of these altered areas, and the $\delta^{18}\text{O}$ analyses can provide insight into the ore-forming process in shallow volcanic environments.

The six areas studied, including the Red Mountain lava ring domes from the Lake City caldera, are: (1) Engineer Pass and Carson Camp,

just outside the Lake City caldera in older volcanic rocks; (2) the productive Red Mountain district on the west edge of the ring fault of the Silverton caldera; (3) Calico Peak, a small deposit located within a quartz latite porphyry intruding Mesozoic sedimentary rocks about 20 km west of the edge of the San Juan volcanic field; and (4) the major Summitville ore district in the eastern San Juan Mountains, just north of the Platoro caldera. The characteristics of these localities are tabulated in Table 5.3, together with information concerning the lithology, alteration, and mineralization associated with each area. The locations of the six areas are shown on Figure 5.10.

5.4.2 Characteristic Features of the Six Localities

The six areas studied in this work exhibit many similarities, which include:

1. All of the altered areas, except Carson Camp, are associated with silicious intrusive rocks of the bimodal assemblage. Quartz latites, with coarse sanidine phenocrysts as large as 5 cm, host the alteration in four of the six areas.

2. Where radiometric or fission-track ages are available for the alteration minerals, the alteration can be shown to be no more than a few million years (generally less than 0.5 million years) younger than the associated host rocks. The spatial association of the alteration to the associated intrusions in areas in which alteration dating has not been reported suggest similar contemporaneity.

3. All of the altered zones are centered on breccias related to intrusion except at Carson Camp, where the altered zones follow linear

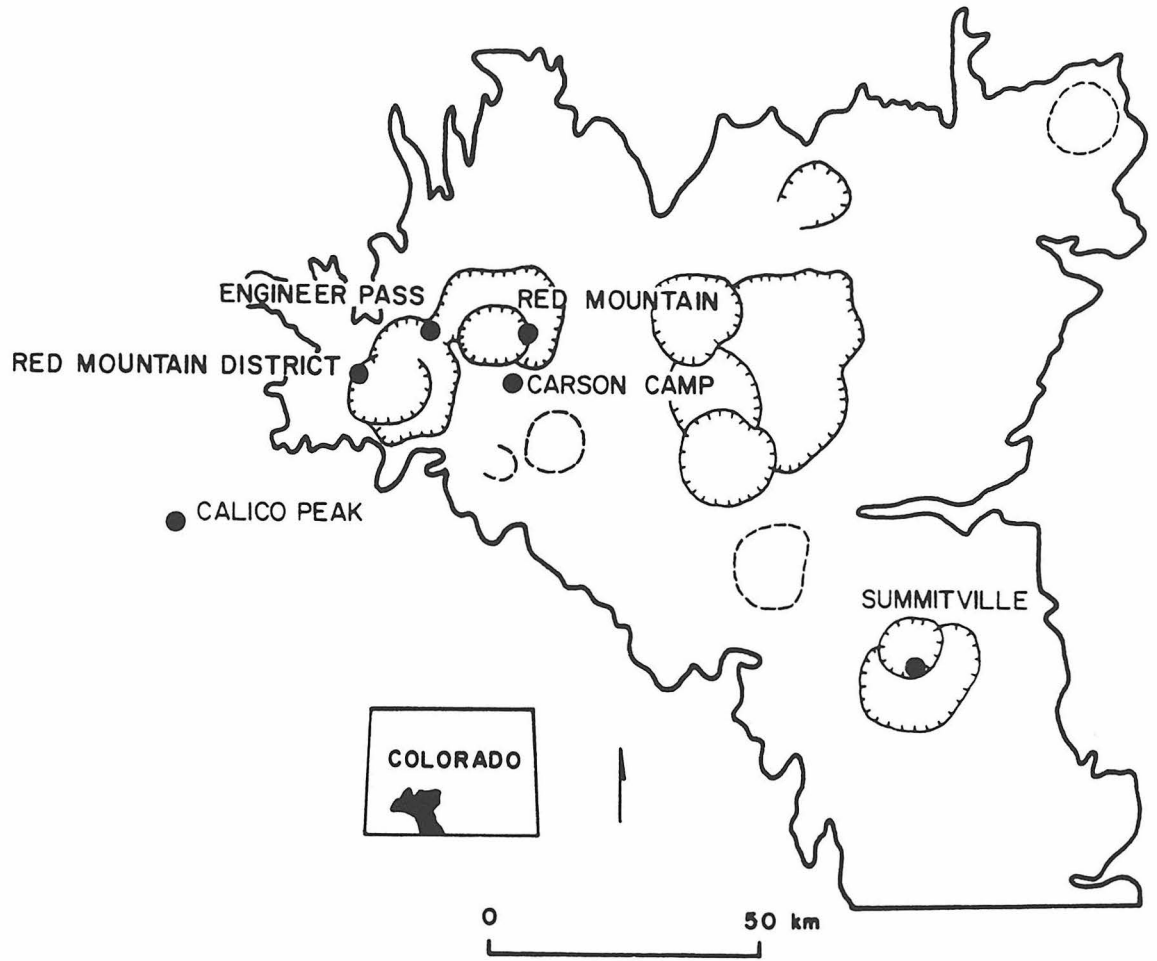
Table 5.3 Summary of characteristics of some solfatarically altered areas in the San Juan Mountains.

Location	¹⁸ O _{QUARTZ} ¹	Host Lithology	Age of Host	Alteration ²	Age of Alteration	Hypogene Ore Minerals ²	Production
Red Mountain	4.9-11.2	Red Mountain quartz latite ³	22.7-22.9 m.y. ⁴	Oz-Al-K/I	22.3-22.9 m.y. ⁵	Py	None
Carson Camp	11.9-11.6	Andersite-rhyodacite prophyry, core of Carson volcano ³	29.6 m.y. ⁶	Oz-Ba zones grade out through Oz-Al-K/I to prop ⁷	Spatially related to core of Carson volcano ⁶	Py-En-Sp-Gn-Cp-Ma-Sulfosalts ⁷	\$150,000 ⁷
Engineer Pass	6.4	Composite rhyolite-basalt stock ^{3,8}	15.4 m.y. ⁶	Oz core, grades out through K/I to prop ⁸	12.0 m.y. ⁸	Py-Gn-Sulfosalts ⁸	None
Red Mountain District-National Belle Mine	10.0-12.3	Quartz latite intrusions ⁹	22.6-22.7 m.y. ⁶	Oz cores with complex clay selvages; Ba-C-Fl ^{9,10}	Spatially related to quartz latite plugs ⁹	Py-En-Sp-Gn-Cp-Cv-Sulfosalts ⁹	\$1,000,000 ⁶
Calico Peak	6.9-9.0	Calico Peak prophyry (quartz latite) ¹¹	4.5-4.6 m.y. ¹²	Oz-Al-Zn-S core with K/I-Se margins ¹¹	Spatially related to Calico Peak porphyry ¹¹	Oz-Mo-Py veinlets, Py-En peripheral to porphyry ¹¹	Minor gold ¹¹
Summitville	13.0-15.5	Quartz latite flows ¹³	22.8-22.9 m.y. ¹⁴	Porous Oz-Al pipes grade out through K/I to prop; Ba ¹³	22.3-22.4 m.y. ¹⁴	Py-Cv-En-S-Au-Cp Sulfosalts ¹³	\$7,400,000 ¹³

Footnotes

- All data is per mil, relative to SMOW.
- Mineral and alteration abbreviations as follows: Al, alunite; Au, gold; Ba, barite; C, carbonate; Cp, chalcopyrite; Cv, covellite; En, enargite; Fl, fluorite; Gn, galena; K/I, kaolinite/illite; Ma, marcasite; Mo, molybdenite; prop, propylitization; Py, pyrite; Oz, quartz; S, sulfur; Se, sericite; Sp, sphalerite; Zn, zunyite.
- Lipman (1976a).
- Mehner et al (1973a).
- Mehner et al (1980).
- Lipman et al (1976).
- Larsen (1911).
- Maheer (1982).
- Luedke and Burbank (1969).
- Luedke and Hosterman (1971).
- Serna-Isaza (1971).
- Naeser et al (1980).
- Steven and Ratte (1960).
- Mehner et al (1973b).

Figure 5.10 Locations of solfatarically altered areas in the San Juan Mountains from which oxygen isotopic data have been obtained. The map shows the outline of the volcanic field, and the location of all known calderas (dashed where buried).



structures. Similar linear control has occurred in some altered areas at Summitville.

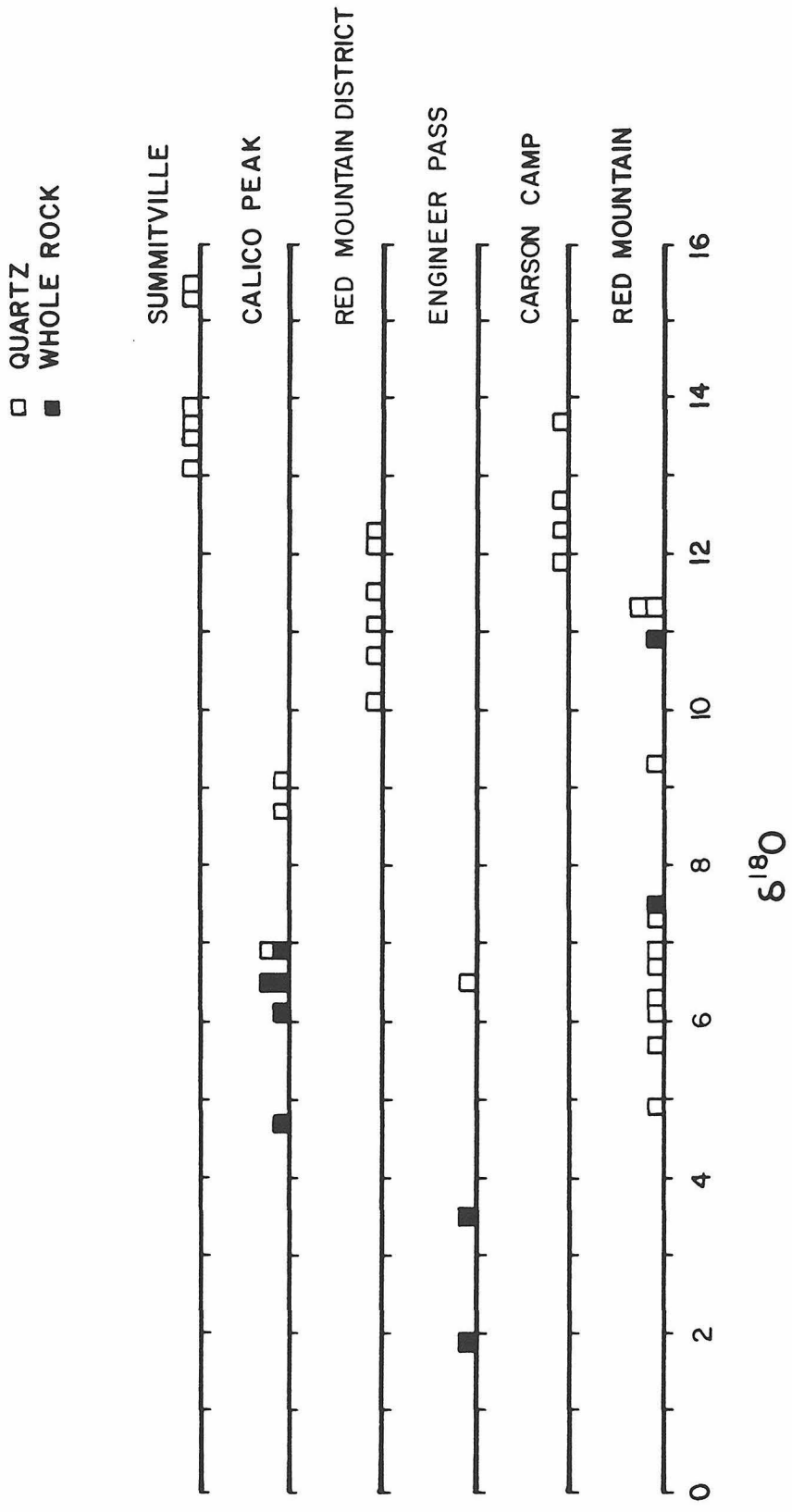
4. Without exception, the solfatarically altered zones consist dominantly of quartz and alunite. Barite is also reported from three of the six areas. The quartz-alunite alteration always grades outward through kaolinite/illite argillized zones to fresh or propylitized rocks. Where detailed analyses have been conducted, this outer argillized zone has been shown to consist of a more complicated clay assemblage, but lack of information precludes generalizations regarding detailed alteration clay mineralogy.

5. Where present, hypogene ore deposits in the altered areas tend to be restricted to the quartz-alunite assemblage, occurring in vuggy leached rocks or in larger solution spaces. The ore mineralogy is dominated by pyrite and enargite. Minor sphalerite, galena, silver sulfosalts, gold, native sulfur, and copper sulfides are widespread. Calico Peak is unique in that quartz veinlets containing molybdenite and pyrite are present, as well as because pyrite-enargite bodies are developed peripheral to the quartz-alunite altered area, not within it.

5.4.3 Discussion of the Isotope Data

Histograms of $\delta^{18}\text{O}$ data from the six areas are compared in Figure 5.11. All samples show varying degrees of ^{18}O enrichment, to as high as +15.5 per mil for Summitville. These ^{18}O enrichments all indicate very low temperature equilibration between the quartz and the hydrothermal fluids, characteristic of the solfataric boiling environment.

Figure 5.11 Histograms comparing oxygen isotopic analyses of samples from solfatarically altered areas in the San Juan Mountains. Data from Red Mountain in the Lake City area are also included (bottom row).



Moreover, native sulfur, which is locally common at Summitville, occurs as euhedral crystals lining vugs. If the temperature had been above 115°C, the melting point of sulfur at atmospheric pressure, the sulfur would most likely occur as rounded droplets. Native sulfur also occurs at Calico Peak and in solfatarically altered rocks in the Red Mountain district, east of the National Belle mine, but the crystalline state of these occurrences is not known.

There is a correlation between $\delta^{18}\text{O}$ and ore enrichment. Summitville, Carson Camp, and the National Belle Mine in the Red Mountain mining district contain the most ore mineralization of the six areas and also have the highest $\delta^{18}\text{O}$ values. The most productive district of all, Summitville, also contains the highest- ^{18}O quartz. The high metal contents and high $\delta^{18}\text{O}$ values in these 3 districts could conceivably be derived from associated magmatic hydrothermal fluids released by the crystallization of the magmas; such fluids would have $\delta^{18}\text{O}$ values in the range of about +7 to +10 per mil. The widespread occurrence of brecciation in these rocks might also be construed to support such a model. In addition, lead isotopic analyses of galena from the Summitville district have shown that this lead is radiometrically similar to lead from the quartz latite hosts (Doe et al, 1979).

Mixing of such high- ^{18}O fluids with an evolved meteoric-hydrothermal fluid having a $\delta^{18}\text{O}$ value of about -8, typical of vein-forming fluids from the Sunnyside mine (Casadevall and Ohmoto, 1977) and from the Lake City caldera, would produce fluids with intermediate $\delta^{18}\text{O}$ values. This would produce a higher- ^{18}O hydrothermal quartz than could be precipitated by purely meteoric water. However, pure magmatic

water of the above composition would produce solfataric quartz with $\delta^{18}\text{O}$ values to as high as 38 per mil for the shallowest portion of the Red Mountain model. Hence, a significant magmatic component in the fluids in all these areas is considered to be highly unlikely. Variations in the isotopic compositions of the hydrothermal quartz are more likely related to local variations in the meteoric water input into the meteoric-hydrothermal system, or to variations in the level of exposure in the various areas.

Any model which accounts for the solfatarically controlled mineralization must invoke meteoric water as the dominant component of the hydrothermal fluid. If a model is constructed whereby the metal components in the fluid are released by a crystallizing magma, then a mechanism must be used to mix and dilute this magmatic emanation with a meteoric-hydrothermal fluid prior to transport of the fluid to the point of deposition.

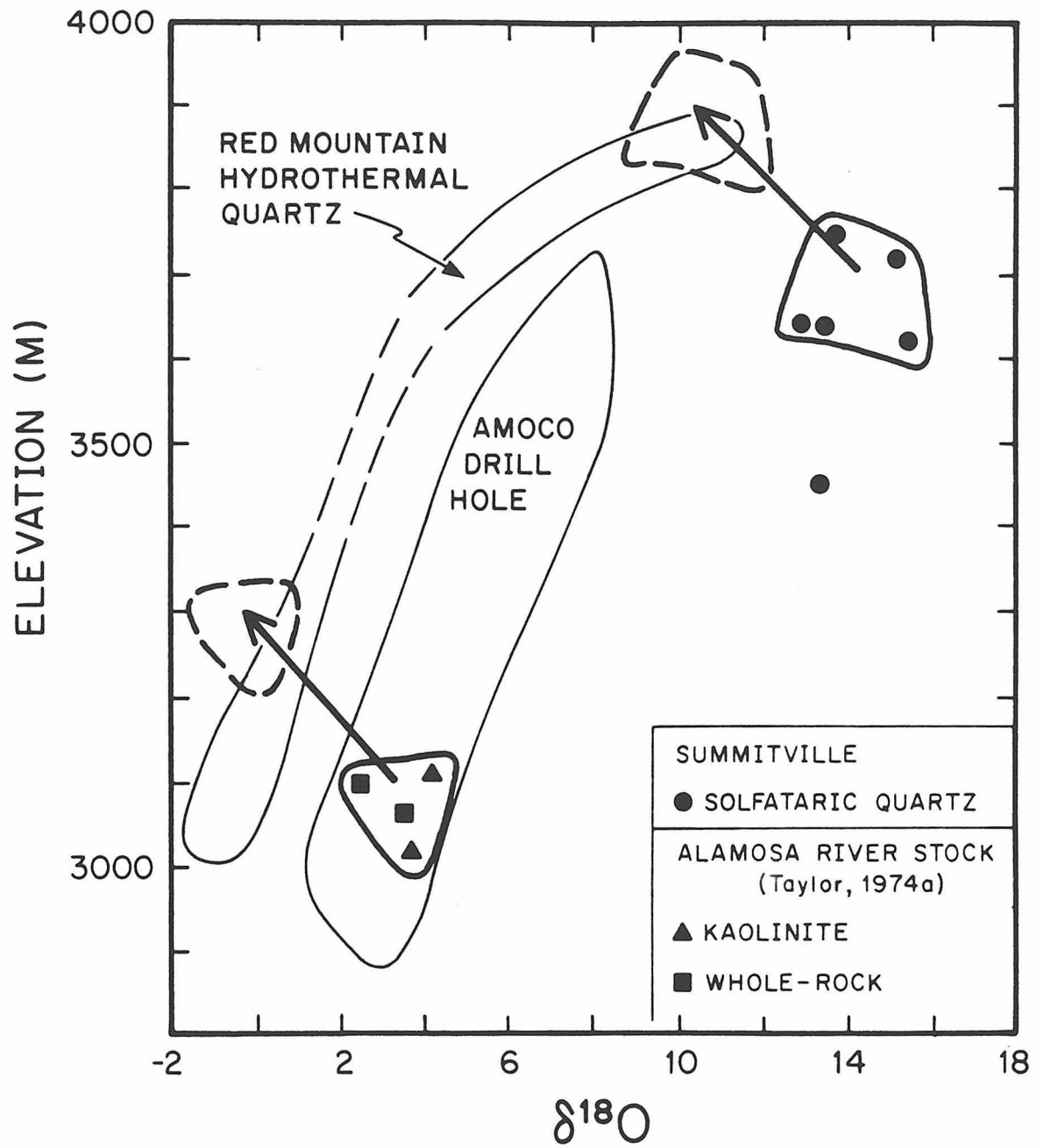
δD analyses of hydrous alteration minerals from the Alamosa River stock, eastern San Juan Mountains, are markedly richer in deuterium than those from the Silverton caldera (about -110 vs. about -145, respectively, see Taylor, 1974a). These data suggest that the initial meteoric water $\delta^{18}\text{O}$ values in the eastern San Juan Mountains were about 5 per mil higher (-10 per mil) than that in the western San Juans (-15 per mil) in mid-Tertiary time. Thus, the heavy quartz $\delta^{18}\text{O}$ values for the Summitville district, which is about 5 km northeast of the Alamosa River stock, may be related to this higher- $\delta^{18}\text{O}$ meteoric water.

Portions of the monzonitic Alamosa River stock, exposed in the Alamosa River canyon 5 km southeast of the Summitville district and

at an elevation 1 km below it, are pervasively altered to a kaolinite-bearing assemblage (Steven and Ratte, 1960). These spatial relationships are compatible with the possibility that deeper argillic alteration associated with the Alamosa River stock may be the eroded roots of the solfataric alteration present in the Summitville district, analogous to the Red Mountain-Alpine Gulch system in the Lake City caldera. However, the available age dating does not support this hypothesis, because the Alamosa River stock has been dated by K-Ar at 28 m.y. (Lipman, 1975), while the Summitville mineralization apparently took place about 22 m.y. ago (Table 5.3). In support of these K-Ar dates, Steven and Ratte (1960) note that the alteration in the Alamosa River stock is continuous with that in the volcanic rocks outside the northern stock contact, and these altered volcanic rocks are unconformably overlain by the extrusive quartz latites that host the Summitville mineralization.

In spite of the above age discrepancies, it is instructive to examine the $\delta^{18}\text{O}$ -elevation trends in the vicinity of Summitville and the Alamosa River stock. $\delta^{18}\text{O}$ values of solfataric quartz from Summitville determined in this study and whole-rock and kaolinite $\delta^{18}\text{O}$ values measured by Taylor (1974a) for the Alamosa River stock are shown in Figure 5.12 as functions of sample elevation. Williams (1978) also presents some generalized $\delta^{18}\text{O}$ data for this intrusion. Included in Figure 5.12 are the fields of Red Mountain hydrothermal quartz and the AMOCO drill core data (see Fig. 5.2). It is apparent on Figure 5.12 that if the elevation of either the Summitville or the Red Mountain $\delta^{18}\text{O}$ values are adjusted so that the highest- ^{18}O , highest elevation

Figure 5.12 $\delta^{18}\text{O}$ values of solfataric quartz from Summitville (this study) and altered rocks and kaolinite from the Alamosa River stock (Taylor, 1974a) plotted as functions of sample elevation. The general distribution of $\delta^{18}\text{O}$ values of hydrothermal quartz from Red Mountain and whole-rocks from the AMOCO drill hole are also shown (see Fig. 5.2). The arrows indicate how the $\delta^{18}\text{O}$ values and elevations at Summitville and the Alamosa River stock would have to be adjusted to make them directly comparable with the Red Mountain solfataric data. See text for discussion.



solofataric quartz values in both groups coincide (that is, adjusting these data sets so the $\delta^{18}\text{O}$ of the fluid and the position of the water table at the time of alteration were identical, and assuming that the temperatures of alteration were similar), the Alamosa River stock whole-rock $\delta^{18}\text{O}$ values would be about 5 per mil lower than the AMOCO drill hole $\delta^{18}\text{O}$ values for an equivalent depth beneath the solofataric zone. These relationships are in agreement with the above described age information, indicating that alteration of the Alamosa River stock is not related to the the Summitville solofataric alteration in a manner similar to that found for the Red Mountain-Alpine Gulch alteration.

$^{18}\text{O}/^{16}\text{O}$ RELATIONSHIPS WITHIN THE LAKE CITY CALDERA6.1 Initial Oxygen Isotopic Compositions of the Intra-Caldera Volcanic and Volcaniclastic Rocks6.1.1 Initial $\delta^{18}\text{O}$ Values of the Sunshine Peak Tuff and Resurgent Intrusive Rocks

Because the Sunshine Peak Tuff and the resurgent intrusive rocks are mineralogically very similar, and probably are derived from the same underlying magma chamber, they are discussed together in this section. The tuff consists of 30 to 50 percent phenocrysts of embayed quartz and euhedral sanidine, with less than 2 volume percent biotite and plagioclase. The groundmass, originally vitrophyric, is recrystallized to fine-grained quartz and sanidine. The tuff can be considered virtually a bimineralic rock containing approximately 40 percent quartz and 60 percent alkali feldspar. The intrusive rocks consist of coarse (to greater than 1.5 cm) alkali feldspar phenocrysts in a matrix of quartz and alkali feldspar (typically 1 to 3 mm grain size). Plagioclase and biotite are generally also present as phenocrysts, but are not abundant. Embayed quartz and pyroxene locally occur as phenocrysts, but generally constitute less than 1 percent of the rock.

The original oxygen isotopic compositions of the Sunshine Peak Tuff and the intrusive rocks from within the caldera cannot be directly measured because of ubiquitous effects of post-crystallization, meteoric-hydrothermal alteration. However, two samples of outflow-facies Sunshine Peak Tuff, CC-7 and CC-8, collected on the eastern side of Jarosa Mesa, about 15 km east of the caldera, are unaltered. The

outflow-facies is equivalent to the lowermost, highest SiO₂, member of the Sunshine Peak Tuff (Tspl) within the caldera. Quartz phenocrysts from these two outflow-facies samples yield identical $\delta^{18}\text{O}$ values of +8.1. Sanidine phenocrysts have $\delta^{18}\text{O} = +7.0$ (CC-7) and +6.8 (CC-8). Quartz phenocrysts separated from three tuff samples collected within the caldera, SC-19, SC-81, and AG-1, are also all identical at $\delta^{18}\text{O} = +8.1$.

The $^{18}\text{O}/^{16}\text{O}$ fractionations between the quartz-sanidine pairs in CC-7 and CC-8 are 1.1 and 1.3 per mil, which are characteristic of unaltered ash-flow tuffs (see Part II of this thesis). The average fractionation of 1.2 per mil indicates an equilibrium temperature of about 625°C (Bottinga and Javoy, 1973), which is slightly lower than the plausible eutectic temperatures in the granite-H₂O system (Tuttle and Bowen, 1958). However, it should also be noted that a quartz-orthoclase fractionation of 1.8 per mil was experimentally determined at 600°C by Blattner and Bird (1974), in which case the (equilibrium) magmatic temperature would be considerably higher than 625°C for a fractionation of 1.2 per mil. Regardless of which geothermometer calibration curves are chosen, the quartz and sanidine $\delta^{18}\text{O}$ analyses in the Sunshine Peak Tuff clearly represent primary, unaltered phenocryst compositions.

Taylor (1968) showed that feldspars in granitic melts are typically 0.2 to 0.4 per mil lower in ^{18}O than the melt; this would indicate an initial $\delta^{18}\text{O}$ of 7.2 ± 0.2 per mil for the magma that produced the outflow facies of the Sunshine Peak Tuff. Sample SC-129, collected from the upper member of the Sunshine Peak Tuff in the southeastern quadrant of the caldera (an area where hydrothermal effects are very

weak or lacking) yields a whole-rock $\delta^{18}\text{O} = +7.3$. This is the average of four replicate analyses with a standard deviation of 0.1 per mil. Both the feldspar and the biotite in this sample are very fresh with no mineralogical alteration effects. We therefore conclude that the Sunshine Peak Tuff rhyolitic magma ($\approx 250 \text{ km}^3$, Steven and Lipman, 1976) was isotopically relatively homogeneous, with a $\delta^{18}\text{O} \approx +7.2$ or $+7.3$, and that all measured whole-rock $\delta^{18}\text{O}$ values different from this value must represent a subsolidus hydrothermal effect.

Whole-rock $^{18}\text{O}/^{16}\text{O}$ analyses of the aforementioned outflow facies samples of the Sunshine Peak Tuff are $+8.2$ (CC-7) and $+7.8$ (BHS-1A, provided by Ken Hon of the U. S. Geological Survey, sample location not identified). Both analyses are slightly heavier than the calculated value of 7.2 per mil. Although this conceivably could indicate an original $\delta^{18}\text{O}$ inhomogeneity in the Sunshine Peak magma, these minor ^{18}O enrichments are better attributed to low-temperature exchange between the vitrophyric, glassy, matrix of the tuff and surface meteoric water. This has been shown by Taylor (1968) to be a very common feature in all hydrated volcanic glasses; in extreme cases the $\delta^{18}\text{O}$ values are raised to as high as $+16$ per mil.

All analyzed samples of resurgent intrusive rocks from within the Lake City caldera have been hydrothermally altered, and are depleted in ^{18}O relative to normal magmatic values. Phenocrystic quartz and alkali feldspar separated from sample SC-161 yield $\delta^{18}\text{O}$ values of $+7.9$ and -1.1 , respectively. Three other alkali feldspar separates from resurgent intrusive rocks have $\delta^{18}\text{O} = -4.0$ to 2.9 . The quartz-alkali feldspar fractionation for sample SC-161 is 9.0 per mil, clearly a

nonmagmatic and a disequilibrium fractionation. In a mid-Tertiary caldera environment eroded to a deeper level than the Lake City area, Criss and Taylor (1983) showed that magmatic quartz exchanges oxygen with hydrothermal fluids very slowly; coarse quartz phenocrysts closely maintain their magmatic $^{18}\text{O}/^{16}\text{O}$ values in a hydrothermal environment, whereas coexisting feldspars exchange quite quickly (Fig. 4.4). The quartz analysis from SC-161, therefore, is probably close to the original magmatic value, suggesting that quartz from both the resurgent intrusions and Sunshine Peak Tuff initially had quite similar $\delta^{18}\text{O}$ values of about +8.1. Thus, as a working hypothesis, we assume that the magmas that formed the Lake City resurgent intrusive rocks all had $\delta^{18}\text{O} \approx +7.2$, and that the whole-rock samples also originally had this value prior to hydrothermal alteration.

6.1.2 Initial $\delta^{18}\text{O}$ Values of the Sunshine Peak Tuff Megabreccia

The Sunshine Peak Tuff megabreccia units were dominantly derived from the older San Juan volcanic rocks (Sapinero Mesa Tuff and andesitic volcanics related to the early calc-alkaline magmatic episode) and the Precambrian granite of Cataract Gulch (Lipman, 1976b), both of which currently form the outer wall of the Lake City caldera ring fault (see Chapter 4). The granite composes a significant proportion of the megabreccia only along the southern margin of the caldera, where the granite actually forms the outer wall of the ring fault.

The initial isotopic compositions of the megabreccia units are difficult to estimate, as the clasts in these units have been derived from a variety of volcanic sources, some of which had been previously

altered during meteoric-hydrothermal activity associated with the Uncompahgre caldera. For example, Lipman et al (1976) noted that altered rocks in the Capitol City area, just outside the northern margin of the Lake City caldera, are truncated by the Lake City caldera ring fault, and that fragments resembling these altered rocks occur in megabreccia units in the Lake City caldera in this area. Similarly, altered rocks with associated vein mineralization make up the eastern topographic wall of the caldera; these are unconformably overlain by the quartz latite ring domes (Lipman et al, 1982). However, in pre-caldera magmatic rocks immediately adjacent to the southern, western, southeastern, and northeastern margins of the caldera we have not found evidence of any pre-Lake City alteration. The ^{18}O depletions in these rocks are clearly spatially related to the Lake City caldera ring fault, indicating that the hydrothermal activity that produced these ^{18}O depletions must have been related to the Lake City caldera hydrothermal system. It was shown above that the initial magmatic $\delta^{18}\text{O}$ value of the Precambrian granite of Cataract Gulch was +9.5. The $\delta^{18}\text{O}$ values of fresh, unaltered volcanic rocks throughout the world (including samples from elsewhere in the San Juan Mountains) are typically in the range +6.0 to +10.0 per mil. It is thus reasonable to conclude that when the masses of Sunshine Peak Tuff megabreccia slid into the collapsed caldera, they probably had normal magmatic $\delta^{18}\text{O}$ values somewhere in the range +6.0 to +10.0 per mil.

6.2 Variations in Alteration Mineralogy and $\delta^{18}\text{O}$ in the Megabreccia

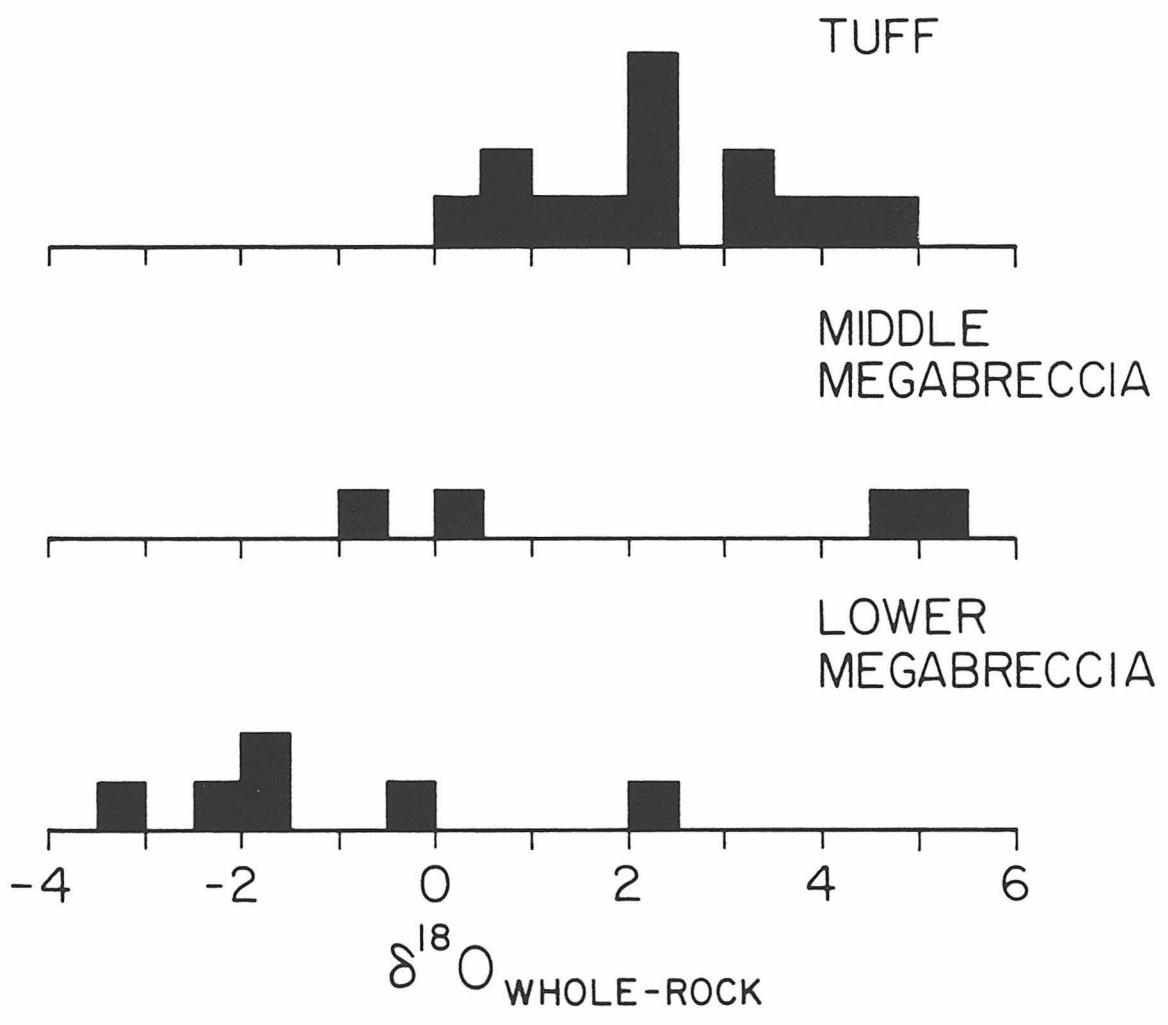
The Sunshine Peak Tuff megabreccia generally is more strongly

depleted in ^{18}O than the caldera-fill Sunshine Peak Tuff (Fig. 6.1). Because it has a mixed initial lithology and because it has been altered to diverse phases, it is not possible to construct meaningful water/rock ratio plots for this unit, as was done for the Precambrian granite in Chapter 4 or as is done below for the Sunshine Peak tuff caldera-fill. However, the overall large ^{18}O depletions within the megabreccias strongly suggest that these units have interacted with large volumes of low- ^{18}O water, or that they have interacted with the meteoric-hydrothermal fluids at relatively high temperature (or both).

The stratigraphically lowest megabreccia units exhibit ^{18}O depletions and alteration products distinct from higher units. Figure 6.1 compares $\delta^{18}\text{O}$ analyses from the lower megabreccia unit in the Burrows Park-Silver Creek-Redcloud Peak area (southwestern part of the caldera) with the $\delta^{18}\text{O}$ values of the upper megabreccia lenses found elsewhere in the caldera. The lower unit, exposed below about 3500 m elevation, is clearly more ^{18}O depleted than the upper unit, to values as low as -2.1. The rocks in the lower unit are generally more than 40 percent altered to calcite, quartz, chlorite, sericite, clay, and pyrite. The upper unit isotopic analyses range to as high as +8.9, and the rocks are fresh or are weakly argillized and silicified. One sample of the upper unit, SC-154, has a $\delta^{18}\text{O}$ value of -0.9, but this sample was collected within an argillized quartz vein selvage.

The variation in alteration mineralogy between the upper and lower megabreccia units is somewhat similar to that observed in the tuff, where argillization is characteristic of higher elevations, while a calcite-chlorite alteration and lower $\delta^{18}\text{O}$ values characterize lower eleva-

Figure 6.1 Comparison between $\delta^{18}\text{O}$ values of megabreccia and tuff in the southwest quarter of the Lake City caldera. The lower histogram shows the whole-rock $\delta^{18}\text{O}$ values from the large megabreccia exposure in Burrows Park, Silver Creek, and Cooper Creek. The upper histogram shows $\delta^{18}\text{O}$ values of Sunshine Peak Tuff ash-flow samples within about 1.5 km horizontally and about 1000 m vertically from the upper contact of this exposure of megabreccia. The middle histogram shows whole-rock $\delta^{18}\text{O}$ values of the upper megabreccia lenses. Note that the megabreccia units are typically more strongly depleted in ^{18}O than the tuff (particularly the lower megabreccia).



tions. This strongly suggests that the lower megabreccia unit exchanged oxygen with the hydrothermal fluid at higher temperatures than the upper unit, as also would be expected in terms of the geothermal gradient. Also, because it contains a significantly greater proportion of alteration product phases, the lower unit almost certainly has undergone exchange with a larger volume of water than the fresh to weakly altered upper unit.

Because of the porous matrix of the megabreccia units (particularly right after their formation 23 m.y. ago), and because the lower unit has clearly undergone a marked degree of water-rock interaction, the lower megabreccia unit probably was a major channel for the meteoric-hydrothermal fluids in the Lake City hydrothermal system. Similar types of alteration and ^{18}O depletions (to $\delta^{18}\text{O} = -1.4$) in the megabreccia in the northeastern part of the caldera (lower Alpine Gulch) show that this zone was also a major fluid channel. The ^{18}O depletions in Sunshine Peak Tuff around these units generally are not as great as in the megabreccias (Fig. 6.1). For example, two samples collected about 8 meters on either side of a tuff-megabreccia contact in lower Cooper Creek exhibit quite distinct isotopic compositions. The megabreccia sample, SC-63, is partially altered to calcite, quartz, sericite, and clays, and has a $\delta^{18}\text{O}$ value of -1.7. The tuff sample, SC-64, with sanidine partially altered to clay and quartz and biotite totally altered to sericite, has a $\delta^{18}\text{O}$ value of +3.4. This 5.1 per mil difference is best explained by a higher water/rock in the more permeable and more porous megabreccia unit.

6.3 Mineralogical Alteration of the Sunshine Peak Tuff

Using the primary $\delta^{18}\text{O}$ values defined above, it is clear that essentially all samples of Sunshine Peak Tuff and the resurgent intrusive rocks from within the caldera were depleted in ^{18}O by 1 to 10 per mil (Fig. 4.2); most samples also exhibit a complementary mineralogical alteration. Because of their fine grain size and simple mineralogy, (basically just quartz and alkali feldspar) it is not possible to examine the water-mineral interactions in these lithologic units with the same detail as was done for the coarser-grained multi-mineralogic Precambrian granite of Cataract Gulch. However, the systematic ^{18}O -depletions in these altered rocks correlate very well with the type and intensity of mineralogical alteration products in the rocks.

Within the high interior of the caldera, areas of most intense mineralogical alteration form bright red to orange surface exposures due to the oxidation of minor amounts of disseminated pyrite in the altered rocks. Quartz veins (typically about one meter wide and bearing base-metal sulfides and pyrite) are central to many of these altered areas. The altered zones thus represent very wide selvages around the quartz veins, some extending farther than 100 m from the veins. Plate 2 (in pocket) shows the distribution of the altered areas within the caldera. Plate 2 was compiled based on field observations of the distribution of mineralogic alteration in the Sunshine Peak Tuff and on petrographic determination of mineralogic alteration in the samples that were analyzed. The alteration facies (defined below) for each sample was recorded on a map, and facies boundaries were then drawn. Detailed mapping of the distribution of alteration facies was not conducted in

the field, and therefore in areas of low sample density some leeway must be assumed for placement of the facies boundaries.

The type and quantity of alteration products in the altered Sunshine Peak Tuff change gradationally away from the quartz veins. Five zones (or facies) can be identified in the altered tuff (Table 6.1), four of which are delineated on the map in Plate 2.

Zone I, developed within a meter or so of the veins, consists of total replacement of the tuff by hydrothermal quartz. Relict zircons are preserved. Primary quartz phenocrysts are recrystallized to finer grained aggregates of quartz grains, but can be recognized in hand samples and thin sections.

Zone II, developed within tens of meters of zone I, is characterized by the total replacement of sanidine and biotite by quartz and a white to light-brown, fine-grained clay, tentatively identified as a mixture of kaolinite and illite. Quartz phenocrysts may show minor recrystallization. The groundmass locally contains thin quartz veinlets.

Zone III grades outward from zone II and comprises partial replacement of sanidine by kaolinite/illite (?) and locally quartz, and total replacement of biotite by sericite. Disseminated pyrite is also characteristic of zones I through III.

Zone IV, the most extensively developed of the 5 alteration facies, also consists of partial replacement of sanidine by kaolinite/illite; it can be subdivided into two sub-zones, IVa and IVb, based on the degree of sericitization of biotite. In IVa, from 50 to 100 percent of the biotite is altered, and in IVb, less than 50 percent of the biotite is altered. Locally in zone IV, chlorite is the alteration product of

Table 6.1

Progressive alteration mineralogy in argillized Sunshine Peak tuff away from quartz veins.

	Zone I*	Zone II*	Zone III	Zone IV	Zone V
Sanidine	Pervasive silicification	Total replacement by quartz and clay	Partial replacement by clay and local quartz	Partial replacement by clay	Turbid
Biotite	Pervasive silicification	Total replacement by quartz and clay	Total sericitization	IVa: total sericitization IVb: fresh	Fresh
Pyrite	Disseminated, 2 to 3 percent	Disseminated, traces	Disseminated, traces	Rare	None

* Zones I and II are shown as a single unit on Plate 2.

the biotite, not sericite. Zone IV grades outward and upward to a caldera-wide weak alteration, zone V.

In zone V, sanidine exhibits only traces of the development of kaolinite/illite (?), and more commonly simply shows turbidity along cleavage planes, fractures, and grain margins. Biotite in zone V is fresh. Alteration in the resurgent intrusive rocks is similar to that in the Sunshine Peak Tuff, except chlorite commonly accompanies the sericite as an alteration product of the biotite.

The alteration zoning described above is best developed in the Sunshine Peak Tuff at elevations above about 12000 ft (3658 m). Weak pervasive alteration in more deeply eroded parts of the caldera, along Burrows Park and the lower portions of the Cooper Creek and Silver Creek drainages in the southwestern part of the caldera, and in the lower elevations in the Alpine Gulch drainage in the northeastern part of the caldera, is different than the typical zone IV alteration described above. In the lower elevations, the biotite is altered to chlorite, not sericite, and the sanidine typically is 30 to 50 percent altered to a carbonate with local green clay. This chloritic type of alteration is indicated as a separate zone on Plate 2. Quartz veins containing pyrite and base-metal sulfides in Burrows Park and in the lower Alpine Gulch drainage have narrow alteration selvages, up to 2 m wide, characterized by the pervasive development of quartz, sericite, pyrite, and minor clay (Krasowski, 1976).

Sunshine Peak Tuff within several hundred meters of the resurgent intrusive rocks has been hornfelsed. This is characterized by the recrystallization of the groundmass to an even-grained mixture of quartz

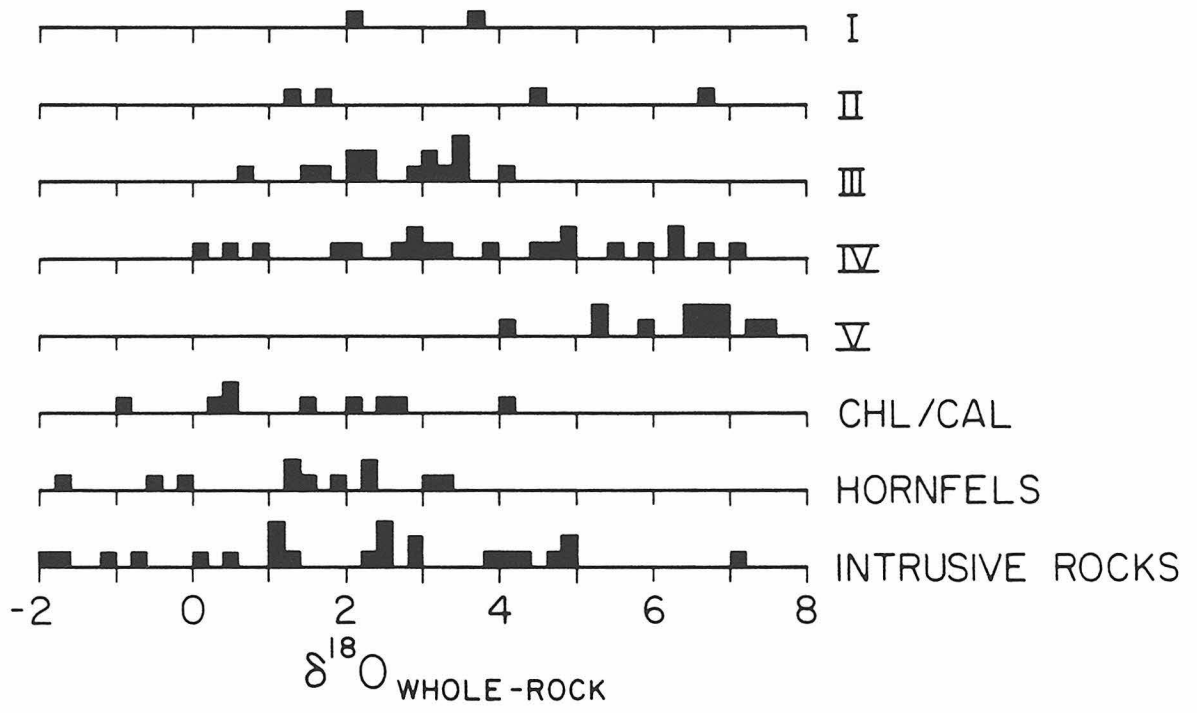
and sanidine, coarser than that typical of devitrification of the tuff throughout the rest of the caldera. The hornfelses matrix has also lost the outlines of compressed pumice shards and the light to dark brown color typical of the non-hornfelses tuff. In hand samples the hornfelses tuff is light tan in color and is somewhat lighter than nonhornfelses samples. Sanidine in the hornfelses tuff is unmixed to an alkali feldspar perthite. Hydrothermal alteration in the hornfelses tuff is typically zone IV, although some zone III and zone II hornfelses tuff is present.

6.4 Correlation between $\delta^{18}\text{O}$ Values and Alteration Assemblages

Figure 6.2 displays the range of ^{18}O analyses of the samples for each of the tuff alteration types discussed above and for the resurgent and ring fracture intrusions. Note that there is a general decrease in the $\delta^{18}\text{O}$ value as alteration progresses from zone V to zone III, but this does not continue to zones I and II (probably because these areas are intensely silicified, and quartz tends to be a very high- ^{18}O mineral). The tuff becomes progressively depleted in ^{18}O closer to the veins as the intensity of alteration increases. As a group, the tuff altered to a chlorite-calcite assemblage at lower elevations is more ^{18}O -depleted than the rocks involved in any of the zones I to V of the argillic alteration.

Variations in the extent of ^{18}O depletions in the tuff and intrusive samples allow us to estimate relative water/rock ratios, as was done for the Precambrian granite. In Figure 4.9, the degree of mineralogic alteration of original magmatic biotite in the granite was plotted

Figure 6.2 Histograms of whole-rock $\delta^{18}\text{O}$ values of the Sunshine Peak Tuff and resurgent intrusive rocks as a function of the type and facies of mineralogic alteration present in the samples. Note that ^{18}O depletions increase as the facies of argillic alteration in the tuff proceeds from stage V (freshest) to stage III. Topographically lower chlorite/calcite alteration in the tuff, however, has produced even more significant ^{18}O depletions. Although not intensely mineralogically altered, the hornfelsed tuff and the resurgent intrusive rocks have overall the lowest ranges of $\delta^{18}\text{O}$ values because they exchanged with the meteoric-hydrothermal fluids at highest temperatures.



against $\delta^{18}\text{O}$, and was used as a measure of the temperature and water/rock ratio under which the rocks had been altered. For the Sunshine Peak Tuff and intrusive rocks, an analogous plot can be made utilizing the degree of mineralogic alteration of the sanidine phenocrysts (Figs. 6.3 and 6.4). However, note that Figures 6.3 and 6.4 are not strictly comparable to Figure 4.9 because, unlike biotite, K feldspar can have a large field of stability at these moderate hydrothermal temperatures, if the pH of the fluids is sufficiently high. The degree of mineralogical alteration of K feldspar in the tuff and intrusive samples is thus only a rough estimate of water/rock ratio, because the production of kaolinite and sericite is strongly dependent on fluid chemistry, as well as on temperature and water/rock ratio (Fig. 6.5). It is important to understand that at high temperatures, or under alkaline conditions, the feldspar can thoroughly exchange oxygen isotopes with the meteoric-hydrothermal fluid without becoming extensively mineralogically altered (perhaps producing only turbidity in the feldspars). The mineralogically "unaltered" but ^{18}O exchanged sanidines in Figures 6.3 and 6.4 typically exhibit considerable turbidity in thin section; this is a normal characteristic of K feldspar that has exchanged with a meteoric-hydrothermal fluid (Taylor, 1974a).

Figure 6.3 is a plot of data from the hornfelsed and chlorite/calcite altered tuff and the resurgent and ring-fracture intrusions. Figure 6.4 is a plot of data from the argillized zones I through V tuff, and it also includes the field of hornfelsed tuff from Figure 6.3 for comparison. Figures 6.3 and 6.4, together with the models discussed in Figures 4.8 and 6.5, imply the existence of three intergradational

Figure 6.3 $\delta^{18}\text{O}$ whole-rock values of hornfelsed tuff, chlorite/calcite altered tuff, and resurgent intrusive rocks, plotted as a function of the degree of mineralogical alteration of K feldspar in the samples. The percent of sanidine in the sample that has been altered to clay and quartz is in some way proportional to the W/R ratio that the rock has experienced, but the alteration of the sanidine is also in large part controlled by fluid chemistry and temperature (Fig. 6.5). The hornfelsed tuff and the resurgent intrusive rocks have low $\delta^{18}\text{O}$ values but are not intensely altered because at high temperatures the K feldspar exchanges readily with the meteoric-hydrothermal fluids without becoming mineralogically altered (analogous to the biotite-chlorite discussion in Fig. 4.8).

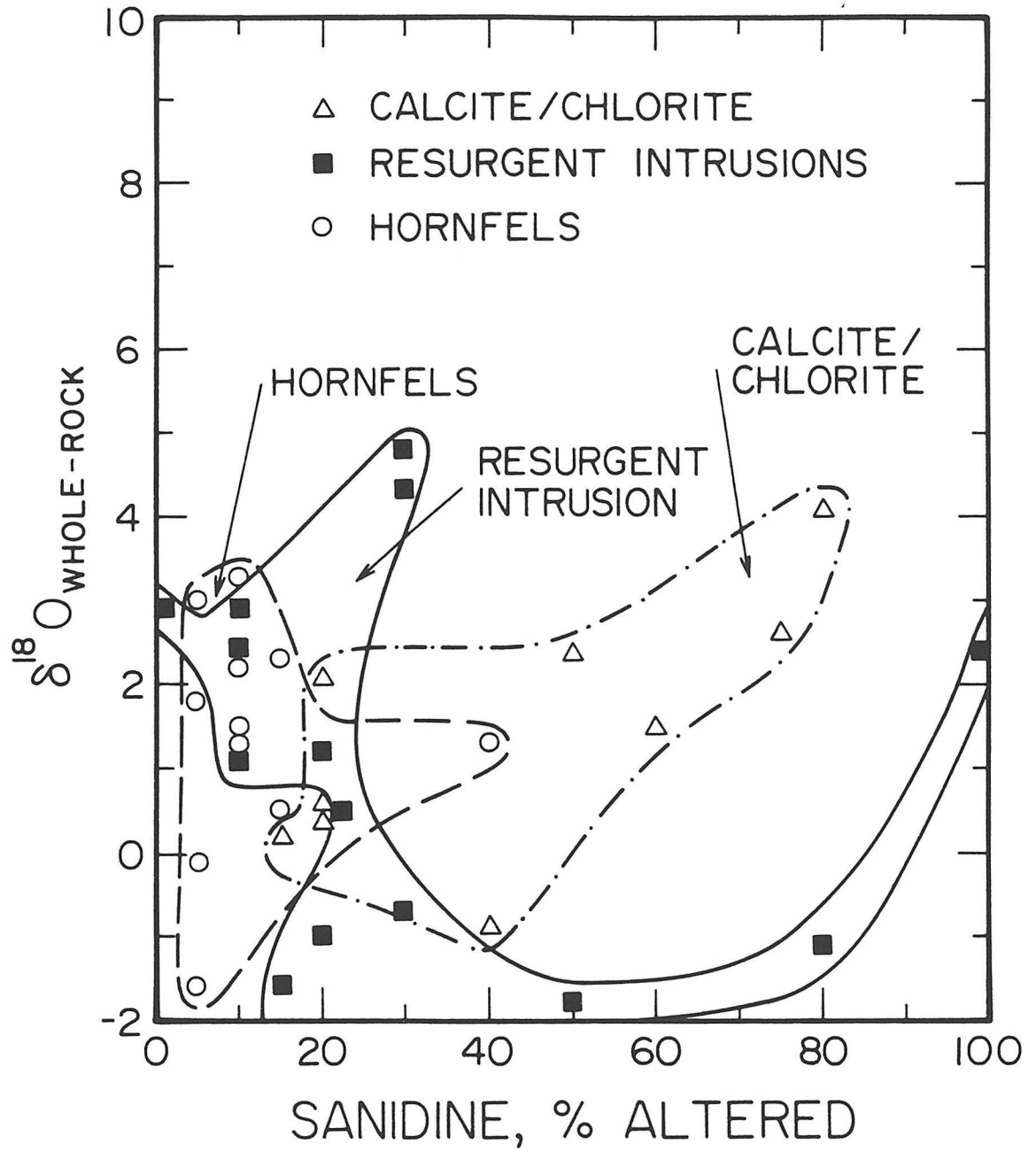


Figure 6.4 Whole-rock $\delta^{18}\text{O}$ values of argillically altered zones I through V tuff plotted as a function of the degree of mineralogical alteration of sanidine in the samples. The field of hornfelsed tuff from Figure 6.3 is also shown. Comparison with Figure 6.5 (and Fig. 4.8) suggests that as the alteration progresses from zone V to zone I the tuff experienced progressively higher W/R ratios. This is consistent with the quantity of alteration products in the sanidine and the geometric distribution of these facies around vein-filled fractures (zone I close to veins grading to zone V far from the veins). Comparison with Figure 6.5 also suggests that the argillization occurred at lower temperatures than the development of hornfels in the tuff (particularly the lower-grade zone IV alteration). This is consistent with the spatial distribution of the hornfelsed tuff around the resurgent intrusion, which also was altered at higher temperatures than the argillized tuff.

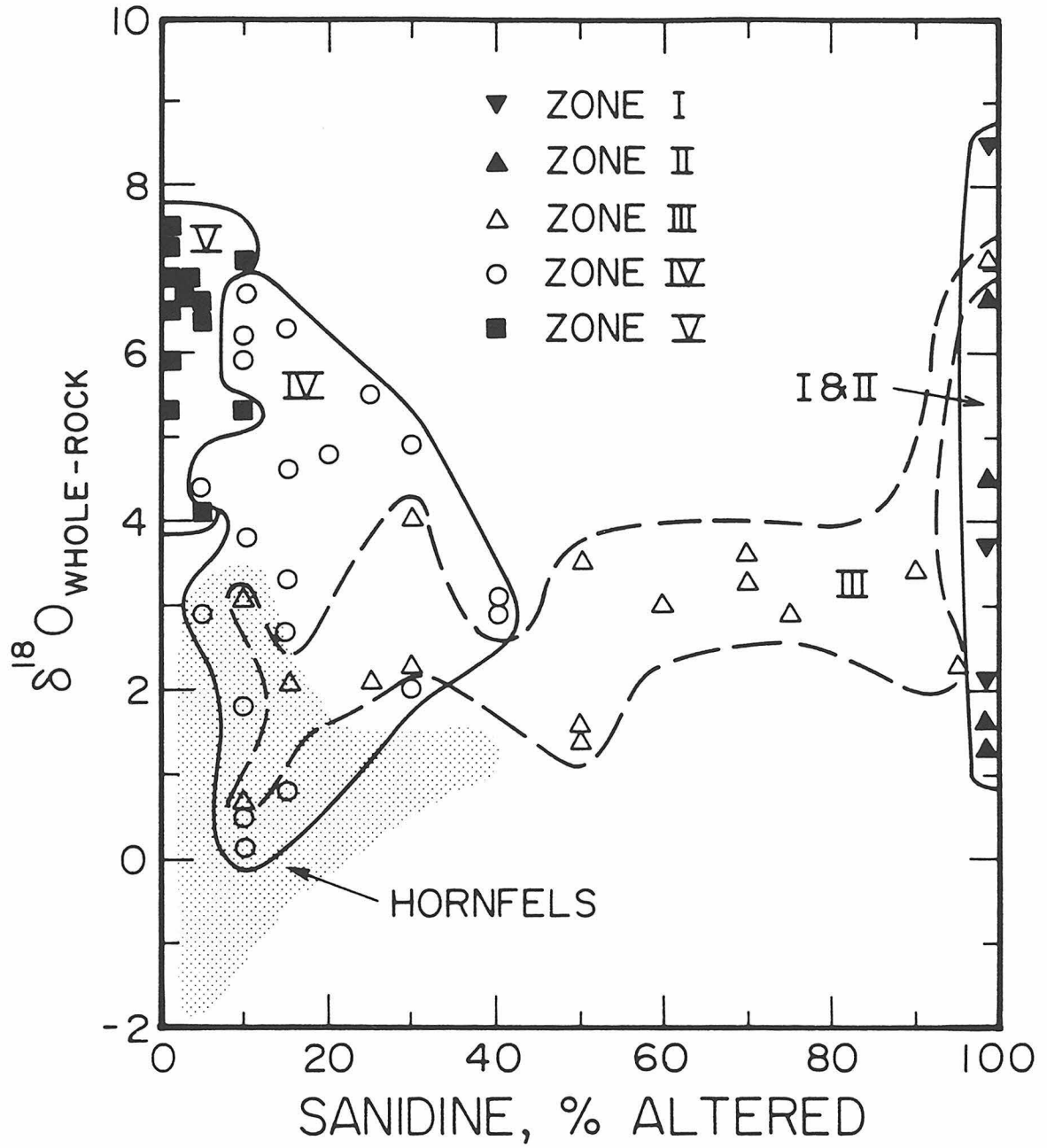
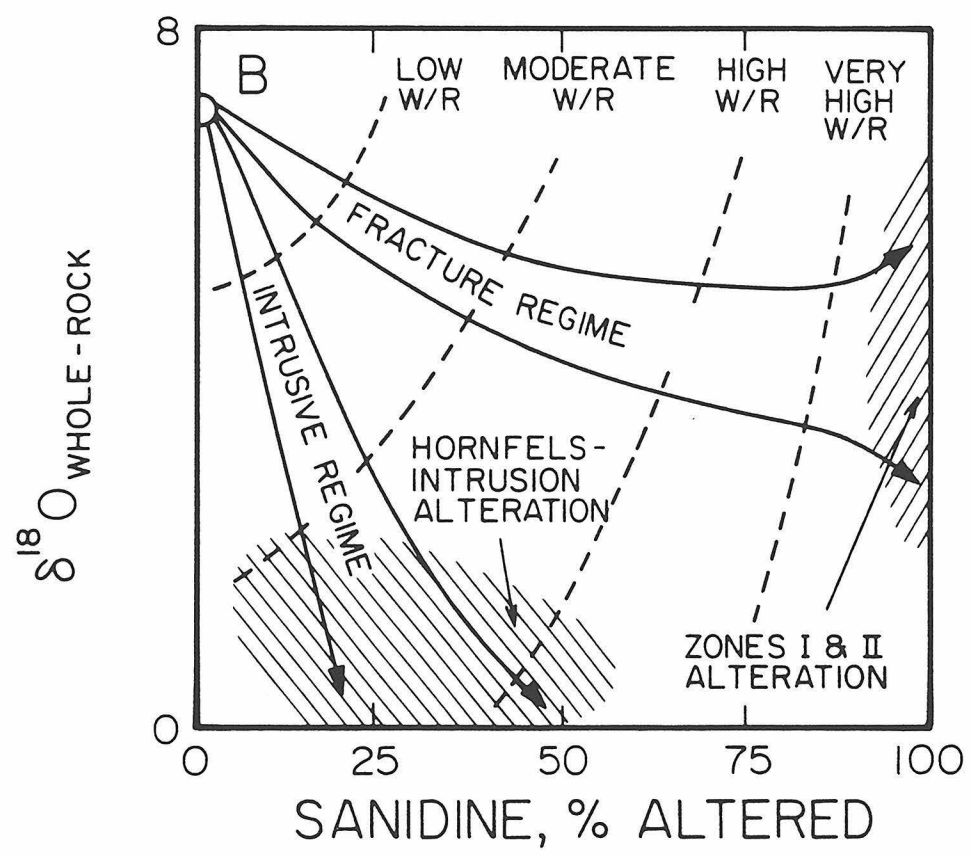
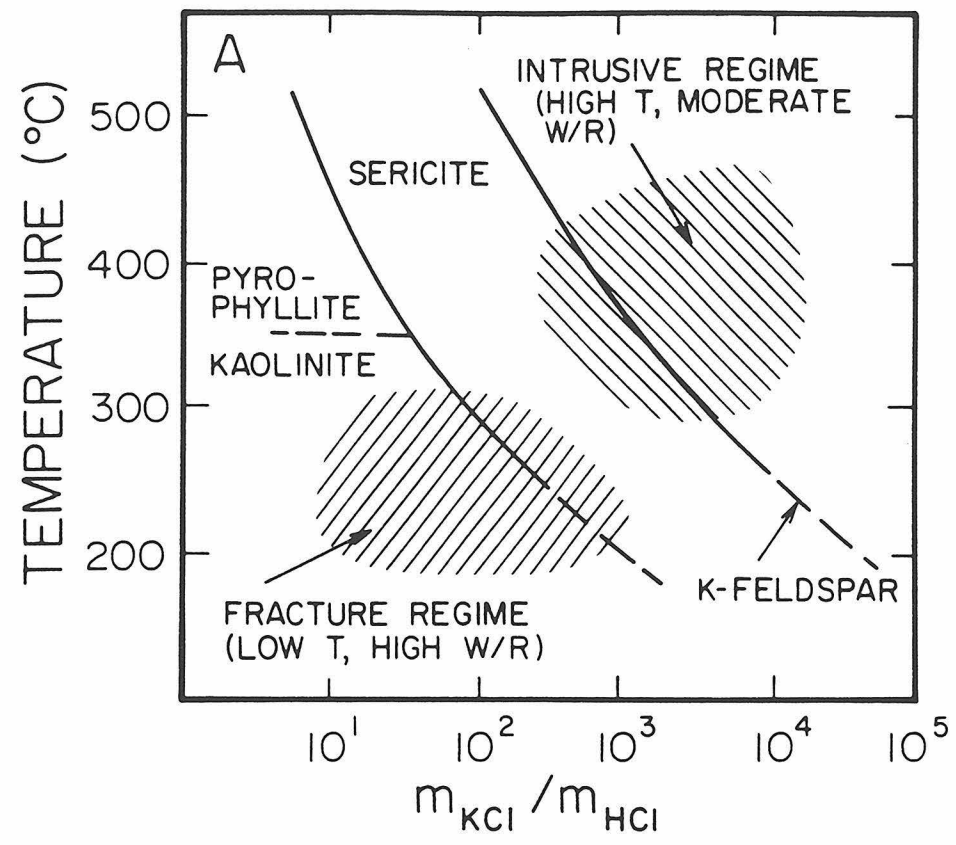


Figure 6.5a Stability fields of K feldspar, sericite, kaolinite, and pyrophyllite as functions of temperature and $m_{\text{KCL}}/m_{\text{HCL}}$ (from Hemley and Jones, 1964). Quartz is also present in all fields. Also shown is the plausible range of fluid composition and temperature appropriate for the Fracture Regime and the Intrusive Regime.

Figure 6.5b Plausible fluid trajectories for the Fracture Regime and Intrusive Regime alteration plotted as functions of whole-rock $\delta^{18}\text{O}$ and the amount of sanidine alteration, for comparison with Figures 6.3 and 6.4. For both regimes the water/rock ratios (W/R) increase in the direction of the arrows, as shown in a highly schematic fashion by the dashed contours. The large amounts of kaolinite and intense silicification found in zones I and II of the Fracture Regime, together with the distribution of zones I and II around obviously permeable fractures, imply very large W/R ratios. Only minor kaolinite is present in the sanidine in rocks altered in the Intrusive Regime, even though these rocks typically have lower $\delta^{18}\text{O}$ values than rocks altered in the Fracture Regime. These relationships could conceivably result from either higher-temperature alteration or higher $m_{\text{KCL}}/m_{\text{HCL}}$ ratios in the Intrusive Regime than in the Fracture Regime, or both. At sufficiently low W/R, the aqueous fluids would be "buffered" by the rocks and would have $m_{\text{KCL}}/m_{\text{HCL}}$ high enough to plot in the K feldspar-stable portion of Figure 6.5a. Alteration under such conditions would still involve extreme oxygen isotopic exchange between the meteoric-hydrothermal fluid and the K feldspar (resulting in low $\delta^{18}\text{O}$ values for these altered rocks), but would not produce intense mineralogical alteration in the K feldspar. At the higher W/R ratios and lower temperatures characteristic

of the Fracture Regime, the aqueous fluids would no longer be buffered and the aqueous fluids could attain very high $m_{\text{KCL}}/m_{\text{HCL}}$ ratios (perhaps through oxidation of H_2S or HS^-), such that intense kaolinite and quartz replacement of the tuff could occur. Thus, the much lower $\delta^{18}\text{O}$ values of the hornfels and resurgent intrusive rocks do not necessarily mean that these rocks have been altered at higher W/R ratios than the argillized zones I, II, and III tuff.



temperature/alteration regimes within the caldera (Table 6.2). These regimes are gradational in the sense that they overlap with one another geographically, and in that they are all produced by similar types of meteoric-hydrothermal fluids. They are, in reality, probably just aspects of a single phenomenon, differing only with respect to their positions in the evolutionary history and geometry of the Lake City hydrothermal system. They are also gradational in the sense that the low-grade alteration zones IV and V are common to all three regimes (or at least we do not at present know how to separate out the zone IV and V rocks that belong to each regime). A fourth regime (solfataric) also may exist, but this regime is essentially absent from the caldera, being almost wholly confined to the ring domes on the east side of the caldera (described in Chapter 5). The solfataric regime may also simply represent the shallowest facies of the fracture regime.

1) Fracture Regime. A relatively uniform temperature regime produced the argillized zone I through zone III tuff, falling off to somewhat lower temperatures in zones IV and V (Fig. 6.4). The major characteristics of this alteration regime were in large part determined by proximity to those fractures that were the principal fluid conduits (Plate 2). The more intensely altered samples lie closest to the veins (zones I and II), and contain sanidine that is essentially 100 percent altered to clay and quartz. The argillized tuff closest to the veins was altered at the highest water/rock ratios, but probably at only slightly higher temperatures than the average zone III samples. Comparison between Figures 6.3, 6.4, 4.8, and 6.5 indicates that even the highest-temperature facies of the Fracture Regime (zones I and II)

probably formed at lower temperatures than the alteration in the hornfelses or chlorite/calcite altered tuff (or the intrusive rocks). In time sequence the alteration types in the Fracture Regime appear to be superimposed on the other regimes described below. The Fracture Regime alteration effects that we can presently examine in the field may represent a late-stage evolution of the caldera-wide hydrothermal system.

2) Intrusive Regime. A generally higher-temperature regime, but one with very strong lateral and vertical temperature gradients, produced the hornfelses tuff and the alteration within the resurgent and ring intrusions. Although these rocks have $\delta^{18}\text{O}$ values lower than the argillized tuff, they exhibit less mineralogical alteration than the argillized tuff because high-temperature alteration allows thorough $^{18}\text{O}/^{16}\text{O}$ exchange between rocks and meteoric-hydrothermal fluids without necessarily producing abundant mineralogical alteration. It is clear that development of the hornfelses in the tuff adjacent to the intrusive contacts occurred at high temperatures. Also, the upper portions of the central resurgent intrusion (the "heat engine" that drove the meteoric-hydrothermal convection system within the caldera) must have been altered at high temperatures. Upward and outward from the contacts of the resurgent intrusion, this alteration regime grades into the successively lower-temperature zones IV and V.

3) Stratigraphic Regime. On Figures 6.3 and 6.4, the chlorite/calcite altered tuff samples as a group plot in an intermediate position between the two regimes described above. This type of alteration occurs deep in the stratigraphic sequence within the caldera, beneath the argillized tuff and peripheral to the hornfelses tuff and resurgent

intrusion (discussed below in Section 6.5.3). This regime appears to be largely stratigraphically controlled, and conceivably could simply represent a deeper (and hotter) facies of the fracture regime. However, it could also represent an early stage in the evolution of the caldera-wide hydrothermal activity, or perhaps a different type of chemical system (see below).

In summary, as shown in Table 6.2, the most intensely affected end-members within the three alteration regimes described above are readily separated both geographically and in diagrams like Figures 6.3 and 6.4. The chlorite/calcite alteration type, the hornfels-intrusion type, and zones I, II, and III all occupy different areas on the map in Plate 2 and different niches on the figures. These alteration types can thus be, respectively, separated out as (1) the Stratigraphic Regime, (2) the Intrusive Regime, or the (3) the Fracture Regime. However, the low-grade alteration types (zones IV and V), which occupy most of the area of the caldera (Plate 2), cannot be so delineated. Although further studies may allow such distinctions to be made, at present zones IV and V must be considered to include the low-grade, low W/R end members of all three alteration regimes.

6.5 Geometry of $^{18}\text{O}/^{16}\text{O}$ Variations in and around the Lake City Caldera

6.5.1 $\delta^{18}\text{O}$ Contour Map

$\delta^{18}\text{O}$ whole-rock values for samples within the caldera and samples of older volcanic and intrusive rocks outside the caldera, together with the calculated K feldspar $\delta^{18}\text{O}$ values for the Precambrian granite (Table 4.1) are contoured on Plate 3 (in pocket). A smaller but identical

Table 6.2

Characteristics of alteration regimes in the Sunshine Peak Tuff of the Lake City caldera. Each regime is defined by the highest-temperature alteration facies achieved for that regime.

GENERAL CHARACTERISTICS	GEOMETRIC RELATIONSHIPS	TEMP.	W/R RATIO	$\delta^{18}\text{O}$ ROCK	TIMING
FRACTURE REGIME	Zones I, II, and III. Restricted to areas above and around the resurgent and ring intrusions. Superimposed upon, and younger than, the hornfelsed and chlorite/calcite tuff. Probably formed at a P and T characteristic of deposition along a hydrostatic boiling curve (see Chapter 5).	150°C to 300°C	High (>> 1)	+1 to +5 (zone III) +2 to +9 (zones I, II) > +7 (solfataric)	Late
INTRUSIVE REGIME	Hornfels and intrusive rocks. Restricted to resurgent and ring-fracture intrusions and adjacent tuff. At low elevations grades outward to chlorite/calcite alteration. At high elevations grades outward and upward to zone IV, or locally to zone III. Formed at relatively high T and high mKCL/mHCL (see Fig. 6.5).	>300°C	Low to moderate (≈ 1)	-2 to +5	Early
STRATIGRAPHIC REGIME	Chlorite/calcite. Occurs in deeper levels of Sunshine Peak Tuff outside the Intrusive Regime. Cut by the Fracture Regime. Also commonly developed at higher elevations in and around the caldera ring fault.	>200°C	Moderate (≈ 1)	-1 to +4	Early to Late (?)
ZONES IV AND V	These facies possibly represent low-temperature end-members of any of the above three regimes. Zone V is typically fresh and unaltered, except for devitrification of the glassy groundmass and some turbidity in the sanidine phenocrysts.	<250°C	Moderate to very low (< 1)	0 to +7 (zone IV) +4 to +8 (zone V)	?

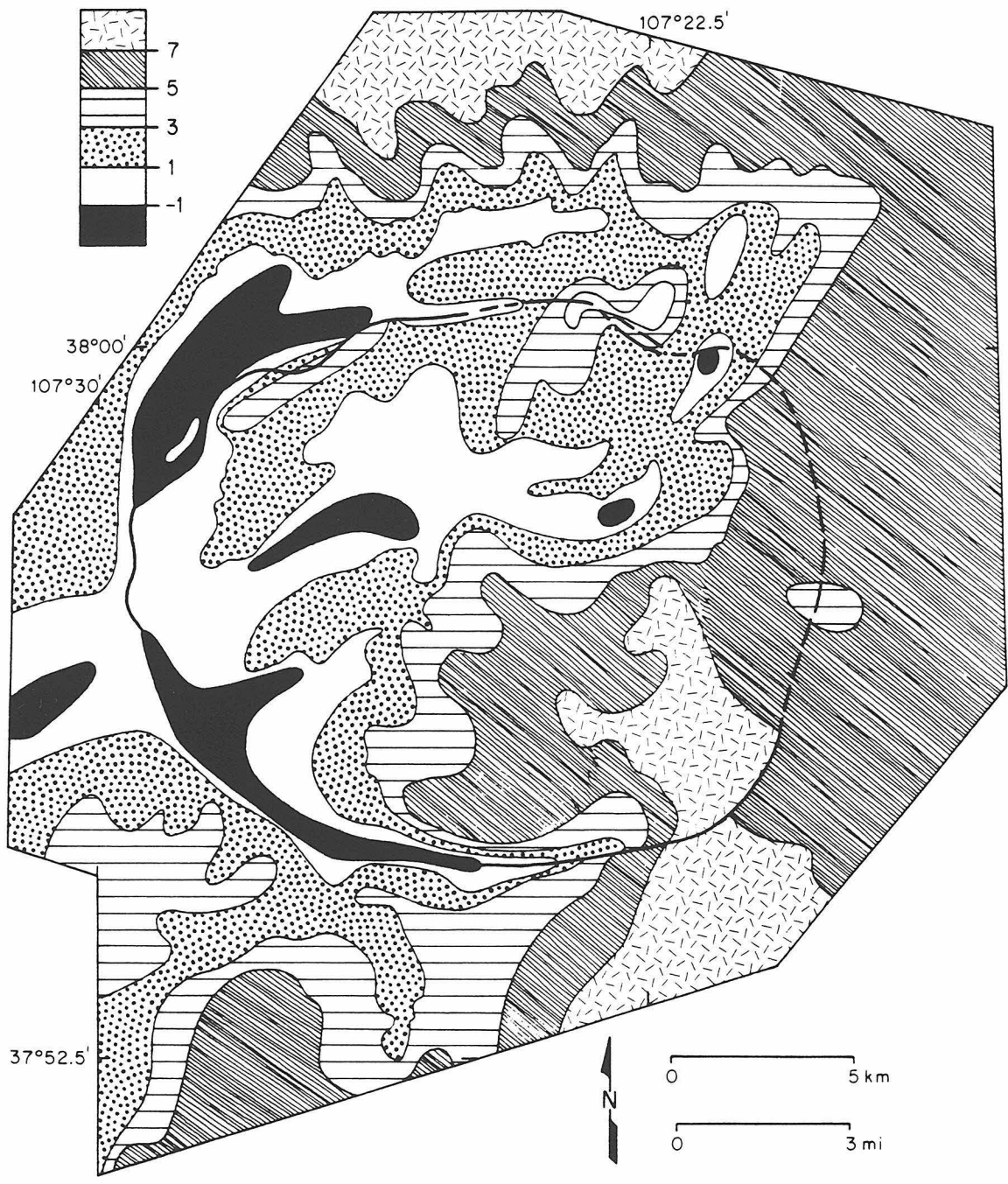
contour map is shown on Figure 6.6. Sample locations are shown on Plate 3 but not on Figure 6.6. The calculated K feldspar values from the Precambrian granite were used in the contouring because the granite had an initial whole-rock $\delta^{18}\text{O}$ value about 2 per mil higher than the Sunshine Peak Tuff, and because the granite initially contained about 30 percent of inert, coarse-grained quartz. Use of the K feldspar data for the granite adjusts these data such that they are compatible with the whole-rock $\delta^{18}\text{O}$ data from the tuff within the caldera. In areas where the density of sample points was low, some latitude was used in drawing the $\delta^{18}\text{O}$ contours, for example making use of the correlations with topography and proximity to intrusions, as described below.

The shape of the lowest- ^{18}O areas on Figure 6.6 resemble an eastward pointing four-tined fork. The handle is the Eureka graben, with two tines positioned along the ring fault, and a couple of central tines in the deeply eroded, low-elevation areas near the central resurgent intrusion. The major influences on the $\delta^{18}\text{O}$ patterns are listed below, and each will be discussed in detail in subsequent sections.

1) The caldera has been asymmetrically tilted to the east. $\delta^{18}\text{O}$ values are lowest in the west and northwest areas of the caldera and highest in the east and southeast areas. This conforms to what we already know about the structural and erosional history of the caldera. Erosion has clearly penetrated more deeply in the west than in the east. Because of the regional tilting, we are looking deeper into the hydrothermal system in the western part of the caldera than in the eastern part.

2) There is an obvious correlation between low- ^{18}O areas and the

Figure 6.6 Contour map of $\delta^{18}\text{O}$ values in the Lake City caldera area. This figure is a smaller but identical version of Plate 3 (in pocket). Sample locations are not shown here but are on Plate 3. Low- ^{18}O areas define a fork-shaped zone with the handle in the Eureka graben, two outer lines along the caldera ring fault, and a couple of central lines in the low-elevation areas near the resurgent intrusion. See text for discussion.



ring fault. The lowest- ^{18}O samples (solid black and white areas on Figure 6.6) all conform nicely to the ring fault (except in the eastern part of the caldera where erosion has not penetrated deeply and the ring domes still cover the ring fault).

3) A positive correlation exists between topography and $\delta^{18}\text{O}$ values. Even a cursory comparison between Figures 3.1 and 6.6 shows a good match between low elevation and low $\delta^{18}\text{O}$ (in Alpine Gulch, Cooper Creek, Silver Creek, Henson Creek, Bent Creek, and in Burrows Park both inside and outside the caldera). Also, high elevation areas correlate with high $\delta^{18}\text{O}$ values (on the middle and eastern parts of Central Ridge, the Sunshine Peak-Redcloud Peak ridge, Alpine Ridge, the Red Mountain-Grassy Mountain ridge, and on Cooper Ridge).

4) Rocks close to and within the central intrusion have low $\delta^{18}\text{O}$ values. This is obvious from Plate 3. Also, Figures 6.2, 6.3, and 6.4 show that the hornfelsed tuff and intrusive groups of samples have lower $\delta^{18}\text{O}$ values than the other tuff alteration groups. All low- ^{18}O areas at high elevations are located near outcrops of the intrusive rocks (near intrusion exposures 1, 9, 10, 11, and 12, Fig. 3.1).

5) Other faults, veins, and fractures exert control over low- ^{18}O areas. Low- ^{18}O areas adjacent to faults occur on the northern end of Cooper Ridge, and in lower Silver and Cooper Creeks.

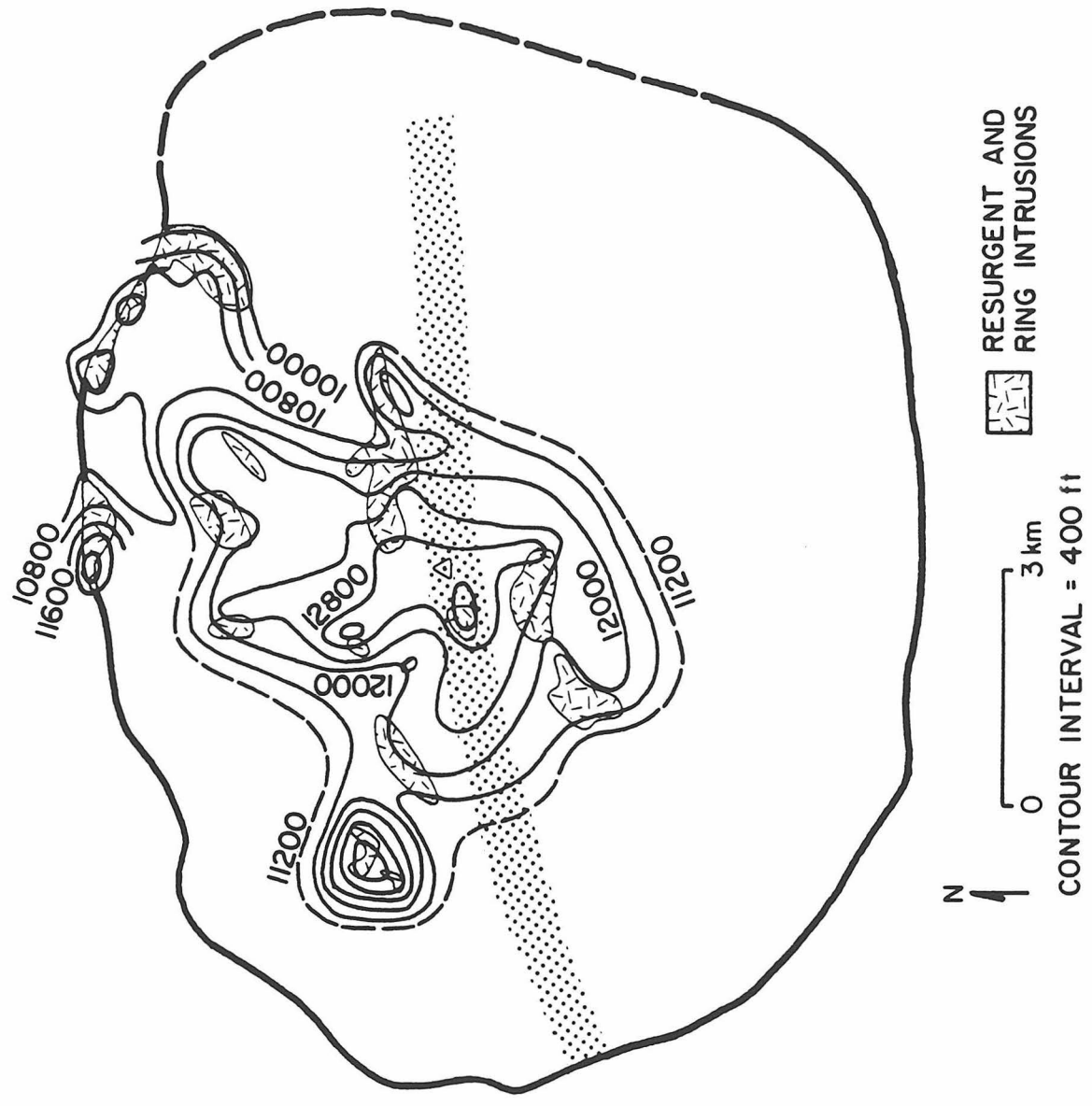
6) Some lithologic control is evident. The megabreccia, Precambrian granite, and the Sunshine Peak Tuff each had a distinct permeability, different grain size, and different initial $\delta^{18}\text{O}$ values. All these factors influenced to varying degrees the reaction of these rocks with the meteoric-hydrothermal fluid.

6.5.2 Shape of the Resurgent Intrusion

Structure contours on the top of the Lake City resurgent intrusion are shown in Figure 6.7. These contours were drawn by connecting points of equal elevation along the intrusive contacts as shown on Plate 1. The intrusion has the form of a broad dome with steep sides, being nearly flat on top. Field examination of some outcrops of the resurgent intrusion (exposures 8, 10, 13, 14, and the western part of 11, Fig. 3.1) revealed the nearly horizontal nature of the upper contact prior to drawing Figure 6.6. Also, the geologic cross sections (Plate 4) show that the upper intrusive contact can be readily connected between intrusive exposures on opposite sides of ridges (for example from exposure 8 to exposure 13 beneath the West End of Central Ridge and from 11 to 14 beneath the Central Ridge). In addition, samples from exposures of the resurgent intrusion visited in the field (8, 10, 11, 12, 13, and 14) are petrographically identical. It is thus clear that erosion within the caldera is just beginning to expose the uppermost portion of the resurgent intrusion, and that all these intrusion exposures within the central part of the caldera (2, 6, 7, 8, 9, 10, 11, 12, 13, and 14, Fig. 3.1) crystallized from the same continuous mass of magma.

In contrast, ring intrusions along the northern caldera ring fault (exposures 3 and 4, Fig. 3.1) are dike-like and have steep contacts. But exposure 5 (also with a steep contact along the ring fault) extends into the caldera away from the ring fault, where it has a flat upper contact similar to that of the resurgent intrusion. It is therefore reasonable to extend the top of the resurgent intrusion to exposure 5 and to consider all these exposures (and perhaps all of the other ring

Figure 6.7 Structural contours drawn on the top of the Lake City caldera resurgent intrusion. These contours were drawn by connecting points of equal elevation of the intrusive contacts as shown on Plate 1. The top of the intrusion is a broad, nearly flat-topped dome, asymmetrically displaced northward from the center of the caldera. Outcrops of the central resurgent intrusion in the caldera can be observed in the field to have nearly flat tops, although the side contacts of the intrusion dip steeply outward. In contrast, the ring intrusions along the northern caldera ring fault are dike-like in form and have very near-vertical contacts. The exposure on Cooper Ridge also has steep contacts and a fine-grained, nearly glassy matrix. This intrusion must be a narrow spike-shaped apophysis of the main resurgent magma that crystallized very quickly. Also shown is the boundary zone between the north and south halves of the caldera used in construction of the composite radial cross section shown in Figures 6.8, 6.9, 6.10, and 6.11. The small triangle near the apex of the resurgent intrusion is the central point from which the sample locations in the composite radial cross section were measured.



intrusions as well) to have crystallized from a single body of magma. The exposure on Cooper Ridge (1 on Fig. 3.1) also has steep contacts. This intrusion is a rhyolite porphyry with a much finer-grained ground-mass than samples from the other exposures. This rhyolite porphyry is clearly a narrow, spike-shaped, intrusive prong of material that crystallized very rapidly. The phenocryst mineralogy of this rhyolite porphyry is, however, nearly identical to that of the main mass of the resurgent intrusion; the Cooper Ridge rhyolite porphyry is thus probably simply an apophysis of the main magma body, and it is shown as such on Figure 6.7.

6.5.3 Radial Cross Sections

A composite radial cross section that incorporates data from all analyzed samples within the caldera was constructed. On this composite cross section we can plot all the data points, the lithologies, the alteration facies, and the whole-rock $\delta^{18}\text{O}$ values (Figs. 6.8, 6.9, 6.10, and 6.11). Two separate sections were made for each diagram, one for the north half, and one for the south half of the caldera, by plotting sample elevation versus the horizontal distance of each sample from a point centrally located near the top of the resurgent intrusion (small triangle on Fig. 6.7). The north and south halves were joined to produce the four composite radial cross sections. Note that there is an enormous vertical exaggeration (>6:1) in all these figures. The boundary between the north and south halves is a nearly east-west, 0.5 km-wide zone passing through the central point (Fig. 6.7). Samples within this boundary strip are plotted on both the north and south halves of

Figure 6.8 A composite radial cross section that includes all samples studied in this work from within the Lake City caldera. This plot was constructed by dividing the caldera into northern and southern halves along a 0.5 km-wide, nearly east-west zone passing through a point near the top of the central resurgent intrusion (Fig. 6.6). Sample distance from this central point is plotted vs. sample elevation. Samples within the narrow east-west strip were plotted on both the north and south halves. The two halves were then joined to produce the composite section. This figure shows sample points and sample numbers.

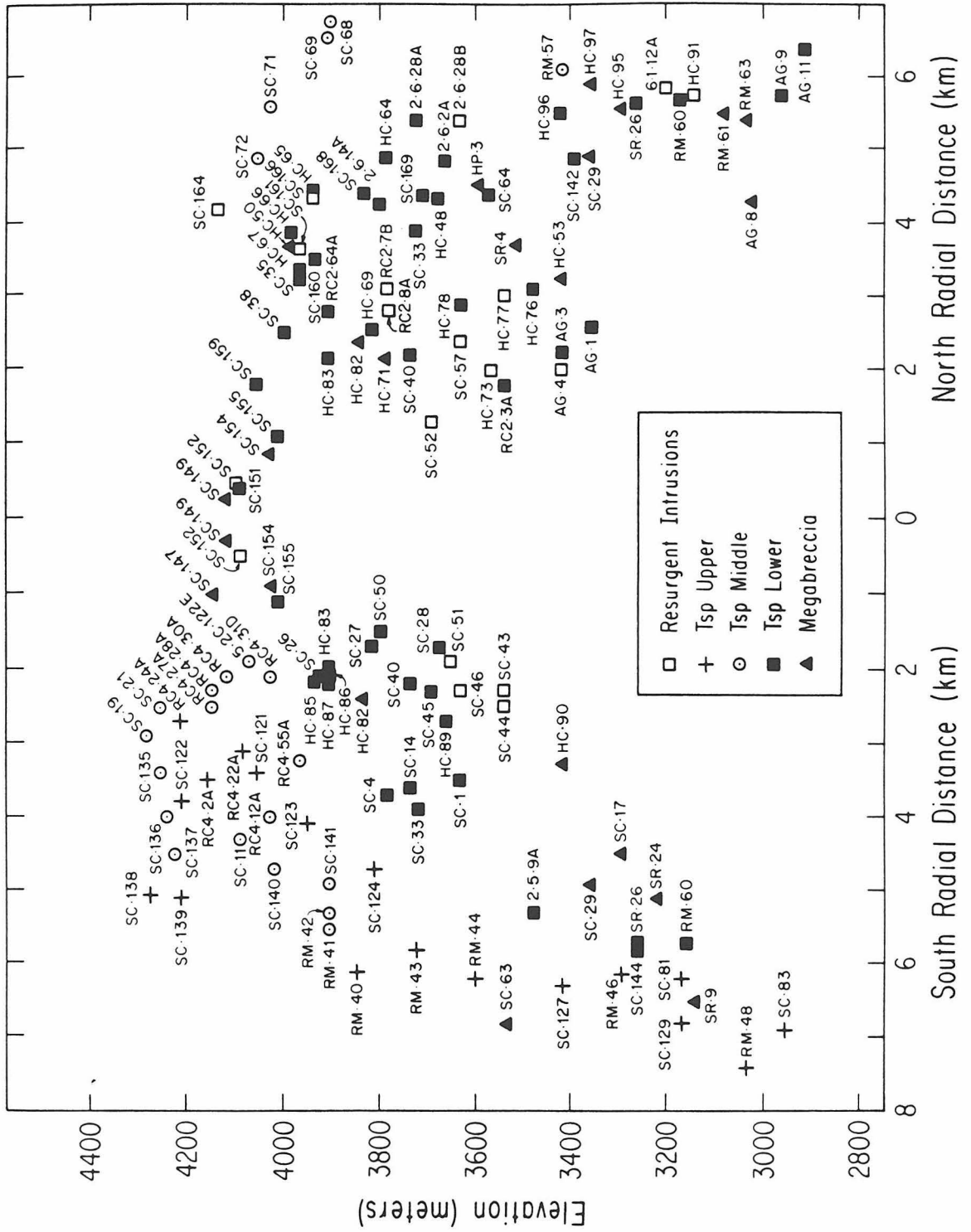


Figure 6.9 Lithology plotted on the composite radial cross section on Figure 6.8. All units of the Sunshine Peak Tuff ash-flows and megabreccias dip away from the central resurgent intrusion. The lithologic symbols are the same as those used on Plate 1. Tspu, Tspm, and Tspl are, respectively, the upper, middle, and lower member of the Sunshine Peak Tuff, Tiq is the resurgent intrusion, and Tsml is the lower megabreccia. Ring intrusions along the northern caldera ring fault plot as distinct separate bodies on the composite section but in reality these are probably connected by feeders to the main mass of the resurgent intrusion. Because the ring fault lies at variable distances from the central point it plots as a wide zone corresponding to its minimum and maximum distance from the central point.

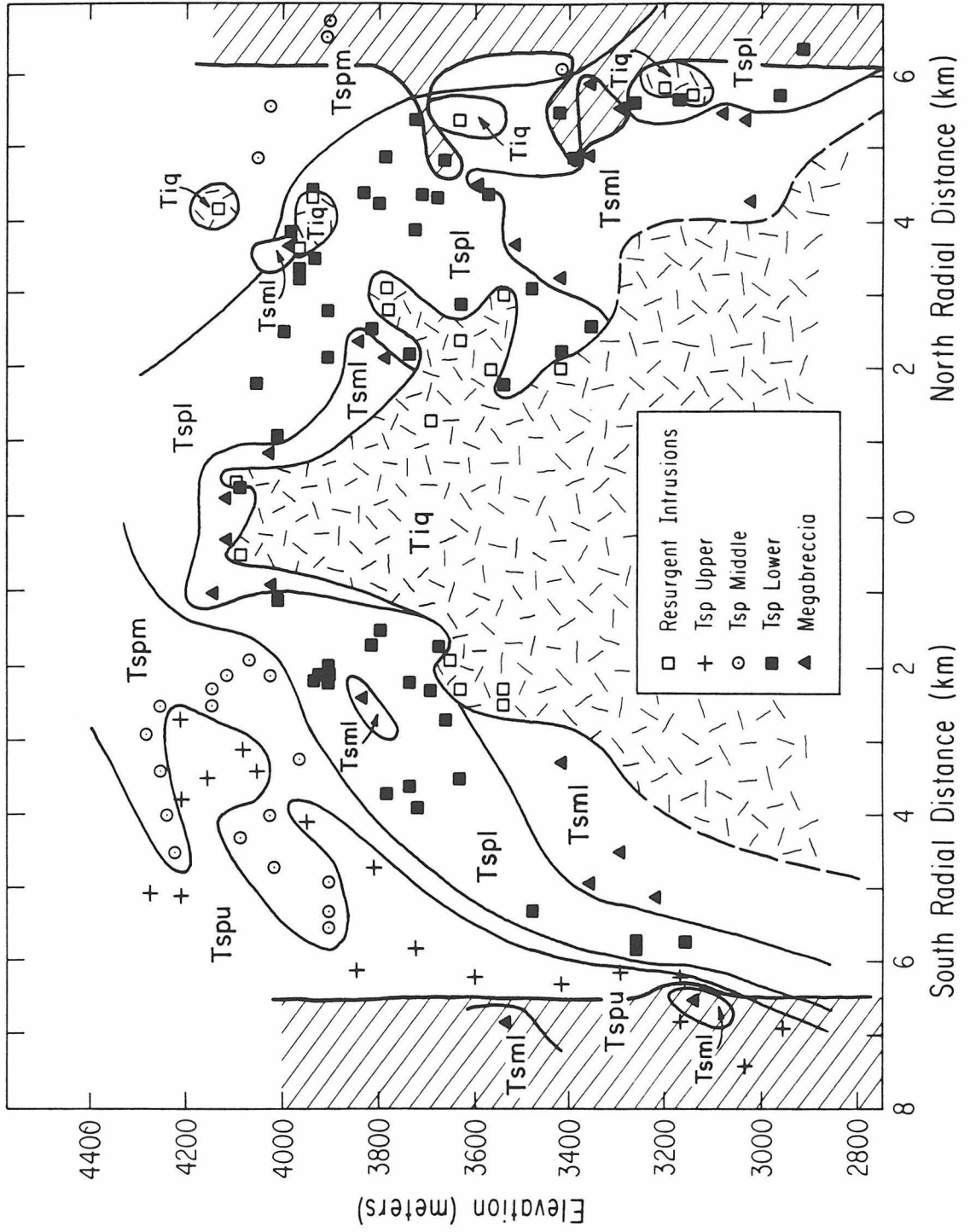


Figure 6.10 Alteration facies of the Sunshine Peak Tuff plotted on the composite radial cross section of Figure 6.8. Hornfelsed tuff is developed adjacent to the resurgent intrusion. Areas of argillized zone I through III tuff occur above the resurgent intrusion and locally in the ring fault zone along the northern caldera margin. Zone IV argillized tuff occurs above and around the resurgent intrusion and grades up into weakly altered (zone V) tuff in the south half. Zone V argillization, restricted to very shallow environments, is lacking in the north half because of deeper and more extensive erosion. Zone IV tuff grades down to chlorite/calcite altered tuff. See text for further discussion.

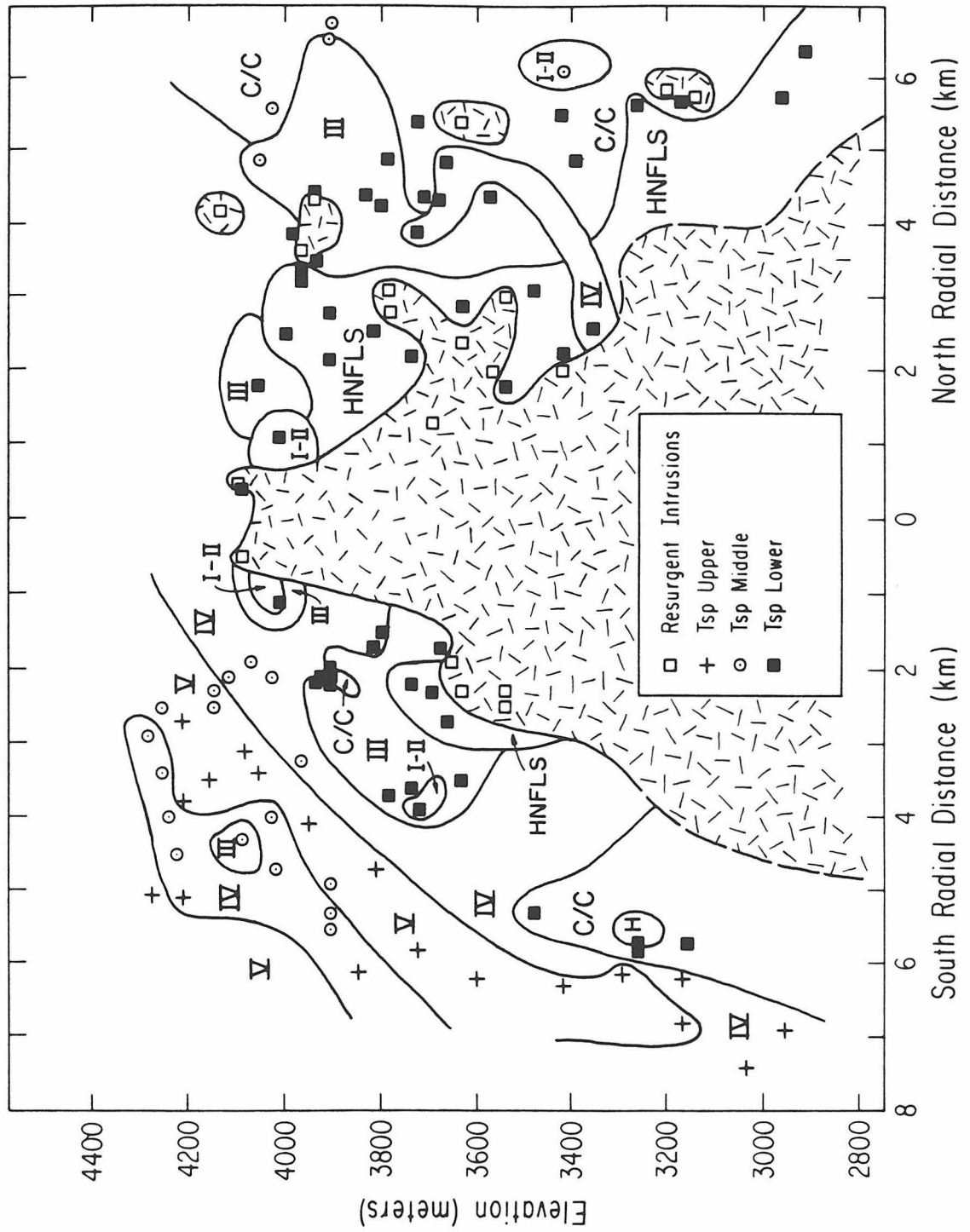
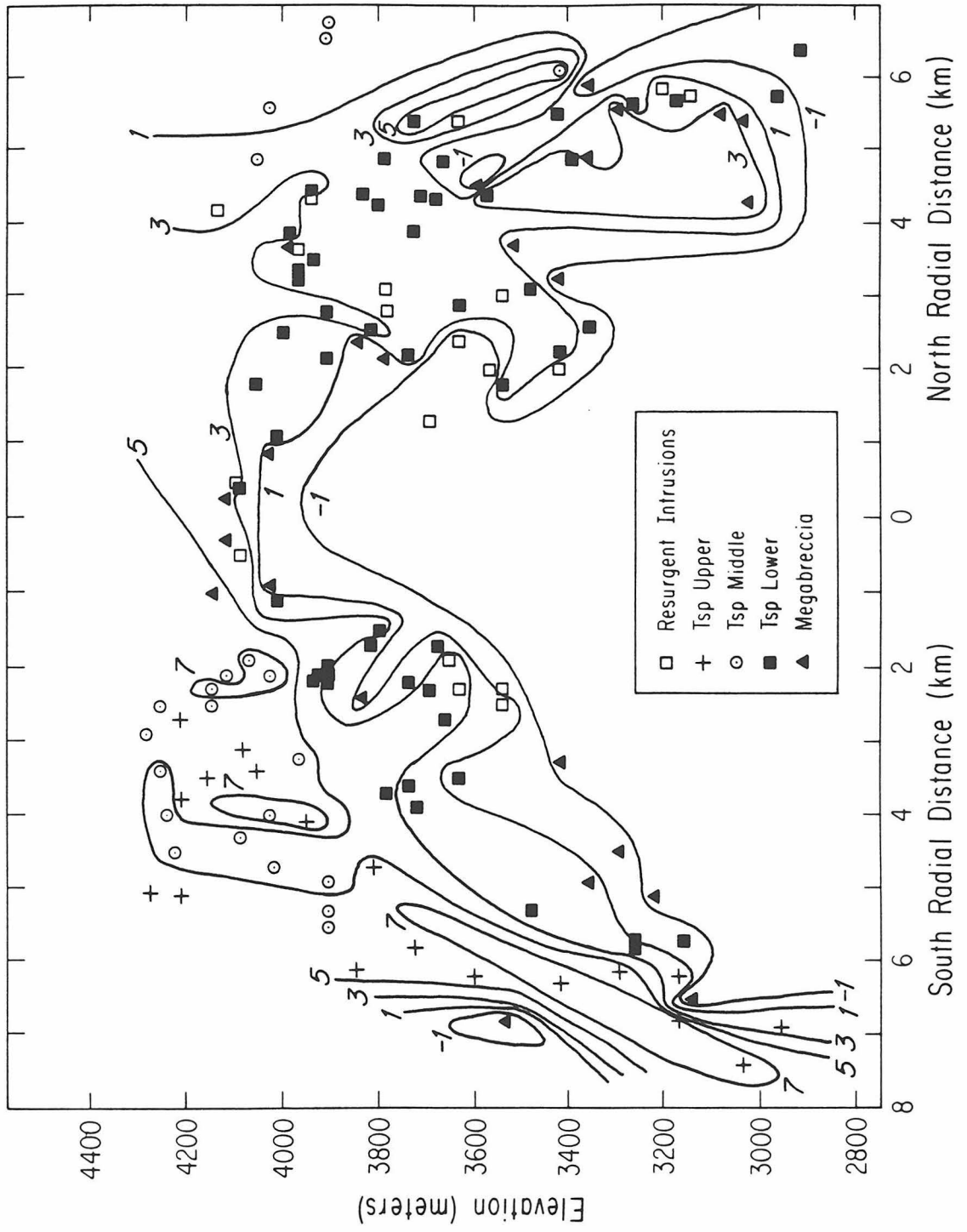


Figure 6.11 Contours of $\delta^{18}\text{O}$ values plotted on the composite radial cross section of Figure 6.8. The contours define a broad domal pattern centered over and concentric with the resurgent intrusion. $\delta^{18}\text{O}$ values decrease systematically with depth throughout the caldera (to less than -1 in the resurgent intrusion but greater than +7 in the shallow upper Sunshine Peak Tuff ash-flow in the south half). Low $\delta^{18}\text{O}$ areas also occur in the ring fault zones in both the north and south halves. See text for further discussion.



all the diagrams. Because the ring fault is oval, not circular, it does not lie at a constant distance from the central point, and thus the ring fault appears as a wide zone corresponding to its minimum and maximum distance from the central point on these figures. Although the assumption of perfect radial symmetry is only an approximation, and it obviously breaks down in going from the north half to the south half of the caldera, Figures 6.8, 6.9, 6.10, and 6.11 provide a remarkably realistic representation, allowing us to plot all of the structural and analytical data on a single series of diagrams.

Figure 6.8 shows the distribution of sample points and sample numbers on these cross sections, and Figure 6.9 shows the distribution of lithologies in the composite cross section. It is gratifying that these simplified, composite cross-sections are consistent with what we already know about the resurgent doming in the caldera; namely, all the units on the radial section are in proper stratigraphic order and dip outward from the central resurgent intrusion. Also, in the south half the uppermost member of the Sunshine Peak Tuff (Tspu) caps the section just as it does on the actual maps and cross-sections (Plate 4). In the north half the upper ash-flow unit has been removed by erosion and the middle ash-flow is the highest lithology. Also, sub-volcanic intrusions only occur along the ring fracture in the north half of the caldera, where they are shown schematically in Figure 6.8 as separate small bodies. In reality these isolated bodies must be connected by feeders to the main resurgent and ring-fracture intrusions.

Mineralogical alteration patterns in the composite cross section are shown in Figure 6.10. The alteration fields in this figure were

delineated by drawing boundaries enclosing all tuff samples that exhibit the same alteration type. Figure 6.10 is complicated somewhat by the regional eastward tilting of the caldera (discussed in detail in Section 6.5.5), but the overall patterns in this figure are compatible with what we already know about the distribution of these facies within the caldera. On Figure 6.10 the hornfelsed tuff lies adjacent to the resurgent intrusion (see also Plate 2). Because the tuff-intrusion contact is exposed by erosion to a greater extent on the north side of the caldera, the hornfelsed field in Figure 6.10 is wider on the north half than on the south half. Zones I through III argillically altered tuff are distributed across the top of the resurgent intrusion. Plate 2 also shows this spatial relationship. Zone IV argillic alteration lies as a broad field upward and outward from the intrusion, and in the south half it is overlain and grades up into zone V tuff. The high-elevation zone V tuff in the south half of Figure 6.10 occurs only in the southeast quarter of the caldera in the stratigraphically high, near-surface, upper Sunshine Peak Tuff ash-flow (compare Figs. 6.9 and 6.10).

In the south half of Figure 6.10 the chlorite/calcite altered tuff occurs only below 3550 m elevation, but in the north half it is exposed as high as 4000 m. This is because the chlorite/calcite alteration in the north half occurs along the western caldera margin and on Cooper Ridge, the part of the caldera that has been uplifted the most due to the regional eastward tilting. Plate 2 shows that the upper boundary of the chlorite/calcite alteration in the western part of the caldera is continuous with the upper boundary of the chlorite/calcite alteration in the south half and that this boundary dips eastward, consistent with the

eastward tilting of the caldera. The small field of zone IV alteration that is enclosed by zone V alteration in the upper left part of Figure 6.10 represents samples from the Sunshine Peak-Redcloud Peak ridge in the western part of the caldera; the "anomalous" high elevation on Figure 6.10 is thus also simply a result of the regional eastward tilting.

The $\delta^{18}\text{O}$ values of all samples within the caldera are contoured on Figure 6.11. These contours define a broad domal pattern parallel to the contact of the resurgent intrusion, with lower $\delta^{18}\text{O}$ values at lower elevations. The lowest values occur in and adjacent to the resurgent intrusion. The highest $\delta^{18}\text{O}$ values are found in the south half in the stratigraphically high, near-surface upper Sunshine Peak Tuff ash-flow, coincident with the zone V mineralogical alteration. Such high $\delta^{18}\text{O}$ values are not found in the north half, because of the great abundance of ring intrusions ("small heat engines"), and because the deeper erosion in that area has removed any such materials. Note that the ring fault in both the north and south halves of Figure 6.11 contains significant amounts of low- ^{18}O rock.

6.5.4 Structural Cross Sections

Five structural cross sections have been drawn (Plate 4, in pocket). These cross sections include both the lithologic units and $\delta^{18}\text{O}$ contours. All five cross sections on Plate 4 also show those sample locations that lie on or very close to the lines of the sections. Three cross sections traverse the study area from north of the caldera to south of the caldera (A-A', B-B', and C-C'). These lines were chosen to examine geologic and $\delta^{18}\text{O}$ changes as one progresses, respectively, from

the Eureka graben eastward through the resurgent dome of the caldera. A fourth section traverses from west of the caldera through the resurgent dome to east of the caldera (D-D'). The fifth cross section zig-zags from north of the caldera to south of the caldera crossing the resurgent intrusion (E-E'). The position of this last section was chosen to include as many $\delta^{18}\text{O}$ data points as possible on or very close to the line of the section.

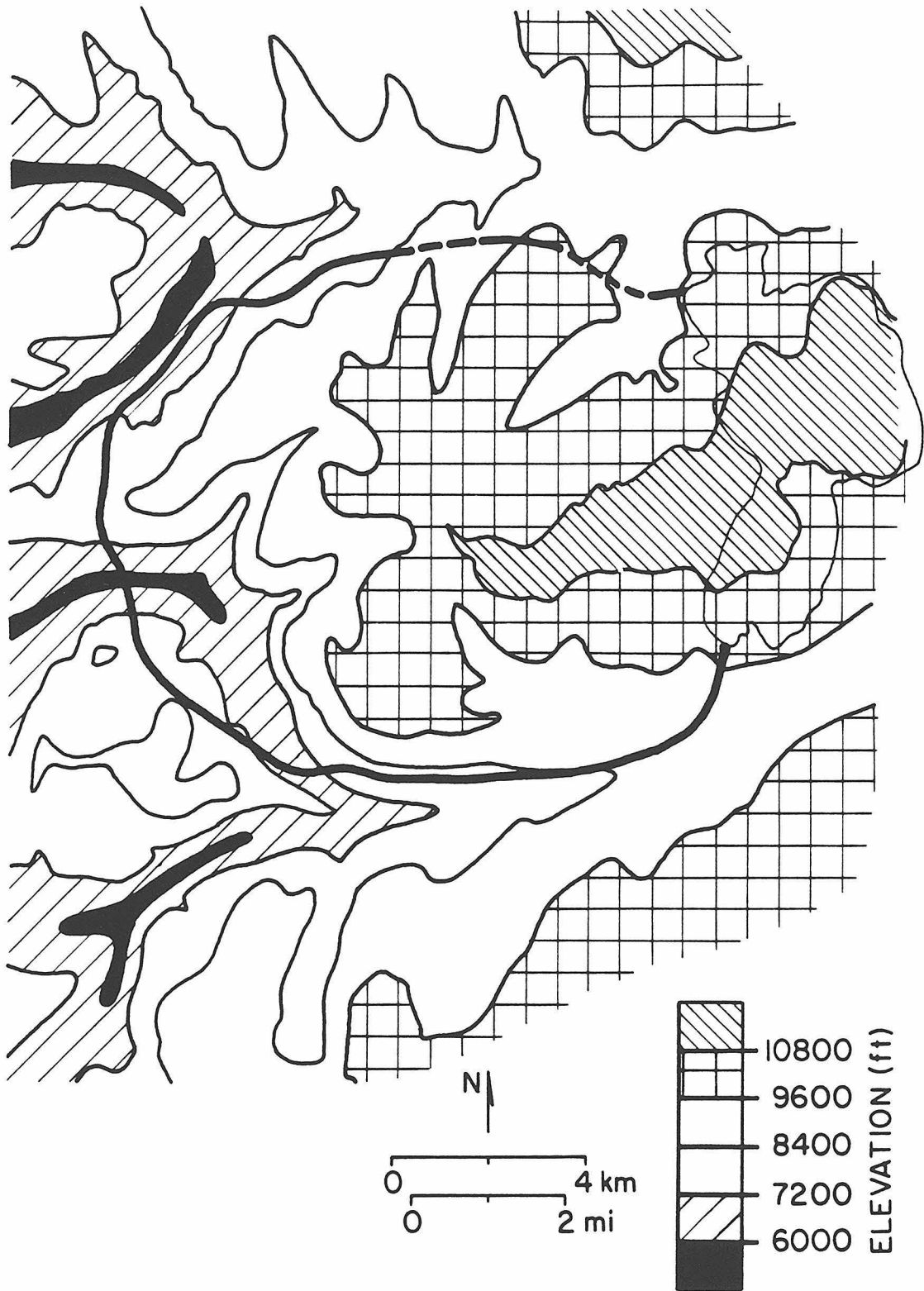
$\delta^{18}\text{O}$ contours on the five sections were drawn after Figures 6.6 (Plate 3) and 6.7 were constructed. Intersections of the $\delta^{18}\text{O}$ contours with the present-day topographic surface on Plate 3 were transferred to their appropriate positions on the cross sections, and the contours on the sections were then drawn to be compatible with the $\delta^{18}\text{O}$ contours on Plate 3. By an iterative process, the $\delta^{18}\text{O}$ contours and geologic contacts were reconciled among all the cross sections of Plate 4 and the maps of Plates 1 and 3.

The $\delta^{18}\text{O}$ contours on all five cross sections show in detail the same general features as the contours on the composite cross sections (Fig. 6.11). The north-south sections that traverse the caldera (B-B', C-C', and D-D') exhibit broad, domal-shaped $\delta^{18}\text{O}$ contours that drape over the resurgent intrusion, with low $\delta^{18}\text{O}$ areas within the intrusion and at low elevations. Low- $\delta^{18}\text{O}$ zones also coincide with the ring fault in the western part of the caldera (B-B', E-E') but are not pronounced in the southeastern part because this area is not deeply eroded and lacks ring intrusions. The domal pattern extends into the Eureka graben (A-A') and the axis of the $\delta^{18}\text{O}$ dome extends from the resurgent intrusion westward into the central part of the graben (D-D').

6.5.5 Effect of Asymmetric Uplift and Tilting

Many lines of evidence show that the area of the Lake City caldera has been asymmetrically uplifted and tilted to the east. The new data in the present study show that this tilting occurred after the bulk of the hydrothermal activity had occurred in the Lake City caldera. A summary of this evidence follows: (1) Stratigraphically high lithologic units are exposed in the eastern part of the caldera (the ring domes and the upper Sunshine Peak Tuff ash-flow), but have been removed by erosion in the topographically higher central and western parts, where the lower Sunshine Peak Tuff ash-flow and the resurgent intrusion are exposed (Plate 1 and Fig. 2.8). (2) Structural contours on the top of the Precambrian granite dip eastward (Fig. 4.17) at the same angle (6°) as the intravolcanic contacts above the granite. (3) Shallow solfataric alteration in the ring domes and nearly fresh, weakly altered tuff (zone V) occur only in the eastern part of the caldera. (4) The deepest alteration facies (chlorite/calcite and hornfels) are exposed at high elevations in the central and western parts, and the upper contact of the chlorite/calcite facies drops to progressively lower elevations from west to east (Plate 2). (5) $\delta^{18}\text{O}$ contours are shifted to higher elevations as one progresses from east to west outside the caldera ring fault in both the Precambrian granite to the south (Figs. 4.12 and 4.13) and the older volcanic rocks to the north (Figs. 4.21 and 4.22). (6) Figure 6.11 and Plate 4 show that $\delta^{18}\text{O}$ values systematically become lower as one goes deeper beneath the original topographic surface. Within the caldera, lower $\delta^{18}\text{O}$ values occur at higher elevations in the western

Figure 6.12 The present erosional surface of the Lake City caldera, after adjustment to remove the eastward, post-alteration tilting. About 6° of tilt (based on the eastward dip of the Precambrian-Tertiary contact and intravolcanic stratigraphic contacts south of the Lake City ring fault) has been removed. The hinge line for this reconstruction trends north-northwest and passes near the summit of Red Mountain; elevations west of this constant-elevation line are shown lower than their present positions (compare with Fig. 3.1). Areas that have been deeply eroded (Henson Creek, Burrows Park, lower Silver Creek, lower Cooper Creek, and lower Alpine Gulch) are also those areas that exhibit the lowest $\delta^{18}O$ values (compare to Fig. 6.6). Areas of little erosion (Red Mountain-Grassy Mountain and the East End of Central Ridge, Fig. 3.1) contain weakly-altered rocks that have high $\delta^{18}O$ values. The upper Sunshine Peak Tuff in the southeast quadrant of the caldera (which must have been just underneath the original surface of the caldera-fill rocks) appears on this diagram to have been fairly deeply eroded in the vicinity of the ring fault. In fact, this topographically low area is a result of its being on the south flank of the resurgent dome, the effects of which have not been removed in this diagram.



part of the caldera than in the eastern part (Fig. 6.6 and Plate 3). For example, except for the solfatarically altered zone, the ring domes are isotopically nearly unaltered ($\delta^{18}\text{O} > +6$), as is the topographically high (< 3950 m elevation) upper Sunshine Peak Tuff ash-flow unit in the southeast quarter of the caldera. However, samples of Sunshine Peak Tuff from similarly high areas (> 3900 m elevation) along the western Central Ridge and Cooper Ridge all have $\delta^{18}\text{O}$ values less than +1, and samples from the Sunshine Peak-Redcloud Peak ridge in the south-central part of the caldera (the highest ridge within the caldera, > 4200 m) have intermediate $\delta^{18}\text{O}$ values less than +3.

Figure 6.12 shows a reconstruction of the caldera at its present level of exposure if the post-alteration eastward tilting is removed. Figure 6.12 was constructed by assuming that about 6° of eastward tilting has occurred (based on the Precambrian-Tertiary contact south of the caldera and the intravolcanic contacts above the Precambrian granite; all these contacts dip about 6° east). Figure 6.12 clearly shows that those parts of the caldera that have the lowest $\delta^{18}\text{O}$ values (compare Figs. 6.6 and 6.12) were altered at very deep levels (> 2 km), and that the relatively unaltered rocks with high $\delta^{18}\text{O}$ values are confined to very shallow levels (< 500 m).

6.5.6 Effect of Proximity to the Resurgent Intrusions

Low $\delta^{18}\text{O}$ values (< +3) are found in and around the central resurgent intrusions (Figs. 6.6 and 6.11, Plates 3 and 4). These low- ^{18}O zones make up the central tines of the fork-shaped, low- ^{18}O pattern discussed above in Section 6.5.1. The lowest $\delta^{18}\text{O}$ values in the central

tines are associated with intrusive exposures 8 (-1.8) and 11 (-1.4); broad zones of low $\delta^{18}\text{O}$ values ($< +1$) surround these two exposures. The cross sections in Plate 4 also show this relationship, particularly sections B-B', C-C', and D-D', in which zones of $\delta^{18}\text{O}$ values less than -1 correspond almost exclusively to areas of the resurgent intrusion. Successively higher $\delta^{18}\text{O}$ contours are dome-shaped, and drape over the resurgent intrusion parallel to the intrusive contact. Comparisons between the geologic (Fig. 6.9) and $\delta^{18}\text{O}$ (Fig. 6.11) composite radial cross sections also show this pattern.

Variations between $\delta^{18}\text{O}$ values and distance from the resurgent intrusion are examined in more detail in Figure 6.13. In this diagram the $\delta^{18}\text{O}$ values of Sunshine Peak Tuff samples that lie above the resurgent intrusion and within the outermost structural contour (Fig. 6.7) are plotted versus sample height above this contact. Note the strong positive correlation in Figure 6.13 between the $\delta^{18}\text{O}$ value and sample height above the intrusion, regardless of sample lithology.

Figure 6.14 is an identical plot to Figure 6.13 but also includes mineralogical alteration data for the Sunshine Peak Tuff samples. Hornfelses tuff and zones I, II, III, and IV argillized tuff can all occur close to the upper intrusive contact, and, except for zones I and II, these alteration facies do not display a very pronounced correlation with height above the intrusive contact. However, the $\delta^{18}\text{O}$ values are lowest (+1.3 to +3.3) for hornfelses tuff and grade to progressively higher values in zone III tuff (+2.1 to +4.1) and zone IV tuff (+2.7 to +5.3). A single sample of zone V tuff lies about 500 m above the intrusive contact with a $\delta^{18}\text{O}$ value of +5.9. The alteration facies in the

Figure 6.13 Sample height above the resurgent intrusion plotted versus the whole-rock $\delta^{18}\text{O}$. This plot includes only those samples which lie within the area enclosed by the structural contours on Figure 6.7. An obvious positive correlation exists between sample height and $\delta^{18}\text{O}$ value.

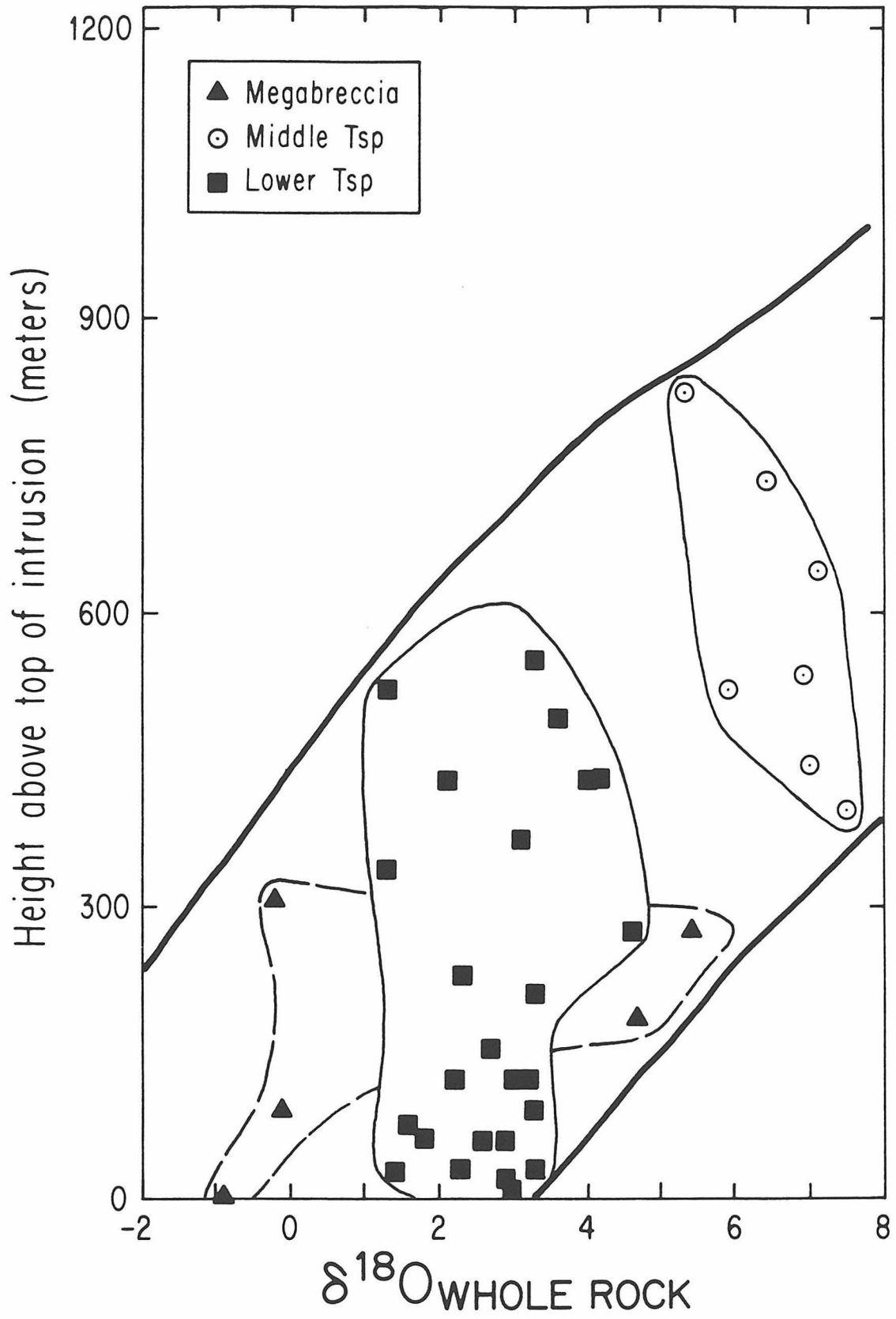
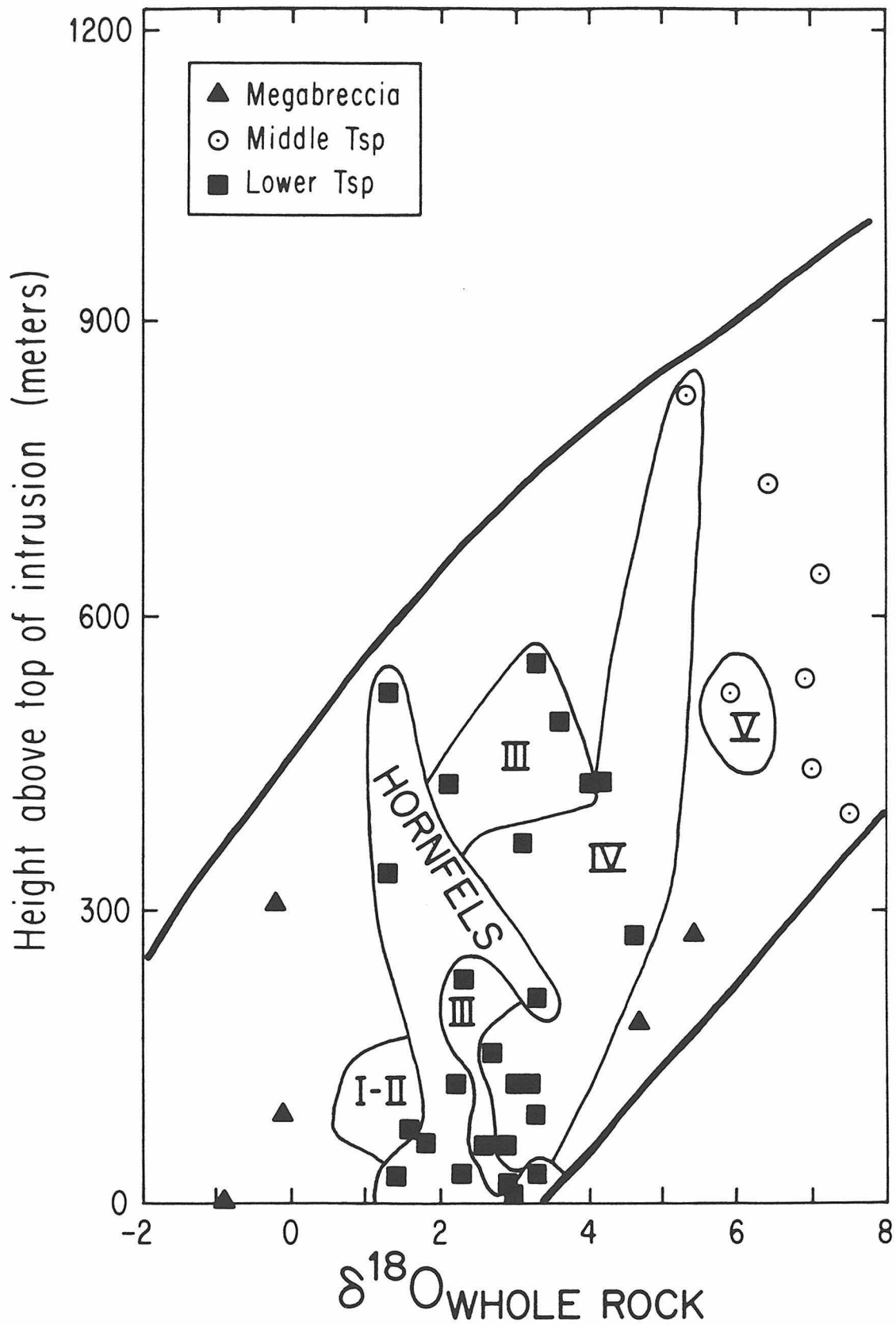


Figure 6.14 Sample height above the resurgent intrusion plotted versus whole-rock $\delta^{18}\text{O}$, with the alteration facies indexed for each Sunshine Peak Tuff sample. Hornfelsed, zone I, and zone II tuff have the lowest $\delta^{18}\text{O}$ values. $\delta^{18}\text{O}$ increases and the field of each facies extends to higher elevations as the alteration progresses from zone I through zone IV. However, except for the hornfels, the alteration facies themselves correlate only weakly with distance from the intrusive contact; they are controlled mainly by proximity to local hydrothermal flow channels (major fractures).



Fracture Regime thus, as might be expected, show only a weak correlation with proximity to the resurgent intrusion; they are much more sensitive to proximity to actual hydrothermal conduits (local fractures).

6.5.7 Effect of Topography

Elevations within the caldera range from greater than 14000 ft (4267 m) at Redcloud Peak and Sunshine Peak to below 9600 ft (2926 m) in Alpine Gulch (Figure 3.1). Topographically low areas occur around the caldera ring fault (Henson Creek on the north and the Lake Fork of the Gunnison River on the south). The interior of the caldera is highest near the center of the resurgent intrusion (along Central Ridge and other high ridges that extend away from it). This high central area has been cut by numerous valleys that drain outward into Henson Creek and the Lake Fork, providing up to 2 km of relief within the resurgent dome of the caldera.

Comparison between Figures 6.6 and 3.1 and examination of the cross sections in Plate 4 show that low $\delta^{18}\text{O}$ values clearly correlate with low elevation areas in: 1) the entire length of Henson Creek, 2) Alpine Gulch, 3) Burrows Park and the upper Lake Fork, 4) Silver Creek, 5) Cooper Creek, 6) Bent Creek, 7) Grizzly Gulch, and 8) upper Owl Gulch.

High $\delta^{18}\text{O}$ values clearly correlate with high elevation areas in: 1) Cooper Ridge, 2) the West End of the Central Ridge, 3) the Sunshine Peak-Redcloud Peak ridge, 4) The Central Ridge and its East End, 5) the high areas around Red Mountain and Grassy Mountain, 6) Alpine Ridge (even though this area lies close to the ring fault and near ring intrusions), 7) the high area north of Henson Creek, and 8) the high area

around Handies Peak. Also, as discussed in detail in Chapter 4, the Precambrian granite exposed on Half Ridge has $\delta^{18}\text{O}$ values higher than topographically lower granite. In fact, the Half Ridge uplift was originally delineated when it became apparent that a high-elevation, high $\delta^{18}\text{O}$, sub-group of granite samples could be singled out.

An even better correlation between $\delta^{18}\text{O}$ and topography is observed if the effects of regional tilting are removed (Fig. 6.12). There is a striking similarity between the adjusted topography of Figure 6.12 and the $\delta^{18}\text{O}$ map of Figure 6.6, particularly after making allowance for the fact that the topographic effect of resurgent doming has not been removed from Figure 6.12.

6.5.8 Effect of the Ring Fault

Areas of low- ^{18}O rocks ($< +1$) occur all along the ring fault in the western half of the caldera (Fig. 6.6). These zones define the two outer tines of the fork-shaped low- ^{18}O zone. The lowest $\delta^{18}\text{O}$ values in the entire area occur in the vicinity of the ring fault, and it is clear that the ring fault zone was a major area of enhanced fracture permeability during the lifetime of the Lake City hydrothermal system. These low- ^{18}O zones steadily narrow to the east along the ring fault, and eventually die out in the eastern half of the caldera because here the ring fault is structurally higher than the ring fault to the west.

The structural cross sections also show these relationship (Plate 4). Where these sections cut across the ring fault in the western half of the caldera (on B-B', in the southern part of E-E', and in the western part of D-D'), the $\delta^{18}\text{O}$ contours are deflected upward into sharp,

narrow spikes that define very steep $\delta^{18}\text{O}$ gradients in the vicinity of the ring fault. This sharpness and narrowness is probably related to the fact that the ring fault is characteristically a single, sharply-defined fracture. In other areas where ring faults are wider zones, or are more deeply eroded (the Idaho batholith and the Silverton caldera, see Chapter 7) the low $\delta^{18}\text{O}$ zone along the ring fault is typically much broader (up to 5 km wide). The northern Lake City ring fault is associated with a broader low- ^{18}O zone than the southern ring fault, presumably because of the abundant ring intrusions along the northern caldera wall (compare Figs. 6.9 and 6.11).

6.5.9 Does a $\delta^{18}\text{O}$ Discontinuity Exist along the Ring Fault ?

The major resurgence of the Lake City caldera and upward movement of the caldera core along the ring fault conceivably could have occurred either just prior to, during, or after the bulk of the meteoric-hydrothermal alteration. These relationships will be examined in more detail in Chapter 7. However, if significant resurgence occurred after most of the hydrothermal activity, low- ^{18}O rocks inside the ring fault would have been displaced upward against higher- ^{18}O rocks (altered at higher elevation and lower temperature) outside the ring fault. This process could explain the juxtaposition of low $\delta^{18}\text{O}$ values just inside the ring fault and high $\delta^{18}\text{O}$ values just outside the fault that is observed in several locations (for example along Bent Creek, +1.8 vs. +7.9; along Alpine Gulch, -1.6 vs. +1.6; and southwest of Sunshine Peak, -2.5 vs. +4.1). However, such movement must have been restricted to the western portion of the ring fault, if it occurred at all, because the

solfatarically altered lava ring domes are not faulted along the extension of the ring fault. In any case, $\delta^{18}\text{O}$ values typically change rapidly as one gets closer to the ring fault (Plate 4); this effect, which is probably a result of increasingly higher W/R ratios approaching a zone of major permeability, also could explain these very steep $\delta^{18}\text{O}$ gradients. Thus, although a case can be made that a $\delta^{18}\text{O}$ discontinuity does exist along the ring fault, much more detailed sampling of this complex area would be necessary to prove it conclusively, one way or the other.

6.5.10 Effects of Other Faults and Fractures

Resurgence-related fractures within the Lake City caldera lie on trends parallel to that of the Eureka graben. Many of these appear to themselves be small, normal faults. Figure 6.6 and Plate 4 show that the $\delta^{18}\text{O}$ values decrease as these structures are approached, even at constant elevation. For example the Sunshine Peak-Redcloud Peak ridge samples are lower in ^{18}O than are a priori expected based on their high elevation (Fig. 6.11). Similar decreases in $\delta^{18}\text{O}$ values at constant elevation are seen as one progresses northwest along the Central Ridge (where low $\delta^{18}\text{O}$ values are also in part due to proximity to the resurgent intrusion) and from northeast to southwest along Cooper Ridge to the extension of the Eureka graben axis. There is thus no doubt that fractures that can be presently observed and mapped in the field were important local conduits for meteoric-hydrothermal fluids within the caldera.

Some samples specifically collected close to fractures also have

anomalously low $\delta^{18}\text{O}$ values (0.0 northeast of Cooper Ridge, -2.1 in lower Silver Creek, -1.7 in Cooper Creek, and 0.4 on the south end of Cooper Ridge). Also, some areas that contain anomalously high fracture densities have anomalously low $\delta^{18}\text{O}$ values (for example the Sunshine Peak-Redcloud Peak ridge and the small ridge south of the east end of resurgent intrusion exposure 11).

6.5.11 Effect of Mineralogy and Lithology

All Sunshine Peak Tuff samples had nearly identical initial $\delta^{18}\text{O}$ values, grain size, and mineralogical composition ($\delta^{18}\text{O} = +7.2$ to $+7.3$, Section 6.1.1). Thus there is virtually no primary lithologic effect to worry about in discussing the alteration of the tuff samples. The resurgent and ring fracture intrusions also probably had initial $\delta^{18}\text{O}$ values nearly identical to those of the tuff. These intrusions may have been slightly less susceptible to alteration than the Sunshine Peak Tuff because of their coarser grain size, but such a relationship is totally obscured by their consistently higher temperature alteration (they are consistently at least as ^{18}O depleted as nearby hornfelsed tuff, see Fig. 6.6).

K feldspar phenocrysts were analyzed for only a few Sunshine Peak Tuff and resurgent intrusion samples. Coarse K feldspar phenocrysts (to 1.5 cm) from intrusive exposures 11 and 13 (Fig. 3.1) have higher $\delta^{18}\text{O}$ values than the whole-rock host material (respectively $+1.6$ vs. -0.7 and $+2.9$ vs. $+0.5$). Phenocrysts in both samples are argillized along their rims and along fractures and cleavage planes, but have mineralogically fresh interiors. Thus their coarse grain size inhibited

interaction between the phenocrysts and the hydrothermal fluid; such interactions apparently occurred mainly along the rims of the phenocrysts and along penetrating cracks. The lower $\delta^{18}\text{O}$ whole-rock values can be attributed to the much smaller grain size of the groundmass K feldspars, which must have totally exchanged with the meteoric-hydrothermal fluid.

Two other intrusive samples from exposures 1 and 9 have $\delta^{18}\text{O}$ K feldspar phenocryst values lower than the $\delta^{18}\text{O}$ whole-rock values (respectively -1.1 vs. +1.2 and -4.0 vs. -1.6). Both these samples contain argillized clots throughout the K feldspar phenocrysts, and thus these feldspar grains appear to have thoroughly exchanged with the hydrothermal fluid. Similar relationships are observed in the three tuff samples from which sanidine phenocrysts were analyzed. One sample in Alpine Gulch contains sanidine phenocrysts altered only along their margins and cleavage planes, and exhibits the "reversed" $\delta^{18}\text{O}$ sanidine-whole-rock relationship (sanidine = +4.8, whole-rock = +2.3). The two other tuff samples, one from near the summit of Redcloud Peak (the highest tuff sample collected) and one from lower Alpine Gulch (coincidentally the lowest tuff sample collected) contain sanidines with scattered clay clots throughout; here, the sanidine $\delta^{18}\text{O}$ values are lower than the whole-rock $\delta^{18}\text{O}$ values (respectively +4.3 vs. +5.3 and -1.9 vs. -1.6).

Lithologic effects are clearly important when comparing Sunshine Peak Tuff data with: 1) the megabreccia (Section 6.2), because those units are composed of fragments of various volcanic and intrusive lithologies that must have had different initial $\delta^{18}\text{O}$ values and because the megabreccias were originally much more permeable to fluid flow; and

2) the Precambrian granite (Chapter 4), because the granite has a higher initial $\delta^{18}\text{O}$ value (+9.2 to +9.8), is much coarser grained, and contains about 30 percent inert quartz.

CHAPTER 7

HYDROTHERMAL CIRCULATION IN THE LAKE CITY CALDERA

7.1 A Review of Caldera-Related Hydrothermal Systems7.1.1 Shallow, Caldera-Related Hydrothermal Activity in the Western United States

Observations in active, caldera-related, meteoric-hydrothermal systems provide considerable information about the fluid-flow patterns in the shallower portions of such environments. A review of such systems is useful for comparison with the Lake City hydrothermal system.

Smith and Bailey (1968) define a model for the evolution of resurgent cauldrons (Table 7.1) which includes, as a last stage (stage VII), terminal solfataric and hot spring activity. In the Smith and Bailey (1968) model, terminal solfataric and hot spring activity follows resurgent doming (stage V) and major ring fracture volcanism (stage VI). Smith and Bailey (1968) also state that hot springs and solfataras are probably active throughout most of the caldera cycle. The evolution of the Lake City caldera follows the Smith and Bailey (1968) model. Stage VII terminal solfataric and hot spring activity is currently active in three young resurgent calderas in the western United States: the Long Valley caldera, California, the Yellowstone caldera, Wyoming, and the Valles caldera, New Mexico.

7.1.2 Long Valley Caldera, California

The Long Valley caldera formed 0.7 m.y. ago in response to the eruption of the Bishop Tuff (Bailey et al, 1976). Subsequent intracaldera volcanism was associated with resurgence or occurred along the

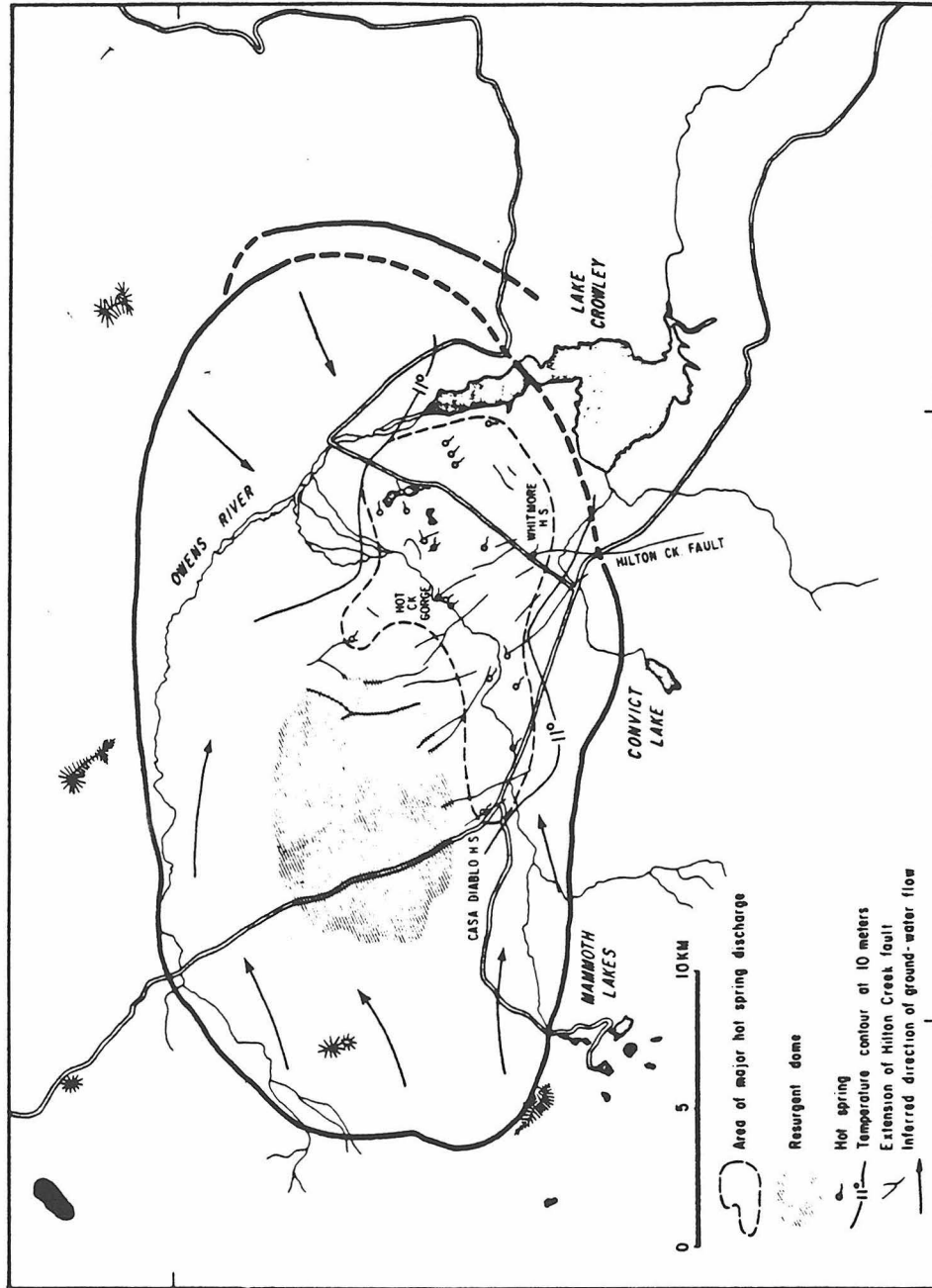
Table 7.1 Stages in the development of resurgent cauldrons (Smith and Bailey, 1968)

Stage	Structural Events	Volcanic Events	Sedimentary Events	Plutonic Events	Duration in the Valles Caldera
I	Regional tumescence and propagation of ring and radial fractures with possible apical graben subsidence.	Eruptions due to leakage along radial or ring fractures.	Erosion of the volcanic highland.	Compositional zonation in magma chambers. Increasing magma pressure. Minor intrusion.	$< 4 \times 10^5$ yrs
II	—	Major ash-flow eruption, 50-500 mi ³ .	—	Degassing and skimming of zoned top of chamber.	$< 10^5$ yrs. (est)
III	Caldera collapse.	Overlap with stage II in some calderas.	Avalanches and slides from caldera walls.	Disequilibrium.	$< 10^5$ yrs. (est)
IV	—	Minor pyroclastic eruptions and lavas on caldera floor in some calderas.	Caldera fill; talus, avalanches, slides, fans, lake deposits.	Consolidation of magma caught in ring fractures (residual ring dikes). Progressive recovery of equilibrium. Beginning of minor ring intrusion.	$< 10^5$ yrs
V	Resurgent doming.	Possible ring-fracture volcanism and/or eruption or intrusion in dome fractures.	Caldera fill continues. (Lake overflows and caldera is breached.)	Rise of central pluton and perhaps a ring-intrusion stage.	
VI	Possible regional tumescence and reopening of ring fractures.	Ring-fracture volcanism. Possible stage II eruption of next cycle	Caldera fill continues, late lake sediment. Erosion of fill. Fill $>$ erosion.	Final emplacement and differentiation of ring intrusions. Possible stopping by central pluton.	8×10^5 yrs $\pm 10^5$ yrs
VII	—	Terminal fumarolic and hot spring activity (hydrothermal alteration).	Erosion. Erosion $>$ fill.	Crystallization of major plutons. Possibly a major ore-forming stage.	$> 10^5$ yrs

ring fracture; this volcanism ranges in age from 0.68 m.y. to as young as 450 years (Bailey et al, 1976). Hot springs and fumaroles are currently active within the collapsed block of the caldera (Rinehart and Ross, 1964; Lachenbruch et al, 1976; Sorey and Lewis, 1976). Most of these active hot springs and fumaroles are located on or near active extensions of the Sierra Nevada frontal Hilton Creek fault (Rinehart and Ross, 1964; Bailey et al, 1976). However, the general distribution of hydrothermal activity within the caldera is in an arcuate zone peripheral to the eastern edge of the resurgent dome (Fig. 5.1) (Bailey et al, 1976; Lachenbruch et al, 1976). Argillized and acid-sulfate altered rocks are widely distributed throughout the caldera, in most cases not associated with active geothermal areas, suggesting that surficial hydrothermal activity was previously much more extensive in the caldera than at present (Bailey et al, 1976). Extensive hot spring deposits in lacustrine sedimentary rocks deposited in the moat of the caldera suggest that hydrothermal activity in the caldera peaked at the time of deposition of these rocks, about 0.3 m.y. ago (Bailey et al, 1976).

Variations in thermal gradients in shallow (< 30 m) wells within the Long Valley caldera define three regions of shallow hydrothermal fluid circulation (Lachenbruch et al, 1976). Group I wells exhibit small thermal gradients and no seasonal temperature variations, suggesting that local shallow heat transfer is predominantly by conduction. Lachenbruch et al (1976) suggest that, for group I wells, heat from greater depth is being absorbed by moving groundwater, a characteristic condition of areas of hydrologic recharge. Thus, the areas near the Long Valley caldera ring fracture, along which group I wells are

Figure 7.1 Distribution of hot springs in the Long Valley caldera
(from Lachenbruch et al, 1976). The hot springs are located inside
the caldera ring fault, in an arcuate zone peripheral to the south-
eastern margin of the resurgent dome of the caldera.



concentrated, may be an area of shallow recharge. Group III wells exhibit large, variable, thermal gradients, from which Lachenbruch et al (1976) infer that group III wells occupy zones of regional discharge. The area of group III wells coincides with the area of current hot spring activity on the southeastern margin of the resurgent dome within the caldera (Fig. 7.1). Group II thermal gradients are intermediate between those for groups I and III, and are similar to background regional gradients. The areas in which group II wells are located probably lie above regions less disturbed by water flow (Lachenbruch et al, 1976). Deeper holes (to 300 m) drilled in areas of group III shallow wells display local gradient reversals; Lachenbruch et al (1976) suggest that this is caused by lateral and vertical circulation of hot water in permeable layers or fractures.

Source areas for fluids circulating in the Long Valley caldera probably lie to the west in the higher Sierra Nevada Mountains (Mariner and Wiley, 1976; Lachenbruch et al, 1976). D/H and $^{18}\text{O}/^{16}\text{O}$ measurements of thermal waters from the Long Valley caldera (Mariner and Wiley, 1976) show that these waters have experienced a small ^{18}O shift (about 5 per mil) along a trajectory parallel to acid sulfate-type geothermal waters (Fig. 4.1) with a slope of about 3. This trajectory intersects the meteoric water line at δD equal to about -130 per mil and $\delta^{18}\text{O}$ equal to about -17.5 per mil. Local surface water on the western caldera margin has a $\delta^{18}\text{O}$ value of -15.9 per mil and a δD value of -115 per mil (Mariner and Wiley, 1976). The fluid sources for the hot spring discharge water are depleted in ^{18}O relative to local meteoric water, and have an isotopic composition similar to that which is found

in the high Sierra Nevada Mountains to the west (Taylor, 1974a). Limited data on water-table elevations (Lewis, 1974, as reported in Lachenbruch et al, 1976) show that flow in the shallow groundwater system is controlled by the surface topographic gradients.

Thus, hydrothermal fluids involved in the Long Valley meteoric-hydrothermal system must have originated in the higher Sierra Nevada Mountains to the west. Flow directions in this system are thus from west to east, even though areas of discharge lie to the east of the resurgent dome, away from the fluid source. Minor recharge occurs along the ring fault, where local meteoric water flows down and infiltrates the system.

7.1.3 Yellowstone Caldera, Wyoming

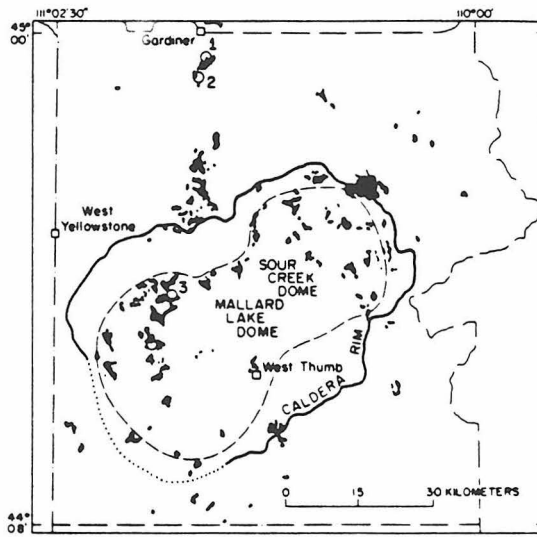
In Yellowstone Park, Wyoming, about 0.6 m.y. ago, a voluminous ash-flow eruption resulted in collapse of the two contiguous blocks of the 70 by 45 km Yellowstone caldera (Eaton et al, 1975). This event occurred within a few days, following 0.6 m.y. of relatively non-explosive rhyolite-flow activity. Resurgent doming of the two blocks, with associated ring-fracture volcanism, followed this collapse. Since then, rhyolitic extrusive activity has continued intermittently right up to the present time. The youngest such dome is about 70,000 years old, and the eruptions are probably not yet permanently ended (Eaton et al, 1975). A variety of geophysical measurements are interpreted by Eaton et al (1975) as strongly suggesting the presence of a large, partially molten magma body beneath the Yellowstone rhyolite plateau.

The development of the Yellowstone caldera follows the Smith

and Bailey (1968) resurgent cauldron model. Stage VII terminal solfataric and hot spring activity is manifest in the numerous, well known, thermal springs in Yellowstone National Park (Fig. 7.2). Within the Yellowstone caldera, this activity is concentrated near ring fracture zones and along the margins of the two resurgent domes (Eaton et al, 1975; Leeman et al, 1977). Heat flow measurements in lake sediments from Yellowstone Lake, which straddles the southeastern caldera boundary, show that conductive heat flow is relatively low outside the caldera margin, but increases through a steep gradient inside the caldera boundary, and is highest in areas of hot spring activity (Morgan et al, 1977). Thermal measurements in deep drill holes (to 300 m) in hot spring areas within the caldera show that convective fluid flow is confined to areas of high permeability, such as in fractures or porous layers (White et al, 1975). Near the surface, hydrothermal fluids flowing up from deeper parts of the system locally mix with surface meteoric waters. Evidence for such mixing is provided by (1) dilution of Cl concentrations, (2) a lowering of the $\delta^{18}\text{O}$ value relative to the typical meteoric-hydrothermal fluids, and (3) shifts in deuterium concentrations (Lower and Shoshone Geysers basins in the caldera, Truesdell et al, 1977). Thermal waters from the Norris basin show no mixing effects (Truesdell et al, 1977).

Craig (1963) first noted that thermal fluids discharging in Yellowstone National Park were of meteoric origin (Fig. 4.1). However, deep thermal waters in the Yellowstone system have a δD of -149 per mil, distinct from local surface meteoric waters, which range from -144 to -133 per mil (Truesdell et al, 1977). This suggests that the deep

Figure 7.2 Distribution of hot springs in the Yellowstone National Park (from Leeman et al, 1977). Inside the caldera, hot spring and fumarole activity is either peripheral to the resurgent Mallard Lake and Sour Creek domes or along the caldera ring faults.



water probably flowed into the caldera from areas of higher elevation outside the caldera (Truesdell et al, 1977). Pb and Sr isotopic compositions of hot spring deposits within Yellowstone Park show that the Pb and Sr in the fluids from which these deposits were precipitated contained significant sedimentary components (Leeman et al, 1977). These components must have been leached from sediments outside the caldera as the fluid flowed into the caldera through deep channels, because there are no known sediments exposed on the surface in the vicinity of the caldera margin (within about 10 km).

Features of the meteoric-hydrothermal system in the Yellowstone caldera, therefore, resemble those found at the Long Valley caldera. Water involved in the system originated as meteoric water in topographically higher areas outside the caldera. The fluid flowed into the caldera through deep channels. Areas of discharge within the caldera are distributed around the margins of the resurgent domes or along the ring structure. Upflowing thermal waters close to the surface mix with small quantities of local meteoric water, and shallow flow is strongly controlled by permeable zones such as fractures or porous layers.

7.1.4 Valles Caldera, New Mexico

Although the Valles caldera, New Mexico, is the "type" resurgent cauldron upon which Smith and Bailey (1968) originated their model, the geothermal system associated with the caldera is not well defined in the published literature. The Union Oil Company has conducted extensive drilling and geophysical investigations in the caldera in an attempt to

define a geothermal resource, but most of the data are proprietary and unavailable (Laughlin, 1981).

The Valles caldera collapsed in response to the eruption of the upper member of the Bandelier Tuff 1.0 m.y. ago (Doell et al, 1968). Rhyolite ring domes along the caldera rim (Fig. 7.3) are as young as 0.1 m.y. old (Doell et al, 1968). Although alteration is widespread in the caldera (Doell et al, 1968), active hot spring activity is restricted to the west side of the caldera, adjacent to the resurgent dome (Smith and Bailey, 1968). Resurgent graben faults and other structures represent important shallow permeable flow conduits (Laughlin, 1981). In these respects the Valles caldera hydrothermal system resembles the Yellowstone and Long Valley systems.

The Lake City caldera is geologically almost a duplicate of the Valles caldera, but is about 22 m.y. older and has been eroded to provide a three-dimensional picture of the paleohydrothermal system. Both calderas conform perfectly to the Smith and Bailey (1968) model. Lambert and Epstein (1980) have published $\delta^{18}\text{O}$ values of hydrothermally altered rocks from a 1687 m-deep drill hole (Baca no. 7, Fig. 7.3) which can be used to compare some aspects of hydrothermal alteration between these two calderas.

The initial unaltered $\delta^{18}\text{O}$ value of the Bandelier Tuff (+7.3 to +7.6, Lambert and Epstein, 1980) is nearly identical to that of the Sunshine Peak Tuff (+7.2, Chapter 6). Both tuffs contain K feldspar and quartz as major phenocryst minerals, but the Bandelier Tuff also contains minor clinopyroxene and fayalite (Doell et al, 1968) whereas the Sunshine Peak Tuff lacks these ferromagnesian minerals but does

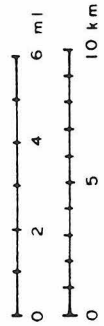
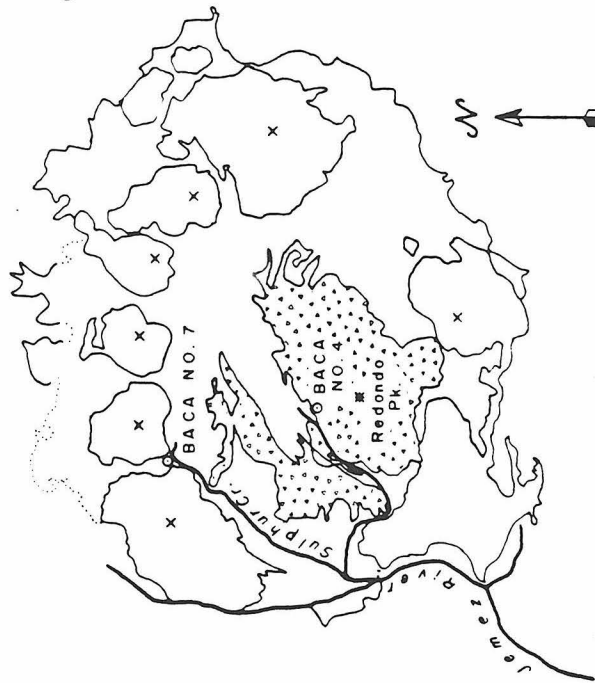
Figure 7.3 Map of the Valles caldera, New Mexico, showing the locations of the ring domes and the Baca no. 7 drill hole (from Lambert, 1975).

VALLES CALDERA

after SMITH, BAILEY, and ROSS
1970



- WELL LOCATION
- × RHYOLITE DOME
-  SURFACE OUTCROPS OF BANDELIER TUFF IN VALLES CALDERA



contain biotite. Permian sedimentary rocks occur beneath the Bandelier Tuff in the Valles caldera, but the Baca no. 7 drill hole in the Valles caldera does bottom in a Precambrian granite similar to the Precambrian granite of Cataract Gulch southwest of the Lake City caldera. Ring domes emplaced along the Valles ring fault (Fig. 7.3) are analogous to the Red Mountain-Grassy Mountain ring dome at Lake City, and the ring intrusions along the northern Lake City caldera ring fault probably were feeders to other such ring domes. Alteration in the Bandelier Tuff samples within the Valles caldera consists of replacement of the groundmass by quartz and kaolinite with minor sericite and calcite (Doell et al, 1968). This alteration is mineralogically similar to the argillized and chlorite/calcite alteration in the Sunshine Peak Tuff. Present-day surface waters from the Valles caldera have $\delta^{18}\text{O}$ values in the range -11 to -13.3 (Lambert and Epstein, 1980), whereas meteoric waters in the western San Juan Mountains had a $\delta^{18}\text{O}$ value of about -15 (Chapter 4) during the Lake City hydrothermal event.

$\delta^{18}\text{O}$ values from the Baca no. 7 drill hole samples (Lambert and Epstein, 1980) are plotted on Figure 7.4 as a function of sample depth. For comparison, $\delta^{18}\text{O}$ values of Sunshine Peak Tuff samples collected within about 2 km of cross section C-C' (Plate 1), from where it crosses Central Ridge north to the intersection with cross section D-D', are also plotted as a function of sample depth beneath the projected top of the upper Sunshine Peak Tuff.

$\delta^{18}\text{O}$ values of samples from above the Bandelier Tuff in Baca no. 7 range from +4.5 to +7.9. Below the upper Bandelier Tuff contact the $\delta^{18}\text{O}$ values are much lower (+1.9 to +3.9). The pattern of lower $\delta^{18}\text{O}$

Figure 7.4 Whole-rock $\delta^{18}\text{O}$ values from the Baca no. 7 drill hole (Lambert and Epstein, 1980) compared to some $\delta^{18}\text{O}$ values from the Lake City caldera. Also shown are calcite-water $^{18}\text{O}/^{16}\text{O}$ fractionation temperatures from the drill hole (Lambert and Epstein, 1980) and the hydrostatic boiling curve for pure water (Haas, 1971) that was used in the Red Mountain solfataric model (Chapter 5). $\delta^{18}\text{O}$ values from both the Valles caldera and Lake City caldera show similar decreases with increasing depth. See text for further discussion.

values with increasing depth in the Valles caldera is nearly identical to that shown for the Lake City caldera samples in Figure 7.4. Also, feldspar from the Precambrian granite at the bottom of Baca no. 7 has a $\delta^{18}\text{O}$ value of +1.3, and igneous quartz from this sample has a value of +8.2. These data are consistent with the $\delta^{18}\text{O}$ values of minerals from the Cataract Gulch granite at Lake City (Fig. 4.4).

Calcite-water fractionation temperatures determined for hydrothermal calcite from Baca no. 7 are also shown on Figure 7.4 (Lambert and Epstein, 1980). These calculated temperatures are known to be within a few degrees Celsius of measured borehole temperatures (Lambert and Epstein, 1980). A temperature measurement of 229°C is reported for the bottom of Baca no. 7 (Lambert, 1975). This temperature is also consistent with the calculated temperatures. The thermal gradient used for the Red Mountain solfataric model at Lake City is also shown on Figure 7.4. This curve has a shape similar to that for the Baca no. 7 well. The similarity of the vertical $\delta^{18}\text{O}$ patterns and thermal gradients between the Lake City and Valles calderas, together with their geological similarities, show that these two hydrothermal systems must be nearly identical.

Lambert and Epstein (1980) conclude that the meteoric-hydrothermal fluid in the Valles geothermal system has undergone only a negligible ^{18}O shift during water/rock interaction, probably because water/rock ratios in this system are very large. Lambert and Epstein (1980) suggest that the history of the hydrothermal activity in the Valles caldera is marked by three isotopically-preserved thermal events: (1) an early event (probably about 100°C) that produced hydrothermal quartz

in the groundmass of the Bandelier Tuff, (2) a second event (150° to 180°C) best preserved in calcite $\delta^{18}\text{O}$ values in Permian limestones in Baca no. 7, and (3) the currently active hydrothermal system involving temperatures greater than 230°C in lower parts of the section in Baca no. 7. Thus, the temperature of the hydrothermal activity at the Valles caldera seems to have risen with time with no evidence of any cooling.

7.1.5 Oxygen Isotopic Evidence for Deep Meteoric-Hydrothermal Fluid Circulation in Eroded Calderas

The deeper portions of active, caldera-related hydrothermal systems cannot as yet be examined directly, owing to the restrictions placed by present-day drilling technology. Where exposed by erosion, however, stable isotopic investigations of the deeper portions of paleo-hydrothermal systems have provided much useful information regarding fluid flow in the caldera environment.

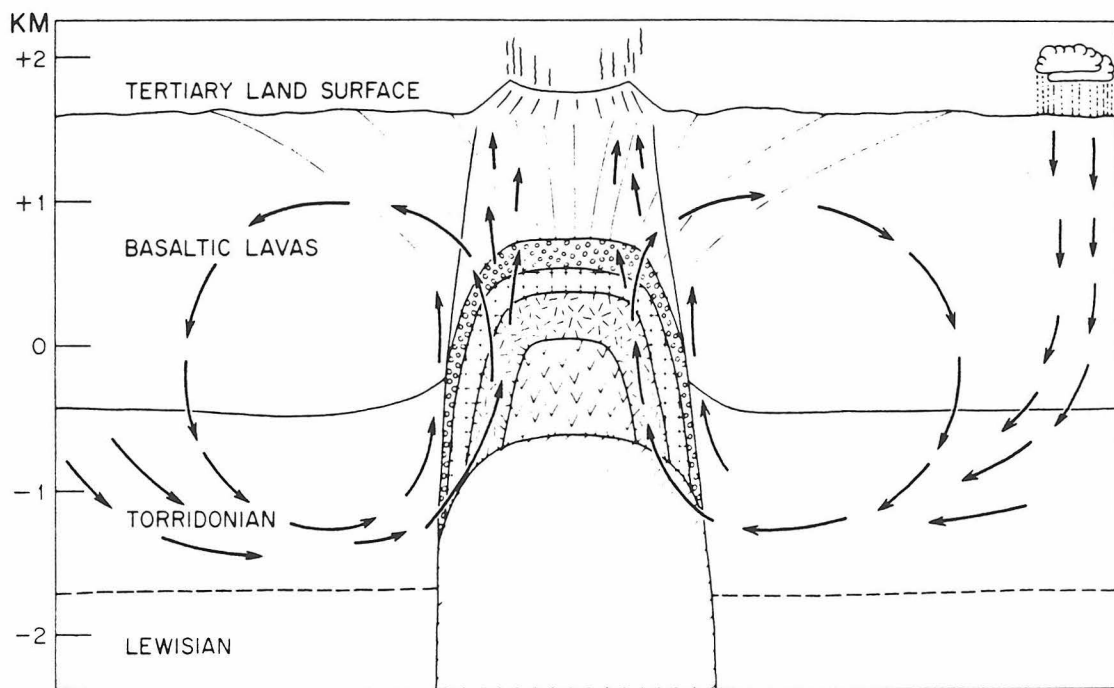
Ring-fracture volcanism typically takes place just before the terminal solfataric and hot spring activity (Table 7.1); this is accompanied by the intrusion of dikes into the caldera ring fractures. After erosion and denudation of resurgent calderas, granitic ring complexes with central plutons are exposed, and can be used to infer the original existence of the calderas. Smith and Bailey (1968) cite several examples of such eroded calderas, including some that occur in the Scottish Hebridian province. In the Hebridian province, ring dikes have been recognized at Mull, Skye, and Ardnamurchan, among other intrusive centers (Emeleus, 1982).

Mull, Skye, and Ardnamurchan were the object of several oxygen and

hydrogen isotopic investigations by Taylor and Forester (1971) and Forester and Taylor (1977a, 1977b). These authors found large areas of ^{18}O -depleted rocks centered on the intrusive complexes. About 400 km^2 around both Skye and Mull were depleted in ^{18}O by as much as 6 or 7 per mil, and about 80 km^2 around Ardnamurchan were depleted by as much as 3 to 6 per mil. Deeply circulating, upflowing, heated meteoric water is the only material that could have caused such ^{18}O depletions (Taylor and Forester, 1971). The strong jointing in the plateau lavas and the fracture-generating effects related to forcible intrusion and caldera collapse both greatly enhanced permeability of the rocks, allowing ground water to flow through the walls adjacent to the ring dikes and other intrusions at all three centers. At Ardnamurchan and Mull, intrusive rocks emplaced directly into the plateau lavas are more ^{18}O depleted than intrusive rocks emplaced into other, much less fractured, intrusive rocks. Also, at Mull, felsic rocks emplaced along the caldera-ring structures are the most ^{18}O depleted rocks associated with the complex. This probably resulted from higher W/R ratios in the ring fracture zone, controlled by the enhanced permeability contributed by the fractures (Taylor and Forester, 1971).

The present levels of exposure at Mull, Skye, and Ardnamurchan are 2 to 3 km below the original eruptive surface. It is apparent, then, that at these depths in caldera-related meteoric-hydrothermal systems, the fluid flow is dominated by permeability, particularly fracture-induced permeability related to the ring structures (Fig. 7.5). The fluids are meteoric water derivatives and are convectively rising at this point. Thus, the dominant volume of recharge into the convective

Figure 7.5 Generalized hydrothermal flow pattern associated with the Scottish Hebridian ring dike complexes (from Taylor and Forester 1971). Upward, convectively-driven circulation is concentrated along the ring intrusions. Recharge into the system is meteoric water derived from some distance away from the caldera. This water flows into the system through porous deep aquifers. Only minor quantities of fluid penetrate into the non-porous crystalline Lewisian basement.



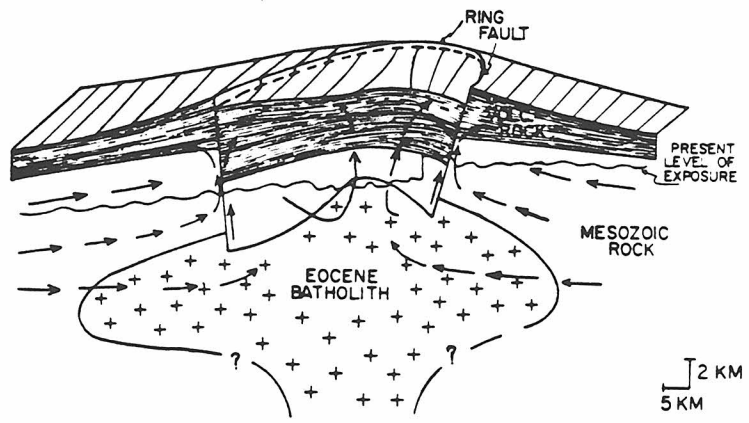
cell must occur at least 2 to 3 km below the eruptive surface.

Annular zones of ^{18}O depletion surrounding Eocene plutons intruded into the Mesozoic Idaho batholith have been interpreted by Criss and Taylor (1983) to have formed in very deep (5 to 7 km) portions of caldera meteoric-hydrothermal convection systems (Fig. 7.6). Criss and Taylor (1983) note that these ^{18}O -depleted zones coincide with intrusive-related faults, which they suggest formed as a result of subsidence during eruption of the Challis ash-flow tuffs associated with the Eocene plutons. Very high W/R ratios are required by low (to -6.7 per mil) $\delta^{18}\text{O}$ values in the ring zones. Criss and Taylor (1983) envisage meteoric-hydrothermal fluids flowing radially inward to the ring zones, where convective flow was dominantly upward.

7.1.6 Summary of Caldera-Related Meteoric-Hydrothermal Systems

Thermal energy to drive meteoric-hydrothermal systems is provided by the crystallizing and cooling intrusive rocks associated with the calderas. Ground water heated by these plutons is less dense than unheated ground water, and rises in the earth's gravitational field. Such convecting systems have been modelled by Norton and Knight (1977) and Norton (1978, 1982). Results of these models indicate that, for sufficiently high permeabilities such as are probably exceeded in highly fractured volcanic rocks, convective heat flux dominates over conductive heat flux as a cooling mechanism for the plutons. Moreover, upward-flowing portions of the modelled convective cells are concentrated near the margins of the cooling plutons. In a caldera environment, shallow resurgent plutons are surrounded by the highly

Figure 7.6 Generalized hydrothermal flow pattern associated with Eocene calderas of the Idaho batholith (from Criss and Taylor, 1983). Ring structures of the calderas exert a strong influence over upward fluid flow adjacent to the Eocene plutons. Recharge into the system occurs at very deep levels, below at least 7 km.



fractured ring fault systems. The enhanced permeability provided by these fractures must exert a strong influence over fluid flow adjacent to the plutons.

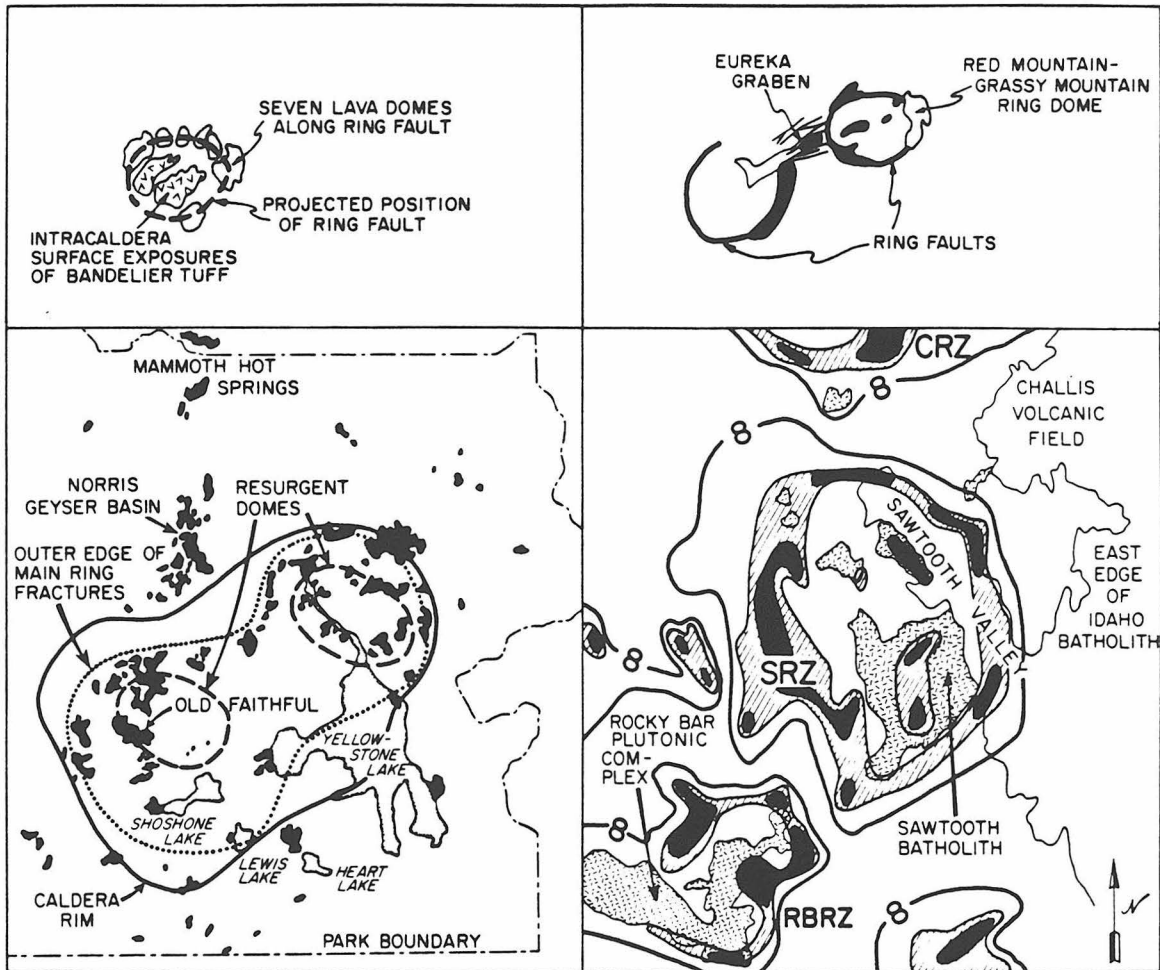
The relationships observed in the active, shallow meteoric-hydrothermal systems at the Long Valley, Yellowstone, and Valles calderas can be integrated with the flow patterns defined by stable isotopic investigations of eroded systems in the Scottish Hebridian province and the Idaho batholith to produce a general model for meteoric-hydrothermal fluid circulation in caldera hydrothermal systems (Figs. 7.7 and 7.8). Both theoretical and empirical models show that upward fluid flow in deeper parts of the systems is strongly controlled by ring-fracture structures and intrusive rocks, to depths of at least 7 km around the Idaho batholith Eocene plutons. Recharge into the ring-fracture systems occurs below at least 3 km and probably below 7 km. The evolved fluids recharging the systems are meteoric in origin and have been shown through radiogenic isotopic analyses at Yellowstone (Leeman et al, 1977) and the Scottish ring complexes (Taylor and Forester, 1971) to have interacted with deeply buried rocks outside the caldera margins. Source regions for these fluids must lie kilometers to tens of kilometers outside the caldera ring faults.

Hot springs and fumaroles in active systems occur around the periphery of resurgent domes, inside the caldera ring faults. At depths less than a kilometer, the evolved meteoric-hydrothermal fluids feeding the thermal vents can mix with small amounts of local pristine meteoric water. In the Long Valley caldera, it has been demonstrated that this pristine water is entering the system by flowing down through

Figure 7.7 Comparison of the sizes and hydrothermal flow patterns of caldera-related hydrothermal systems (modified from Criss and Taylor, 1983). Black areas shown in the Lake City-Silverton calderas and the Idaho batholith indicate zones of the lowest $\delta^{18}\text{O}$ values for these calderas. Thermal springs in Yellowstone National Park are also shown as black areas. The map of the Valles caldera is shown for size comparison.

VALLES CALDERA

LAKE CITY-SILVERTON
CALDERAS



YELLOWSTONE
NATIONAL
PARK

IDAHO
BATHOLITH

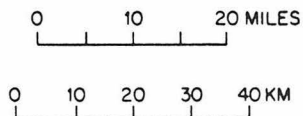
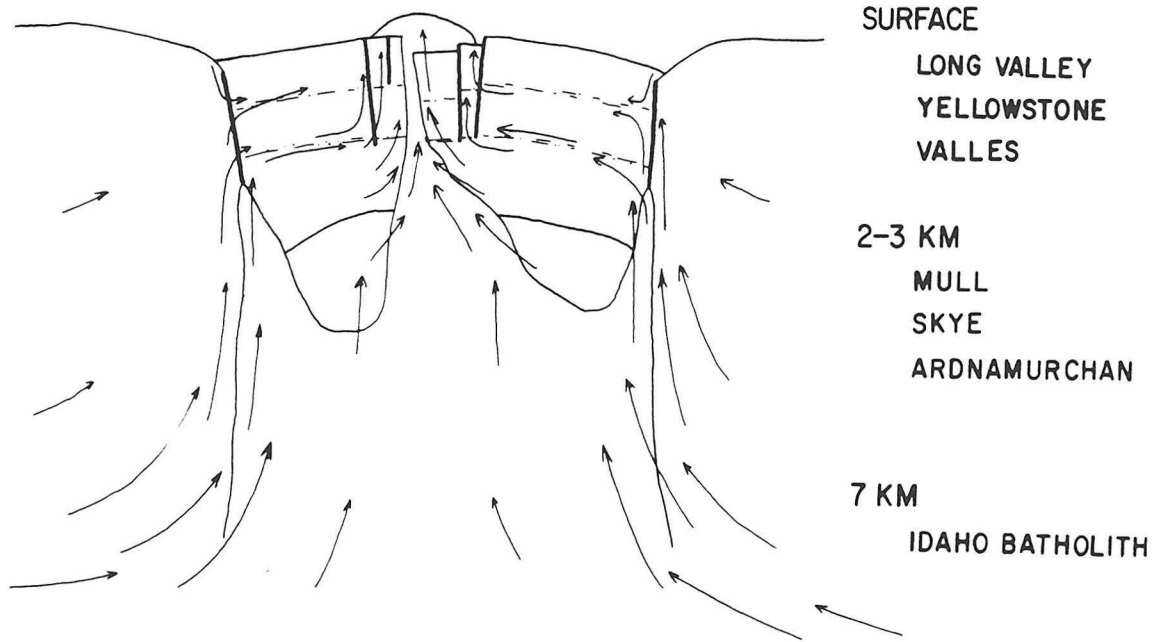


Figure 7.8 Model of meteoric-hydrothermal fluid flow patterns associated with resurgent calderas. This model is based on observations of flow patterns in active caldera hydrothermal systems at the Yellowstone, Long Valley, and Valles calderas. Deeper portions of the model are derived from isotopic studies of the hydrothermal systems associated with the Scottish Hebridian ring dike complexes and Eocene plutons in the Idaho batholith, both of which are eroded resurgent calderas. At deep levels, below 2 to 3 km, upward flow is controlled by permeable zones related to the caldera ring structures and ring intrusions. At shallow levels, less than 1 km, upward flow is controlled by permeable zones within the downdropped, resurged block, and convection is controlled by the resurgent intrusions. Between these two levels, fluid flows from the deeper regime to the shallow regime along permeable layers within the caldera-fill rocks. Deep fluids are derived from meteoric water drawn from well outside the caldera margins. Local pristine meteoric water can infiltrate the shallow part of the system by flowing down the ring fractures and mixing with the evolved water.



the ring faults. Thus, at some point, within 2 to 3 km of the surface, upward-flowing meteoric-hydrothermal fluid is probably channelled from the ring fault zone toward the central resurgent dome of the caldera.

The resurgent intrusion has domed the stratigraphic units within the caldera, causing these units to dip outward from their centers. The collapsed caldera block also commonly contains stratigraphically controlled porous layers, such as poorly welded basal or upper portions of ash-flow units, or poorly consolidated air-fall tuffs. Where these layers are truncated by the ring fault, fluids flowing up the fault will be at least partially deflected into the caldera; the fluids can then flow up the dip through the permeable horizons toward the convective system associated with the resurgent intrusions. The highest portions of the resurgent magmas are small epizonal apophyses which feed resurgence-related extrusive domes. Convective systems developed around these apophyses would have small radii in plan view relative to the systems developed around the much larger deeper plutons. These small convective systems within the domes could effectively draw the meteoric-hydrothermal fluids radially inward; the fluids would be forced to rise along the deeper portions of the ring structures, through the permeable aquifers in the resurgent dome, and into the convective system in the central part of the collapsed block.

Where nearly-vertical, resurgence-related structures are intersected by the porous layers near the intrusive apophyses, fluid flow would typically be expected to be deflected upward and would vent where these structures intersect the surface as hot springs or fumaroles. Such layers and structures have been shown to strongly control fluid

flow in the Yellowstone and Long Valley calderas. Where shallow recharge along the ring fault is restricted by ring dikes and domes, the evolved, unmixed, meteoric-hydrothermal fluid could continue, in part, to flow up along the ring structure and discharge where these structures intersect the surface.

7.2 The Meteoric-Hydrothermal System Associated with the Lake City Caldera

7.2.1 Introduction

Most of the $^{18}\text{O}/^{16}\text{O}$ features displayed by the individual lithologic units associated with the Lake City caldera, as discussed in Chapters 4, 5, and 6, resulted from water-rock interaction between the rocks and the Lake City meteoric-hydrothermal fluid. In this section, these isotopic-lithologic relationships will be integrated to produce a model for the convectively-driven hydrothermal system associated with the caldera. This system ends up as the Smith and Bailey (1968) stage VII terminal solfataric and hot spring activity of the Lake City caldera. The shallow (eastern end) to deep (western end) erosion within the caldera provides us with the opportunity to place important vertical constraints on the nature of this system, and allows valid comparisons to be made to the general caldera fluid flow models presented in the previous section. Upon this framework, a general model of vein and epithermal mineralization in calderas can be constructed.

7.2.2 A Circulation Model for the Lake City Hydrothermal System

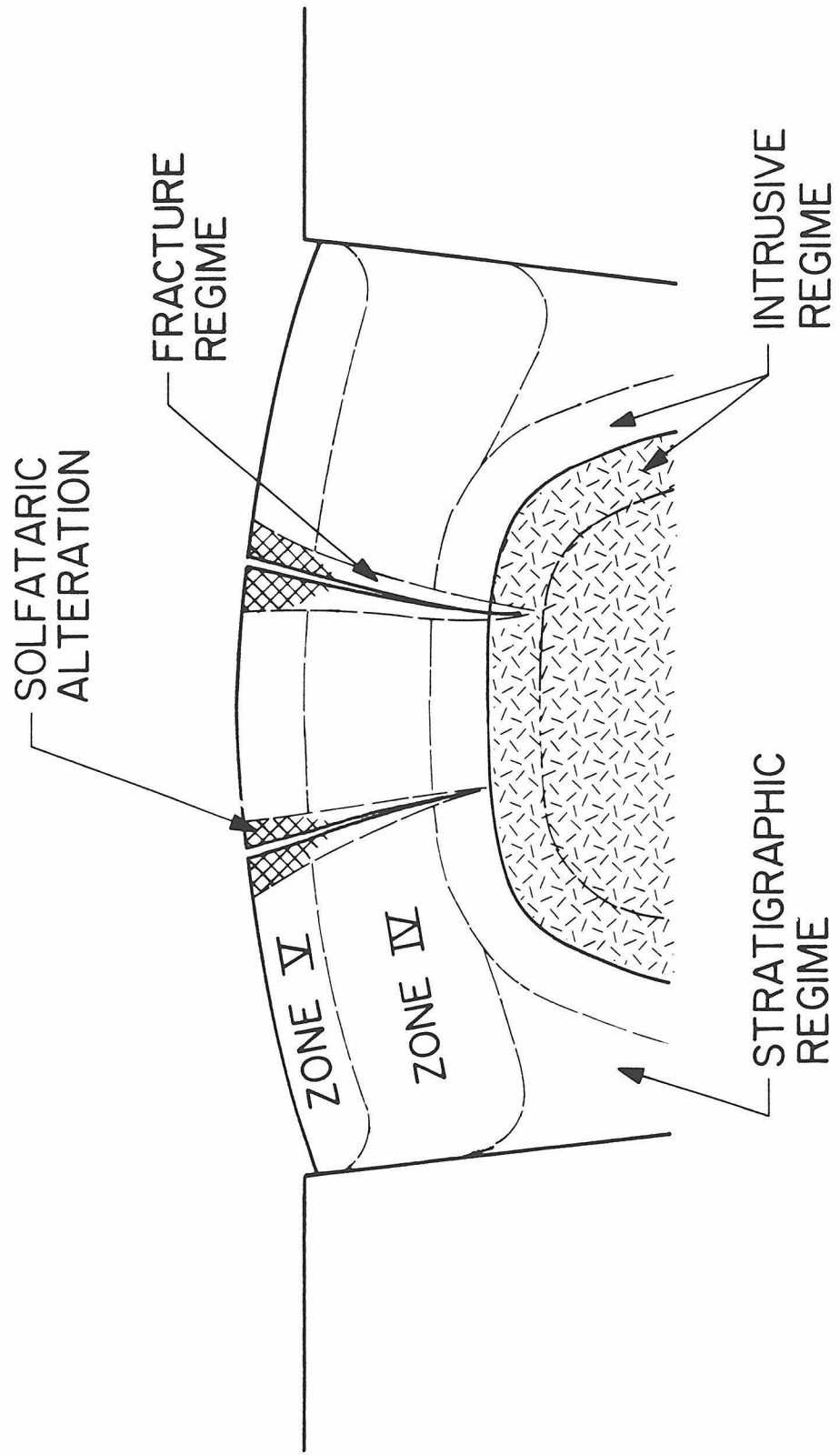
The whole-rock isotopic data from the caldera are contoured in Figure 6.6 and on Plate 3 (in pocket). As shown in Figure 6.6, the ^{18}O

depletions are controlled by permeable zones and are generally spatially related to the resurgent intrusions. Plate 5 (in pocket) reproduces the composite radial cross section showing the whole-rock $\delta^{18}\text{O}$ contours (Fig. 6.11) together with contours of the whole-rock $\delta^{18}\text{O}$ values from the older volcanic rocks north of the caldera and contours of the calculated K feldspar $\delta^{18}\text{O}$ values from the Cataract Gulch granite south of the caldera (excluding Graben Group samples from both data sets). Both these data sets were plotted on Plate 5 as functions of distance from the Lake City caldera ring fault. Also, Plate 5 has a vertical exaggeration identical to that of the structural cross sections on Plate 4. Figure 7.9 is a schematic picture of the relationships among the alteration regimes (Table 6.2) within the Lake City caldera. The important aspects of the ^{18}O variations, as detailed in Chapters 4, 5, and 6 and shown on Figures 6.6 and 7.9 are:

- 1) Rocks just outside the caldera ring fault exhibit ^{18}O depletions controlled by this structure. In the Precambrian granite of Cataract Gulch, rocks adjacent to the ring fault experienced relatively high water/rock ratios. Southwest-trending Eureka graben structures in the granite controlled circulation of meteoric-hydrothermal fluids, producing high water/rock ratios in the area of the graben. A clear-cut east-west gradient in $\epsilon^{18}\text{O}$ within the granite is mainly related to tilting of this Precambrian crystalline block to the east; this gradient in $\delta^{18}\text{O}$ is thus attributable to increasing temperature with depth within the hydrothermal system.

- 2) $\delta^{18}\text{O}$ values in the older volcanic rocks north of the caldera margin are lower in the west than in the east. This can also be best

Figure 7.9 Schematic distribution of alteration regimes within the Lake City caldera. The Intrusive Regime probably developed earliest, during and shortly after emplacement of the resurgent magma. Fracture Regime alteration clearly cuts this earlier alteration. The Stratigraphic Regime may have been operative at the same time as the Intrusive Regime; it is found away from the Intrusive Regime, below the zones IV and V alteration, and it may in part be controlled by proximity to the ring fault. Zones IV and V alteration are shallow and may be the low-temperature end members of any of the three regimes.



attributed to eastward tilting of the rocks north of the caldera ring fault. Decreasing $\delta^{18}O$ values with depth north of the caldera can also be best attributed to increasing temperature with depth within the hydrothermal system.

3) Although the resurgent intrusive rocks are generally strongly depleted in ^{18}O , they have not experienced unusually large water/rock ratios. The ^{18}O depletions are a result of the fact that water/rock interaction in this intrusion occurred at a relatively high temperature. Hornfelsed Sunshine Peak Tuff adjacent to the intrusion exhibits the same characteristics.

4) In and around the area of the resurgent dome that contains the resurgent intrusion, the Sunshine Peak Tuff is most intensely altered and depleted in ^{18}O along resurgence-related, vein-filled fractures. Although the tuff in these altered areas experienced much higher water/rock ratios than did the intrusion, it displays similar degrees of ^{18}O depletion because it interacted with the meteoric-hydrothermal fluids at a lower temperature. Away from the area of intrusive activity and high in the stratigraphic section (in the southeastern quadrant of the caldera) very little water-rock interaction took place, except along the caldera ring fault. Here, Sunshine Peak Tuff along the fault experienced low-temperature alteration at a relatively high water/rock ratio, similar to the effects observed in the immediately adjacent Precambrian granite.

5) The Sunshine Peak Tuff megabreccia units in the Burrows Park and lower Alpine Gulch areas are more highly altered, are much more depleted in ^{18}O , and experienced higher water/rock ratios than the

immediately adjacent Sunshine Peak Tuff. These lower units are also more ^{18}O -depleted and more mineralogically altered than stratigraphically higher megabreccia units.

6) The ring domes, erupted on the eastern caldera margin, were altered in a solfataric, near-surface, environment characterized by ascending, boiling, meteoric-hydrothermal fluids. This area is less deeply eroded than any other part of the caldera. Alteration in the ring domes grades downward to an argillic-type of alteration that is mineralogically and isotopically similar to that found in the Sunshine Peak Tuff within the caldera. Thus, we interpret these altered areas within the caldera to be the roots of eroded shallow solfataric systems, similar to that observed in the quartz latite of the Red Mountain ring dome.

Water/rock ratios for altered Sunshine Peak Tuff and resurgent intrusive rocks in the central part of the resurgent dome of the caldera have been calculated. Figure 7.10 shows calculated water/rock ratios for the Sunshine Peak Tuff assuming open system behavior (see Chapter 4 for discussion of the water/rock calculation) for temperatures of 100°C, 200°C, 300°C, and 400°C and a reasonable ^{18}O -shifted fluid $\delta^{18}\text{O}$ value of -5. Figure 7.11 shows 300°C and 400°C isotherms over the resurgent intrusion in the resurgent dome. The 400°C isotherm is assumed to be coincident with the upper contact of the resurgent dome. This is consistent with heat flow models of cooling plutons (for example see Norton, 1978) that show that the 400°C isotherm is nearly coincident with upper pluton contacts throughout most of the cooling history of a pluton. The 300°C isotherm was placed at 1100 m beneath

Figure 7.10 Calculated water/rock ratios for altered Sunshine Peak Tuff. These curves are also valid for the resurgent intrusive rocks as they have initial $\delta^{18}\text{O}$ values identical to that of the tuff. Curves for open system water-rock interaction at 100°C, 200°C, 300°C, and 400°C are shown for an initial fluid $\delta^{18}\text{O}$ value of -5 (a plausible ^{18}O -shifted hydrothermal fluid). 200°C and 400°C curves are also shown for an initial fluid $\delta^{18}\text{O}$ value of -15 (pristine mid-Tertiary San Juan meteoric water).

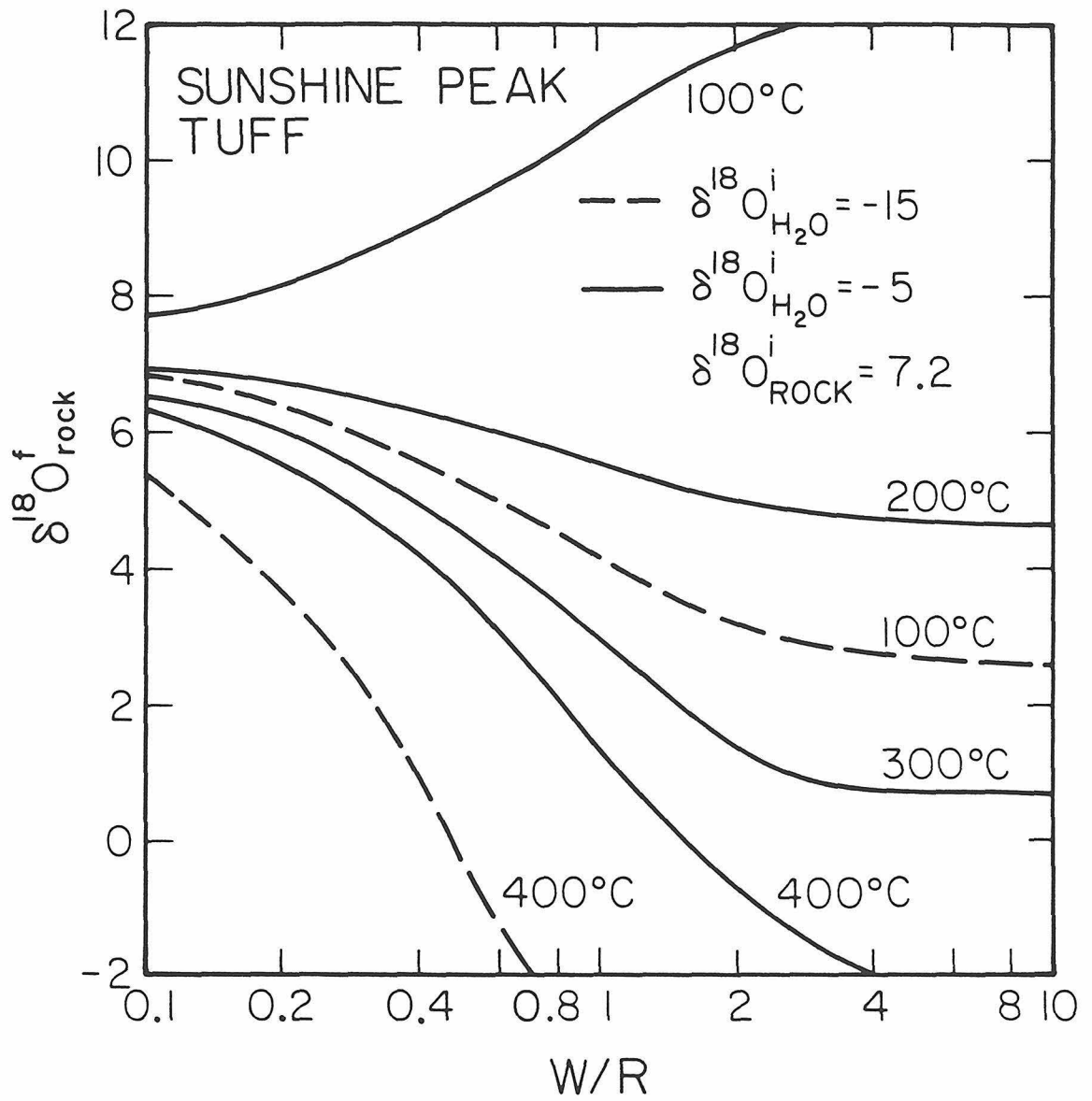


Figure 7.11 300°C and 400°C isotherms associated with the resurgent intrusion. The 400°C isotherm is assumed to be coincident with the upper contact of the intrusion. The 300°C isotherm was placed at 1100 m depth beneath the uneroded top of the caldera-fill rocks (initially at least 1600 m thick).

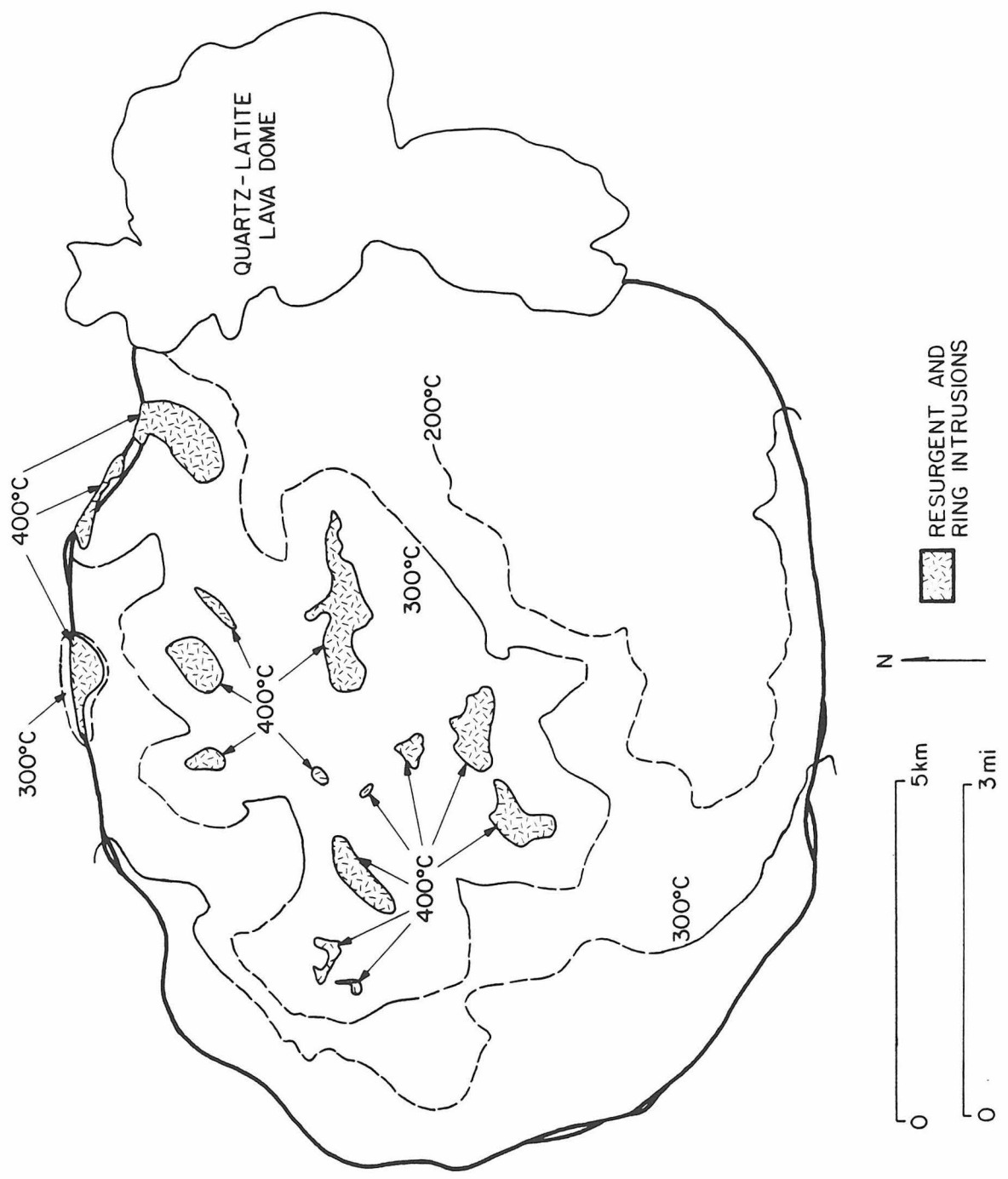
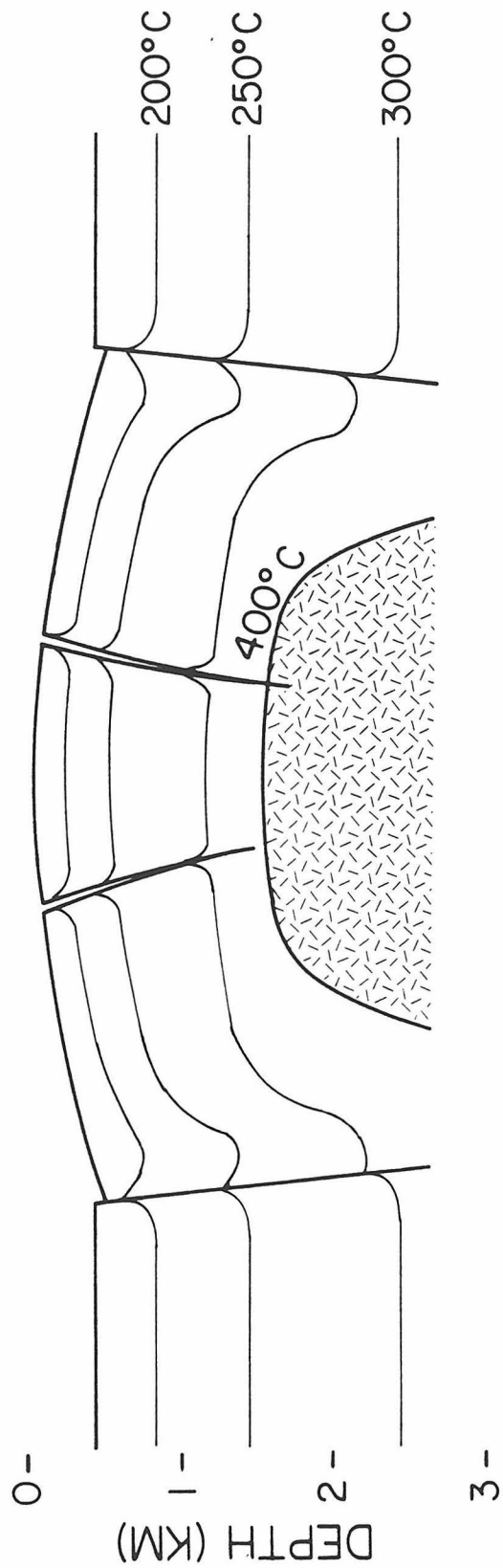


Figure 7.12 A schematic cross section showing the distribution of isotherms in the Lake City hydrothermal system. The 400°C isotherm is assumed to be coincident with the contact between the resurgent intrusion and the caldera-fill rocks. The 200°C, 250°C, and 300°C isotherms were placed at approximately 150 m, 400 m, and 1100 m below the surface (along the hydrostatic boiling curve, see Fig. 5.5). The isotherms are deflected upward along the ring fault and fractures within the caldera because of upward flow of hot hydrothermal fluids along these permeable zones. These isotherms represent the distribution of temperatures within the caldera when the bulk of the hydrothermal activity was occurring.



the surface of the caldera-fill rocks prior to erosion. This is about the depth at which boiling would begin in a rising, 300°C hydrothermal fluid (Fig. 5.5). A minimum of 1600 m of rocks overlay the top of the resurgent intrusion during the hydrothermal circulation; thus, the 300°C isotherm was placed 500 m above the upper contact of the central resurgent intrusion as shown in Figure 6.7. Water/rock ratios for samples within 0.3 km of the two isotherms were then read from the respective water/rock curve on Figure 7.10 using the measured whole-rock $\delta^{18}\text{O}$ value of the sample. These water/rock ratios are contoured on Figure 7.13. Rocks on the north and northwest side of the central part of the resurgent intrusion experienced the highest water/rock ratios (> 2). Rocks on the southern part of the resurgent intrusion experienced the lowest water/rock ratios (< 1).

Using the relationships described above, a generalized fluid flow model for the Lake City caldera stage VII hydrothermal system has been constructed and is presented in Figure 7.14. In this model, meteoric water, which has evolved and become enriched in ^{18}O through deep-seated interaction with mid-Tertiary volcanic rocks and Precambrian crystalline rocks, recharges the caldera system primarily through the Eureka graben but also probably radially inward to some extent from all other directions.

Deep circulation of the meteoric-hydrothermal fluids in the western San Juan meteoric-hydrothermal systems was originally suggested by Taylor (1974a), who documented ^{18}O depletions along the eroded ring fault of the Silverton caldera. Other isotopic evidence also requires deep fluid circulation. Measurements of the isotopic composition of Pb

Figure 7.13 Contours of water/rock ratios above the resurgent intrusion, along the present day erosion surface within the Lake City caldera. These were constructed by reading the water/rock ratio for whole-rock $\delta^{18}O$ values from the appropriate curves on Figure 7.10 for initial water $\delta^{18}O = -5$ and for samples that lie within 0.3 km of the isotherms shown in Figure 7.11, and then contouring those data. The highest water/rock ratios (> 2) occur in and above the northern part of the resurgent intrusion. Rocks in or above the southern half of the resurgent intrusion have been altered at low (< 1) water/rock ratios.

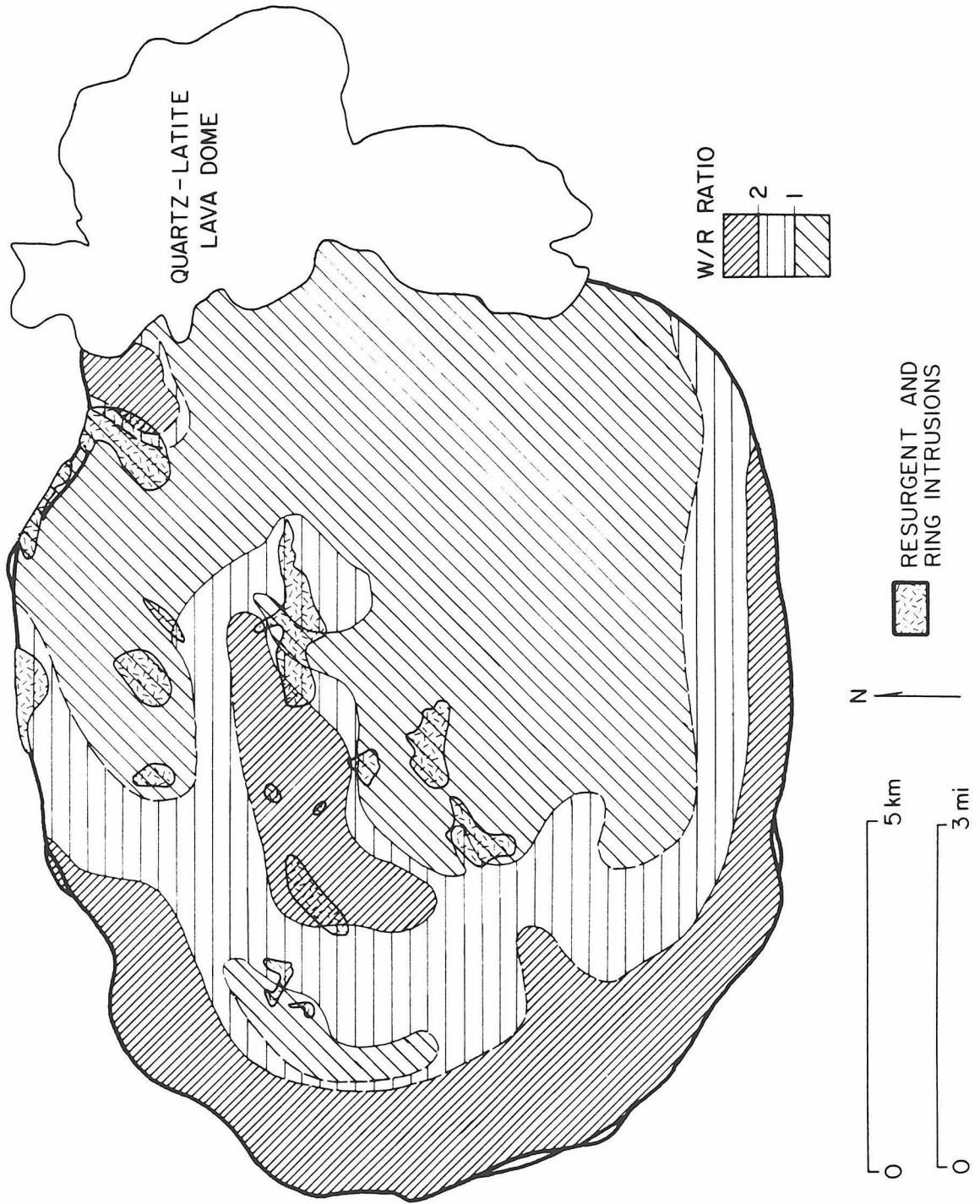
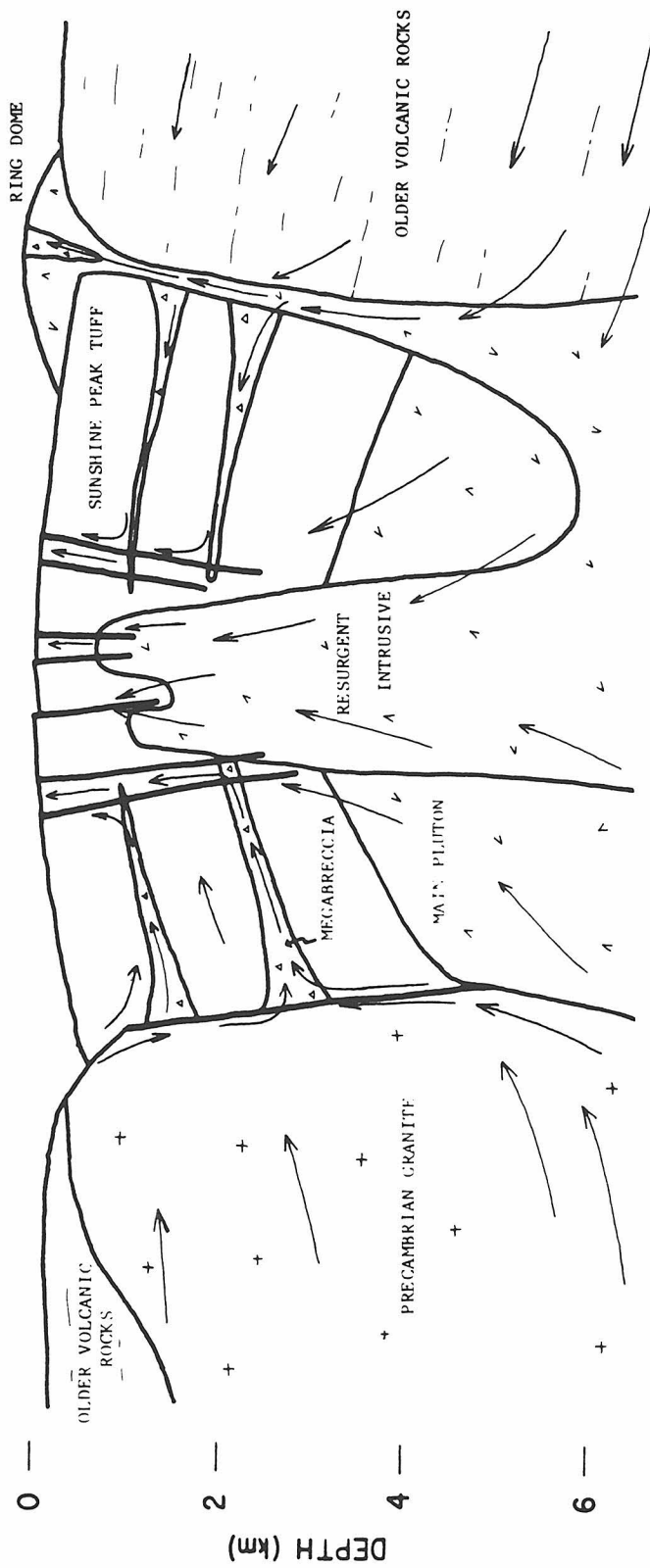


Figure 7.14 Hydrothermal flow model for the Lake City caldera. Arrows denote generalized fluid flow paths. Compare this model to Figure 5.5. Deeply circulated fluids, rising through the caldera ring zone, intersect the lower megabreccia units within 2 to 3 km of the surface. These fluids are drawn as recharge, along the lower megabreccia units, into the convection system associated with the resurgent intrusions. The fluids are deflected upward where resurgence related faults and fractures intersect the megabreccia units near the resurgent intrusions. Boiling occurs in shallow portions of the system. Local recharge of pristine meteoric water occurs along the shallow portions of the ring fault. Where the ring structures are plugged by ring dikes, fluids continue to rise to the surface through permeable zones.



in ore deposits throughout the San Juan Mountains (Doe et al, 1979) show that the ore leads are distinctly more radiogenic than lead in the associated Tertiary igneous rocks (Lipman et al, 1978). The ore leads are isotopically similar to lead in the Precambrian crystalline rocks and Phanerozoic sedimentary rocks, suggesting that the ore-depositing fluids leached lead from the basement below the volcanic rocks. Such interaction requires deep circulation of meteoric water in the hydrothermal system (Doe et al, 1979). Samples analyzed by Doe et al (1979) include vein galena from Alpine Gulch, within the Lake City caldera. Similar deep circulation was invoked by Casadevall and Ohmoto (1977) to account for Pb and Rb/Sr isotopic characteristics in minerals from the Sunnyside vein system.

The resurgent intrusive rocks occur in the central and northern part of the Lake City caldera (Fig. 6.7). The intrusions provided the thermal energy which drove the hydrothermal convection systems within 1 to 2 km of the surface. This can be inferred from the spatial distribution of intensely altered tuff around the resurgent intrusions, and the fact that the intrusions experienced higher temperature water-rock interactions and lower water/rock ratios than the adjacent tuff. The intrusions did not interact with such large volumes of fluid because they are not as porous as or extensively fractured and jointed as the tuff. Note that discharge of hydrothermal fluids is also spatially related to resurgent intrusions in the hydrothermal systems at the Long Valley caldera (Fig. 7.1) (Bailey et al, 1976; Lachenbruch et al, 1976), the Yellowstone caldera (Fig. 7.2) (Eaton et al, 1975; Leeman et al, 1977), and the Valles caldera (Smith and Bailey, 1968).

Within the Lake City caldera, two types of permeable zones exerted control over the hydrothermal fluid flow: the resurgence-related faults and fractures, and the porous megabreccia units. The deeper megabreccia units are more altered than the higher units, and experienced higher temperature alteration and much greater water/rock ratios than the higher units. Caldera-fill rocks tend to dip quaquaversally away from the central part of the collapsed block as a result of resurgent doming. The lower megabreccia units must therefore have been aquifers which channelled fluids up into the central part of the caldera where the resurgent intrusions were driving convective hydrothermal circulation. The lens-like, upper megabreccia units apparently did not act as significant aquifers. Note that fluid flow control by permeable horizons has been demonstrated for hydrothermal systems in the collapsed blocks of the Long Valley caldera (Lachenbruch et al, 1976) and the Yellowstone caldera (White et al, 1975).

On their downdip extensions, the megabreccias terminate at the caldera ring fault. This structure probably focused and conducted deeply circulating, evolved, meteoric-hydrothermal fluids upward to a level where they could enter the down-dip portions of the lower megabreccia units. The fluid was drawn into the lower megabreccia units because of the hydrostatic pressure gradients ("up-dip suction") provided by the convection system associated with the resurgent intrusions. Smaller amounts of fluid rose further along the ring structures to intersect the higher megabreccia units.

In fact, cool, pristine, local meteoric water was probably flowing down the ring fault and mixing with the evolved hydrothermal fluid in

the down-dip portions of the megabreccia units; thus, the fluids moving toward the central part of the resurgent dome very likely were mixtures of two different end-members. Such fluids would have been cooler and lower in ^{18}O than the deeply circulating hydrothermal fluid. Evidence for this is given by sericitic biotite alteration in the Precambrian granite adjacent to the ring fault along the southern caldera margin, which was apparently produced by lower-temperature water-rock interaction than the chloritic biotite alteration away from the fault. This sericitically altered granite along the ring fault exchanged oxygen with a lower- ^{18}O fluid than did the chloritized granite. Note that similar infiltration of surface meteoric water along the ring fault has been demonstrated for the Long Valley caldera hydrothermal system (Lachenbruch et al, 1976). Mixed pristine and evolved hydrothermal fluids are also observed in the Yellowstone hydrothermal system (Truesdell et al, 1977).

Close to the resurgent intrusions in the Lake City caldera, fluid flow was again directed upward where resurgence-related faults and fractures intersect the megabreccia aquifers. These nearly vertical channels are now filled with vein quartz and display intensely altered selvages, indications of very high water/rock ratios. High water/rock ratios are not surprising, as the cross-sectional areas available to flow in the megabreccias are quite large when compared to that in the veins. At low elevations in the caldera, the veins have narrow quartz-sericite selvages, and often contain base-metal sulfides and pyrite. At higher elevations, the veins are enclosed in broad argillized selvages and lack base metal sulfides. These broad selvages are similar

mineralogically and isotopically to the roots of the Red Mountain solfataric zone, and are very likely related to the initiation of boiling in the rising hydrothermal fluid.

The precipitation of sulfides prior to boiling in the rising fluids eliminates boiling as a significant mineralization-controlling process. The mechanism that controls this mineralization is at present unclear. Mixing of the evolved, metal-bearing, hydrothermal fluids with pristine meteoric water infiltrating down the ring fractures would cause cooling of the mixed fluid, which would decrease the solubility of the sulfide minerals (Helgeson, 1969). However, oxygen isotopic compositions of vein quartz from throughout the caldera show no mixing effects. The pristine meteoric water (-15 per mil) should have produced significantly lighter $\delta^{18}\text{O}$ values in quartz veins if mixed with the ^{18}O -shifted evolved meteoric-hydrothermal fluid, although if it was fairly cool, this effect might be counteracted. Thus, only small quantities of pristine meteoric water may have been added to the system.

As boiling proceeded in the rising fluid, interaction between the fluid and rocks produced the solfataric alteration at shallow levels, as seen in the brecciated portion of the Red Mountain quartz latite dome. Intrusion of the quartz latite dome magmas through the ring fracture, and the intrusion of other ring-fracture magmas along the northeastern caldera ring fault, prevented local meteoric water from infiltrating the system in these areas, and possibly prevented significant amounts of upflowing evolved hydrothermal fluids from entering the porous megabreccia in these areas. The intrusions may also have generated their own shallow convective systems, but significant zones

of ^{18}O depletion and alteration are not centered on them, as is the case with the resurgent intrusive rocks.

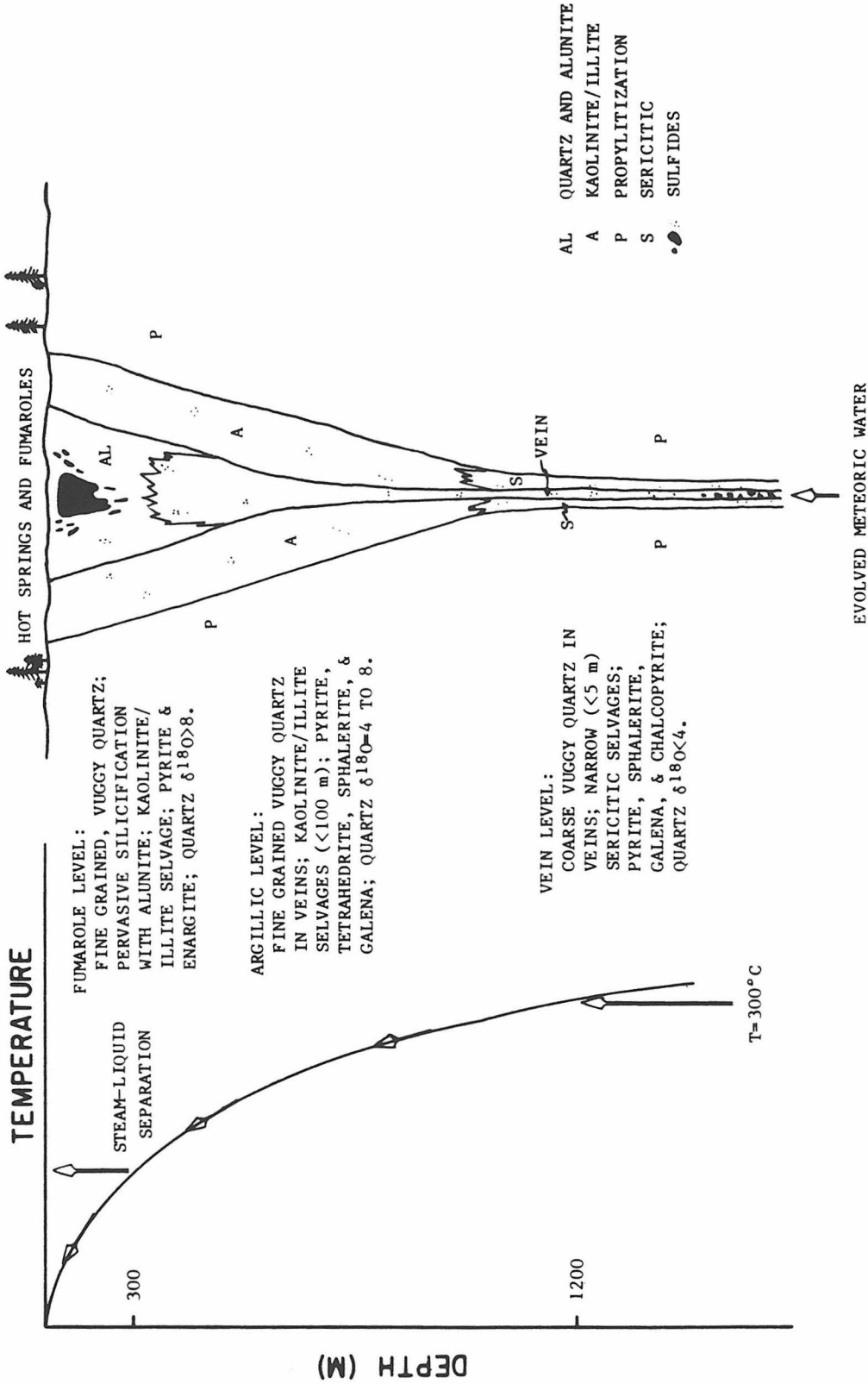
The Lake City hydrothermal model correlates closely with phenomena observed in active caldera-related hydrothermal systems (compare Fig. 7.8 and Fig. 7.14). The nature of hydrothermal fluid flow in deeper parts of caldera-related systems, as inferred from stable isotopic studies of such systems, are more tenuously applied to the Lake City model. However, if this model is correct, the ring-fracture zone below the current level of exposure in the Lake City caldera must have been supplying upflowing, evolved, meteoric-hydrothermal fluid to the down-dip extensions of the lower megabreccia units.

7.3 Implications for Mineralization in Shallow Volcanic Environments

Vertical variations in the distribution and structural control of sulfide mineralization and hydrothermal alteration in the Lake City caldera are described in Chapters 5 and 6. The distribution of alteration facies within the caldera are schematically shown on Figure 7.9. A boiling model for the solfataric alteration at Red Mountain was developed in Chapter 5. Solfatarically altered areas throughout the San Juan Mountains exhibit mineralogic and isotopic similarities to the Red Mountain system, although only a few of these are economically mineralized. The characteristics of these areas will be integrated below to produce a vertical model of alteration and mineralization that relates deeper vein mineralization to the shallow solfataric alteration and mineralization.

The model is shown in Figure 7.15. This model relates vertical

Figure 7.15 Relationships between vein mineralization and solfataric mineralization. This model is derived from vertical variations in alteration and mineralization in the Lake City caldera. The mineralogy and lateral alteration variations in the solfataric zone are also based in part on observations at other solfatarically altered areas in the San Juan Mountains. The same evolved meteoric-hydrothermal fluid responsible for vein mineralization at depth rises along the hydrostatic boiling curve to produce the solfataric alteration in shallow environments.



- AL QUARTZ AND ALUNITE
- A KAOLINITE/ILLITE
- P PROPYLITIZATION
- S SERICITIC
- SULFIDES

variations in vein and alteration mineralogy to the position of an upflowing meteoric-hydrothermal fluid on the hydrostatic boiling curve. Fluids involved in the solfataric alteration and mineralization have been shown to be dominantly meteoric in origin. Furthermore, relationships in the Lake City caldera show that, with depth, alteration associated with the solfataric level grades down into, first, quartz veins with broad argillized selvages and, next, quartz-base metal sulfide-pyrite veins with narrow sericitic selvages. Sulfide mineralization is common at the vein level and at the solfataric level, but is not abundant in the argillic level.

At the vein level, fluids are rising along steep thermal gradients until they intersect the hydrostatic boiling curve. Vein-level mineralization and alteration continue to be produced while a small but growing vapor phase is generated in the rising fluid. At some shallower depth, argillization replaces sericitization as a vein selvage and significant sulfide mineralization ceases. At still shallower depths, the argillized selvage expands to tens of meters, or further, away from the vein. At very shallow depths, enough vapor is generated such that a vapor phase separates from the fluid and can rise independently. Also, at very shallow depths, alunite and quartz pervasively replace the rock, accompanied in some areas by the renewed precipitation of sulfide ore minerals. This solfataric alteration grades out through an argillized zone to fresh or propylitized wall rock.

The common occurrence of solfatarically altered areas with contemporaneous intrusive rocks does not in any way prove that metals and fluids in these systems were directly derived from a crystallizing

magma; although mixing with small amounts of metal-rich magmatic brine cannot be ruled out, the metals also could have been leached out of surrounding rocks under sub-solidus conditions. These magmatic rocks provided thermal energy which drove meteoric-hydrothermal convection systems, and permeable structures within or adjacent to the intrusions provided convenient channels which controlled fluid flow in these systems. At Carson Camp, and locally at Summitville, the solfataric alteration is distributed along linear trends that appear to be fault or fracture controlled.

The above model does not preclude the existence of porphyry-style mineralization associated with these rocks. Indeed, such mineralization is observed to occur in the Calico Peak solfataric zone. Deeper levels of similar systems are probably represented by the stockwork molybdenum mineralization in argillized zones in the Ophir-Silverton area (Jackson et al, 1980; Ringrose et al, 1981). This porphyry mineralization is derived from dominantly magmatic fluids (Ringrose et al, 1981), but at Calico Peak the magma contributed negligible amounts of fluid to the meteoric-hydrothermal fluids responsible for the solfataric alteration.

CHAPTER 8

SUMMARY AND CONCLUSIONS

Meteoric-hydrothermal fluid circulation in the Lake City caldera 23 m.y. ago has been mapped out in a general way by measuring ^{18}O depletions in the rocks that underwent oxygen isotope exchange with this hydrothermal fluid. The magnitudes of these ^{18}O depletions in the samples, in conjunction with (1) the estimated depths beneath the original mid-Tertiary surface, (2) the quantity and type of mineral alteration products in the rocks, and (3) the distances from the contact of the resurgent intrusion, were used as measures of the temperatures of alteration and the degree of evolution of the hydrothermal fluids interacting with the rocks. It was shown that both fracture permeability and lithologic permeability and porosity exerted a strong control over fluid flow, not a surprising result. The resurgent intrusion within the caldera was the heat engine that drove the convective system.

The variable, but relatively shallow, depths of erosion within the caldera exposed rocks from the very near-surface hydrothermal environment down through at least 2 km into the center of the hydrothermal system. This has furnished a unique opportunity to investigate water-rock interactions in the upflowing, shallow portions of a fossil hydrothermal system. The model of fluid circulation developed from this investigation provides an important link between observations of surface hot spring activity in active caldera-related hydrothermal systems, and models of fluid circulation around much deeper intrusive complexes inferred to be the roots of eroded calderas. Boiling of the rising

meteoric-hydrothermal fluid is important in shallow parts of the convection system, and such a model has important ramifications when applied to the nexus between deeper vein-controlled mineralization and shallow, solfataric bonanza-type ores.

The major conclusions of this study are:

1) Fluids involved in the Lake City hydrothermal system were dominantly, if not entirely, of meteoric origin. The $\delta^{18}\text{O}$ value of mid-Tertiary meteoric waters in the western San Juan Mountains, estimated to have been -15 per mil by Sheppard et al (1969), Taylor (1974a), Taylor and Forester (1972), and Casadevall and Ohmoto (1976), is consistent with the low- ^{18}O fluid required to produce the ^{18}O depletions measured in the present study on the altered Lake City rocks. However, measured $\delta^{18}\text{O}$ values of vein quartz within the caldera indicate that the meteoric-hydrothermal fluid that precipitated this quartz was ^{18}O -shifted upward to about $\delta^{18}\text{O} \approx -8$ prior to entering the shallow convective system associated with the resurgent intrusive rocks. This shift is the result of water-rock interaction in deeper (> 2 to 3 km) levels of the meteoric-hydrothermal system. These deeper parts of the system were recharged by lateral inward flow of groundwater infiltrating the hydrologic system in areas peripheral to the Lake City caldera. The highly fractured Eureka graben, southwest of the caldera, is probably the principal source for this meteoric water, but there was undoubtedly radial inflow toward the caldera from all points of the compass.

2) Analyses of mineral separates from the Precambrian granite of Cataract Gulch, which forms the southern and western wall of the Lake City caldera, show that muscovite exchanges oxygen with the meteoric-

hydrothermal fluid faster than quartz, but much slower than orthoclase. Meteoric-hydrothermal alteration of biotite in the granite produces sericite at lower temperatures and chlorite at higher temperatures. Because of higher permeabilities and consequently higher W/R ratios along the Lake City ring fault, granite altered at relatively low temperatures along the ring fault may be locally more ^{18}O -depleted than granite altered at higher-temperatures farther from the ring fault. In part, this effect may also be the result of migration of cold, low- ^{18}O , meteoric waters down the ring fault from the surface to mix, at deeper levels, with the upflowing evolved meteoric-hydrothermal fluids. This is analogous to present-day flow patterns in the young Long Valley caldera in eastern California.

3) Fluid flow within the Lake City caldera was dominated by permeable zones: (A) the porous megabreccia units, which dip outward from the resurgent dome, and (B) vertical fractures and faults related to resurgence. The megabreccia units and tuff adjacent to the fractures exhibit marked ^{18}O depletions, and they are also intensely mineralogically altered. Stratigraphically lower megabreccia units are more ^{18}O -depleted than higher units, showing that the lower units were probably major aquifers that exerted a strong control over fluid flow in deeper parts of the caldera. Where resurgence-related fractures intersect the megabreccia units near the resurgent intrusions, fluid flow was apparently channelled into the fractures and diverted vertically upward.

4) The resurgent intrusive stock within the caldera, and its contact metamorphosed aureole of hornfelsed Sunshine Peak Tuff, both experienced water/rock ratios lower than the permeable zones, but they

typically have even lower $\delta^{18}\text{O}$ values because they were altered at higher temperatures; the intrusion was, of course, the main source of heat for the hydrothermal fluids. The resurgent intrusion is located in the center of the area of most intense mineralogical alteration developed along fractures in the Sunshine Peak Tuff. These relationships all show that the shallow convection system within the caldera was driven by the resurgent intrusion. Convective fluid circulation in this system was controlled by the permeable zones in areas around the intrusions, where the largest volumes of upflowing fluid were concentrated.

5) A relatively shallow thermal gradient, typical of a convective hydrothermal system, was present throughout the vertical section now exposed within the caldera. The shallower portion of this gradient was controlled by the temperature drop associated with the evolution of boiling in the uprising fluid. In the deeper portion of the system, the fossil thermal gradient can be approximately calculated by vertical variations in the $\delta^{18}\text{O}$ values and the quantity and type of alteration products developed within the caldera-fill Sunshine Peak Tuff. Deeper exposures of tuff are more depleted in ^{18}O than shallow portions away from the argillized vein selvages. The deeper tuff was altered at higher temperatures than the shallow tuff, and it was probably also subjected to lower water/rock ratios.

6) The vertical variations in alteration mineralogy developed adjacent to flow channels are in part the result of boiling in the upflowing fluid. Within several hundred meters of the original surface (the solfataric zone), the alteration assemblage is characterized by the development of pervasive zones of silicification and alunitization.

High $\delta^{18}\text{O}$ values in this zone result from the large quartz-water fractionation at low temperatures (100°C to 200°C) along the shallowest portion of the hydrostatic boiling curve. Below this zone is a level of argillization where clays and quartz pervasively replace wall rocks in broad selvages adjacent to the flow channels. The channels are filled with vein quartz precipitated from the fluid, which contained only a minor vapor phase at this point. In the deepest levels of exposure, quartz and sericite replace wall rocks in narrow selvages adjacent to the flow channels, which locally contain abundant base metal sulfides and pyrite in addition to the vein-filling quartz. These deep veins precipitated from the fluid prior to or just after the fluid intersected the hydrostatic boiling curve. A single type of upward-flowing, evolved meteoric-hydrothermal fluid could have produced all the observed variations in vein and alteration mineralogy throughout all three levels. The high $\delta^{18}\text{O}$ values of quartz from both mineralized and barren solfataric zones throughout the San Juan Mountains show that all these solfataric areas were altered and mineralized by evolved meteoric fluids.

7) Integration of all the above aspects of fluid-rock interaction in the Lake City caldera leads to a convective, fluid-flow model for this meteoric-hydrothermal system. Deeply circulating meteoric water rose along caldera ring structures 3 to 5 km beneath the mid-Tertiary surface. This convective circulation was driven by the large cooling pluton that initially produced the eruption of the Sunshine Peak Tuff. Resurgent intrusions in the resurged dome of the caldera produced smaller, shallower, convective systems centered within the dome. The

deeper fluids, rising along the deeper ring zone, were drawn into the shallow convective system through the lower, porous, megabreccia units. These units are apparently truncated down dip by the Lake City caldera ring faults. Near the resurgent intrusions, fluid flow was again directed upward where resurgence-related, near-vertical, fractures intersect the megabreccia units. At the present outcrop level, which probably varies from about 200 to 2500 m beneath the original mid-Tertiary surface, the flow regime within these fractures was locally shallow enough that boiling began in the fluid (at depths of approximately 1000 m).

At the surface, discharge of the boiling fluid produced a zone of hot spring and solfataric activity peripheral to the resurgent core of the caldera, but generally inside the ring fault. Where the ring fault controlled magma intrusion, such as for the eastern tier of quartz-lattite ring domes, surface fluid discharge was apparently deflected into and along the ring fault zone. This is either because these magmatic bodies "sealed" the ring fault-megabreccia channels, or because they themselves acted as "heat engines" and thus were centers for local convective circulation systems. Minor recharge of local meteoric water into the shallow convective system occurred through the ring structure where it was not intruded and sealed. Small amounts of this pristine meteoric water probably mixed with the evolved fluid in the megabreccia units. The $\delta^{18}\text{O}$ effects and the hydrothermal model described above for the Lake City caldera give us insight into the deeper, unexplored parts of currently active geothermal systems associated with recently-formed silicic calderas, particularly the Long Valley caldera and the Valles

caldera, both of which seem to be in many respects virtually identical to the Lake City caldera.

PART II

$^{18}\text{O}/^{16}\text{O}$ RELATIONSHIPS IN TERTIARY ASH-FLOW TUFFS
FROM COMPLEX CALDERA STRUCTURES IN CENTRAL NEVADA AND
THE SAN JUAN MOUNTAINS, COLORADO

CHAPTER 1

INTRODUCTION

1.1 Object of the Research

In part I of this thesis, we presented a detailed study of the oxygen isotope relationships in hydrothermally altered rocks in and around a mid-Tertiary caldera complex. Assimilation of, or exchange between, such altered low- $\delta^{18}\text{O}$ country rocks and the underlying magma can cause a lowering of the $\delta^{18}\text{O}$ value of the magma below the range of "normal" magmatic $\delta^{18}\text{O}$ values. Such ^{18}O depletions have in fact been observed in ash-flow sheets and other rocks erupted sequentially from the tops of silicic magma chambers that are analogous to the one that formed the Lake City caldera (Friedman et al, 1974; Lipman and Friedman, 1975). The caldera-forming process provides a mechanical means to catastrophically fracture the roof above the magma chamber, thereby allowing the stoping of a large quantity of hydrothermally altered, low- $\delta^{18}\text{O}$ wall rocks into the top of the magma chamber. Assimilation of these blocks, or oxygen isotopic exchange between the blocks and the magma, is a plausible mechanism for producing ^{18}O -depleted magmas (Taylor, 1977). Moreover, ash-flow eruptions provide "snapshots" of $\delta^{18}\text{O}$ profiles that existed in the upper portions of the magma chamber prior to eruption. Sequential eruptions record the evolution of these profiles, as well as recording the overall $\delta^{18}\text{O}$ variations with time in a sub-volcanic magma chamber.

The purpose of this study is to document such variations. Two caldera complexes, the central Nevada caldera complex, Nye County,

Nevada, and the central San Juan caldera complex, San Juan volcanic field, Colorado, were chosen for study, because: (1) the rocks are well exposed; (2) these areas are logistically relatively easy to sample; and (3) the geological relationships and eruptive products from these caldera complexes have previously been described in detail in the literature.

1.2 Low- ^{18}O Igneous Rocks

The oxygen isotopic compositions of "normal" igneous rocks lie within well-defined, restricted ranges (Taylor, 1968, 1978, 1980a). Deviations from these "normal" $\delta^{18}\text{O}$ values indicate that the magmas or crystalline igneous rocks interacted in some way with other reservoirs that have $\delta^{18}\text{O}$ values higher or lower than the "normal" range. One important grouping of such rocks are those that have $\delta^{18}\text{O}$ values below the "normal" range because they crystallized from low- ^{18}O magmas.

Evidence for low- $\delta^{18}\text{O}$ magmas has been found in a number of areas, including the Tertiary granitic rocks at Mull and Skye, Scotland (Forester and Taylor, 1976, 1977; Taylor, 1978), the Tertiary inner diorite at Stony Mountain, Colorado (Forester and Taylor, 1972, 1980), young basaltic lava flows on Iceland (Muehlenbachs et al, 1974), some young rhyolitic ash-flow tuffs from the western United States (Friedman et al, 1974; Lipman and Friedman, 1975; Hildreth et al, 1980), and in granophyre phases of the Skaergaard and Jabal at Tif mafic complexes (Taylor and Forester, 1979; Taylor, 1980a). The development of such low- ^{18}O magmas is explained by a number of mechanisms by these and other authors: (1) direct interaction between the magmas and meteoric

ground waters; (2) isotopic exchange between the magmas and country rocks that had previously been altered and thus have $\delta^{18}\text{O}$ values lower than "normal"; (3) partial or complete assimilation of hydrothermally altered, low- $\delta^{18}\text{O}$, country rocks derived from the roof zones above the magma chambers; or (4) fractional crystallization and gravitational removal of cumulus phases having high $\delta^{18}\text{O}$ values.

Direct solution of meteoric water into magmas or large-scale oxygen isotopic exchange between meteoric waters and magmas are both difficult to envision as significant processes for lowering the $\delta^{18}\text{O}$ values of magmas, for the following reasons: (1) Diffusion of water through silicate liquids is extremely slow (Shaw, 1974). (2) Pressure gradients outside the wall of the magma chamber are hydrostatic, whereas within the magma chamber they are lithostatic ($P_{\text{lithostatic}} \approx 3P_{\text{hydrostatic}}$); thus, water cannot physically flow up this gradient through fissures into the magma chamber. However, if $(P_{\text{H}_2\text{O}})_{\text{hydrostatic}} > (P_{\text{H}_2\text{O}})_{\text{magma}}$, then grain-boundary diffusion of water up a thermal gradient adjacent to the magma body may allow small amounts of water to enter the magma chamber (Taylor, 1978). (3) Extremely large amounts of meteoric water would have to enter a magma chamber, exchange with the magma, and then bubble out again in order to produce a several per mil shift in the $\delta^{18}\text{O}$ of an epizonal magma chamber, because magmas at shallow depths in the Earth's crust can only dissolve 2 to 4 weight percent H_2O ; this is not enough to drastically alter the $\delta^{18}\text{O}$ of the magma, especially since this water would have already been ^{18}O -shifted to higher $\delta^{18}\text{O}$ values as a result of prior exchange with the wall rocks (Taylor, 1978).

As stated by Taylor (1977, 1980a), the most likely mechanism for

generating low- $\delta^{18}\text{O}$ magmas is assimilation of, or exchange with, low- $\delta^{18}\text{O}$ country rocks by the magmas. Oxygen isotopic exchange between the magma and stopped blocks of altered, ^{18}O -depleted country rocks is likely to be important in every volcanic-plutonic terrane where meteoric-hydrothermal activity is common, particularly in rift-zone environments (Taylor, 1977). Physical evidence for assimilation is widespread in magmatic rocks of diverse composition emplaced in diverse tectonic environments (McBirney, 1979). Also, where sufficient analytical data are available, initial $^{87}\text{Sr}/^{86}\text{Sr}$ ratios define mixing curves when plotted against $\delta^{18}\text{O}$ in some igneous rock series, and Taylor (1980b) has shown that in such cases altered volcanic rocks or sedimentary rocks were assimilated by mantle-derived magmas. Heat balance requires that large-scale assimilation be accompanied by fractional crystallization in the magma (Taylor, 1980b; Bowen, 1928). Because mineral-magma oxygen isotopic fractionations are small at magmatic temperatures, fractional crystallization by itself contributes negligibly to $\delta^{18}\text{O}$ variations in the magmas (Garlick, 1966; Anderson et al, 1971).

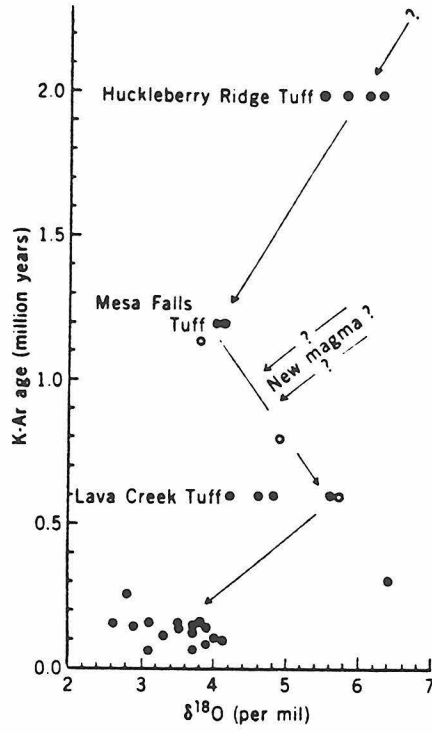
1.3 Previous $\delta^{18}\text{O}$ Studies of Ash-Flow Tuffs

Ash-flow tuff magmas with $\delta^{18}\text{O}$ values significantly lower than "normal" igneous rocks have been found in two areas: Quaternary rhyolites associated with the Yellowstone caldera (Friedman et al, 1974; Hildreth et al, 1980); and Tertiary ash-flow sheets erupted from the Claim Canyon-Oasis Valley caldera complex in southwestern Nevada (Friedman et al, 1974; Lipman and Friedman, 1975). Ash-flow tuff magmas with "normal" $\delta^{18}\text{O}$ values have been found in the Superstition volcanic field

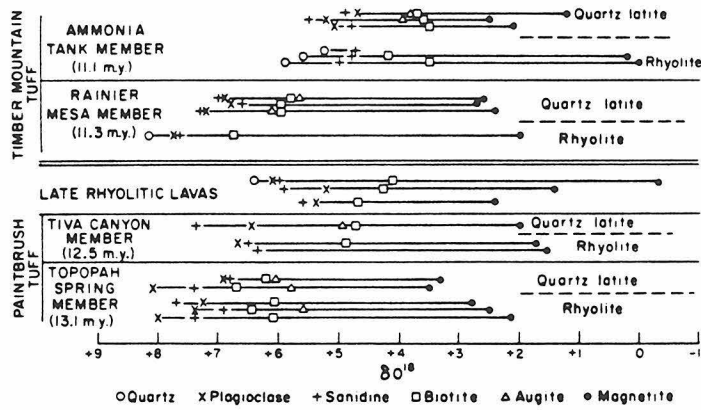
in central Arizona (Taylor, 1968; Stuckless and O'Neil, 1973), the Bishop Tuff, erupted from Long Valley, California (Hildreth, personal communication), and the Bandelier Tuff, erupted from the Valles Caldera, New Mexico (Lambert and Epstein, 1980). The latter two calderas are described in Part I, Chapter 7, of this work. A number of other "normal" Tertiary ash-flow magmas from scattered locations throughout North America were found by Taylor (1968).

Analyses of sanidine and quartz phenocrysts in rhyolites sequentially erupted from the Yellowstone caldera, including both ash-flows and domes, have shown that $\delta^{18}\text{O}$ values in these rocks decrease with age (Fig. 1.1; Friedman et al, 1974; Hildreth et al, 1980). Similar relationships for suites of phenocrysts were found in the Paintbrush and Timber Mountain zoned ash-flow sheets, erupted from the Claim Canyon-Oasis Valley caldera complex, Nevada (Fig. 1.1; Friedman et al, 1974; Lipman and Friedman, 1975). These authors suggest that the ^{18}O -depletions resulted from direct interaction of the upper portions of the magma chambers with meteoric water. However, both caldera complexes were emplaced into sedimentary strata capped by Tertiary volcanic rocks. Hydrothermal systems developed within these rocks, such as the system currently active at Yellowstone, would provide a reservoir of rocks with $\delta^{18}\text{O}$ values below the "normal" range that, upon high-level stopping and assimilation or oxygen isotopic exchange, could have produced the ^{18}O depletions observed in these rocks. Note that Noble and Hedge (1969) interpreted Sr isotopic data from the Paintbrush and Timber Mountain tuffs to indicate at least minor assimilation of wall rocks by the upper, most silicic parts of the magma chamber.

Figure 1.1ab $\delta^{18}\text{O}$ values of phenocrysts separated from some low- ^{18}O ash-flow tuffs and associated lavas from the western United States. (a) Analyses of sanidine phenocrysts from ash-flow tuffs and lavas erupted from the Yellowstone caldera (from Friedman et al, 1974). (b) Analyses of phenocrysts from the Paintbrush and Timber Mountain Tuffs and related lava flows, Nevada (from Lipman and Friedman, 1975). In both cases note that sequentially younger eruptives may have lower $\delta^{18}\text{O}$ values than older eruptives. However, renewed influx of new magma from below can produce an ^{18}O increase. Such variations most likely result from some type of direct or indirect interaction between the magmas and low- ^{18}O meteoric waters.



A



B

CENTRAL NEVADA CALDERA COMPLEX

2.1 Evolution of the Central Nevada Caldera Complex

Three nested collapse structures are recognized in the central Nevada caldera complex, located 110 km ENE of Tonopah, Nevada (Ekren et al, 1972; Ekren et al, 1973a, 1973b, 1974; Quinlivan et al, 1974; Quinlivan and Rogers, 1974; Snyder et al, 1972). The lithologic evolution and structural evolution of this caldera complex are shown in Table 2.1 and Figure 2.1.

The caldera complex was emplaced into a section of Paleozoic dolomite, limestone, shale, and quartzite (Ekren et al, 1973a; Quinlivan et al, 1974). This caldera complex is 15 to 20 m.y. older and 110 km northeast of the southwestern Nevada (Claim Canyon-Oasis Valley) caldera complex (Fig. 1.1b) studied by Lipman and Friedman (1975).

Each of the three collapse structures produced a distinct suite of volcanic rocks, and it is therefore convenient to divide these rocks into three cycles (Table 2.1): (1) the early sequence consists of one major and two minor ash-flow tuffs, all of similar chemical composition, that were erupted from the oldest collapse structure; (2) the giant, 3000 km³, middle eruptive is the only recognized product of the intermediate-age caldera collapse; (3) a late sequence consists of a major ash-flow tuff sheet erupted from the Lunar Lake caldera, as well as smaller ash-flow tuffs and lava domes subsequently erupted from the ring dome of this caldera. Major element analyses of rocks erupted from these calderas define a calc-alkaline trend (Ekren et al, 1974). The

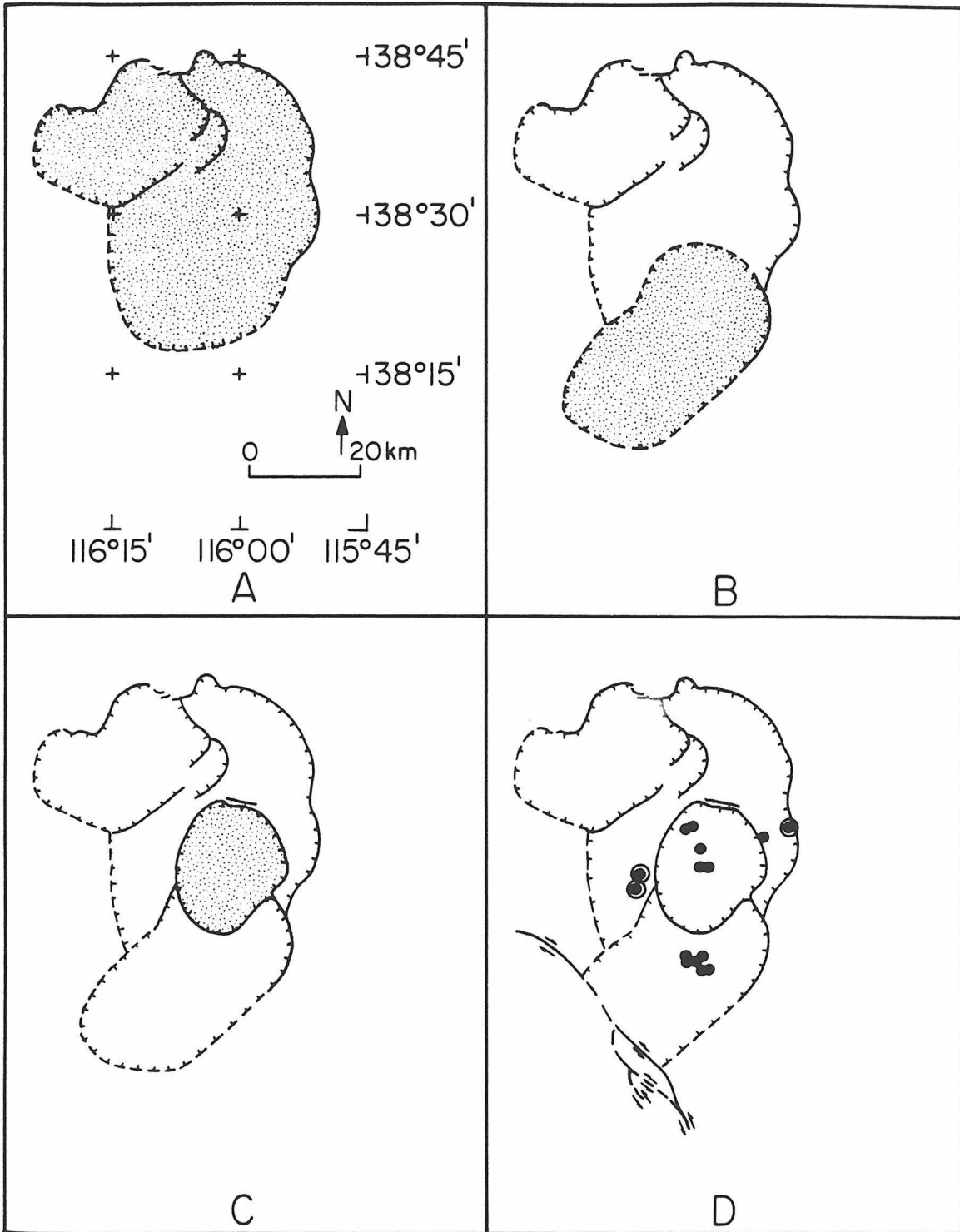
Table 2.1 Volumes and ages of rocks erupted from the central Nevada caldera complex. The rocks are listed in stratigraphic order, the youngest on top. The units are divided into three sequences based on their source caldera. Also shown are the abbreviations for the units as used in the text.

<u>Unit</u>	<u>Volume</u>	<u>Age⁽¹⁾</u>
<u>LATE SEQUENCE</u>		
Tuff of Black Beauty Mesa (Tbb)	10 km ³	
Tuff of Buckwheat Rim (Tbr)	45 km ³	
Andesite (Ta)	13 km ³	
<u>Ring Eruptive Sequence</u>		
Quartz Latite (Tql)	3 km ³	
Tuff of Buckskin Point (Tbp)	15 km ³	25.4±1.3 bi ⁽²⁾
Rhyolite of Big Sand Spring Valley	20 km ³	25.8 wr ⁽²⁾
*Tuff of Lunar Cuesta (Tlc)	370 km ³ (2)	25.5±0.8 bi ⁽²⁾
<u>MIDDLE ERUPTIVE</u>		
*Monotony Tuff (Tm)	3000 km ³ (3)	27.0±0.8 bi ⁽⁴⁾
<u>EARLY SEQUENCE</u>		
Tuff of Palisade Mesa (Tp)	25 km ³	29.9±1.2 bi ⁽⁴⁾ 30.3±0.9 bi ⁽⁴⁾
Tuff of Halligan Mesa (Th)	75 km ³	
*Tuff of Williams Ridge and Morey Peak (Twm) (outflow facies = Windous Butte Tuff?)	+2500 km ³	31.6±0.9 bi ⁽⁴⁾ 30.7±0.8 bi ⁽⁵⁾ 31.7±0.8 bi ⁽⁵⁾

(1) All ages are m.y. ago, K-Ar; bi = biotite, wr = whole rock. (2) Ekren et al (1972). (3) Ekren et al (1971). (4) Marvin et al (1973). (5) Gromme et al (1972).

* Denotes eruptions related to caldera collapse

Figure 2.1abcd Structural evolution of the central Nevada caldera complex. (a) Initial collapse was in response to the eruption of the Tuff of Williams Ridge and Morey Peak about 31 m.y. ago. (b) The southern margin of the earlier caldera was truncated by collapse associated with eruption of the 3000 km³ Monotony Tuff about 27 m.y. ago. (c) The Lunar Lake caldera, nested within the two older calderas, formed about 25.5 m.y. ago in response to eruption of the Tuff of Lunar Cuesta. (d) The southern portion of the complex has been displaced by post-collapse, right-lateral faulting. Sample locations or traverses are shown as dots; localities where 3 or more samples were collected are indicated by circled dots. See text for data sources.



alkali-lime index for the tuffs and lavas is approximately 62, within the calc-alkalic field of Peacock (1931). The analyses vary from SiO_2 = 65 weight percent to 77 weight percent but there is no indication of any systematic chemical variations as eruptions proceeded, starting about 31 m.y. ago (age of the Windous Butte Formation) and ending about 25 m.y. ago (age of the tuff of Buckskin Point). The youngest rocks include the most basic as well as the most silicic of the suite (Ekren et al, 1974). Most of the ash-flow tuff cooling units in the Lunar Lake area are characterized by a mafic-poor rhyolitic base and a mafic-rich quartz latitic top. Although the Windous Butte shows more extreme chemical variations within a single cooling unit than any of the other principal units in the area, the contrasting lithologies in the Windous Butte all plot neatly along the curves defined by the major oxides of the younger ash-flow sheets.

The early sequence began with eruption of Twm, the Tuff of Williams Ridge and Morey Peak (Ekren et al, 1973a, 1974). This was a very large ash-flow eruption, and a thick section of this tuff fills the collapsed block (Fig. 2.1a) of the early-sequence caldera. A core hole collared within the block penetrated 1830 m of Twm and bottomed in this unit without drilling out of it (Ekren et al, 1973). Ekren et al (1974) believe that the tuff of the Windous Butte Formation is the outflow facies of the upper part of Twm. Twm is an unzoned quartz latite containing 48 to 56 percent phenocrysts of, in order of abundance, plagioclase, quartz, sanidine, and hornblende (Ekren et al, 1973).

In the western part of this collapsed block, Twm is overlain successively by the Tuff of Halligan Mesa (Th) and the Tuff of Palisade

Mesa (Tp). No specific source for these units has been identified, but their small volumes (75 and 25 km³, respectively) and spatial association with Twm suggest that the three units were erupted in rapid succession from the same source area (Ekren et al, 1974). The early sequence is comprised of these three units. Both Tp and Th are zoned from lower crystal-poor rhyolites (about 25 percent phenocrysts; quartz = sanidine > plagioclase > biotite) to upper crystal-rich quartz latites (about 45 percent phenocrysts; plagioclase > quartz > sanidine > biotite) (Snyder et al, 1972). The crystal-poor Tuff of Black Rock Summit overlies Twm in the eastern part of the collapsed block; this unit was not sampled in the present study.

Eruption of the voluminous (3000 km³) Monotony Tuff (Tm) resulted in caldera collapse that truncated the southern part of the earlier Twm caldera (Fig. 2.1b). This middle eruptive tuff (Tm) consists of a uniform phenocryst-rich (40 to 50 percent phenocrysts) quartz latite (plagioclase > sanidine = quartz = biotite > hornblende; Ekren et al, 1971, 1973b). Tm is widespread in Nye County, Nevada (Ekren et al, 1971). Outside the source area, this tuff is generally about 300 m thick, but in the collapsed block it locally exceeds 1500 m (Ekren et al, 1971, 1973b).

The youngest collapse structure in the central Nevada caldera complex, the Lunar Lake caldera (Fig. 2.1c), formed in response to the eruption of the Tuff of Lunar Cuesta (Tlc) (Ekren et al, 1974). Tlc, the oldest member of the late sequence, is a quartz latite with 20 to 35 percent phenocrysts (plagioclase > quartz > sanidine > biotite; Ekren et al, 1974). The Lunar Lake caldera is entirely nested within the

older two calderas; it truncates the northern portion of the caldera that is the source of the Monotony Tuff.

Ring-fracture volcanism is developed along the margins of the Lunar Lake caldera. The nearly aphyric rhyolite of Big Sand Spring Valley (not sampled in this work) erupted as lavas from multiple vents in the eastern and northern ring-fracture zone (Ekren et al, 1974). Also, small ash-flows, quartz latite lavas, and andesite lavas erupted sequentially along the southern margin of the Lunar Lake caldera. This sequence, referred to as the Citadel Mountain section, began with eruption of the Tuff of Buckskin Point (Tbp). Tbp, 75 m thick, is zoned from a crystal-poor rhyolite base (10 percent phenocrysts; plagioclase >> pyroxene > quartz = biotite = hornblende) to a crystal-rich quartz latite top (35 percent phenocrysts; plagioclase > quartz > biotite > hornblende; Snyder et al, 1972). Quartz latite lavas (Tql), up to 200 m thick, overlie Tbp and contain 30 to 55 percent phenocrysts (plagioclase > quartz = sanidine > biotite > hornblende; Snyder et al, 1972). Up to 350 m of andesite (Ta) overlies Tql (8 to 30 percent phenocrysts; plagioclase > pyroxene; Snyder et al, 1972).

Two small ash-flows, the Tuff of Buckwheat Rim (Tbr) and the Tuff of Black Beauty Mesa (Tbb), cap the Citadel Mountain section (Snyder et al, 1972; Ekren et al, 1974). Tbr consists of up to 150 m of a basal rhyolite (25 percent phenocrysts) and an upper quartz latite (35 percent phenocrysts; Snyder et al, 1972). Tbb, up to 18 m thick, is similarly zoned (Snyder et al, 1972).

All of the units described above erupted in mid- to late-Oligocene time (Table 2.1) (Gromme et al, 1972; Marvin et al, 1973; Ekren et al,

1974). In Miocene and Pliocene time, the caldera complex was deformed during basin-range extensional faulting. During this time the southern portion of the Tm-source caldera was displaced by left-lateral movement along the Tybo-Reveille fault system (Fig. 2.1) (Ekren et al, 1974). In Quaternary time basalts of the Lunar Crater volcanic field erupted within and around the Lunar Lake caldera (Scott and Trask, 1971).

2.2 Oxygen Isotopic Analyses of Coexisting Minerals From the Central Nevada Caldera Complex

Unweathered samples, approximately 3 to 5 kg in size, were collected along traverses specifically laid out in sequential stratigraphic order to sample a wide compositional range in the various units of the central Nevada caldera complex. Some units were sampled at widely separated outcrops (for example Tm and Twm), because complete stratigraphic sequences are not exposed in accessible areas. Samples were collected near the bases and tops of most of the units, and samples from the interior of each unit were also collected.

Analyses of mineral separates from these samples are tabulated in Table 2.2. Mineral separates of about 20 to 50 mg were prepared for analyses by hand picking 30 to 50 g of crushed rock. Biotite and feldspar separates are greater than 95 percent pure. It was not possible to separate K feldspar from plagioclase, and the tabulated feldspar analyses in general represent mixtures of these two phenocryst minerals. However, in all samples the K feldspar (sanidine) makes up more than two-thirds of the separated feldspar sample. Quartz separates were routinely treated with HF to dissolve any fragments of matrix or other

Table 2.2

Oxygen isotopic analyses of rocks and mineral separates from the central Nevada caldera complex. The following explanatory remarks refer to the column headings, as enumerated on the first page of data.

- (1) Latitude is N, longitude is W.
- (2) All data are per mil, relative to SMOW. Data for which replicate analyses were made show the average of the two analyses with the range denoted as ±.
- (3) Abbreviations are as follows:

bg	black glass	og	orange glass
OF	outflow facies	ICF	intracaldera facies
RF	ring fracture extrusive		
- (4) Abbreviations for units are as follows:

Tm	Monotony Tuff
Tp	Tuff of Palisade Mesa
Th	Tuff of Halligan Mesa
Tbp	Tuff of Buckskin Point
Tlc	Tuff of Lunar Cuesta
Tql	Quartz Latite
Tbb	Tuff of Black Beauty Mesa
Twm	Tuff of Williams Ridge and Morey Peak

Central Nevada Caldera Complex

Field #:	Location ¹ : Lat/Long	Relative Height: (0 to 1h)	δ ¹⁸ O Analyses ² :			Unit ⁴ :	Remarks ³ :
			Quartz	Feldspar	Biotite		
CN-1	38°32.38' 115°47.89'	center of unit		7.3		Tm	OF
CN-2	38°32.41' 115°47.91'	center of unit	10.2	9.1±0.3	7.1±0.0	Tm	OF
CN-3	38°32.49' 115°47.96'	center of unit	10.3		8.2	Tm	OF
CN-5	38°29.14' 116°04.73'	0.78	10.9		8.2	Tm	OF
CN-6	38°25.24' 116°10.75'	0.25	10.5	9.5	8.5	Tp	ICF
CN-7	38°25.25' 116°10.79'	0.05	10.9±0.1	9.3	8.4±0.0	Tp	ICF
CN-8	38°25.26' 116°10.81'	0.96	10.3	9.4±0.2	8.2±0.1	Th	ICF
CN-9	38°25.26' 116°10.85'	0.84	10.5	9.5	7.6	Th	ICF
CN-10	38°25.28' 116°10.89'	0.67	10.7	9.5		Th	ICF
CN-11	38°26.72' 116°09.47'	0.44	10.1	8.9	8.3	Tm	OF

Field #:	Location: Lat/Long	Relative Height: (0 to 1h)	$\delta^{18}O$ Analyses:				Unit:	Remarks:
			Quartz	Feldspar	Biotite	Other		
CN-12	38°26.73' 116°09.62'	0.28	10.5	7.6		Tm	OF	
CN-12.5	38°26.72' 116°09.75'	0.85	10.5	9.0	8.9	Tp	ICF	
CN-13	38°18.18' 116°07.48'	0.08		8.2		Tbp	RF 9.6 og 9.8 bg	
CN-14	38°18.22' 116°07.45'	0.90	10.7	9.3±0.2	7.3±0.2	Tlc	OF	
CN-15	38°17.81' 116°07.33'	0.60	10.9	9.1	7.8	Tlc	OF 8.3 og	
CN-16	38°17.38' 116°06.83'	0.67 (?)	10.4±0.1	8.2	7.2±0.1	Tq1	RF	
CN-17	38°16.96' 116°06.34'	0.08				Tbb	RF 10.0 bg	
CN-19	38°17.08' 116°06.39'	0.90 (?)	10.4	8.9±0.3	8.0±0.1	Tq1	RF	
CN-21	38°32.71' 116°06.05'	30 to 50 m from top of unit	11.2±0.1		7.6±0.2	Twm	ICF	
CN-21X	38°32.71' 116°06.05'	30 to 50 m from top of unit	11.0	9.4	7.3	?	Xenolith in CN-21, ICF	
CN-22	38°27.97' 116°03.89'	0.32	10.5	9.0	7.8	Tlc	ICF	

Field #:	Location: Lat/Long	Relative Height: (0 to 1h)	$\delta^{18}O$ Analyses:				Unit:	Remarks:
			Quartz	Feldspar	Biotite	Other		
CN-23	38°28.01' 116°03.93'	0.24	10.9±0.1	9.8	6.8±0.0	Tlc	ICF	
CN-24	38°30.46' 115°54.62'	within 30 m of top of unit	10.4		7.9	Twm	ICF	

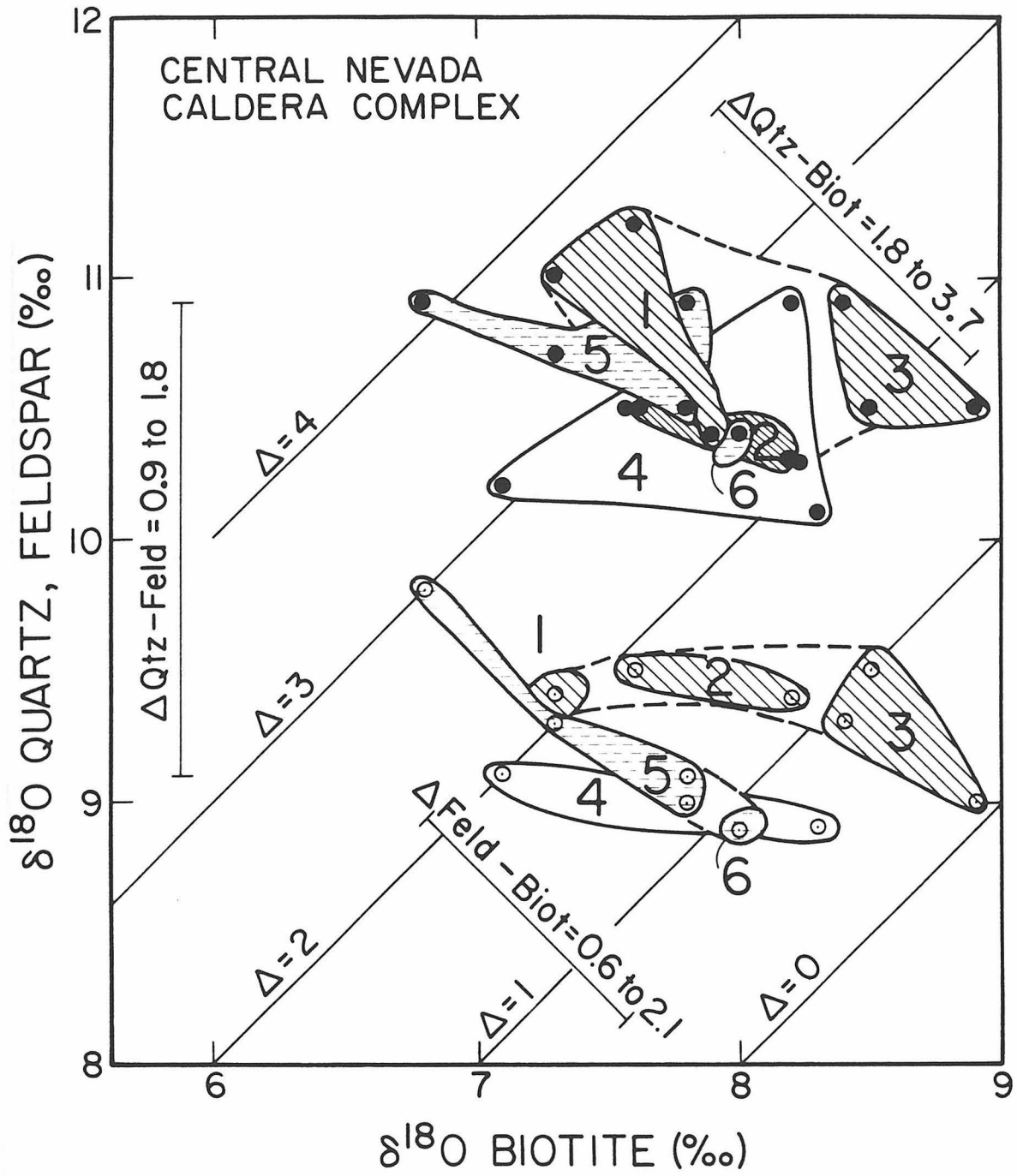
minerals adhering to the quartz phenocrysts; the quartz separates are thus nearly 100 percent pure. The matrix of some samples of densely welded, vitrophyric tuff consists of volcanic glass; black or reddish-orange to orange glass was hand picked from several samples and also analyzed.

2.3 Possible Effects of Post-Magmatic Alteration on the $^{18}\text{O}/^{16}\text{O}$ Ratios

Based on field and petrographic observations, the analyzed volcanic rocks from the Central Nevada caldera complex all appear to be fresh and free from alteration. However, it should be remembered that these rocks have been exposed to weathering and groundwater alteration for up to 25 or 30 million years, and also, during the original magmatic activity, some of the samples could have undergone weak hydrothermal alteration. It is important to take into account any such alteration effects on the measured $^{18}\text{O}/^{16}\text{O}$ ratios, before using these data to interpret the $\delta^{18}\text{O}$ variations associated with the mid-Tertiary magmatism.

The $\delta^{18}\text{O}$ values of quartz and feldspar are plotted against $\delta^{18}\text{O}$ of biotite in Figure 2.2. One sample was deleted from this figure, CN-16 from the quartz-latitude ring dome of the Late Eruptive Sequence (Tq1). This sample has an anomalously large $\Delta^{18}\text{O}$ quartz-feldspar fractionation of 2.2 per mil, much larger than the typical values observed even in slowly cooled plutonic rocks (Taylor, 1968). Inasmuch as this sample is from a lava-dome erupted along the ring-fracture zone of the Lunar Lake caldera, by analogy with the data from the Lake City caldera discussed in Chapters 4, 5, and 6 (Part I), it is not unlikely that the feldspar phenocrysts in this rock underwent some ^{18}O depletion during

Figure 2.2 $\delta^{18}\text{O}$ of quartz and feldspar plotted vs. the $\delta^{18}\text{O}$ of biotite for the central Nevada caldera complex samples. The numbers in the fields refer to the following units: (1) Twm; (2) Th; (3) Tp; (4) Tm; (5) Tlc; (6) Tq1. The units are numbered sequentially in order of their eruption, from oldest to youngest. The fields with the diagonal pattern are from the Early Sequence; the blank field is the Middle Eruptive, and the fields with the cross pattern are from the Late Sequence. See text for discussion.



meteoric-hydrothermal alteration. However, this hypothetical alteration must have been very weak because the $\Delta^{18}O$ quartz-biotite value is not unusually large and the biotite is not chloritized.

Only one other sample in Table 2.2 has an anomalously low $\delta^{18}O$ feldspar value (+8.2) that possibly ought to be attributed to weak meteoric-hydrothermal alteration. This is CN-13, from the Tuff of Buckskin Point (Tbp). Like the Tq1 sample described above, this unit is also from the ring-eruptive sequence. No coexisting minerals were analyzed from this sample, however, so this unit cannot be plotted on Figure 2.2, and we can only speculate about the reason for the low $\delta^{18}O$ value. It perhaps should be pointed out that this phenocryst feldspar is much lower in ^{18}O than the coexisting orange glass or black glass (Table 2.2). These cannot represent equilibrium relationships at magmatic temperatures; either the volcanic glass became enriched in ^{18}O or the feldspar became depleted in ^{18}O . Both are plausible possibilities.

Two other samples that are plotted on Figure 2.2 have somewhat anomalous $\Delta^{18}O$ feldspar-biotite, mainly attributable to their unusual $\delta^{18}O$ biotite values. These are: (1) Sample CN-12.5 (Tp), which has the highest $\delta^{18}O$ biotite in the entire suite, and a $\Delta^{18}O$ feldspar-biotite value that is much too small to represent isotopic equilibrium (0.1 per mil); and (2) Sample CN-23 (Tlc), which has the lowest $\delta^{18}O$ biotite in the suite of samples. Neither of these unusual samples appears to be hydrothermally altered, and in fact there is no obvious way that hydrothermal alteration would produce the entire set of $\delta^{18}O$ values and $^{18}O/^{16}O$ fractionation effects described above. Thus, we simply note

the existence of these somewhat anomalous data-points on Figure 2.2, and we shall not place much emphasis on these samples in the following discussion of magmatic $\delta^{18}\text{O}$ variations.

All of the other data-points plotted in Figure 2.2 form very tight, close-knit groupings. The phenocryst mineral assemblages exhibit the following $^{18}\text{O}/^{16}\text{O}$ fractionations:

	$\Delta^{18}\text{O}_{\text{Qtz-Feld}}$	$\Delta^{18}\text{O}_{\text{Qtz-Bio}}$	$\Delta^{18}\text{O}_{\text{Feld-Bio}}$
Range (per mil)	0.9 to 1.8	1.8 to 3.7	0.6 to 2.1
Mean (per mil)	1.3	2.7	1.4
No. of Samples	12	16	11

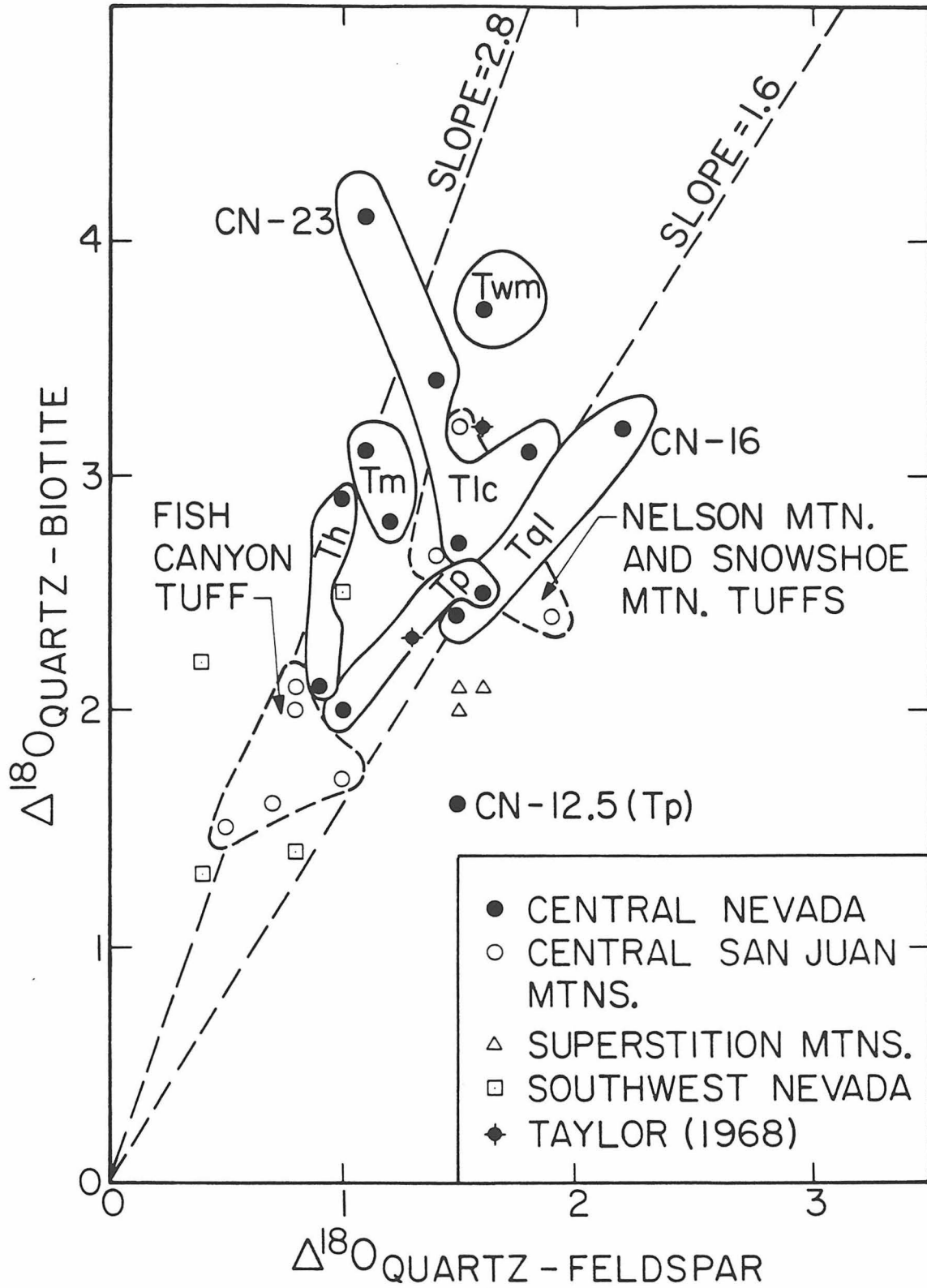
Although we cannot rule out the possibility that some of the above phenocrysts were slightly disturbed by post-magmatic alteration, there is no reason to invoke such an explanation; all of the data can be thought of as "quenched-in" primary igneous values, and the $\delta^{18}\text{O}$ variations can be attributed to phenomena taking place in the respective magma chambers prior to eruption. The above values are very similar to values obtained by other workers studying fresh, unaltered volcanic rocks (Taylor, 1968; Stuckless and O'Neil, 1973; Friedman et al, 1974; Lipman and Friedman, 1975).

2.4 Oxygen Isotopic Fractionations Among Coexisting Minerals

2.4.1 General Statement

Figure 2.3 is a plot of $\Delta^{18}\text{O}$ quartz-biotite vs. $\Delta^{18}\text{O}$ quartz-feldspar comparing data from the Central Nevada caldera complex with data

Figure 2.3 $\Delta^{18}\text{O}$ quartz-biotite fractionations plotted vs. $\Delta^{18}\text{O}$ quartz-feldspar fractionations for ash-flow tuffs from the central Nevada complex, the central San Juan complex, and other published studies of ash-flow tuffs (see text for data sources). The field of equilibrium $^{18}\text{O}/^{16}\text{O}$ fractionations at magmatic temperatures should lie between the two lines emanating from the origin with slopes of 1.6 and 2.8. These data could be interpreted as indicating that the phenocryst assemblage in the Fish Canyon Tuff formed at relatively high temperatures ($\approx 850^\circ\text{C}$?) whereas that in Tlc and Twm formed at relatively low temperatures ($\approx 700^\circ\text{C}$?). However, a possible complicating factor is the existence of very high fluorine concentrations in the biotites of the Fish Canyon Tuff; fluorine substitution for hydroxyl in biotite might also produce small $\Delta^{18}\text{O}$ quartz-biotite and $\Delta^{18}\text{O}$ feldspar-biotite fractionations (see Section 3.7).



from other literature sources, as well as with other data from this thesis on volcanic rocks from the San Juan Mountains, Colorado. Figure 2.3 backs up the discussion in the previous section with respect to the 3 anomalous samples CN-12.5, CN-16, and CN-23. All three of these samples plot well outside the two lines with slope of 1.6 and 2.8 that emanate from the origin on Figure 2.3 and which enclose most of the available $^{18}\text{O}/^{16}\text{O}$ data on coexisting quartz, feldspar, and biotite phenocrysts from ash-flow tuffs.

If all of the feldspars and biotites that are plotted on Figure 2.3 inherently had identical oxygen isotopic properties, and if equilibrium had been "frozen in" at the time of eruption in all these rocks, then the data-points ought to all plot close to a single straight line (Clayton and Epstein, 1958; Taylor and Epstein, 1962b). The most likely equilibrium line on such a diagram would be one with a slope of about 2.2. However, there could in reality be a family of such lines depending, for example, on the fluorine content of the biotite or the Al/Si ratio of the feldspar (Taylor and Epstein, 1962b; O'Neil and Taylor, 1967). In fact, at the present time there is insufficient information to decide which of the data-points lying between the lines of slope 1.6 and 2.8 represent non-equilibrium, if any! Such a determination must await more detailed laboratory calibrations of the pertinent $^{18}\text{O}/^{16}\text{O}$ equilibrium curves, as well as more complete chemical information on the mineral separates. Because the hydroxyl oxygen in biotite is probably intrinsically lower in ^{18}O than the immediately adjacent oxygen within the sheets of linked silica tetrahedra (Taylor and Epstein, 1962b; Hamza and Epstein, 1980), substitution of F for OH

would produce an equilibrium line with a smaller slope on Figure 2.3, perhaps even approaching the 1.6 line.

2.4.2 Early Eruptive Sequence

A series of diagonal 45° lines are shown on Figure 2.2 at $\Delta = 0$, 1, 2, 3, and 4 per mil. Such a plot of $\delta^{18}\text{O}$ quartz and $\delta^{18}\text{O}$ feldspar vs. $\delta^{18}\text{O}$ biotite is very useful, because both the ^{18}O fractionations (Δ values) and the bulk $^{18}\text{O}/^{16}\text{O}$ variations (δ values) can be simultaneously displayed on a single diagram.

The individual ash-flow tuff eruptive units from the Central Nevada caldera complex each plot in a distinctive position on Figures 2.2 and 2.3. Therefore, although the $^{18}\text{O}/^{16}\text{O}$ variations are small, they clearly are not random; each eruptive unit has a characteristic oxygen isotopic signature. In the feldspar-biotite plot (lower series of data points on Fig. 2.2) there is a systematic, marked increase in Δ feldspar-biotite going from the oldest unit (Twm) through the intermediate unit (Th) to the youngest unit (Tp), all within the Early Eruptive Sequence. This trend also shows up on Figure 2.3 and the upper part of Figure 2.2, but in a less systematic fashion. These systematics are best interpreted as indicating a sequentially increasing equilibration temperature, with the gigantic Tuff of Williams Ridge and Morey Peak ($> 2500 \text{ km}^3$) having been erupted at the overall lowest temperature. This could perhaps be interpreted as indicating that the Twm magma chamber was relatively H_2O -rich, which would make sense in terms of the size of the Twm eruption, as this was very likely triggered by a pressure-release event and rapid exsolution of the dissolved magmatic H_2O (however, reverse

effects are observed in the gigantic Fish Canyon Tuff from the central San Juan Mountains, as discussed below in Chapter 3!).

Although on the basis of Δ feldspar-biotite, unit Tp appears to have been erupted at a higher temperature than the immediately preceding unit Th, this is less clear for Δ quartz-biotite (Fig. 2.2) and not supported at all by Δ quartz-feldspar (Fig. 2.3). If the Tp biotite had higher fluorine contents than the Th biotites, these discrepancies would be removed, and we would conclude that Tp and Th were erupted at roughly similar temperatures. We should also point out, however, that Tp is a much smaller eruption than Th (Table 2.1), so that the sequence of increasing feldspar-biotite "temperatures" correlates very well with decreasing size of eruption (and decreasing H₂O content in the magma chamber?).

2.4.3 The Middle Eruptive

About 27 m.y. ago, after about 3 m.y. of quiescence, an event occurred that was comparable in magnitude to the eruption of the Tuff of Williams Ridge and Morey Peak. This was the eruption of the 3000 km³ Monotony Tuff. The measured ¹⁸O/¹⁶O fractionations in this single unit cover much of the range exhibited by the various units of the Early Sequence, but they in general occupy an intermediate position (particularly on Fig. 2.3). If interpreted literally, these data would suggest intermediate, but quite variable, "temperatures" of phenocryst equilibration.

The most significant $\delta^{18}\text{O}$ effect observed in the Monotony Tuff is the small, but nevertheless distinct, lowering of the $\delta^{18}\text{O}$ in the feld-

spars compared to those of the Early Sequence. This indicates that there was a decrease in the $\delta^{18}\text{O}$ of the magma chamber of about 0.3 per mil during the 3 m.y. prior to eruption of the Monotony Tuff (see below).

2.4.4 Late Eruptive Sequence

The Late Eruptive Sequence is quite complex, and not all of the units were analyzed for $\delta^{18}\text{O}$ (Table 2.1). Nonetheless it is clear that Tlc, the Tuff of Lunar Cuesta, was a fairly "low-temperature" eruptive, similar in this respect to the Tuff of Williams Ridge and Morey Peak. This was also a major eruption with a volume of about 370 km^3 . Just as is the case in the Early Sequence, following the eruption of Tlc, a smaller-volume and later-stage eruption (Tql) displays a higher isotopic "temperature" on Figures 2.2 and 2.3.

The statements made above, which assume isotopic equilibrium, must be particularly qualified for these Late Sequence samples, because of the indications of disequilibrium in one sample of Tql and one sample of Tlc (Fig. 2.3). Nevertheless, there are some very strong indications of both a close approach to isotopic equilibrium and of systematic temperature differences among these various magmas. It appears that in each sequence the latest-stage, smallest volume eruptives exhibit the highest equilibration temperatures, compatible with lower H_2O contents in the magmas (and thus less likelihood of a truly violent eruption?).

2.5 $\delta^{18}\text{O}$ Variations in the Eruptive Units with Time

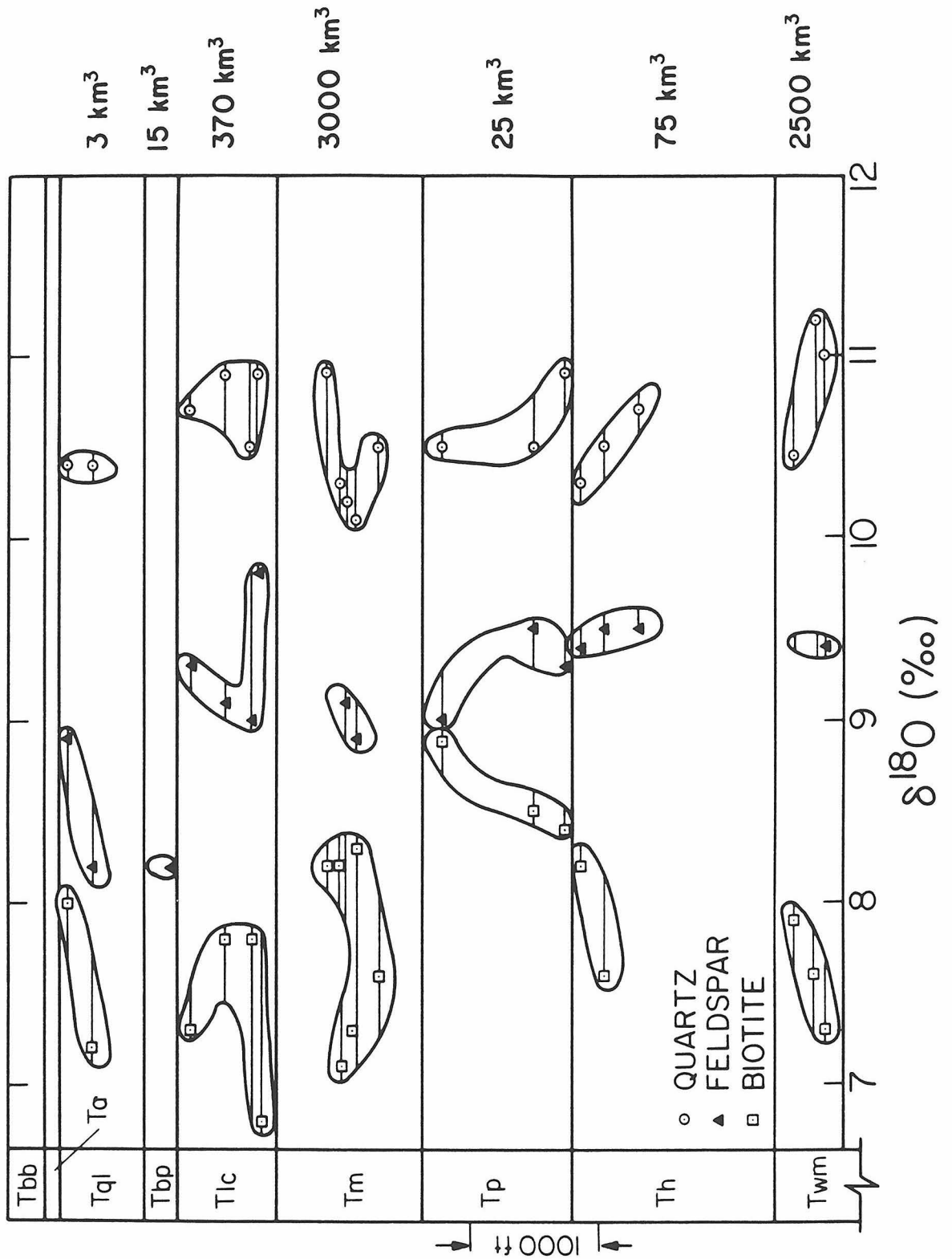
The $\delta^{18}\text{O}$ values of mineral separates of quartz, feldspar, and

biotite phenocrysts from the central Nevada complex are plotted in Figure 2.4 in their respective stratigraphic order. Except for a few analyses of orange glass and black glass (Table 2.2), whole-rock $\delta^{18}\text{O}$ values of rocks were not measured because their glassy matrices probably have exchanged oxygen with local near-surface meteoric water (Taylor, 1968). However, the original magma $\delta^{18}\text{O}$ values can be fairly accurately calculated from the feldspar analyses, because at high (magmatic) temperatures, magma-feldspar fractionations in rhyolitic rocks are 0.2 to 0.3 per mil (Taylor, 1968). Most of the feldspar $\delta^{18}\text{O}$ values lie within the range +8.9 to +9.5 (Fig. 2.2) indicating $\delta^{18}\text{O}$ values of about +9.1 to +9.8 for the original magmas (quartz latite to rhyolite).

The central Nevada complex lies within the Great Basin high- ^{18}O belt (Solomon and Taylor, 1981) defined by Cretaceous plutonic rocks with whole-rock $\delta^{18}\text{O}$ values greater than +9.0. Solomon and Taylor (1981) note that this high- ^{18}O belt corresponds spatially with a belt of late Precambrian-early Paleozoic, high- ^{18}O , geosynclinal sediments, which they consider to be the dominant source material for these Cretaceous magmas. These geosynclinal rocks thus also probably account for at least one source of the magmas with similar $\delta^{18}\text{O}$ values that formed the Oligocene central Nevada complex.

The variation in $\delta^{18}\text{O}$ in the magmas of the central Nevada eruptive sequences can be discerned on both Figures 2.2 and 2.4. Throughout the Early Sequence, with the exception of the one anomalous sample of late-stage Tp ($\delta^{18}\text{O} = +9.0$), the feldspar $\delta^{18}\text{O}$ values remain constant within experimental error (+9.3 to +9.5, average = +9.4). These $\delta^{18}\text{O}$ values show a small, but definite decrease to an average value of +9.0 in the

Figure 2.4 Mineral $\delta^{18}\text{O}$ values from central Nevada complex rocks plotted as a function of stratigraphic height, based on the stratigraphic relationships worked out by Ekren et al (1972, 1973a, 1973b, 1974). The relative thickness of each stratigraphic unit is based on the thickness at the actual sample locality; this thickness bears little or no relation to the actual volume of the eruptive unit, which is given along the right-hand side of each unit.



Middle Sequence. The $\delta^{18}\text{O}$ of quartz shows a similar decrease. However, quartz also exhibits a greater $^{18}\text{O}/^{16}\text{O}$ variability (+10.3 to +11.2, average = +10.7 in the Early Sequence versus +10.1 to +10.9, average = +10.4 for the Middle Sequence); this is in part attributable to temperature variations (Fig. 2.3). These feldspar and quartz values indicate that the 3000 km^3 mass of Monotony Tuff magma had become about 0.3 to 0.4 per mil depleted in ^{18}O during the three million years following the close of the Early Sequence eruptive cycle. This small ^{18}O depletion in the Monotony Tuff could be the result of (a) assimilation of altered, ^{18}O -depleted, volcanic country rocks (which have not been looked for in the area of the calderas); or (b) a change in the $\delta^{18}\text{O}$ of the primary magmas, possibly related to a different source region. Inasmuch as all the magma batches have similar chemical compositions (quartz latite to rhyolite) with no correlation between $\delta^{18}\text{O}$ and petrographic type, it is simpler to explain the $\delta^{18}\text{O}$ variations as resulting from differences in the amount and type of high-level assimilation of country rocks by the primary magmas.

Following the great Monotony Tuff eruption, there was another quiescent period of 1.0 to 1.5 m.y. prior to eruption of the much less voluminous Tuff of Lunar Cuesta (Tlc). The latter exhibits higher feldspar $\delta^{18}\text{O}$ values (+9.0 to +9.8, average = +9.3), similar to those of the Early Sequence and possibly indicating a return to the primary $\delta^{18}\text{O}$ value for the magma in this area. Very shortly after the Tlc eruption, the relatively tiny eruptions of Tbp and Tql occurred, and this may have been accompanied by another decrease in $\delta^{18}\text{O}$ attributable to assimilation of low- ^{18}O roof rocks (Tbp: +8.2; Tql: +8.2 to +8.9,

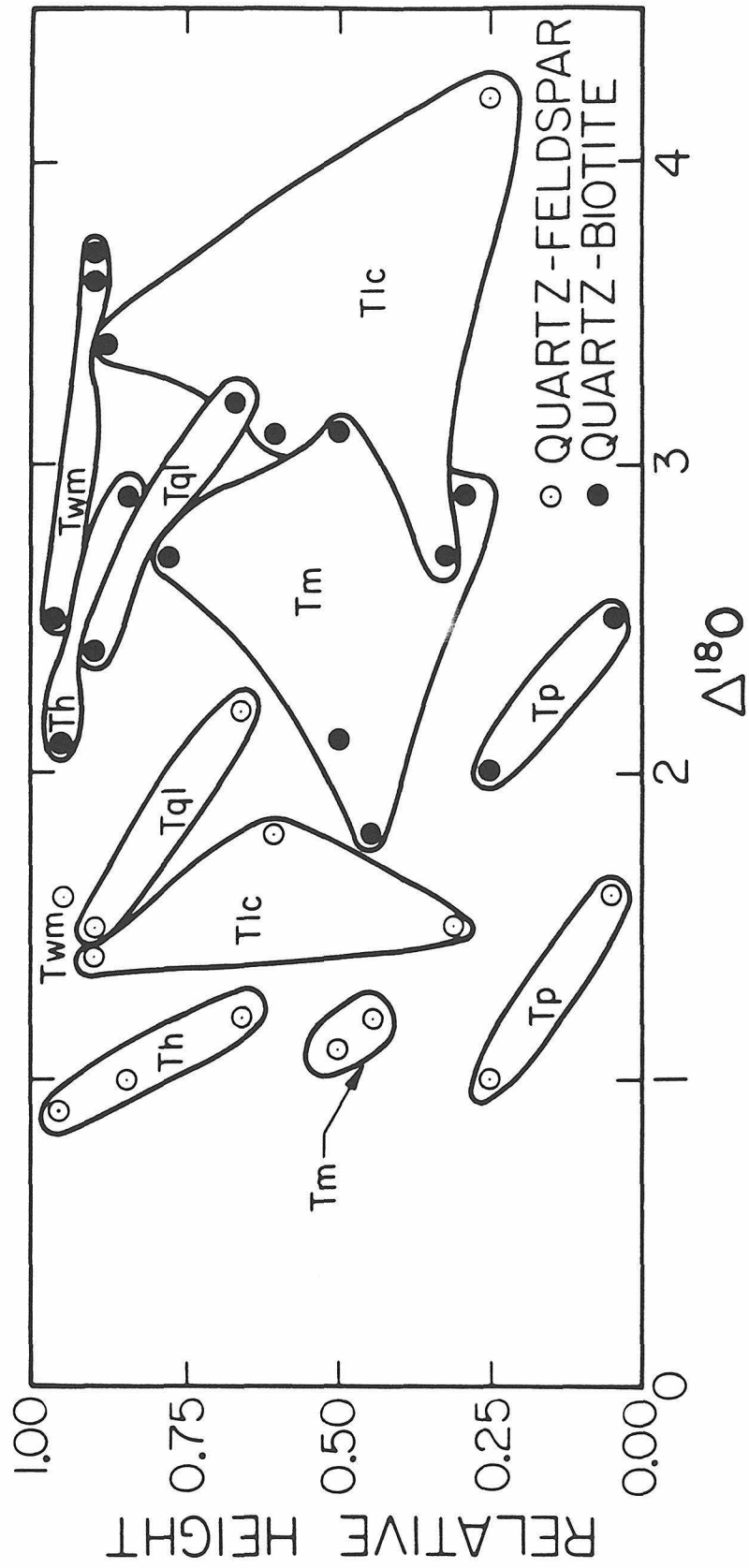
average = +8.6). However, as indicated above, these small changes in $\delta^{18}\text{O}$ conceivably could be due to minor hydrothermal alteration, or to changes in the $\delta^{18}\text{O}$ of the source materials of the original magmas.

Although we have emphasized the changes in $\delta^{18}\text{O}$ with time in the above discussion, the major conclusion indicated by the data in Figures 2.2 and 2.4 is the remarkable constancy in $\delta^{18}\text{O}$ of the rhyolite and quartz latite magmas erupted over a period of more than 6 m.y. in the central Nevada caldera complex. This is particularly true if we assume that some of the later-stage magmas such as the Tq1 ring dome have been hydrothermally altered. Thus, although we specifically entered this project looking for low- ^{18}O magmas of the type found by Friedman et al (1974) and Lipman and Friedman (1975) in the Yellowstone and southwestern Nevada caldera complexes, it is clear that such low- ^{18}O magmas are either very rare or totally non-existent in the central Nevada caldera complex. It is not at all obvious why the ^{18}O depletions should be so extensive and dramatic at Yellowstone and in the Claim Canyon-Oasis Valley caldera complexes, and virtually non-existent in the rocks we have studied. Perhaps the development of low- ^{18}O rhyolitic magmas requires a unique set of circumstances involving an interplay between the timing and location of caldera collapse and the vagaries of the hydrothermal circulation system.

2.6 $^{18}\text{O}/^{16}\text{O}$ Variations within Individual Ash-Flow Tuffs

Mineral $\delta^{18}\text{O}$ data are plotted as functions of stratigraphic positions within each volcanic unit in Figure 2.4, and the $\Delta^{18}\text{O}$ fractionation data are plotted in a somewhat analogous fashion in Figure 2.5.

Figure 2.5 $\Delta^{18}\text{O}$ quartz-feldspar and quartz-biotite fractionations for the central Nevada complex plotted as a function of relative height of the sample. Fields for all the units show negative slopes for both fractionations. These slopes indicate a vertical temperature gradient in the magma chamber, with larger fractionations (lower equilibration temperatures) characterizing the phenocryst assemblages near the roof of the magma chamber prior to eruption of each of these units.



The thicknesses of the tuffs and flows are variable, and the thicknesses used in Figure 2.4 correspond to the thickness of a unit where it was sampled. T_{wm} is at least 1 km thick and the base of the unit is not exposed. The two samples of this unit (CN-21 and CN-24) were both collected within 50 m of the top of the unit and are plotted as such on Figure 2.4.

Mineral-mineral fractionations typically decrease systematically within each tuff unit as one goes from the lower to the higher samples. This supports the previous interpretations in Section 2.4 that these are close to equilibrium ¹⁸O fractionations because: (1) We would a priori expect that the temperatures would increase upward in each unit, as the upside-down stratigraphy means we are actually sampling deeper into the magma chamber; and (2) The equilibrium $\Delta^{18}\text{O}$ values within a single tuff unit should all decrease systematically with an increase in temperature, because any chemical variations (fluorine, etc.) are expected to be smaller within a single unit than they would be in a whole series of different ash-flow sheets. Thus, the isotope data in Figure 2.5 indicate that a thermal gradient existed along the upper margin of the magma chamber prior to the eruption of most of the tuff units. The lowermost portions of the ash-flows (uppermost portions of the magma chamber) exhibit the largest mineral-mineral ¹⁸O fractionations, compatible with cooler temperatures adjacent to the roof of the magma chamber.

The effects described above are best developed in the Early Sequence eruptives. The middle eruptive (T_m) does not exhibit very systematic patterns on Figure 2.5, particularly for $\Delta^{18}\text{O}$ quartz-biotite.

The late sequence eruption (Tlc) also does not show this pattern, particularly if the lowermost Tlc sample (CN-23, the one with the very large quartz-biotite fractionation, +4.1 per mil) were to be deleted from the diagram. CN-22, collected just above CN-23, has the smallest quartz-biotite fractionation (+2.7 per mil) of the Tlc samples, and the two uppermost Tlc samples (CN-14 and CN-15) exhibit intermediate fractionations of +3.1 and +3.4, respectively. It may not be a coincidence that the least systematic $\Delta^{18}\text{O}$ fractionation patterns are found in those units (Tm and Tlc) that have the lowest bulk $\delta^{18}\text{O}$ values. This might be taken as indicating that the small degree of $\delta^{18}\text{O}$ lowering in these magma chambers was indeed caused by stoping and assimilation of hydrothermally altered roof-rocks, thereby imparting a relatively heterogeneous ^{18}O pattern to the upper parts of these particular magma chambers.

CENTRAL SAN JUAN CALDERA COMPLEX

3.1 Evolution of the Central San Juan Caldera Complex

The central San Juan caldera complex is a product of the caldera-forming calc-alkaline magmatism of the San Juan volcanic province described in Part I of this thesis. Eight ash-flow tuffs related to collapse in the central San Juan caldera complex are recognized (Ratte and Steven, 1967; Steven and Lipman, 1976). The distribution of these units in and adjacent to the complex were studied by Lipman and Steven (1976), Steven (1967), Steven and Lipman (1973), Steven and Ratte (1973). Evolution of the caldera complex is summarized in Table 3.1, and the structural evolution of the caldera complex is shown in Figure 3.1abc. The rocks into which the caldera complex were emplaced consist of the products of the earlier San Juan intermediate calc-alkaline volcanism.

The earliest major eruption from the central San Juan complex, the Fish Canyon Tuff (Tfc), had a volume greater than 3000 km³. This eruption is the largest single event in the history of the central San Juan Mountains, and it resulted in collapse of the great La Garita caldera (Fig. 3.1a) (Steven and Lipman, 1976). This widespread tuff is a chemically and mineralogically homogeneous quartz latite, and contains about 40 percent phenocrysts (plagioclase > sanidine > hornblende = biotite > quartz) (O'Leary and Whitney, 1981; Whitney and Stormer, 1983). Analyses of iron-titanium oxides suggest magmatic temperatures of about 760°C at the stratigraphic base and about 810°C at the top (O'Leary and

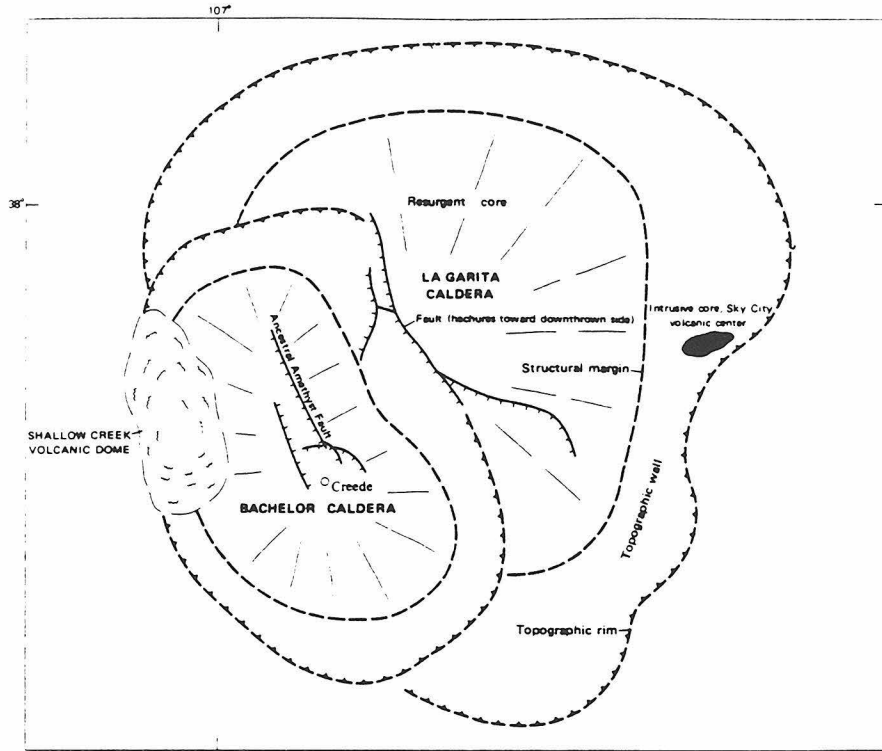
Table 3.1 Volumes and ages of rocks erupted from the central San Juan caldera complex. The rocks are listed in stratigraphic order, with the youngest above and the oldest at the bottom. Also shown are abbreviations for the units as used in the text.

Unit	Volume	Age ⁽¹⁾	Caldera
Fisher quartz latite (Tf)	10-100 km ³ (2)	26.4 bi ⁽³⁾	
*Snowshoe Mountain Tuff (Ts)	>500 km ³ (3)		Creede
Volcanics of Stewart Peak	?		
*Nelson Mountain Tuff (Tnr)	>500 km ³ (3)		San Luis
*Rat Creek Tuff (Tnr)	<100 km ³ (3)		early San Luis
*Wason Park Tuff (Tw)	100-500 km ³ (3)		Creede area
*Mammoth Mountain Tuff (Tm)	100-500 km ³ (3)	26.7 bi ⁽⁴⁾	Creede area
Farmers Creek Tuff	10-100 km ³ (2)		
Shallow Creek Quartz Latite (Tsc)	+5 km ³		
*Carpenter Ridge Tuff (Tcr)	>500 km ³ (3)		Bachelor
Miners Creek Rhyolite (Tmc)	1 km ³		
*Fish Canyon Tuff (Tfc)	>3000 km ³	27.7±0.8 bi ⁽⁴⁾	La Garita

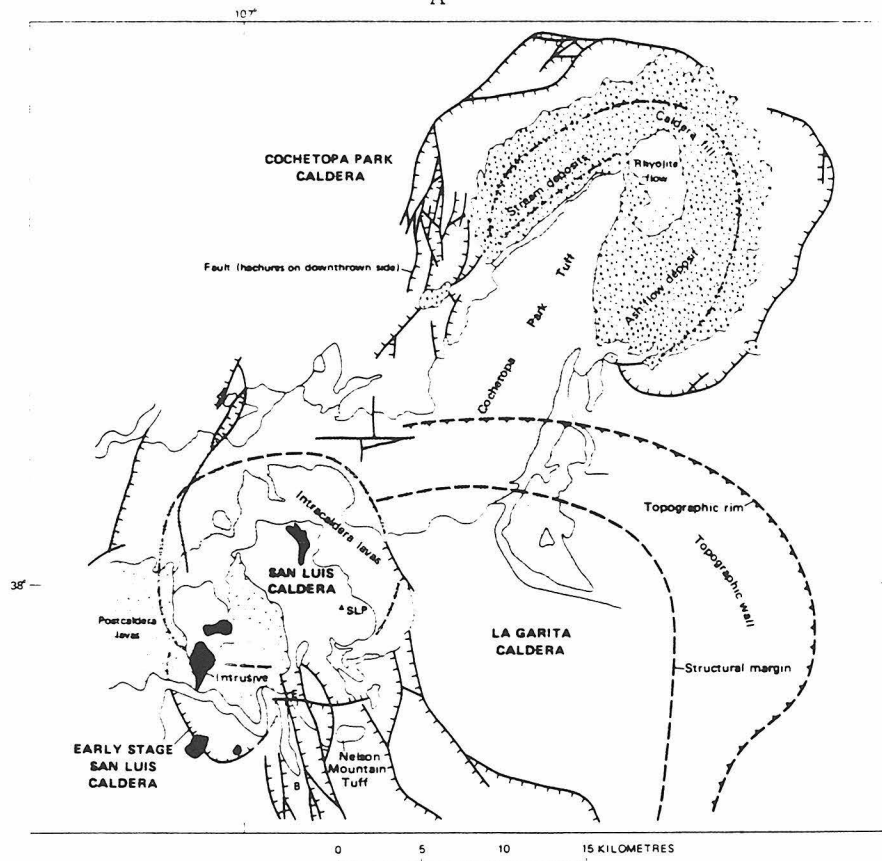
(1) All ages are m.y. ago, K-Ar; bi = biotite; analytical uncertainty given where listed by original authors. (2) Ratte and Steven (1964). (3) Steven and Lipman (1976). (4) Lipman et al (1970).

* denotes eruption related to caldera collapse

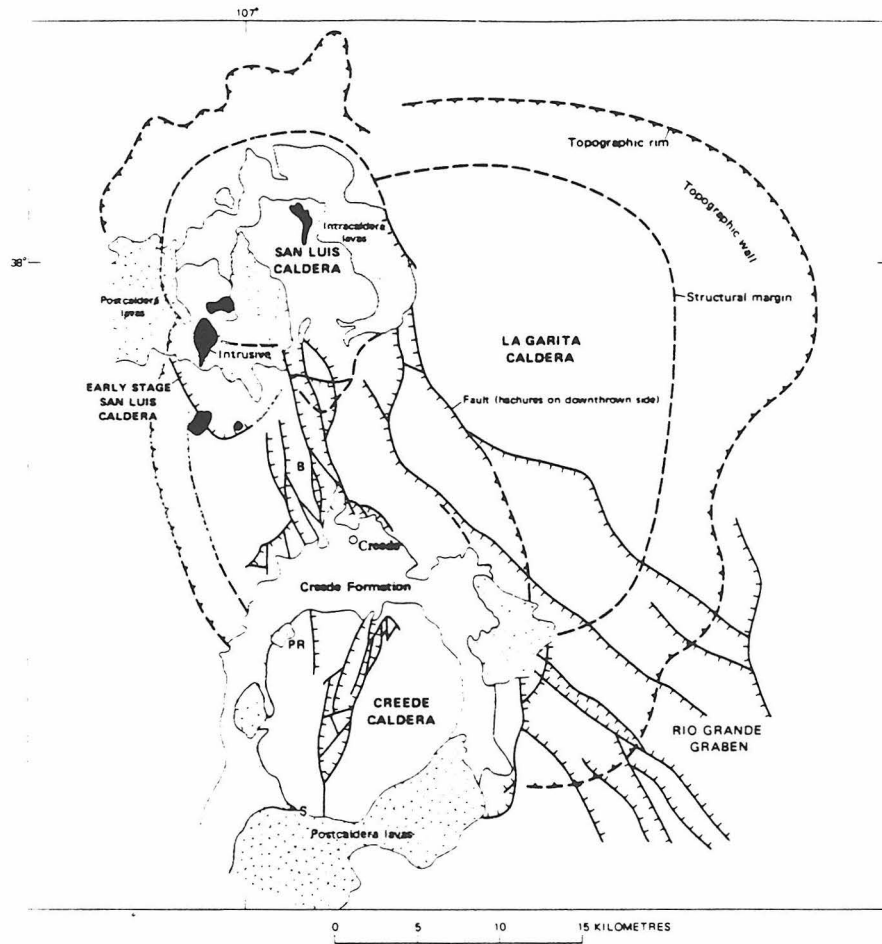
Figure 3.1abc Evolution of the central San Juan caldera complex (from Steven and Lipman, 1976). (a) Volcanism began with eruption of the voluminous Fish Canyon Tuff (3000 km^3) and collapse of the La Garita caldera about 28 m.y. ago. This was followed by eruption of the Carpenter Ridge Tuff and collapse of the Bachelor caldera on the western margin of the La Garita caldera. (b) The only intermediate-age ash-flows in this complex that can be traced to well-defined sources are the Rat Creek Tuff and Nelson Mountain Tuff, both of which erupted from the San Luis caldera on the northwestern margin of the La Garita caldera. The eruption of the Cochetopa Park Tuff to the north closely followed the collapse of the San Luis caldera. (c) The final caldera collapse in the central San Juan complex, the Creede caldera, occurred in response to the eruption of the Snowshoe Mountain Tuff. Lavas of the Fisher quartz latite (about 26.4 m.y. old) occur as domes around the periphery of the Creede caldera.



A



B



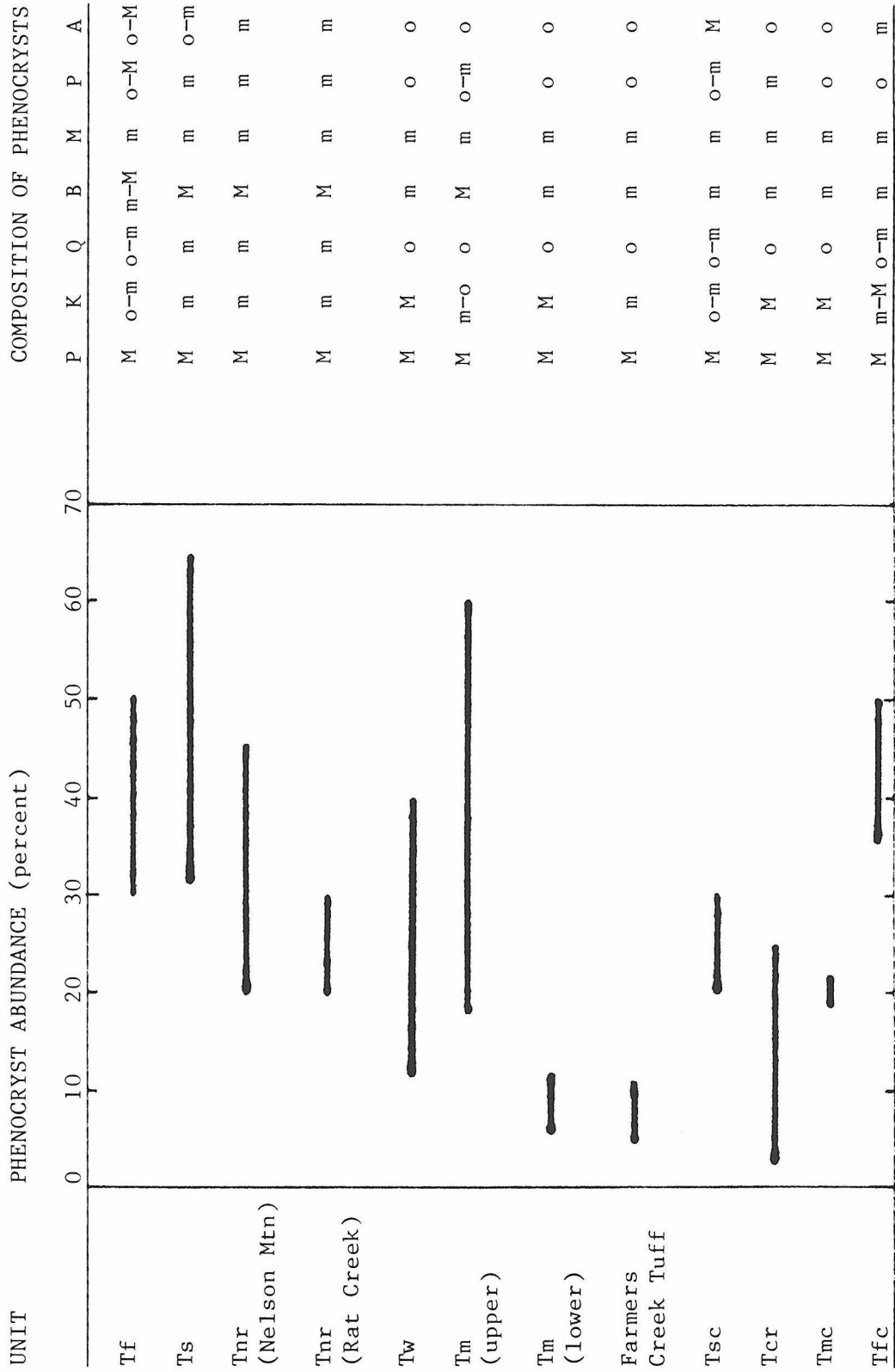
C

Whitney, 1981). Outside the La Garita caldera the tuff ranges from 30 to 200 m thick, and accumulated to greater than 1.4 km thick within the caldera (Steven and Lipman, 1976). The only ring-fracture volcanism possibly related to the La Garita caldera is the porphyritic rhyolite dome of Miners Creek (Tmc), which may have erupted from a source on the western caldera margin. Tmc comprises 20 percent phenocrysts (sanidine = plagioclase > biotite) (Steven and Ratte, 1965).

The other ash-flows and lavas produced from the caldera complex after the gigantic eruption of Fish Canyon Tuff all erupted from sources along the western margin of the La Garita caldera (Fig. 3.1bc). The mineralogy of most of these units is summarized by Ratte and Steven (1964) and is shown on Figure 3.2. The Bachelor caldera formed in response to the eruption of the Carpenter Ridge Tuff (Tcr) (Steven and Lipman, 1976). The Bachelor Mountain member of Tcr (Bachelor Mountain rhyolite of Ratte and Steven, 1964) fills the collapsed block of the Bachelor caldera to 1.5 km (Steven and Lipman, 1976). Outflow Tcr is less than 400 m thick and is in places compositionally zoned from a lower rhyolite to an upper quartz latite. The Shallow Creek quartz latite lava dome (Tsc) was then extruded along the western margin of the Bachelor caldera. Steven and Ratte (1965) note that samples of fresh, unaltered Tsc are very rare.

Eruption of the small Farmers Creek Tuff (Farmers Creek rhyolite of Ratte and Steven, 1964) initiated the Mammoth Mountain eruptive cycle (Steven and Lipman, 1976). This was followed by eruption of the Mammoth Mountain Tuff (Tm) (Mammoth Mountain rhyolite of Ratte and Steven, 1964). Tm is highly variable in thickness and accumulated to

Figure 3.2 Mineralogy of some of the ash-flows and lavas erupted from the central San Juan caldera complex (modified after Ratte and Steven, 1964; Steven and Ratte, 1965; and Lipman, 1975). Note that Steven and Lipman (1976) have significantly reinterpreted the evolution of these calderas, and this list has been expanded to include all units listed in Tables 3.1 and 3.2 (consult those tables for an explanation of the unit symbols). Mineral abbreviations for composition of phenocrysts are: P, plagioclase; K, sanidine; Q, quartz; B, biotite; M, magnetite; P, pyroxene; A, amphibole. M indicates that mineral makes up more than 10 percent of total phenocrysts; m indicates less than 10 percent; and o indicates a trace or not present. Except for the earliest ash-flow (Tfc), phenocryst abundances tend to increase in the successively younger eruptions (Ratte and Steven, 1964).



greater than 500 m in topographic lows (Steven and Lipman, 1976). Locally, T_m is zoned from a basal crystal-poor rhyolite to an upper crystal-rich quartz latite (Ratte and Steven, 1964, 1967). T_m is postulated to have erupted from a source in the area of the subsequent Creede caldera (Steven and Lipman, 1976). Similarly, the Wason Park Tuff (T_w) (Wason Park rhyolite of Ratte and Steven, 1964), which followed the Mammoth Mountain Tuff, has a postulated source within the area of the subsequent Creede caldera (Steven and Lipman, 1976).

The Rat Creek and Nelson Mountain Tuffs (collectively T_{nr}) were then sequentially erupted from the San Luis caldera (Fig. 3.1b) (Steven and Lipman, 1976). The rhyolitic Rat Creek Tuff varies widely in thickness (to a maximum of about 200 m) because of rough underlying topography, whereas the quartz latitic Nelson Mountain Tuff accumulated to at least 1.5 km thickness within the collapsed block of the San Luis caldera and to 300 m thickness outside the caldera (Steven and Lipman, 1976). Intermediate to silicic volcanics of Stewart Peak were then erupted within the collapsed block of the San Luis caldera (Steven and Lipman, 1976). Eruption from the Cochetopa Park caldera, north of the central San Juan complex, deposited the Cochetopa Park Tuff in the San Luis caldera area (Steven and Lipman, 1976)

The final ash-flow eruption from the central San Juan complex was the Snowshoe Mountain Tuff (T_s) (Snowshoe Mountain quartz latite of Ratte and Steven, 1964), which erupted from the Creede caldera (Fig. 3.1c). Smith and Bailey (1968) used the Creede caldera as one example of a typical resurgent cauldron. Perhaps up to 2 km of T_s fill the Creede caldera, but outflow T_s is thin and not widespread (Steven and

Lipman, 1976). Caldera-fill Ts is pervasively weakly altered (Steven and Ratte, 1965). Eruption of Ts was followed by the extrusion of flows of the Fisher quartz latite (Tf) around the periphery of the Creede caldera.

3.2 Oxygen Isotopic Analyses of Coexisting Minerals from the Central San Juan Caldera Complex

Sampling procedures for rocks from the central San Juan caldera complex are similar to those described in Chapter 2 for rocks from the central Nevada caldera complex. Sample preparation was identical to that of the Nevada samples. Analyses of mineral separates from the central San Juan samples are shown in Table 3.2. Quartz is only rarely found as a phenocryst mineral in the San Juan ash-flows and this is reflected by the small number of quartz analyses shown in Table 3.2. Also, the central San Juan calderas have been affected by widespread hydrothermal alteration; this alteration is not always manifest in hand samples, and thus some data in Table 3.2 represent analyses of altered rocks. The $\delta^{18}O$ values in such rocks are lower than those in unaltered igneous rocks. Feldspar analyses in Table 3.2 include both K feldspar and plagioclase, because these minerals are not readily separated during hand picking. However, the feldspar separates generally were made up of more than 50 percent sanidine. Hornblende, magnetite, and pyroxene are found as accessory phases in many of the ash-flows from the central San Juan caldera complex. In rocks where these minerals occur in sufficient quantity as large grains, they were hand picked and analyzed. The matrix of the Miners Creek rhyolite dome consists of green and

Table 3.2

Oxygen isotopic analyses of rocks and mineral separates from the central San Juan caldera complex. The following explanatory remarks refer to the column headings, as enumerated on the first page of data.

- (1) Latitude is N, longitude is W.
- (2) All data are per mil, relative to SMOW. Data for which replicate analyses were made show the average of the two analyses with the range denoted as \pm .
- (3) Abbreviations are as follows:
- | | | | |
|----|-------------|----|--------------|
| gg | green glass | M | magnetite |
| H | hornblende | og | orange glass |
| P | pyroxene | WR | whole-rock |
- (4) Abbreviations for units are as follows:
- | | |
|-----|-------------------------------------|
| Tfc | Fish Canyon Tuff |
| Tw | Wason Park Tuff |
| Tnr | Nelson Mountain and Rat Creek Tuffs |
| Tcr | Carpenter Ridge Tuff |
| Tf | Fisher Quartz Latite |
| Ts | Snowshoe Mountain Tuff |
| Tm | Mammoth Mountain Tuff |
| Tsc | Shallow Creek Quartz Latite |
| Tmc | Miners Creek Rhyolite |

Central San Juan Caldera Complex

Field #:	Location ¹ : Lat/Long	Relative Height: (0 to 1h)	δ ¹⁸ O Analyses ² :			Unit ⁴ :	Remarks:
			Quartz	Feldspar	Biotite		
SP-1	37°33.49' 106°46.27'	0.39	7.2	5.8	7.5 WR 3.1 M 6.0 H	Tfc	
SP-2	37°30.54' 106°46.36'	0.80	7.1	6.2		Tfc	
SF-2	37°30.65' 106°42.21'	0.01	7.1	5.8	9.0 WR 6.0 H	Tfc	
SF-3	37°32.76' 106°41.73'	0.20	7.1	5.9	8.5 WR 5.8 H	Tfc	
SF-5	37°34.61' 106°43.79'	0.20	7.5	6.0	7.0 WR	Tfc	Numerous xenoliths
CC-1	37°58.25' 107°10.87'	0.44	6.7	5.8	7.7 WR	Tw	
CC-2	37°58.01' 107°10.37'	0.13	6.8	5.8	7.3 WR	Tw	
CC-4	37°57.58' 107°10.08'	0.95	8.1	6.4		Tfc	
CC-6	37°56.27' 107°10.04'	Near base			6.6 WR	Hinsdale basalt	
CC-9	37°54.41' 107°09.48'	6 m from top of unit	8.2	5.6	5.8 WR 5.6 H 5.7 P	Tnr	

Field #:	Location: Lat/Long	Relative Height: (0 to 1h)	$\delta^{18}O$ Analyses:				Unit:	Remarks:
			Quartz	Feldspar	Biotite	Other		
CC-10	37°52.92' 107°08.77'	0.60 (?)	6.9	5.8	7.6 WR	Tnr		
CC-14	37°56.85' 107°07.08'	0.12	6.8	5.7	8.2 WR 5.4 P	Tw		
CC-16	37°55.17' 107°05.68'	0.90	7.2	6.6	8.9 WR	Tcr		
CC-17	37°51.80' 106°55.54'	?	7.2	9.1 WR	Tcr	Plagioclase altered to clay		
CC-18	37°52.72' 106°55.68'	?	6.1	21.8 WR 8.6 clay	Tcr	Plagioclase altered to clay	405	
CC-19	37°46.35' 106°49.84'	0.03	7.6	6.0±0.0	7.3 WR 6.8 H	Tf		
CC-20	37°46.46' 106°49.29'	0.53	6.4	6.0	8.5 WR	Tf	Weak alteration along fractures	
CC-23	37°42.09' 106°55.97'	?	6.4	6.4		Ts	Clinopyroxene 50% altered to calcite	
CC-25	37°42.87' 106°54.78'	?	8.2±0.1	6.7	7.7 WR	Ts		
CC-26	37°44.03' 106°54.27'	?	8.2	6.3	5.9 P	Ts		

Field #:	Location: Lat/Long	Relative Height: (0 to lh)	δ ¹⁸ O Analyses:			Unit:	Remarks:
			Quartz	Feldspar	Biotite		
CC-30	37°53.66' 106°54.38'	0.07	7.2±0.1	6.3	Tm		
CC-31	37°53.68' 106°54.28'	0.16	7.1	6.1	Tm		
CC-32	37°53.74' 106°54.25'	0.36	7.3±0.1	6.3	Tm		
CC-33	37°53.81' 106°54.21'	0.59	7.2	6.3	Tm		
CC-34	37°53.88' 106°54.14'	0.73	7.2	5.5±0.1	Tm		
CC-35	37°53.86' 106°53.95'	0.87	7.2±0.2	6.3	Tm		
CC-38	37°50.74' 106°59.54'	0.31			Tsc	9.6±0.5 WR	
CC-39	37°50.54' 106°59.50'	0.12			Tsc	9.4 WR Feldspars altered	
CC-40	37°50.42' 106°59.29'	Float			Tsc	5.7 WR Groundmass recrystalline	
CC-41	37°52.38' 106°59.65'	Near base of dome	7.1	6.0	Tmc	11.8±0.0 WR 12.4 gg 12.9 og Perlitic, same outcrop as CC-42	

Field #:	Location: Lat/Long	Relative Height: (0 to 1h)	$\delta^{18}O$ Analyses:				Unit:	Remarks:
			Quartz	Feldspar	Biotite	Other		
CC-42	37° 52.38' 106° 59.65'	Near base of dome	6.9	6.4		Tmc	Perlitic, oxidized, same outcrop as CC-41	
CC-47	37° 35.31' 106° 38.61'	0.09	7.2±0.0	6.4		Tcr		
CC-48	37° 35.40' 106° 38.63'	0.15	6.8±0.0	6.1		Tw		

orange devitrified volcanic glass. Fragments of these two glass types were hand picked and analyzed. Analyses were also made on a number of whole-rock samples, all from aliquots prepared by crushing one to two grams of unweathered rock.

3.3 Possible Effects of Post-Magmatic Alteration on the $^{18}\text{O}/^{16}\text{O}$ Ratios

Large volumes of volcanic rocks in the central San Juan caldera complex have been hydrothermally altered; these hydrothermally altered rocks host the Creede and Spar City mining districts (Steven et al, 1974; Steven and Ratte, 1965). Any such alteration effects on the measured $^{18}\text{O}/^{16}\text{O}$ ratios must be taken into account before using these data to interpret the $\delta^{18}\text{O}$ variations associated with the mid-Tertiary magmatism.

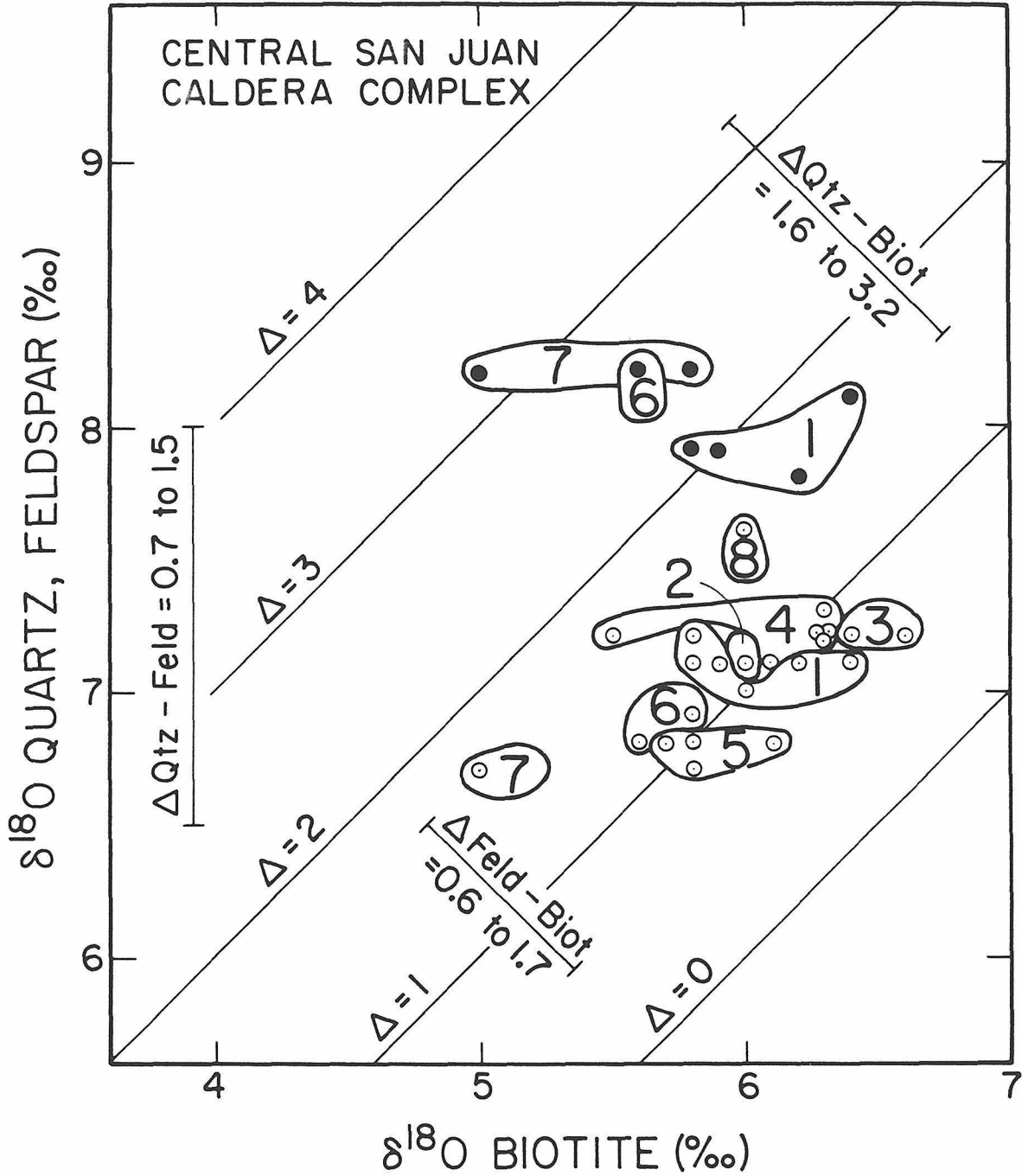
Areas that contain mineralogically altered rocks were routinely avoided during sampling, but some outcrops that were sampled and analyzed were subsequently found to exhibit mineralogical alteration under the petrographic microscope. For example, two specimens of Tcr (CC-17, CC-18) were found to contain heavily argillized plagioclase. Even though this plagioclase could be avoided in the mineral separations (the analyzed feldspars from these two samples were nearly pure sanidine), the sanidine from CC-18 was found to have a $\delta^{18}\text{O}$ value of +6.1, 1.1 per mil lower than feldspars from the other three analyzed Tcr samples. This low- $\delta^{18}\text{O}$ value suggests that the sanidine in CC-18 exchanged oxygen with the low ^{18}O meteoric-hydrothermal fluid that was probably responsible for the alteration of the plagioclase. Note, however, that sanidine from the other altered sample (CC-17) has a $\delta^{18}\text{O}$ value of +7.2,

identical to feldspar from two unaltered Tcr samples (CC-16, CC-47). The sanidine from CC-17 thus does not appear to have exchanged appreciably with meteoric-hydrothermal fluids.

The $\delta^{18}\text{O}$ values of quartz and feldspar are plotted against $\delta^{18}\text{O}$ of coexisting biotite in Figure 3.3. Sample CC-20, from a Tf ring dome of the Creede caldera, was deleted from this figure; this was done on the basis of the anomalously small Δ feldspar-biotite fractionation of 0.4 per mil, as well as because this sample contains hydrothermal calcite and quartz in microveinlets. The small fractionation indicates non-equilibrium, and means that one (or both) of these minerals probably exchanged oxygen with the same hydrothermal fluid that produced the microveinlets; however, in thin section, there is no obvious mineralogical alteration of the feldspar or biotite.

Two samples of Ts (CN-23, CN-26) were also excluded from Figure 3.3 because they show evidence of hydrothermal alteration: (1) CC-23 exhibits carbonate alteration of pyroxene phenocrysts; the Δ feldspar-biotite fractionation for this sample is much too small to represent equilibrium (0.0 per mil). (2) CC-26 is not obviously mineralogically altered, but it has a low Δ feldspar-biotite fractionation of 0.5 per mil and an anomalously large Δ quartz-feldspar value of 1.9 per mil. The most plausible explanation for the anomalous $\Delta^{18}\text{O}$ values in these two samples is post-crystallization oxygen isotope exchange with a meteoric-hydrothermal fluid. Also, both samples are intracaldera facies from the Creede caldera; by analogy with what we know about the Lake City and other caldera hydrothermal systems (Part I of this thesis), it is not unreasonable that caldera-wide meteoric-hydrothermal activity occurred

Figure 3.3 $\delta^{18}\text{O}$ of quartz and feldspar plotted vs. the $\delta^{18}\text{O}$ of biotite for the central San Juan complex samples. The numbers in the fields refer to the following units: (1) Tfc; (2) Tmc; (3) Tcr; (4) Tm; (5) Tw; (6) Tnr; (7) Ts; (8) Tf. These units are numbered sequentially in order of their eruption, from oldest to youngest. See text for discussion.



in the Creede caldera shortly after it formed.

Three samples of the Shallow Creek Quartz Latite dome (CC-38, CC-39, CC-40) were found to be so intensely mineralogically altered that analyses of mineral separates for these samples were not even attempted. A whole-rock $\delta^{18}\text{O}$ value of +5.7 for CC-40 is suggestive of relatively high temperature oxygen isotopic exchange with a meteoric-hydrothermal fluid. Lower temperature hydration and alteration is probably responsible for the intensely argillized feldspars in CC-39, which has a whole-rock $\delta^{18}\text{O}$ value of +9.4. By analogy to CC-39, CC-38 (whole-rock $\delta^{18}\text{O} = +9.6$) is also probably altered, although a petrographic thin section of this sample is not available to confirm mineralogical alteration. In hand sample, feldspars in CC-38 show the same clouded, white discoloration that is evident in both CC-39 and CC-40.

The two samples of perlitic Miners Creek Rhyolite (CC-41, CC-42) were collected within a meter of each other at the same outcrop. No evidence of hydrothermal alteration in this outcrop was noted during sampling, although sample CC-42 is highly oxidized. Because perlitites are typically enriched in ^{18}O by low-temperature hydration processes (Taylor, 1968), it was not surprising to find glass and whole-rock $\delta^{18}\text{O}$ values of +11.8 to +12.9 in these samples. However, it was somewhat surprising to find that the $\Delta^{18}\text{O}$ feldspar-biotite fractionations in the phenocrysts from these two samples were quite different (1.1 and 0.5, respectively). The 1.1 per mil fractionation for CC-41 is within the normal range of magmatic values. The 0.5 per mil fractionation for oxidized sample CC-42 lies below the normal range, and thus these data are not plotted on Figure 3.3 and are not considered in the following

discussion of magmatic $\delta^{18}\text{O}$ values of the central San Juan caldera complex. The unoxidized sample CC-41 is used in the discussions below as the only representative of the Miners Creek Rhyolite.

All of the other data-points plotted on Figure 3.3 form very tight, close-knit groupings. A similar plot (Fig. 2.2, discussed in Chapter 2) shows similar tight groupings for the central Nevada caldera complex. The phenocryst mineral assemblages for the central San Juan caldera complex, excluding Tfc sample SF-5 (see below), but including two samples of outflow-facies Sunshine Peak Tuff from the Lake City caldera (Part I of this thesis) exhibit the following $^{18}\text{O}/^{16}\text{O}$ fractionations:

	$\Delta^{18}\text{O}_{\text{Qtz-Feld}}$	$\Delta^{18}\text{O}_{\text{Qtz-Bio}}$	$\Delta^{18}\text{O}_{\text{Feld-Bio}}$
Range (per mil)	0.8 to 1.6	1.6 to 3.2	0.6 to 1.7
Mean (per mil)	1.2	2.2	1.1
No. of Samples	8	6	23

The above values are very similar to values obtained on the central Nevada caldera complex, as well as those obtained by other workers studying fresh, unaltered volcanic rocks (Taylor, 1968; Stuckless and O'Neil, 1973; Friedman et al, 1974; Lipman and Friedman, 1975). Thus, although we cannot rule out the possibility that some of these phenocrysts were slightly disturbed by post-magmatic alteration, there is no reason to invoke such an explanation; all of the data can be thought of as "quenched-in" primary igneous values, except those specifically mentioned above in connection with the discussion of hydrothermal alteration. The $\delta^{18}\text{O}$ variations and $\Delta^{18}\text{O}$ effects can be attributed to

phenomena taking place in the respective magma chambers prior to eruption.

3.4 Oxygen Isotopic Fractionations among Coexisting Minerals and Rocks

The individual ash-flow eruptive units from the central San Juan caldera complex each plot in a distinctive position on Figures 2.3 and 3.3. As was the case for the central Nevada caldera complex, although the $^{18}\text{O}/^{16}\text{O}$ variations are small, they clearly are not random; each eruptive unit has a characteristic oxygen isotopic signature. There is no obvious systematic variation in Δ feldspar-biotite (lower series of data points on Fig. 3.3) in going from older to younger units. These data thus might be taken as indicating that most of the magmas from the central San Juan caldera complex erupted at about the same average temperature. Although some suggestion of a temperature effect appears in the Δ quartz-biotite values (upper series of data points on Fig. 3.3), there really are not enough $\delta^{18}\text{O}$ quartz analyses to establish a pattern (remember that quartz phenocrysts are very rare in most of the central San Juan tuffs).

The above statements need to be qualified to a certain extent, because for some of the units (notably Tw and Tnr), the data-points plotted on Figure 3.3 do not cover the complete stratigraphic range. Comparison with Figures 3.5 and 3.6 below shows that the Tw samples are all from near the roof of the Tw magma chamber whereas the Tnr samples are all from the deeper parts of the Tnr magma chamber. Thus, if we were to neglect any complications caused by variable fluorine concentrations in the biotite (see Section 3.7), and assuming a close approach

to equilibrium, we can make a tentative ranking of these eruptions according to their average $^{18}\text{O}/^{16}\text{O}$ "temperatures". Figures 3.3, 3.5, and 3.6 suggest the following sequence from highest temperature to lowest: (1) Tcr, (2) Tm and Tw, (3) Tfc, (4) Tnr, and (5) Ts. It is interesting to note that the lowest temperatures are observed in the latest-stage units Tnr and Ts, which are also the ones that characteristically have the highest phenocryst contents and the highest concentrations of hydrous minerals like biotite and amphibole (see Fig. 3.2). Thus, all of these data are compatible with higher $P_{\text{H}_2\text{O}}$ (and lower T) in some of the later-stage magmas from the central San Juan complex. These magmas also display slightly lower overall $\delta^{18}\text{O}$ values (see Section 3.5 below), compatible with some direct or indirect involvement with meteoric ground waters.

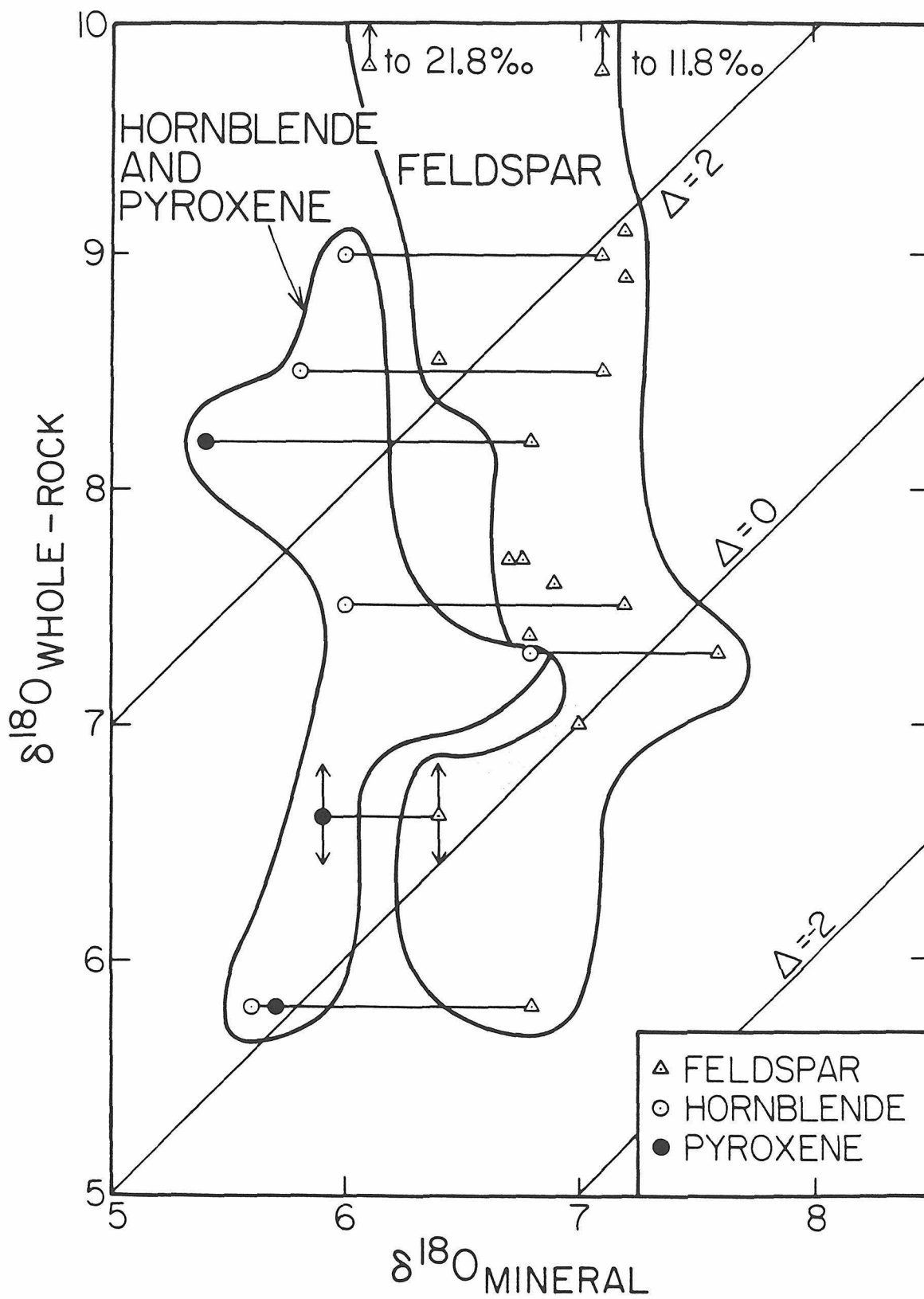
The giant, earliest-stage eruption in the central Nevada caldera complex (Tuff of Williams Ridge and Morey Peak) has very large Δ feldspar-biotite and Δ quartz-biotite values. These data can be interpreted (Section 2.4.2) as indicating that the magma chamber from which this tuff erupted was relatively H_2O -rich. However, the gigantic Fish Canyon Tuff (3000 km^3), the earliest and largest ash-flow to erupt from the central San Juan caldera complex, shows the opposite relationship: the Tfc samples have Δ feldspar-biotite values that are consistently about as low or lower than in any other ash-flow studied in this work. If the large Tm and Tfc eruptions were both triggered by the same mechanism (e.g. a pressure-release event and rapid exsolution of the dissolved magmatic H_2O), it is clear that this mode of eruption does not produce consistent $\delta^{18}\text{O}$ patterns, nor does it lead to similar $\delta^{18}\text{O}$ effects in

subsequent eruptions from the magma chambers (compare Figs. 2.2 and 3.3).

Although the Tfc samples are in general amazingly uniform, with $\Delta^{18}\text{O}$ quartz-feldspar = 0.7, 0.8, 0.8, and 1.0, and $\Delta^{18}\text{O}$ feldspar-biotite = 1.1 ± 0.2 (6 samples), one sample of Fish Canyon Tuff (SF-5) has an unusually low $\delta^{18}\text{O}$ quartz of +7.5 and a very small $\Delta^{18}\text{O}$ quartz-feldspar value of 0.5. This sample has not been affected by hydrothermal alteration, but it does contain numerous xenoliths. This outcrop of Tfc contains about 20 percent xenoliths up to 3 cm in length. These xenoliths consist of about equal proportions of older ash-flow tuffs and andesitic volcanic rocks, both of which must have been derived from the older San Juan volcanic rocks. The xenolith-bearing sample was collected from a relative height of 0.20 above the base of Tfc, along the same traverse that includes samples SF-2 and SF-3. In fact, SF-3 also was collected from the same relative height of 0.20 above the base of Tfc. Therefore, little weight is attached to sample SF-5 in the following discussion.

Hornblende, pyroxene, and feldspar $\delta^{18}\text{O}$ values from the central San Juan caldera complex are plotted vs. the whole-rock $\delta^{18}\text{O}$ values of the samples in Figure 3.4. Δ feldspar-hornblende fractionations range from 0.8 to 1.4 per mil, and Δ feldspar-pyroxene fractionations range from 0.4 to 1.6. A series of diagonal 45° lines are shown on Figure 3.4 at $\Delta = -2, 0, \text{ and } +2$ per mil. The shaded region on Figure 3.4 represents the normal magmatic wholerock-feldspar fractionations of 0.0 to +0.3 per mil (Taylor, 1968). If the Δ wholerock-feldspar fractionations from the central San Juan caldera complex represent equilibrium magmatic

Figure 3.4 $\delta^{18}\text{O}$ whole-rock values from the central San Juan complex plotted vs. $\delta^{18}\text{O}$ values of feldspar, hornblende, and pyroxene. Also shown are 45° lines of $\Delta = -2, 0, \text{ and } +2$ per mil. The shaded area in the feldspar field shows the range of normal magmatic Δ wholerock-feldspar fractionations of 0.0 to +0.3 per mil (Taylor, 1968). Most of the whole-rock $\delta^{18}\text{O}$ values are higher than predicted from the feldspar $\delta^{18}\text{O}$ values and the normal magmatic fractionations. This is probably a result of low-temperature oxygen isotopic exchange between volcanic glass and meteoric ground waters (Taylor, 1968).



fractionations they should plot within this shaded region. Nearly all of the data plot outside this shaded region on Figure 3.4, indicating that these fractionations are not magmatic. Both the feldspar and the hornblende-pyroxene fields on Figure 3.4 are elongate parallel to the $\delta^{18}\text{O}$ whole-rock axis; this indicates that the whole-rock $\delta^{18}\text{O}$ values have been increased by a post-magmatic process that has not affected the phenocryst mineral $\delta^{18}\text{O}$ values. The most plausible process that can account for these data is near-surface, low-temperature oxygen isotopic exchange between meteoric ground water and the glassy matrix of the ash-flows and lava domes. Taylor (1968) noted that this process is widespread in young, glassy volcanic rocks, and our work again emphasizes that it is virtually useless to try to study magmatic phenomena by analyzing whole-rock $\delta^{18}\text{O}$ values of volcanic rocks, unless the rocks were erupted very recently. This interpretation is supported by $\delta^{18}\text{O}$ values of perlitic orange glass (+12.9) and perlitic green glass (+12.4) from CC-41 (Tmc).

3.5 $\delta^{18}\text{O}$ Variations in the Eruptive Units with Time

Like the rocks erupted from the central Nevada caldera complex, rocks erupted from the central San Juan caldera complex have monotonously nearly consistent mineral $\delta^{18}\text{O}$ values, both from one eruptive unit to the next and within any one particular unit (Fig. 3.3). In fact, the San Juan samples are, if anything, more uniform than the central Nevada samples, even though hydrothermal alteration is more widespread and more pervasive in the central San Juans (Section 3.3).

All analyses of minerals separated from the central San Juan cal-

dera complex are plotted in Figure 3.5 in their respective stratigraphic order. Based on stratigraphic relationships and the feldspar $\delta^{18}\text{O}$ data, it is possible to divide these units into two groups: (1) an early, higher- ^{18}O sequence that includes all units erupted sequentially from Tfc through Tm, with feldspar $\delta^{18}\text{O}$ values all practically identical within experimental error, +6.9 to +7.3, and (2) a later, lower- ^{18}O sequence that includes Tw, Tnr, and Ts, that has feldspar $\delta^{18}\text{O}$ values in the range +6.3 to +6.9. Inclusion of the Snowshoe Mountain Tuff samples in the latter group must be qualified because the Ts samples contain visible mineralogic alteration (clinopyroxenes partially altered to calcite); thus the feldspar $\delta^{18}\text{O}$ values in the Ts samples may have undergone some change from their original igneous values, as the feldspars very likely exchanged some oxygen with the same hydrothermal fluids that altered the clinopyroxene phenocrysts. Note that the lowest- ^{18}O feldspars in the central San Juan complex come from these altered Ts samples (Figs. 3.3 and 3.5). However, arguing against this is the fact that the $\delta^{18}\text{O}$ values of quartz phenocrysts from two Ts samples (both +8.2) are identical to the +8.2 value for one sample of Tnr, suggesting similar $\delta^{18}\text{O}$ values for both magmas.

Using a magma-feldspar fractionation of 0.3 (Taylor, 1968), we can infer that the early, higher- ^{18}O sequence had magma $\delta^{18}\text{O}$ values in the range +7.2 to +7.5, whereas the later, lower- ^{18}O sequence had a range of +6.8 to +7.2 (perhaps extending down as low as +6.6 if the $\delta^{18}\text{O}$ values of the Snowshoe Mountain feldspars indeed represent primary igneous values). These values are all well within the range of "normal" intermediate to silicic igneous rocks (Taylor, 1968). Note also that the

outflow facies of the Sunshine Peak Tuff from the Lake City caldera plots within this range, overlapping most closely with the later sequence Tnr and Tw rocks (Fig. 3.5). The shift in $\delta^{18}\text{O}$ values from the early to the late sequences (about 0.3 per mil) is small, and similar to the ^{18}O shift observed between the Early and Middle Sequence in the central Nevada complex (Chapter 2). Even though these variations are very small and in fact barely greater than analytical uncertainty (± 0.1 per analysis, thus for comparison of two data points is ± 0.2), it is clear from the consistency of the results that the trend is real. This ^{18}O shift must be a result of: (1) A significant change in magmatic temperature from the earlier sequence to the later sequence, enough to affect the $^{18}\text{O}/^{16}\text{O}$ fractionations between the phenocrysts and the magma by at least 0.3 per mil. However, the feldspar-biotite fractionations (Fig. 3.3) change most markedly at the Tw-Tnr boundary, not at the early-late sequence boundary, suggesting that variation in temperature is not the explanation; (2) Fractional crystallization that is dominated by some high- $\delta^{18}\text{O}$ mineral, like quartz; (3) Assimilation of altered, ^{18}O -depleted volcanic rocks; or (4) Variations in the $\delta^{18}\text{O}$ values in the primary deep-seated magma sources. Fractional crystallization of quartz can be ruled out in general, and particularly in these magmas, which contain only very tiny amounts of phenocryst quartz (Fig. 3.2). Thus, the most likely explanation of the shift to lower $\delta^{18}\text{O}$ values is either a relatively modest amount of assimilation of low- ^{18}O , hydrothermally altered roof rocks or a change in the deep-seated source regions from which the magmas were derived (thus pushing the problem so far down that we are unable to say much of anything about it).

3.6 $^{18}\text{O}/^{16}\text{O}$ Variations within Individual Ash-Flow Tuffs

Mineral $\delta^{18}\text{O}$ values and isotopic fractionations (Δ values) are plotted as functions of stratigraphic position in individual ash-flow units in Figures 3.5 and 3.6. Unit thicknesses in Figure 3.5 are thicknesses of the units where they were sampled. Mineral-mineral ^{18}O fractionations for most of the units show small, but systematic variations as a function of sample height within a given volcanic unit (Fig. 3.6). In particular, the $\Delta^{18}\text{O}$ quartz-biotite values for the Fish Canyon Tuff (Tfc) show a well-defined decrease upward in the section, indicating a small thermal gradient (temperatures decreasing roofward) in the magma chamber prior to eruption of this voluminous ($> 3000 \text{ km}^3$) ash-flow. These data are consistent with the temperature gradients in Tfc as defined by analyses of iron-titanium oxides (O'Leary and Whitney, 1981). Although we cannot say anything about the absolute temperatures from the $\delta^{18}\text{O}$ data, based on these oxide analyses, O'Leary and Whitney (1981) determined a magmatic temperature of 760°C at the stratigraphic base of Tfc and 810°C at the top.

Except for one anomalous sample (CC-34), feldspar-biotite fractionations for Tm (Fig. 3.6) are remarkably uniform throughout the section where this unit was sampled. This suggests either (1) little or no temperature variation in the phenocryst assemblage throughout this entire sample traverse through the Mammoth Mountain Tuff (from 0.07 to 0.87 relative height, Table 3.2), or (2) that any temperature-gradient effect is counteracted by fluorine concentration gradients of the type found for the Fish Canyon Tuff (Section 3.7). Ratte and Steven (1967) note that Tm is locally zoned from a lower crystal-poor rhyolite to an

Figure 3.5 $\delta^{18}\text{O}$ values of the mineral separates of rocks from the central San Juan caldera complex plotted as a function of stratigraphic position. The $\delta^{18}\text{O}$ values are generally very uniform; however, an abrupt lowering of $\delta^{18}\text{O}$ feldspar (and thus of $\delta^{18}\text{O}$ magma?) occurs at the boundary between Tm and Tw, and the late sequence is consistently lower in ^{18}O than the early sequence. The $^{18}\text{O}/^{16}\text{O}$ variability within individual units is not quite as pronounced as noted for the central Nevada caldera complex samples (compare with Figs. 2.4 and 2.5).

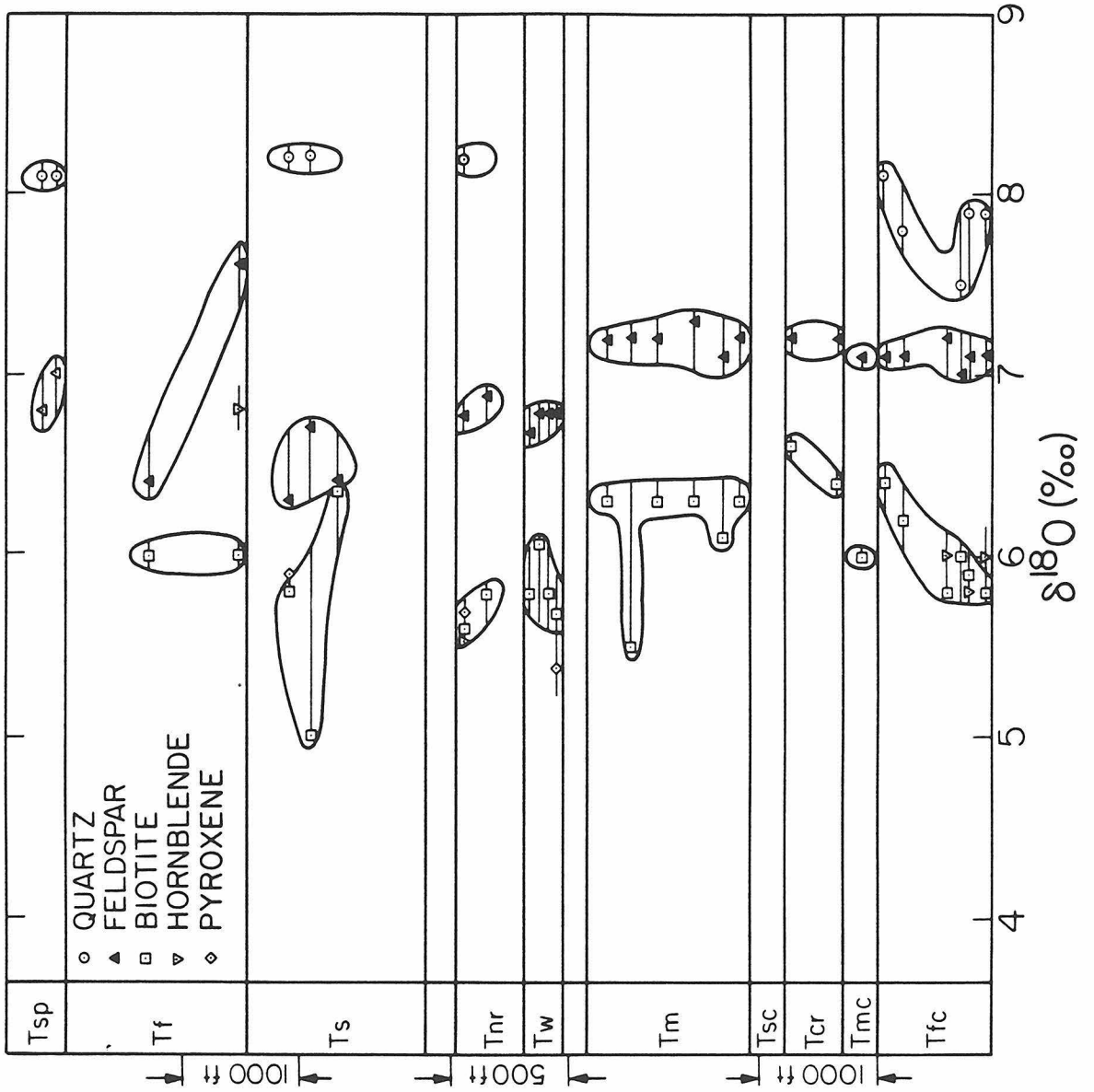
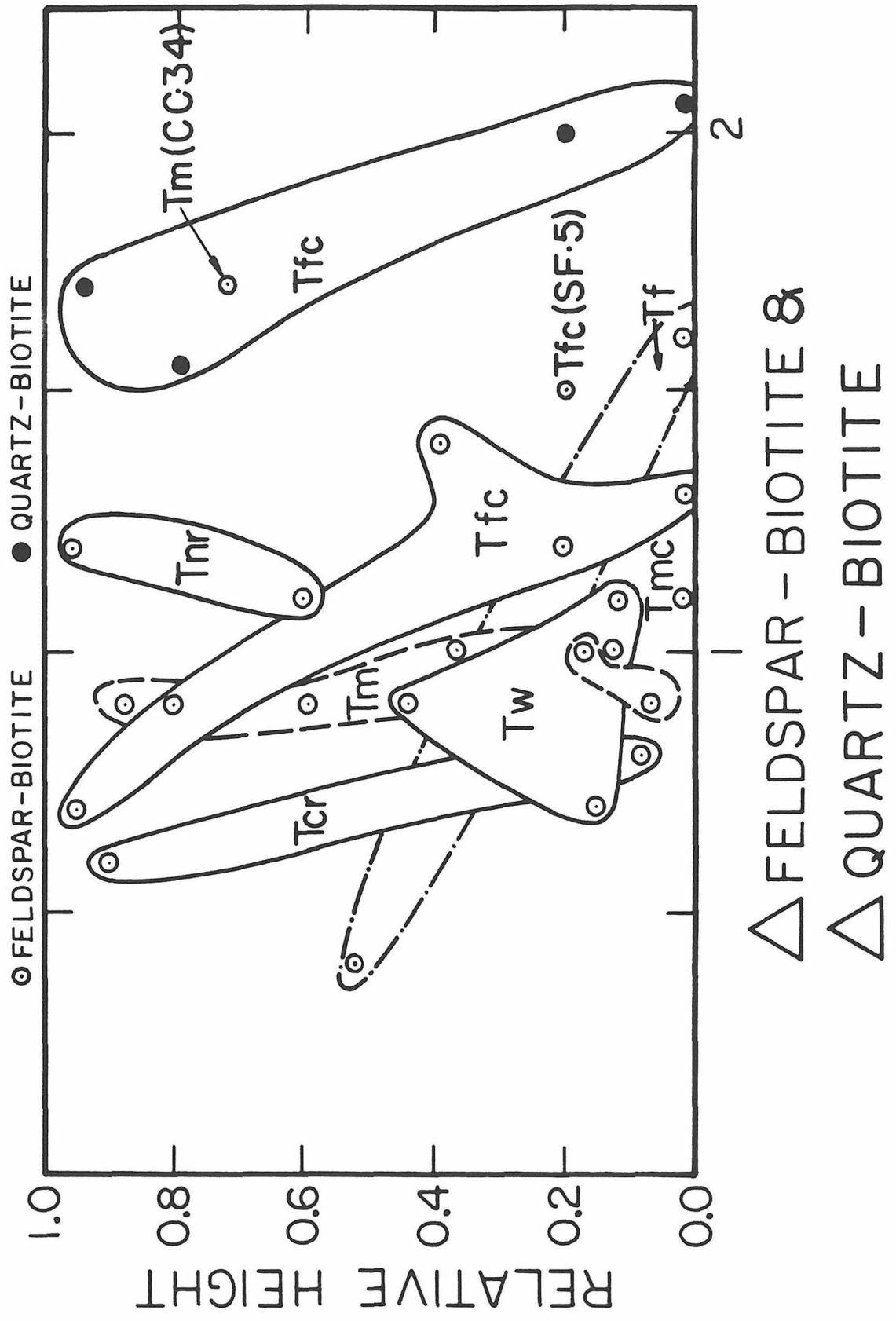


Figure 3.6 $\Delta^{18}\text{O}$ feldspar-biotite and $\Delta^{18}\text{O}$ quartz-biotite fractionations plotted vs. relative sample height for the central San Juan complex. Data from Tfc exhibit a slight decrease in fractionation with stratigraphic height, but data from Tm, a chemically and mineralogically zoned ash-flow, are remarkably consistent through the entire thickness of the unit (also see Figs. 3.3 and 3.5). The units that exhibit smaller $\Delta^{18}\text{O}$ values upward in the stratigraphic sequence were probably derived from magma chambers having lower temperatures near their roofs prior to eruption. Note that the gradients in $\Delta^{18}\text{O}$ (and hence temperature?) in the rocks from the San Juan caldera complex are typically steeper and better defined than those observed in the central Nevada complex (Fig. 2.5).



upper crystal-rich quartz latite. Samples analyzed in this study were collected from the First Fork section of Ratte and Steven (1967), who describe the tuff from this section as consisting of a lower 1000 feet of the crystal-poor facies and an upper 500 to 600 feet of the crystal-rich facies. All samples from both facies exhibit nearly identical phenocryst $\delta^{18}\text{O}$ values, except sample CC-34, which contains an unusually low- ^{18}O biotite but a typical feldspar $\delta^{18}\text{O}$ value. We do not have any idea why sample CC-34 should have such a unique $\delta^{18}\text{O}$ biotite value; there are no indications of any complications, such as hydrothermal effects (see Sections 3.3 and 3.4). One possible explanation would be that this particular biotite has a very low fluorine content (see below).

3.7 Possible Complications Attributable to High Fluorine Contents in the Biotites

Taylor and Epstein (1962a) hypothesized that $\delta^{18}\text{O}$ value of the hydroxyl oxygen in igneous biotite and hornblende is lower than the adjacent silicat-lattice oxygen, and that it might be as much as 10 to 15 per mil lower than the $\delta^{18}\text{O}$ value of coexisting igneous quartz. Hamza and Epstein (1980) obtained some experimental evidence for this idea. If this is true, then substitution of fluorine for hydroxyl groups would markedly raise the $\delta^{18}\text{O}$ value of igneous biotite relative to the value it would have if the hydroxyl position were occupied wholly by OH; this substitution would thus produce lower $\Delta^{18}\text{O}$ feldspar-biotite values compared to assemblages where the biotites contain no fluorine. Therefore, comparison between the $\Delta^{18}\text{O}$ feldspar-biotite values from the central Nevada (0.6 to 2.1, mean = 1.4) and the central

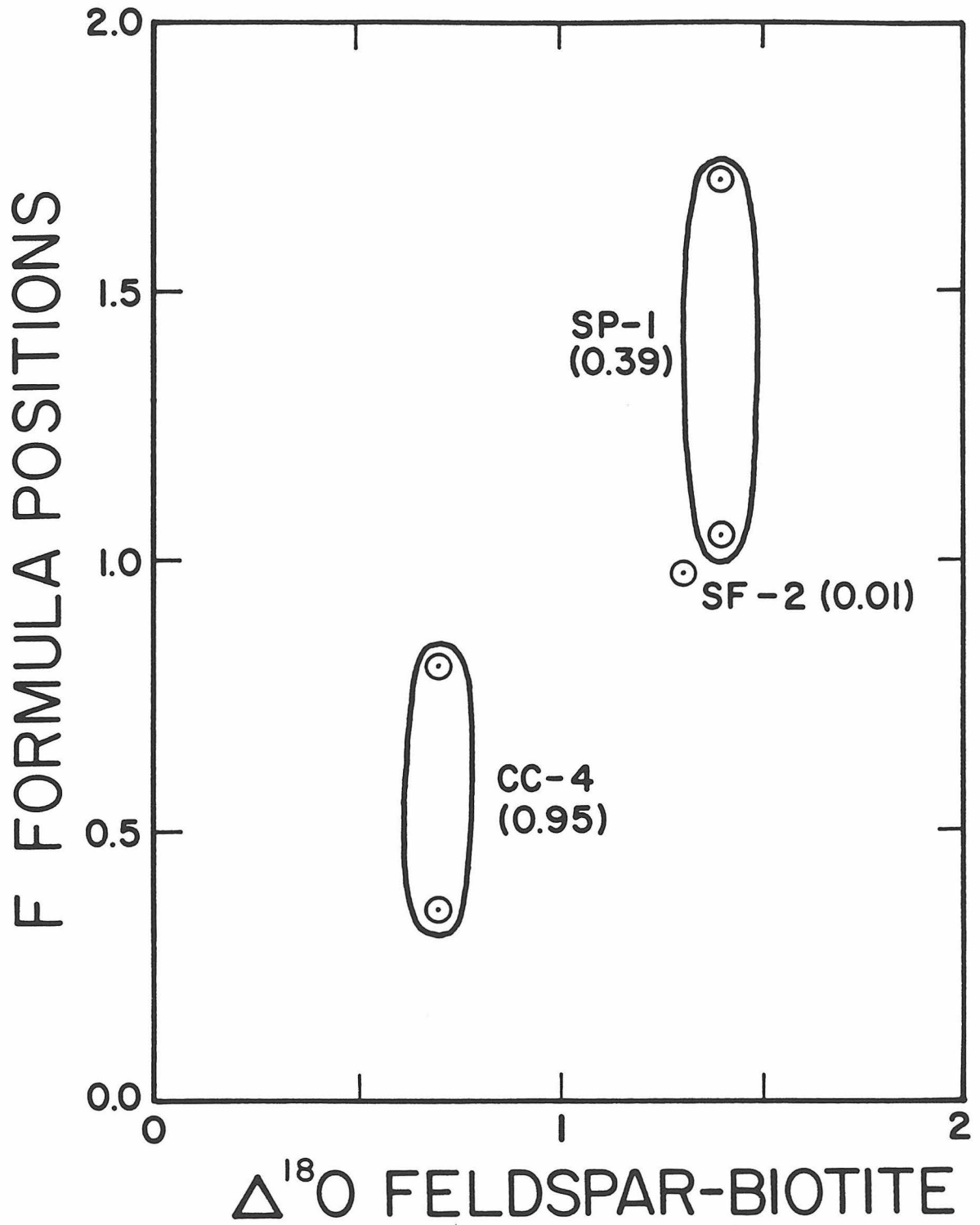
San Juan (0.6 to 1.7, mean = 1.1) complexes conceivably could be interpreted as suggesting higher fluorine contents in the San Juan biotites. Fluorine analyses of biotites from the central Nevada complex are not available. However, microprobe analyses of 5 biotites from 3 samples of Fish Canyon Tuff showed that some of these biotites do indeed have very high fluorine contents:

	<u>F (weight percent)</u>	<u>F (formula positions based on two hydroxyl sites)</u>
SP-1 (A)	6.01	1.57
SP-1 (B)	4.42	1.04
SF-2	4.01	0.97
CC-4 (A)	3.37	0.80
CC-4 (B)	1.46	0.35

Unfortunately, the anomalous biotite from sample CC-34 has not yet been analyzed for fluorine.

$\Delta^{18}\text{O}$ feldspar-biotite values are plotted vs. F formula positions in biotite for the Tfc samples on Figure 3.7. Opposite to what we might have predicted, the $\Delta^{18}\text{O}$ feldspar-biotite values increase with increasing fluorine in the biotite. However, another factor must be considered; note that sample CC-4 was collected at a relative height of 0.95, corresponding to a deep level within the original magma chamber. This sample must have equilibrated at higher temperatures than SP-1 and SF-2, which were collected at relative heights of 0.39 and 0.01, respectively. Thus, the roofward temperature gradients in the Tfc magma chamber may be more dramatic than might be inferred by the small variation in $\Delta^{18}\text{O}$ feldspar-biotite. O'Leary and Whitney (1981)

Figure 3.7 $\Delta^{18}O$ feldspar-biotite values plotted vs. F formula positions for three samples of Fish Canyon Tuff (Tfc). CC-4 was collected at a relative height of 0.95 in Tfc, whereas SP-1 and SF-2 were collected at relative heights of 0.39 and 0.01, respectively. Biotites from sample CC-4 have the lowest F concentrations, and this sample also has the smallest $\Delta^{18}O$ feldspar-biotite value, contrary to the effect expected when fluorine substitutes for hydroxyl in biotite (see text). Thus, the small $\Delta^{18}O$ feldspar-biotite value in CC-4 therefore must reflect equilibration at higher temperatures in the Tfc magma chamber than for SP-1 and SF-2, compatible with its higher position in the upside-down stratigraphic sequence.



used iron-titanium oxides to define a temperature gradient of 760°C at the top to 810°C near the base of the Tfc magma. The fluorine effect, if it exists, is apparently counteracted by the temperature gradient effects.

4.1 Comparison with Plutonic Rocks

Ash-flow magmas erupted from calderas are more-or-less instantaneously quenched, and the $\delta^{18}\text{O}$ values of phenocrysts are thus "frozen in" with their original high-temperature, magmatic values at the time of eruption. However, plutonic rocks cool very slowly compared to ash-flow tuffs; therefore, subsolidus oxygen isotopic exchange can be expected to occur, and has in fact been documented in numerous instances. Accordingly, $\Delta^{18}\text{O}$ values for igneous minerals from plutonic rocks reflect lower-temperature equilibration and are larger than $\Delta^{18}\text{O}$ values for minerals from ash-flow tuffs (Taylor, 1968). In Figures 4.1 and 4.2, $\Delta^{18}\text{O}$ quartz-biotite and $\Delta^{18}\text{O}$ feldspar-biotite values from a typical granodiorite pluton in the Southern California batholith (Turi and Taylor, 1971) are compared with $\Delta^{18}\text{O}$ values for ash-flow tuffs from the central Nevada and central San Juan complexes (this study), as well as with previous data on other ash-flow tuffs (southwest Nevada caldera complex, Lipman and Friedman, 1975; Superstition volcanic field, Arizona, Stuckless and O'Neil, 1973).

Figures 4.1 and 4.2 clearly show that $\Delta^{18}\text{O}$ quartz-biotite and $\Delta^{18}\text{O}$ feldspar-biotite values for the granodiorite pluton from the Southern California batholith are much larger than values for the ash-flow tuffs. $\Delta^{18}\text{O}$ quartz-biotite values in the former range from +3.8 to +6.1, whereas the range of $\Delta^{18}\text{O}$ quartz-biotite values from all the ash-flow tuffs is only +1.3 to +3.2. Distinct differences in $\Delta^{18}\text{O}$ feldspar-

Figure 4.1 $\Delta^{18}\text{O}$ quartz-biotite values plotted vs. the $\delta^{18}\text{O}$ values of biotites, for a granodiorite pluton from the Southern California batholith and for various ash-flow tuffs discussed in the text. Data sources are listed in the text. Plutonic rocks cool more slowly than ash-flow tuffs, which quench upon eruption. Thus, $\Delta^{18}\text{O}$ values for plutonic rocks are larger than for ash-flow tuffs, reflecting lower-temperature, sub-solidus oxygen isotope exchange among the plutonic igneous minerals. The steep negative slopes displayed by the various data-point envelopes are a reservoir effect; because biotite is an accessory mineral (modal abundance < 10 percent in most of these rocks), its $\delta^{18}\text{O}$ value responds very sensitively to temperature, whereas the $\delta^{18}\text{O}$ values of the much more abundant quartz and feldspar change only slightly.

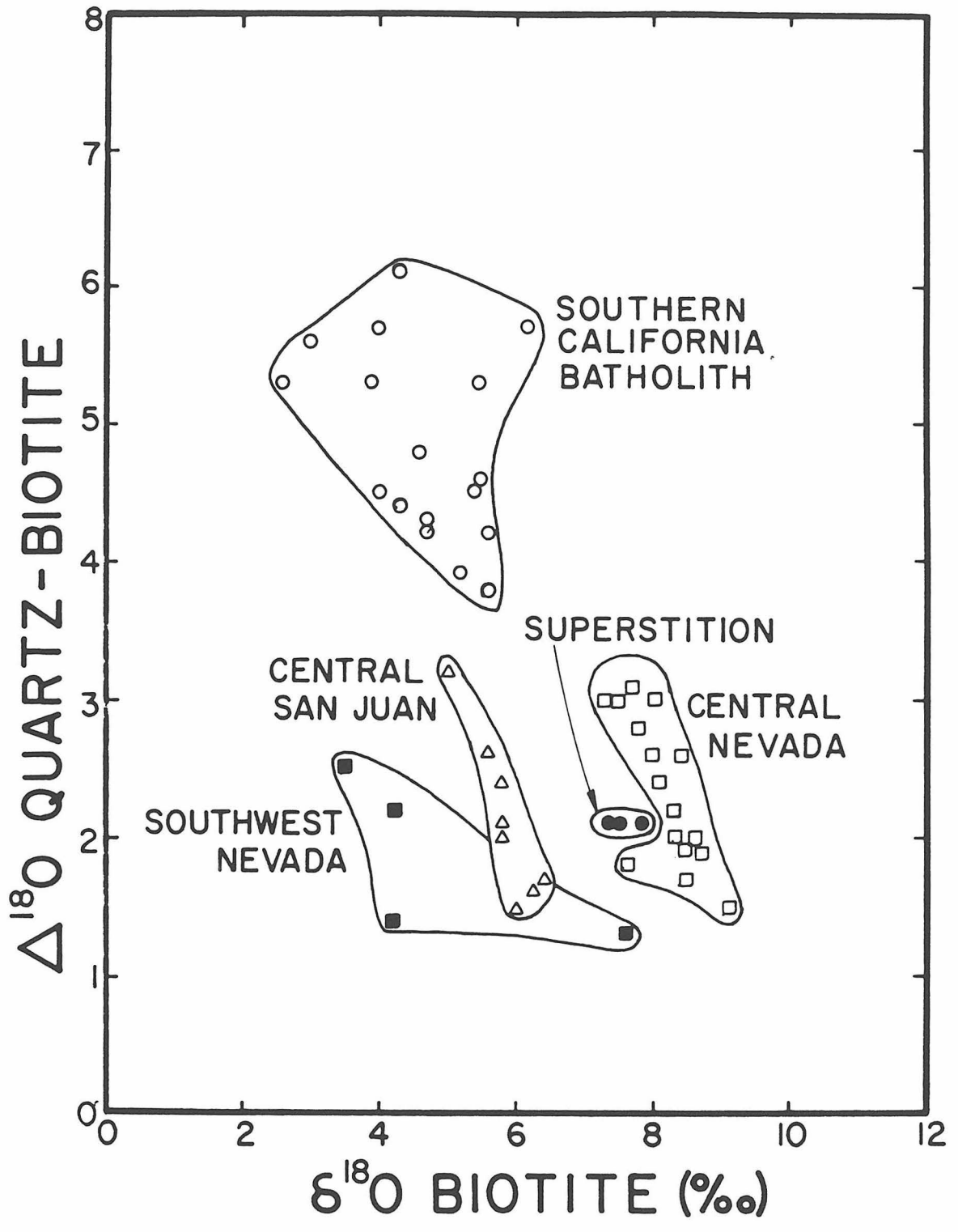
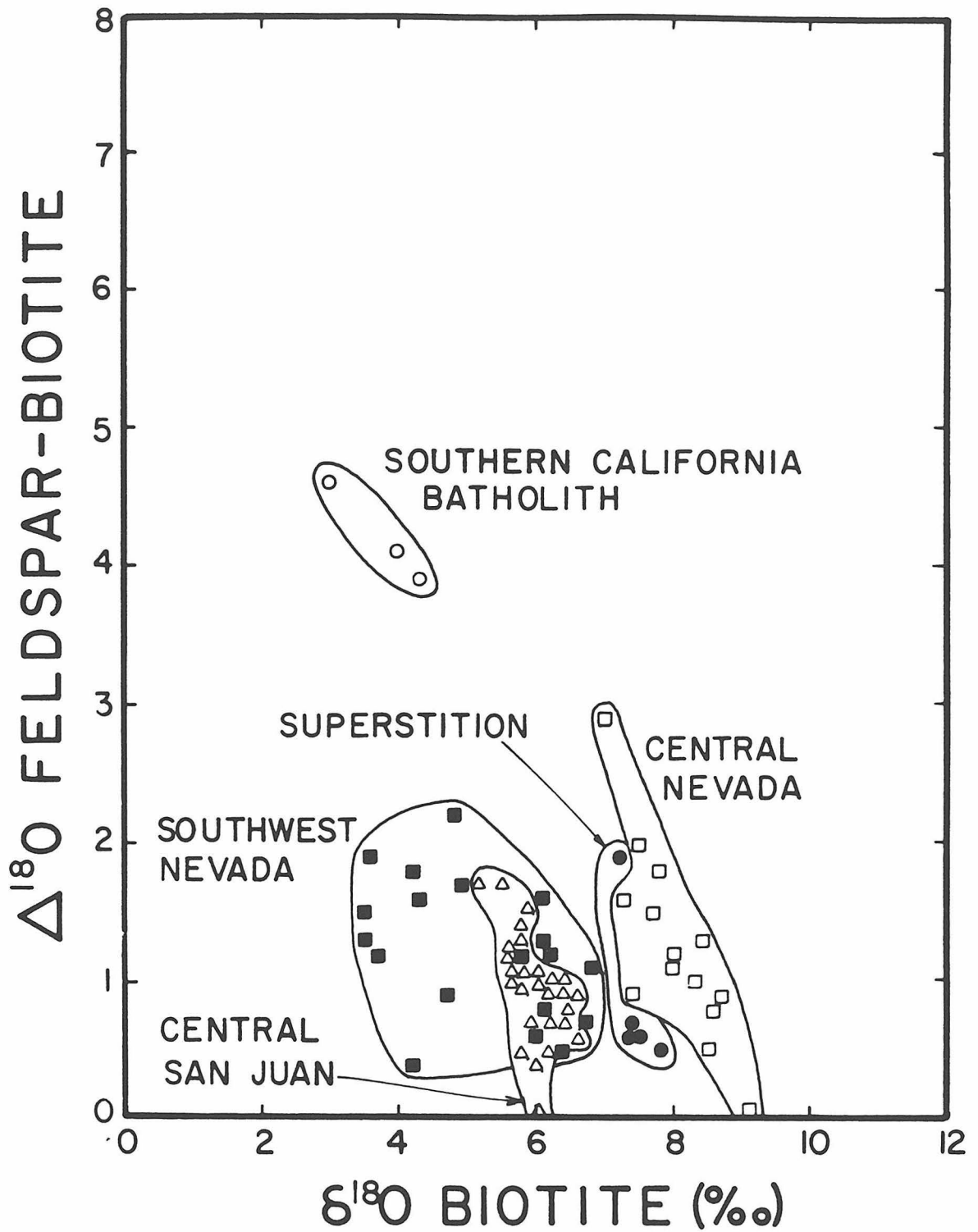


Figure 4.2 $\Delta^{18}\text{O}$ feldspar-biotite values from the Southern California batholith and ash-flow tuffs plotted vs. the $\delta^{18}\text{O}$ values of biotite. Data sources are listed in the text. $\Delta^{18}\text{O}$ values for plutonic rocks are larger than for ash-flow tuffs, reflecting lower-temperature, subsolidus oxygen isotope exchange among the plutonic igneous minerals. See Figure 4.2 for an explanation of the steep negative slopes of the data-point envelopes.



biotite are also observed between the pluton (+3.9 to +4.6) and the ash-flow tuffs (0.0 to +2.9), although the granodiorite values are confined to three data points. The granodiorite pluton is, however, only used as an example; similar features are found in all plutonic igneous rocks. These data demonstrate unequivocally that the minerals in the granodiorite continued to exchange oxygen isotopes with one another down to well below the solidus temperatures; this took place in the absence of meteoric-hydrothermal fluids (Turi and Taylor, 1971).

It is clear that higher equilibration temperatures are the main reason why the ash-flow tuffs have smaller Δ -values than the granodiorite. However, another effect that needs to be considered is the probable higher fluorine content of the ash-flow tuff biotites compared to plutonic biotites; this would act in the same direction as increased temperature (Section 3.7). A summary of plutonic biotite analyses by Deer, Howie, and Zussman (1962) shows that such biotites generally contain less than 2 weight percent fluorine. A compilation of volcanic biotite analyses by Stormer and Carmichael (1971) shows that biotites in volcanic rocks typically contain up to 3.5 weight percent fluorine; in fact the lowest fluorine content of any volcanic biotite reported by Stormer and Carmichael is 1.55 weight percent. Fluorine analyses of biotites from a few samples of Fish Canyon Tuff in this thesis are in agreement with these generalizations. This literature review of biotite analyses is certainly not exhaustive, and is used only to point out the relatively high fluorine contents of volcanic biotites. A more detailed study of fluorine- $\delta^{18}\text{O}$ correlations in igneous biotites would be required to definitively determine the

relative importance of equilibration temperatures vs. fluorine content of biotite in explaining the differences between volcanic and plutonic igneous rocks on Figures 4.1 and 4.2.

4.2 Temperatures of the Ash-Flow Magmas

Because the $\delta^{18}\text{O}$ values of phenocrysts from ash-flow tuffs are "frozen in" at the time of eruption, vertical $\Delta^{18}\text{O}$ gradients in ash-flow tuffs are also "frozen in" in the upside-down ash-flow stratigraphy; these can be used to infer the presence of temperature gradients in ash-flow magmas prior to eruption (Figs. 2.5 and 3.6). Figure 2.3 is a plot of $\Delta^{18}\text{O}$ quartz-biotite values vs. $\Delta^{18}\text{O}$ quartz-feldspar values for the various ash-flow tuffs. With the exception of some possibly altered samples from the central San Juan and central Nevada complexes (discussed in Chapters 2 and 3), most of the data points in Figure 2.3 fall between two lines emanating from the origin with slopes of +1.6 and +2.8. This suggests a close approach to equilibrium.

Figures 2.5 and 3.6 plot the relative height of samples from the central Nevada and central San Juan caldera complexes vs. the $\Delta^{18}\text{O}$ quartz-biotite and $\Delta^{18}\text{O}$ feldspar-biotite values of the samples. Data points for all these units define fields with negative slopes on Figures 2.5 and 3.6. The basal portions of the units (upper levels of the magma chambers) typically have much larger $\Delta^{18}\text{O}$ values than the upper portions of the units (lower levels of the magma chambers). These data show that essentially all the magma chambers from which these volcanic rocks erupted were thermally stratified; the lowest temperatures existed near the roofs of the magma chambers (largest $\Delta^{18}\text{O}$ values) and the highest

temperatures existed in the lower levels of the magma chambers (smallest $\Delta^{18}\text{O}$ values). Although we cannot at present assign any absolute values to these $\Delta^{18}\text{O}$ "temperatures", the Fish Canyon Tuff gradient is confirmed by O'Leary and Stormer (1981), who used analyses of iron-titanium oxides to estimate temperatures of about 760°C at the base of Tfc (top of the magma chamber) and 810°C at the top of Tfc (deeper level of the magma chamber).

Lipman (1971) also used iron-titanium oxide analyses to estimate magmatic temperatures of the Topopah Spring and Tiva Canyon Members of the Paintbrush Tuff and the Ranier Mesa and Ammonia Tanks Members of the Timber Mountain Tuff, all of which erupted from the southwest Nevada caldera complex. Temperatures in the basal parts of these members (upper parts of the magma chambers) are 720°C, 660°C, 700°C, and 680°C, respectively. Temperatures in the upper parts of these tuffs (deeper levels of the magma chambers) are 900°C, ?, 930°C, and 930°C, respectively (the temperature of the upper part of the Tiva Canyon Member was not determined by Lipman, 1971). Thus the upper parts of the later, low- ^{18}O magma chambers formed in the southwest Nevada complex were 20° to 60°C lower than the upper parts of the early, high- ^{18}O magma chambers. $\Delta^{18}\text{O}$ feldspar-magnetite fractionations for the southwest Nevada ash-flow tuffs confirm these temperature gradients and are in good qualitative agreement with the iron-titanium oxide temperature estimates (Lipman and Friedman, 1975).

The above discussion makes it clear that similar "temperatures" and temperature gradients existed in the ash-flow tuffs erupted from all caldera complexes, irrespective of whether strongly ^{18}O -depleted magmas

were developed (southwest Nevada) or were not (central Nevada, central San Juans). There are, however, some weak indications that the later-stage, slightly lower- ^{18}O magmas in the latter complexes typically had somewhat lower temperatures, analogous to the effects described above for the southwest Nevada complex.

4.3 The Problem of Low- ^{18}O Magmas

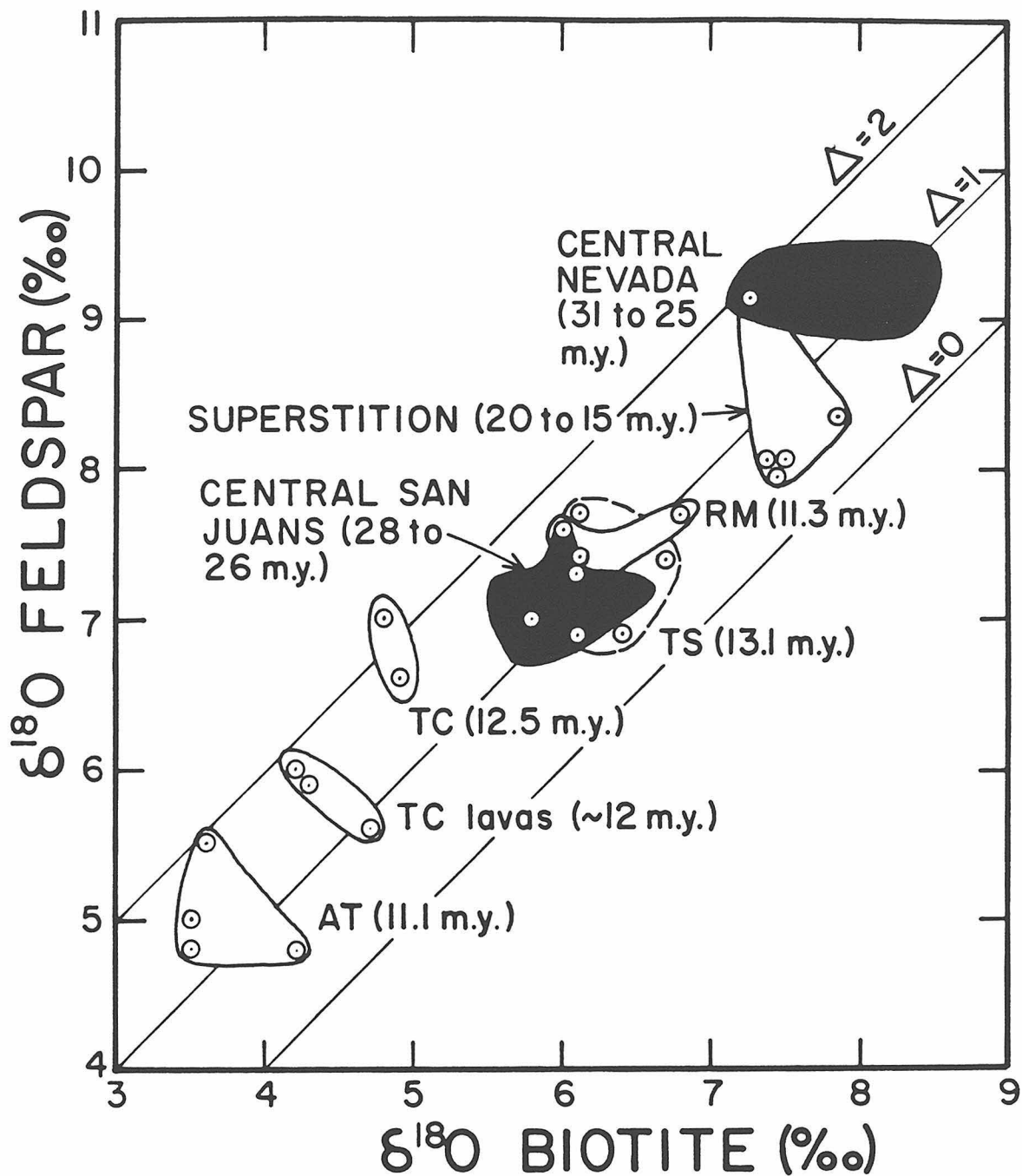
This study of $\delta^{18}\text{O}$ variations in ash-flow tuffs was initially stimulated by earlier investigations of $\delta^{18}\text{O}$ variations in Tertiary ash-flow tuffs erupted from the southwest Nevada caldera complex (Friedman et al, 1974; Lipman and Friedman, 1975) and the Yellowstone caldera (Friedman et al, 1974). These authors found that the sequentially later volcanic rocks erupted from these caldera complexes commonly had much lower $\delta^{18}\text{O}$ values than the earliest erupted rocks (by about 3 per mil for both complexes, see Fig. 1.1). Because catastrophic ash-flow eruptions can shatter hydrothermally altered roof rocks above magma chambers, mechanisms involving stoping and assimilation of these low- ^{18}O rocks can readily be called upon to account for the development of such low- ^{18}O magmas. The data of Friedman et al (1974) and Lipman and Friedman (1975), together with earlier data of Muehlenbachs et al (1974) on volcanic rocks from Iceland, seemed to indicate that the development of low- ^{18}O magmas would be commonplace in such volcanic terranes.

We were therefore quite surprised that our analyses from the central Nevada and central San Juan caldera complexes showed only minor negative shifts in $\delta^{18}\text{O}$ (typically less than 0.3 per mil) in the

sequentially erupted ash-flow tuffs and lava domes. In the central Nevada complex, $\delta^{18}\text{O}$ values decrease by about 0.3 from the Early Sequence to the Middle Eruptive. This is followed by a reestablishment of the higher Early Sequence $\delta^{18}\text{O}$ values in the first Late Sequence eruption, and the values again decrease by about 0.3 to 0.6 in the later Late Sequence eruptions (see Figs. 2.2 and 2.4). Variations in $\delta^{18}\text{O}$ values for rocks erupted from the central San Juan complex are also small. A consistent ^{18}O difference of about 0.3 per mil is observed between the early magmas and the lower- ^{18}O , later-stage tuffs erupted from the central San Juan complex (Figs. 3.3 and 3.5).

On Figure 4.3, feldspar $\delta^{18}\text{O}$ values are plotted vs. biotite $\delta^{18}\text{O}$ values for a number of mid- to late-Tertiary ash-flow tuffs in the western United States. This includes data from the central Nevada and central San Juan complexes (this study), the Superstition volcanic field, Arizona (Stuckless and O'Neil, 1973), and the Timber Mountain-Paintbrush Tuff, southwest Nevada caldera complex (Friedman et al, 1974; Lipman and Friedman, 1975). Nearly all of these data points fall within the diagonal $\Delta^{18}\text{O}$ feldspar-biotite boundaries of +0.5 to +2.0. Thus, all these tuffs were erupted within basically the same temperature range (see also Fig. 2.3). However, note that, whereas the central Nevada, central San Juan, and Superstition volcanic rocks each define distinctive, very tight groupings on Figure 4.3, implying virtually no magmatic $^{18}\text{O}/^{16}\text{O}$ variation, the southwest Nevada samples exhibit a distinct lowering of $\delta^{18}\text{O}$ values (by about 3 per mil) from the older eruption in each sequence (Ranier Mesa and Topopah Springs Members) to the younger eruption (Ammonia Tank and Tiva Canyon Members).

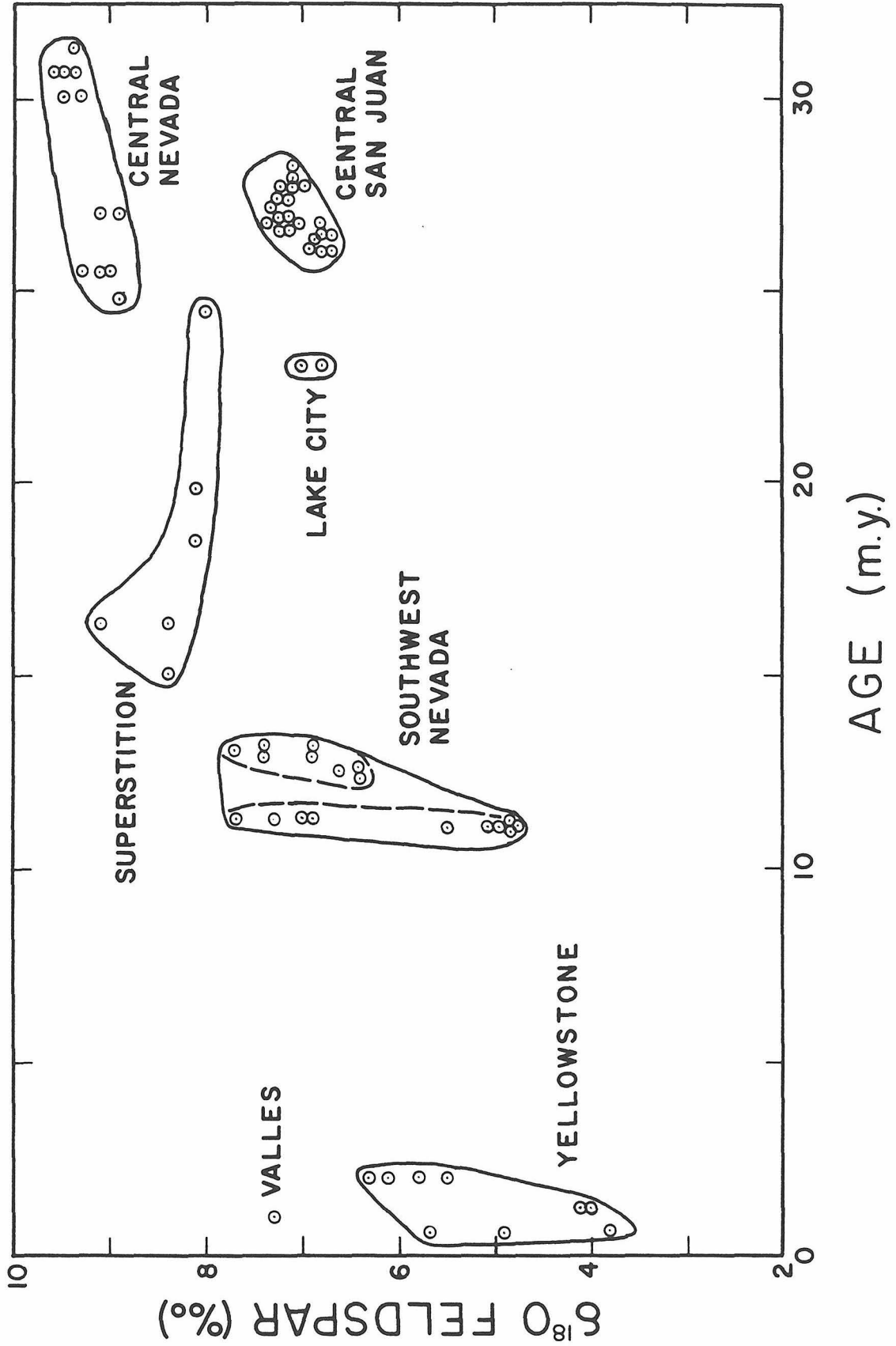
Figure 4.3 $\delta^{18}\text{O}$ feldspar values plotted vs. $\delta^{18}\text{O}$ biotite values for ash-flow tuffs. Data sources are listed in the text. Diagonal lines with 45° slopes are shown for $\Delta^{18}\text{O} = 0, 1, \text{ and } 2$. Note the extremely narrowly defined, but distinctive, ranges in $\delta^{18}\text{O}$ exhibited by each of the central Nevada, Superstition, and central San Juan caldera complexes; this contrasts sharply with the large $\delta^{18}\text{O}$ variations in the southwest Nevada complex. Ash-flow tuff members from the southwest Nevada caldera complex are abbreviated as: RM, Ranier Mesa; TS, Topopah Springs; TC, Tiva Canyon; and AT, Ammonia Tank. The Ranier Mesa and Ammonia Tank Members make up the Paintbrush Tuff and the Topopah Springs and Tiva Canyon Members make up the Timber Mountain Tuff. Nearly all the data points lie within the $\Delta^{18}\text{O}$ feldspar-biotite range of 0.5 to 2.0. Thus, all of these ash-flows erupted within basically the same temperature range. See text for further discussion.



Why should the southwest Nevada and Yellowstone volcanic fields show an order of magnitude greater ^{18}O depletion than the central Nevada and San Juan volcanic fields? This is the most striking and remarkable problem raised by the present study. Also, why should the first two detailed $^{18}\text{O}/^{16}\text{O}$ studies of complex caldera structures show abundant evidence for strongly ^{18}O -depleted magmas, whereas the next two (this work) show such miniscule ^{18}O depletions (barely outside analytical error)? These dramatic $^{18}\text{O}/^{16}\text{O}$ differences cannot be attributed to variations in the $\delta^{18}\text{O}$ of the associated meteoric ground waters. They must be due to some differences in the way the magma chambers at Yellowstone and the southwest Nevada complex interacted with their environment. For some reason, these particular sub-volcanic magma chambers interacted much more strongly with hydrothermally altered roof rocks or with the meteoric ground waters themselves. Based on the new data obtained in the present work, this process (whatever it is) must be much less common than heretofore believed (e.g. Lipman and Friedman, 1975, page 701, last sentence).

Figure 4.4 is plot of feldspar $\delta^{18}\text{O}$ values vs. age for the ash-flow tuffs shown in Figure 4.3; it also includes data for the Sunshine Peak Tuff erupted from the Lake City caldera, San Juan Mountains, Colorado (this study, Part I), for the Bandelier Tuff erupted from the Valles caldera, New Mexico (Lambert and Epstein, 1980), and for the ash-flows erupted from the Yellowstone caldera, Wyoming (Friedman et al, 1975). Note that ash-flows from all the caldera complexes plotted on Figure 4.4 show some degree of negative $\delta^{18}\text{O}$ shifts from older to younger eruptions, except the Valles caldera and the Lake City caldera where only

Figure 4.4 $\delta^{18}\text{O}$ feldspar values from ash-flows plotted vs. the age of the ash-flow eruptions. See text for data sources. $\delta^{18}\text{O}$ values decrease by about 3 per mil from early eruptions to later eruptions for two caldera complexes that are less than 15 m.y. old. Only small $\delta^{18}\text{O}$ shifts occur in ash-flows erupted from caldera complexes with ages greater than 25 m.y. This gap in time also corresponds to the initiation of Basin-Range crustal extension in the western United States. This extension produced fractures that conceivably could have led to greatly enhanced circulation of meteoric waters deeply into the continental crust; thus, the Yellowstone and southwest Nevada caldera complexes may have been depleted much more strongly in ^{18}O at great depth than the central Nevada and central San Juan caldera complexes, leading to much greater amounts of assimilation and partial melting of low- ^{18}O country rocks by the sub-volcanic magma chambers.



limited data are available, and the Superstition volcanic rocks, which are also a limited data set and not clearly related to any recognized calderas (in fact these rocks may have been erupted from totally unrelated calderas; note that their ages span a greater range than any of the other groups plotted on Figure 4.4).

At this stage, we can only speculate as to why some caldera complexes produce volcanic rocks with much larger negative ^{18}O shifts than other complexes. More detailed studies are required on a variety of other areas before we can develop sufficient statistics to answer these questions. Nevertheless, we can at least address some of the salient points that might be important in such considerations.

Scale and Size of Eruptions. The nature and size of the eruptions does not seem to be important in determining the $^{18}\text{O}/^{16}\text{O}$ effects. All four caldera complexes that have been studied in detail (Yellowstone, southwest Nevada, central Nevada, and central San Juans) have a history of at least one or two giant ($> 2000 \text{ km}^3$) eruptions. The Ammonia Tanks Member of the Timber Mountain Tuff, the youngest ash-flow from the southwest Nevada complex, has the lowest sanidine $\delta^{18}\text{O}$ values (+4.8 to +5.5) of any of the four members and also has the largest volume ($+ 2000 \text{ km}^3$). The oldest ash-flow (Topopah Spring Member of the Paintbrush Tuff) has the highest sanidine $\delta^{18}\text{O}$ values (+6.9 to +7.7) and has the smallest volume ($+ 300 \text{ km}^3$).

The earliest ash-flows erupted from the central San Juan and central Nevada complexes are both gigantic (Fish Canyon Tuff, $> 3000 \text{ km}^3$, the largest ash-flow erupted from the central San Juan complex; Tuff of Williams Ridge and Morey Peak, $> 2500 \text{ km}^3$, the second largest ash-flow

erupted from the central Nevada complex). Both of these ash-flows belong to the earlier, slightly higher- ^{18}O sequences erupted from these two normal- ^{18}O complexes. However, in the low- ^{18}O Yellowstone caldera complex, the earliest eruption was also gigantic (Huckleberry Ridge Tuff, 2500 km³). Thus, the $\delta^{18}\text{O}$ values of ash-flow tuffs do not vary in any systematic manner as a function of the volumes of the eruptions, or of the position of the largest eruption in the age sequence.

Duration and Intensity of Magmatism. The duration and intensity of magmatic activity does not seem to have exerted any obvious control on the magnitude of the $^{18}\text{O}/^{16}\text{O}$ effects observed for the four complex calderas that have been studied in detail. Vast volumes of magmas were erupted from both the southwest Nevada and the Yellowstone calderas over a short period of time (about 2.5 m.y.), and rocks erupted from both these complexes exhibit the most dramatic variations in $\delta^{18}\text{O}$ values. However, the central San Juan complex produced even greater volumes of ash-flow tuff over an equally short time span, and this complex shows only a small ^{18}O shift. Nevertheless, this subject warrants further study, because the two caldera complexes that displayed the longest duration of eruptive activity both show negligible depletion in ^{18}O ; the central Nevada complex and Superstition volcanic field were both active for more than 6 m.y., more than twice the time span of the other three complexes. Note also that in the southwest Nevada complex there was only a very short (200,000-year) hiatus between eruption of the high- ^{18}O Ranier Mesa Member and the extremely ^{18}O -depleted Ammonia Tanks Member.

Nature of Associated Tectonic Activity. The two caldera complexes

that exhibit the greatest $\delta^{18}\text{O}$ shifts on Figure 4.4 are both younger than 15 m.y., and those which exhibit only small shifts are older than 24 m.y. It is interesting to note (remember, this is only speculation!) that this gap in time between 15 and 24 m.y. also corresponds to the transition between non-extension in the western United States and the extensional tectonic regime of the Basin-Range province (for example, see Stewart, 1978). The Yellowstone caldera, in fact, lies on the eastern end of the currently-active Snake River Plain rift system, and the southwest Nevada caldera complex lies right in the midst of abundant Basin-Range extensional features. Such region-wide extension must produce fractures that penetrate deeply into the crust. These fractures could allow meteoric water to circulate very deeply into the crust, as they clearly have in Iceland (Muehlenbachs et al, 1974). Therefore, the Yellowstone and southwest Nevada caldera complexes conceivably could have been subjected to much greater rifting and regional extension than the central Nevada or central San Juan caldera complexes, allowing for much more massive stoping and assimilation of hydrothermally altered, low- ^{18}O country rocks. This hypothesis could be tested by carrying out more comparative $^{18}\text{O}/^{16}\text{O}$ studies of caldera complexes developed in rift and non-rift environments.

Complexity of the Eruptive Cycle. When this study was initiated, it a priori seemed likely that low- ^{18}O magmas might be most abundantly developed in those caldera complexes exhibiting the most complicated history of eruption and overlapping caldera collapse. This assumption was mainly predicated on the following basis: (1) The two known low- ^{18}O caldera complexes, Yellowstone and southwest Nevada, were both

geologically complex, and (2) in terms of our assimilation-stopping model, the more complicated and intense the eruptive and fracturing history, the more likely there would be large-scale interaction between the magma chamber and the roof rocks. The central Nevada and central San Juan caldera complexes were thus (in part) chosen for study because of their complexity. As a result of the present $^{18}\text{O}/^{16}\text{O}$ study, we now, of course, know that factors other than a complicated eruptive history must be involved. Nonetheless, there are some features of this argument that bear more detailed consideration, because low- ^{18}O magmas were apparently not developed in any of the relatively simple caldera complexes on which $^{18}\text{O}/^{16}\text{O}$ studies have been made (Valles, Long Valley, Lake City). It is obvious that eruptive complexity is not a sufficient condition for development of low- ^{18}O ash-flow magmas. However, it may be a necessary condition for their development!

Chemical Composition. Examination of Figure 1 in Hildreth (1981) shows that all of the known low- ^{18}O ash-flow tuffs belong to his Groups I and II (high- SiO_2 rhyolites and high- SiO_2 rhyolites zoned to intermediate compositions). The extremely ^{18}O -depleted tuffs thus all exhibit SiO_2 contents up to and above 77 weight percent, indicative of very strong differentiation. This is probably the most clear-cut correlation with $\delta^{18}\text{O}$ of any of the parameters discussed previously. All of the normal- ^{18}O ash-flow tuffs described in Chapters 2 and 3 from the central Nevada and central San Juan complexes are either monotonous intermediates (e.g. Fish Canyon and Monotony Tuffs), or, if they do include rhyolites, the rhyolites are zoned to SiO_2 contents no higher than 74-76 weight percent. The only known counter-examples to the above

correlation are the Bishop Tuff, erupted from Long Valley caldera 700,000 years ago, the Bandelier Tuff, erupted from the Valles caldera 1 m.y. ago, and the Sunshine Peak Tuff, erupted from the Lake City caldera 23 m.y. ago. The Bishop Tuff is extremely uniform in $\delta^{18}\text{O}$ (Hildreth, 1981) and is not depleted in ^{18}O to any measurable degree (Taylor, 1968); the Sunshine Peak Tuff shows similar characteristics (Part I of this thesis).

It is plausible that a relationship should exist between ^{18}O depletion and extreme fractional crystallization, because the latter is expected to go hand-in-hand with assimilation and stoping of roof-rocks (Bowen, 1928; Taylor, 1980). Magma chambers stable enough to develop extremely high- SiO_2 differentiates at their roof are also the ones that would have undergone the least amount of stirring and mixing with any new influx of primitive, normal- ^{18}O magma from depth. The roof-ward portions of such stabilized chambers would also have the best chance of interacting with adjacent ground waters and with the hydrothermally altered country rocks above the magma chamber.

Why then do we observe "normal" $\delta^{18}\text{O}$ values in the Bishop Tuff, Bandelier Tuff, and Sunshine Peak Tuff, all of which contain abundant, strongly differentiated, 77 weight percent SiO_2 , rhyolitic material? The best explanation of the absence of low- ^{18}O magma in these three ash-flow tuffs is that each of them was erupted from a relatively simple caldera environment that had not undergone a prior history of intense meteoric-hydrothermal alteration. Thus, although further work is required, we tentatively conclude that two conditions probably need to be satisfied in order to produce significant volumes of low- ^{18}O

ash-flow magma: (1) a complex eruptive and fracturing history that pre-dates the low-¹⁸O eruption and which produces significant meteoric-hydrothermal alteration; and (2) a period of quiescence during which a stabilized magma chamber develops underneath a carapace of low-¹⁸O, hydrothermally altered, highly fractured roof-rocks. This magma chamber must be free of disruption from additions of primitive magma from depth, and it should undergo strong fractional crystallization and differentiation, enhanced by addition of relatively cold blocks of hydrothermally altered roof-rocks that remove heat and add water of dehydration to the magma. Judging by the K-Ar data from the southwest Nevada caldera complex, this interval can be as short as 200,000 years.

REFERENCES CITED

- Allen, E. T., and Day, A. L., 1935, Hot springs of Yellowstone National Park: Carnegie Institute of Washington, Publication 466, 525 p.
- Anderson, A. T., Clayton, R. N., and Mayeda, T. K., 1971, Oxygen isotope geothermometry of mafic igneous rocks: *Jour. Geology*, v. 75, p. 323-332.
- Bailey, R. A., Dalrymple, G. B., and Lanphere, M. A., 1976, Volcanism, structure, and geochronology of Long Valley caldera, Mono County, California: *Jour. Geophys. Research*, v. 81, p. 725-744.
- Barker, F., 1969, Precambrian geology of the Needle Mountains, southwestern Colorado: U. S. Geol. Survey Prof. Paper 644-A, 33 p.
- Barton, P. B., Jr., Bethke, P. M., and Roedder, E., 1977, Environment of ore deposition in the Creede mining district, San Juan Mountains, Colorado: Part III. Progress toward interpretation of the chemistry of the ore-forming fluid for the OH vein: *Econ. Geol.*, v. 74, p. 1832-1851.
- Barton, P. B., Jr., and Toulmin, P., 1961, Some mechanisms for cooling hydrothermal fluids: U. S. Geol. Survey Prof. Paper 424-D, p. 348-352.
- Bethke, P. M., and Rye, R. O., 1979, Environment of ore deposition in the Creede mining district, San Juan Mountains, Colorado: Part IV. Source of fluids from oxygen, hydrogen, and carbon isotope studies: *Econ. Geol.*, v. 74, p. 1832-1851.
- Bickford, M. E., Barker, F., Wetherill, G. W., and Lee-Hu, C., 1967, Geochronology of Precambrian rocks of the Needle Mountains, southwestern Colorado: Part II: Rb-Sr results [abstract]: *Geol. Soc. America Spec. Paper* 115, p. 14.
- Bickford, M. E., Wetherill, G. W., Barker, F., and Lee-Hu, C., 1969, Precambrian Rb-Sr chronology in the Needle Mountains, southwestern Colorado: *Jour. Geophys. Research*, v. 74, p. 1660-1676.
- Blattner, P., and Bird, G. W., 1974, Oxygen isotope fractionation between quartz and K-feldspar at 600°C: *Earth Planet. Sci. Letters*, v. 23, p. 21-27.
- Bottinga, Y., 1968, Calculation of fractionation factors for carbon and oxygen exchange in the system calcite-carbon dioxide-water: *Jour. Phys. Chemistry*, v. 72, p. 800-808.
- Bottinga, Y., and Craig, H., 1968, High-temperature liquid-vapor fractionation factors for H_2O - HDO - H_2O^{18} [abstract]: *Trans. Amer. Geophys. Union (EOS)*, v. 49, p. 356.

- Bottinga, Y., and Javoy, M., 1973, Comments on oxygen isotope geothermometry: *Earth Planet. Sci. Letters*, v. 20, p. 250-265.
- Bowen, N. L., 1928, *The evolution of igneous rocks*: Princeton University Press, Princeton, New Jersey, 332 p.
- Burbank, W. S., 1930, Revision of the geologic structure and stratigraphy in the Ouray district of Colorado, and its bearing on ore deposition: *Colorado Sci. Soc. Proc.*, v. 12, p. 151-232.
- Burbank, W. S., 1941, Structural control of ore deposition in the Red Mountain, Sneffels, and Telluride districts of the San Juan Mountains, Colorado: *Colorado Sci. Soc. Proc.*, v. 14, p. 142-264.
- Burbank, W. S., 1950, Problems of wall rock alteration in shallow volcanic environments: *Colorado Sch. Mines Quarterly*, v. 45, no. 1B, p. 287-319.
- Burbank, W. S., 1960, Pre-ore propylitization, Silverton caldera, Colorado: *U. S. Geol. Survey Prof. Paper* 400-B, p. 12-13.
- Burbank, W. S., and Luedke, R. G., 1964, Geology of the Iron-ton quadrangle, Colorado: *U. S. Geol. Survey Map* GQ-291 (1:24000).
- Burbank, W. S., and Luedke, R. G., 1968, Geology and ore deposits of the western San Juan Mountains, Colorado: in Ridge, J. D., ed., *Ore Deposits of the United States, 1933-1967*: New York, Am. Inst. Mining, Metall., Petroleum Engineers, v. 1, p. 714-733.
- Burbank, W. S., and Luedke, R. G., 1969, Geology and ore deposits of the Eureka and adjoining districts, San Juan Mountains, Colorado: *U. S. Geol. Survey Prof. Paper* 535, 73 p.
- Burt, D. M., Sheridan, M. F., Bikun, J. V., and Christiansen, E. H., 1982, Topaz rhyolites-distribution, origin, and significance for exploration: *Econ. Geol.*, v. 77, p. 1818-1836.
- Casadevall, T., and Ohmoto, H., 1977, Sunnyside mine, Eureka mining district, San Juan County, Colorado: geochemistry of gold and base metal ore deposition in a volcanic environment: *Econ. Geol.*, v. 72, p. 1285-1320.
- Christiansen, R. L., and Lipman, P. W., 1972, Cenozoic volcanism and tectonism in the western United States and adjacent parts of the spreading ocean floor. Pt. 2, Late Cenozoic: *Royal Soc. London Trans.*, v. 271, p. 249-284.
- Clark, K. F., 1972, Stockwork molybdenum deposits in the western Cordillera of North America: *Econ. Geol.*, v. 67, p. 731-758.

- Clayton, R. N., and Epstein, S., 1958, The relationship between O^{18}/O^{16} ratios in coexisting quartz, carbonate, and iron oxides from various geological deposits: *Jour. Geology*, v. 66, p. 352-373.
- Clayton, R. N., Muffler, L. J. P., and White, D. E., 1968, Oxygen isotope study of calcite and silicates of the River Ranch No. 1 well, Salton Sea geothermal field, California: *Amer. Jour. Sci.*, v. 266, p. 968-979.
- Clayton, R. N., O'Neil, J. R., and Mayeda, T. K., 1972, Oxygen isotope exchange between quartz and water: *Jour. Geophys. Research*, v. 74, p. 3057-3067.
- Craig, H., 1961, Isotopic variations in meteoric waters: *Science*, v. 133, p. 1702-1703.
- Craig, H., 1963, The isotopic geochemistry of water and carbon in geothermal areas: in Tongiorgi, E., ed., *Nuclear Geology on Geothermal Areas*, Consiglio Nazionale della Ricerche, Laboratorio de Geologica Nucleare, Pisa, p. 17-53.
- Criss, R. E., and Taylor, H. P., Jr., 1983, An $^{18}O/^{16}O$ and D/H study of Tertiary hydrothermal systems in the southern half of the Idaho Batholith: *Geol. Soc. America Bull.*, v. 94, p. 640-663.
- Criss, R. E., Lanphere, M. A., and Taylor, H. P., Jr., 1982, Effects of regional uplift, deformation, and meteoric-hydrothermal metamorphism on K-Ar ages of biotites in the southern half of the Idaho batholith: *Jour. Geophys. Research*, v. 87, p. 7029-7046.
- Cross, W., and Hole, A. D., 1910, Description of the Engineer Mountain quadrangle, Colorado: *U. S. Geol. Survey Geol. Atlas*, folio 171.
- Cross, W., and Howe, E., 1905, Description of the Needle Mountain quadrangle, Colorado: *U. S. Geol. Survey Geol. Atlas*, folio 131.
- Cross, W., and Larsen, E. S., 1935, A brief review of the geology of the San Juan region of southwestern Colorado: *U. S. Geol. Survey Bulletin* 843, 138 p.
- Cross, W., and Purington, C. W., 1899, Description of the Telluride quadrangle, Colorado: *U. S. Geol. Survey Geol. Atlas*, folio 57.
- Cross, W., Howe, E., and Ransome, F. L., 1905, Description of the Silverton quadrangle, Colorado: *U. S. Geol. Survey Geol. Atlas*, folio 120.
- Cross, W., Howe, E., and Irving, J. D., 1907, Description of the Ouray quadrangle, Colorado: *U. S. Geol. Survey Geol. Atlas*, folio 153.

- Day, A. L., and Allen, E. T., 1925, The volcanic activity and hot springs of Lassen Peak: Carnegie Institute of Washington, Publication 360, 190 p.
- Deer, W. A., Howie, R. A., and Zussman, J., 1962, Rock-forming minerals. Volume 3. Sheet silicates: Longman Group, Ltd., London, 270 p.
- Dickinson, R. G., Leopold, E. B., and Marvin, R. F., 1968, Late Cretaceous uplift and volcanism on the north flank of the San Juan Mountains: Colorado Sch. Mines Quarterly, v. 63, p. 125-148.
- Doe, B. R., Steven, T. A., Delevaux, M. H., Stacey, J. S., Lipman, P. W., and Fisher, F. S., 1979, Genesis of ore deposits in the San Juan volcanic field, southwestern Colorado-lead isotope evidence: Econ. Geol., v. 74, p. 1-26.
- Doell, R. R., Dalrymple, G. B., Smith, R. L., and Bailey, R. A., 1968, Paleomagnetism, potassium-argon ages, and geology of rhyolites and associated rocks of the Valles caldera, New Mexico: Geol. Soc. America Memoir 116, p. 211-248.
- Eaton, G. P., Christiansen, R. L., Iyer, H. M., Pitt, A. M., Mabey, D. R., Blank, H. R., Jr., Zietz, I., and Gettings, M. E., 1975, Magma beneath Yellowstone National Park: Science, v. 188, p. 787-796.
- Ekren, E. B., Anderson, R. E., Rogers, C. L., and Noble, D. C., 1971, Geology of northern Nellis Air Force base bombing and gunnery range, Nye County, Nevada: U. S. Geol. Survey Prof. Paper 651, 91 p.
- Ekren, E. B., Hinrichs, E. N., and Dixon, G. L., 1972, Geologic map of the Wall quadrangle, Nye County, Nevada: U. S. Geol. Survey Map I-719 (1:48000).
- Ekren, E. B., Hinrichs, E. N., Quinlivan, W. D., and Hoover, D. L., 1973a, Geologic map of the Moores Station quadrangle, Nye County, Nevada: U. S. Geol. Survey Map I-756 (1:48000).
- Ekren, E. B., Rogers, C. L., and Dixon, G. L., 1973b, Geologic and bouguer gravity map of the Reveille quadrangle, Nye County, Nevada: U. S. Geol. Survey Map I-806 (1:48000).
- Ekren, E. B., Quinlivan, W. D., Snyder, R. P., and Kleinhampl, F. J., 1974, Stratigraphy, structure, and geologic history of the Lunar Lake caldera of northern Nye County, Nevada: U. S. Geol. Survey Jour. Research, v. 2, p. 599-608.
- Ellis, A. J., 1979, Explored geothermal systems: in Barnes, H. L., ed., Geochemistry of Hydrothermal Ore Deposits, John Wiley and Sons, New York, p. 632-683.

- Emeleus, C. H., 1982, The central complexes: in Sutherland, D. S., ed., *Igneous Rocks of the British Isles*, John Wiley and Sons, New York, p. 369-414.
- Eslinger, E. V., and Savin, S. M., 1973, Mineralogy and oxygen isotope geochemistry of the hydrothermally altered rocks of the Ohaki-Broadlands, New Zealand geothermal area: *Amer. Jour. Sci.*, v. 273, p. 240-267.
- Fenner, C. N., 1936, Bore-hole investigations in Yellowstone Park: *Jour. Geology*, v. 44, p. 225-315.
- Fisher, R. P., Luedke, R. G., Sheridan, M. J., and Raabe, R. G., 1968, Mineral resources of the Uncompahgre primitive area, Colorado: *U. S. Geol. Survey Bull.* 1261-C, 91 p.
- Forester, R. W., and Taylor, H. P., Jr., 1972, Oxygen and hydrogen isotope data on the interaction of meteoric ground waters with a gabbro-diorite stock, San Juan Mountains, Colorado: *Internat. Geol. Cong.*, 24th, Montreal, v. 10, p. 254-263.
- Forester, R. W., and Taylor, H. P., Jr., 1976, ^{18}O -depleted igneous rocks from the Tertiary complex of the Isle of Mull, Scotland: *Earth Planet. Sci. Letters*, v. 32, p. 11-17.
- Forester, R. W., and Taylor, H. P., Jr., 1977, $^{18}\text{O}/^{16}\text{O}$, D/H, and $^{13}\text{C}/^{12}\text{C}$ studies of the Tertiary complex of Skye, Scotland: *Amer. Jour. Sci.*, v. 277, p. 136-177.
- Forester, R. W., and Taylor, H. P., Jr., 1980, Oxygen, hydrogen, and carbon isotope studies of the Stony Mountain complex, western San Juan Mountains, Colorado: *Econ. Geol.*, v. 75, p. 362-383.
- Friedman, I., Redfield, A. C., Schoen, B., and Harris, J., 1964, The variation of the deuterium content of the natural waters in the hydrologic cycle: *Rev. Geophysics*, v. 2, p. 177-224.
- Friedman, I., Lipman, P. W., Obradovich, J. D., and Gleason, J. D., 1974, Meteoric waters in magmas: *Science*, v. 184, p. 1069-1072.
- Garlick, G. D., 1966, Oxygen isotope fractionation in igneous rocks: *Earth Planet. Sci. Letters*, v. 1, p. 361-368.
- Gromme, C. S., McKee, E. H., and Blake, M. C., Jr., 1972, Paleomagnetic correlations and potassium-argon dating of middle Tertiary ash-flow sheets in the eastern Great Basin, Nevada and Utah: *Geol. Soc. America Bull.*, v. 83, p. 1619-1638.
- Haas, J. L., Jr., 1971, The effect of salinity on the maximum thermal gradient of a hydrothermal system at hydrostatic pressure: *Econ. Geol.*, v. 66, p. 940-946.

- Hall, R. B., 1978, World non-bauxite aluminum resources: U. S. Geol. Survey Prof. Paper 1076-A, 35 p.
- Hamza, M. S., and Epstein, S., 1980, Oxygen isotopic fractionation between oxygen of different sites in hydroxyl-bearing silicate minerals: *Geochim. et Cosmochim. Acta*, 44, p. 173-182.
- Hansen, W. R., 1971, Geologic map of the Black Canyon of the Gunnison River and vicinity, western Colorado: U. S. Geol. Survey Map I-584 (1:31680).
- Hansen, W. R., and Peterman, Z. E., 1968, Basement-rock geochronology of the Black Canyon of the Gunnison, Colorado: U. S. Geol. Survey Prof. Paper 600-C, p. 80-90.
- Helgeson, H. C., 1969, Thermodynamics of hydrothermal systems at elevated temperatures and pressures: *Amer. Jour. Sci.*, V. 267, p. 729-804.
- Hemley, J. J., and Jones, W. R., 1964, Chemical aspects of hydrothermal alteration with emphasis on hydrogen metasomatism: *Econ. Geol.*, v. 59, p. 538-569.
- Hildreth, W., 1981, Gradients in Silicic Magma Chambers: Implications for Lithospheric Magmatism: *Jour. Geophys. Research*, v. 86, p. 10153-10192.
- Hildreth, W., Christiansen, R. L., and O'Neil, J. R., 1980, Catastrophic isotopic modification of rhyolitic magma by creation of the Yellowstone caldera [abstract]: *Geol. Soc. America Abstracts with Programs*, v. 12, p. 111.
- Hon, K., Lipman, P. W., and Mehnert, H. H., 1983, The Lake City caldera, western San Juan Mountains, Colorado [abstract]: *Geol. Soc. America Abstracts with Programs*, v. 15, p. 389.
- Irving, J. D., and Bancroft, H., 1911, Geology and ore deposits near Lake City, Colorado: U. S. Geol. Survey Bull. 478, 128 p.
- Jackson, S. E., Harmon, R. S., Lux, D. R., Rice, C. M., and Ringrose, C. R., 1980, Isotopic geochemistry and chronology of porphyry-style mineralisation near Ophir, San Juan Mountains, Colorado [abstract]: *Geol. Soc. America Abstracts with Programs*, v. 12, p. 454.
- Knauth, L. P., and Epstein, S., 1976, Hydrogen and oxygen isotope ratios in nodular and bedded cherts: *Geochim. et Cosmochim. Acta*, v. 40, p. 1095-1108.
- Krasowski, D. J., 1976, Geology and ore deposits of Burrows Park, Hinsdale County, Colorado: M. S. thesis, Colorado State Univ., Ft. Collins, 111 p.

- Kulla, J. B., and Anderson, T. F., 1978, Experimental oxygen isotope fractionation between kaolinite and water: U. S. Geol. Survey Open File Report 78-701, p. 234-235.
- Lachenbruch, A. H., Sorey, M. L., Lewis, R. E., and Sass, J. H., 1976, The near-surface hydrothermal regime of Long Valley caldera: Jour. Geophys. Research, v. 81, p. 763-768.
- Lambert, S. J., 1975, Stable isotope studies of some active hydrothermal systems: Ph.D. thesis, California Institute of Technology, Pasadena, 362 p.
- Lambert, S. J., and Epstein, S., 1980, Stable isotope investigations of an active geothermal system in Valles caldera, Jemez Mountains, New Mexico: Jour. Volcan. Geotherm. Research, v. 8, p. 111-129.
- Larsen, E. S., Jr., 1911, The economic geology of Carson Camp, Hinsdale County, Colorado: U. S. Geol. Survey Bull. 470, p. 30-38.
- Larsen, E. S., Jr., 1913, Alunite in the San Cristobal quadrangle, Colorado: U. S. Geol. Survey Bull. 530, p. 179-183.
- Larsen, E. S., Jr., and Cross, W., 1956, Geology and petrology of the San Juan region, southwestern Colorado: U. S. Geol. Survey Prof. Paper 258, 303 p.
- Laughlin, A. W., 1981, The geothermal system of the Jemez Mountains, New Mexico, and its exploration: in Rybach, L., and Muffler, L. J. P., eds., Geothermal Systems: Principles and Case Histories, John Wiley and Sons, New York, p. 295-320.
- Leeman, W. P., Doe, B. R., and Whelan, J., 1977, Radiogenic and stable isotope studies of hot-spring deposits in Yellowstone National Park and their genetic implications: Geochem. Jour., v. 11, p. 65-74.
- Lewis, R. E., 1974, Data on wells, springs, and thermal springs in Long Valley, Mono County, California: U. S. Geol. Survey Open File Report, 52 p.
- Lipman, P. W., 1971, Iron-titanium oxide phenocrysts in compositionally zoned ash-flow sheets from southern Nevada: Jour. Geology, v. 79, p. 438-456.
- Lipman, P. W., 1974, Geologic map of the Platoro caldera area, southeastern San Juan Mountains, southwestern Colorado: U. S. Geol. Survey Map I-828 (1:48000).
- Lipman, P. W., 1975, Evolution of the Platoro caldera complex and related volcanic rocks, southeastern San Juan Mountains, Colorado: U. S. Geol. Survey Prof. Paper 852, 128 p.

- Lipman, P. W., 1976a, Geologic map of the Lake City caldera area, western San Juan Mountains, southwestern Colorado: U. S. Geol. Survey Map I-962 (1:48000).
- Lipman, P. W., 1976b, Caldera-collapse breccias in the western San Juan Mountains, Colorado: Geol. Soc. America Bull., v. 87, p. 1397-1410.
- Lipman, P. W., and Friedman, I., 1975, Interaction of meteoric water with magma: an oxygen isotope study of ash-flow sheets from southern Nevada: Geol. Soc. America Bull., v. 86, p. 695-702.
- Lipman, P. W., and Steven, T. A., 1976, Geologic map of the South Fork area, eastern San Juan Mountains, southwestern Colorado: U. S. Geol. Survey Map I-966 (1:48000).
- Lipman, P. W., Steven, T. A., and Mehnert, H. H., 1970, Volcanic history of the San Juan Mountains, Colorado, as indicated by potassium-argon dating: Geol. Soc. America Bull., v. 81, p. 2329-2352.
- Lipman, P. W., Steven, T. A., Luedke, R. G., and Burbank, W. S., 1973, Revised volcanic history of the San Juan, Uncompahgre, Silverton, and Lake City calderas in the western San Juan Mountains, Colorado: U. S. Geol. Survey Jour. Research, v. 1, p. 627-642.
- Lipman, P. W., Fisher, F. S., Mehnert, H. H., Naeser, C. W., Luedke, R. G., and Steven, T. A., 1976, Multiple ages of mid-Tertiary mineralization and alteration in the western San Juan Mountains, Colorado: Econ. Geol., v. 71, p. 571-588.
- Lipman, P. W., Doe, B. R., Hedge, C. E., and Steven, T. A., 1978, Petrologic evolution of the San Juan volcanic field, southwestern Colorado: Pb and Sr isotope evidence: Geol. Soc. America Bull., v. 89, p. 59-82.
- Lipman, P. W., Bethke, P. M., Casadevall, T. J., and Steven, T. A., 1982, Field trip guide: Society of Economic Geologists field conference on relationship of mineralization to volcanic evolution of the San Juan Mountains, Colorado, 56 p.
- Luedke, R. G., and Burbank, W. S., 1962, Geology of the Ouray quadrangle, Colorado: U. S. Geol. Survey Map GQ-152 (1:24000).
- Luedke, R. G., and Burbank, W. S., 1963, Tertiary volcanic stratigraphy in the western San Juan Mountains, Colorado: U. S. Geol. Survey Prof. Paper 475-C, p. 39-44.
- Luedke, R. G., and Burbank, W. S., 1968, Volcanism and cauldron development in the western San Juan Mountains, Colorado: Colorado Sch. Mines Quarterly, v. 63, p. 175-208.
- Luedke, R. G., and Hosterman, J. W., 1971, Clay minerals, Longfellow mine, San Juan County, Colorado: U. S. Geol. Survey Prof. Paper 750-C, p. 104-111.

- McBirney, A. R., 1979, Effects of assimilation: in Yoder, H. S., Jr., ed., *The Evolution of Igneous Rocks*, Princeton Univ. Press, Princeton, New Jersey, p. 307-338.
- Maher, B. J., 1982, Geology, geochemistry, and genesis of the Engineer Pass breccia pipe and intrusive complex, western San Juan Mountains, Colorado [abstract]: *Geol. Soc. America Abstracts with Programs*, v. 14, p. 341.
- Mariner, R. H., and Wiley, L. M., 1976, Geochemistry of thermal waters in Long Valley, Mono County, California: *Jour. Geophys. Research*, v. 81, p. 792-800.
- Marvin, R. F., Mehnert, H. H., and McKee, E. H., 1973, A summary of radiometric ages of Tertiary volcanic rocks in Nevada and eastern California. Part III: southeastern Nevada: *Isochron/West*, no. 6, p. 1-30.
- Mayor, J. N., and Fisher, F. S., 1972, Middle Tertiary replacement ore bodies and associated veins in the northwest San Juan Mountains, Colorado: *Econ. Geol.*, v. 67, p. 214-230.
- Mehnert, H. H., Lipman, P. W., and Steven, T. A., 1973a, Age of the Lake City caldera and related Sunshine Peak Tuff, western San Juan Mountains, Colorado: *Isochron/West*, no. 6, p. 31-33.
- Mehnert, H. H., Lipman, P. W., and Steven, T. A., 1973b, Age of mineralization at Summitville, Colorado, as indicated by K-Ar dating of alunite: *Econ. Geol.*, v. 68, p. 399-401.
- Mehnert, H. H., Slack, J. F., and Cebula, G. T., 1980, K-Ar age of alunite alteration at Red Mountain, Lake City area, western San Juan Mountains, Colorado: *Isochron/West*, no. 28, p. 9-11.
- Morgan, P., Blackwell, D. D., and Spafford, R. E., 1977, Heat flow measurements in Yellowstone Lake and the thermal structure of the Yellowstone caldera: *Jour. Geophys. Research*, v. 82, p. 3719-3732.
- Muehlenbachs, K., Anderson, A. T., Jr., and Sigvaldason, G. E., 1974, Low-¹⁸O basalts from Iceland: *Geochim. et Cosmochim. Acta*, v. 38, p. 577-588.
- Naeser, C. W., Cunningham, C. G., Marvin, R. F., and Obradovich, J. D., 1980, Pliocene intrusive rocks and mineralization near Rico, Colorado: *Econ. Geol.*, v. 75, p. 122-133.
- Noble, D. C., and Hedge, C. E., 1969, Sr⁸⁷/Sr⁸⁶ variations within individual ash-flow sheets: *U. S. Geol. Survey Prof. Paper* 650-C, p. 133-139.

- Norton, D., 1978, Sourcelines, sorceregions, and pathlines for fluids in hydrothermal systems related to cooling plutons: *Econ. Geol.*, v. 73, p. 21-28.
- Norton, D., 1982, Fluid and heat transport phenomena typical of copper-bearing pluton environments: in Titley, S. R., ed., *Advances in Geology of the Porphyry Copper Deposits*, University of Arizona, Tucson, p. 59-72.
- Norton, D., and Knight, J., 1977, Transport phenomena in hydrothermal systems: cooling plutons: *Amer. Jour. Sci.*, v. 277, p. 937-981.
- O'Leary, W. J., and Whitney, J. A., 1981, Magmatic paragenesis of the Fish Canyon ash-flow tuff, central San Juan Mountains, Colorado [abstract]: *Geol. Soc. America Abstracts with Programs*, v. 13, p. 521.
- O'Neil, J. R., and Taylor, H. P., Jr., 1967, The oxygen isotope and cation exchange chemistry of feldspars: *Am. Mineralogist*, v. 52, p. 1414-1437.
- O'Neil, J. R., and Taylor, H. P., Jr., 1969, Oxygen isotope equilibrium between muscovite and water: *Jour. Geophys. Research*, v. 74, p. 6012-6022.
- O'Neil, J. R., and Silberman, M. L., 1974, Stable isotope relations in epithermal Au-Ag deposits: *Econ. Geol.*, v. 69, p. 902-909.
- O'Neil, J. R., Silberman, M. L., Fabbi, B. P., and Chesterman, C. W., 1973, Stable isotope and chemical relations during mineralization in the Bodie mining district, Mono County, California: *Econ. Geol.*, v. 68, p. 765-784.
- Peacock, M. A., 1931, Classification of igneous rock series: *Jour. Geology*, v. 39, p. 54-67.
- Plouff, D., and Pakiser, L. C., 1972, Gravity study of the San Juan Mountains, Colorado: *U. S. Geol. Survey Prof. Paper 800-B*, p. 183-190.
- Pratt, W. P., McKnight, E. T., and DeHon, R. A., 1969, Geologic map of the Rico quadrangle, Dolores, and Montezuma Counties, Colorado: *U. S. Geol. Survey Map GQ-797 (1:24000)*.
- Quinlivan, W. D., and Rogers, C. L., 1974, Geologic map of the Tybo quadrangle, Nye County, Nevada: *U. S. Geol. Survey Map I-821 (1:48000)*.
- Quinlivan, W. D., Rogers, C. L., and Dodge, H. W., Jr., 1974, Geologic map of the Portuguese Mountain quadrangle, Nye County, Nevada: *U. S. Geol. Survey Map I-804 (1:48000)*.

- Ransome, F. L., 1901, Economic geology of the Silverton quadrangle, Colorado: U. S. Geol. Survey Bull. 182, 265 p.
- Ratte, J. C., and Steven, T. A., 1964, Magmatic differentiation in a volcanic sequence related to the Creede caldera, Colorado: U. S. Geol. Survey Prof. Paper 475-D, p. 49-53.
- Ratte, J. C., and Steven, T. A., 1967, Ash flows and related volcanic rocks associated with the Creede caldera, San Juan Mountains, Colorado: U. S. Geol. Survey Prof. Paper 524-H, 58 p.
- Rinehart, C. D., and Ross, D. C., 1964, Geology and mineral deposits of the Mount Morrison quadrangle, Sierra Nevada, California: U. S. Geol. Survey Prof. Paper 385, 106 p.
- Ringrose, C. R., Harmon, R. S., Jackson, S. E., and Rice, C. M., 1981, Stable isotopic composition of fluid inclusions in a porphyry-style hydrothermal system near Silverton, San Juan Mountains, Colorado [abstract]: Geol. Soc. America Abstracts with Programs, v. 13, p. 538.
- Rose, A. W., and Burt, D. M., 1979, Hydrothermal alteration: in Barnes, H. L., ed., Geochemistry of Hydrothermal Ore Deposits, John Wiley and Sons, New York, p. 173-235.
- Schmitt, L. J., and Raymond, W. H., 1977, Geology and mineral deposits of the Needle Mountains district, southwestern Colorado: U. S. Geol. Survey Bull., 1434, 40 p.
- Scott, D. H., and Trask, N. J., 1971, Geology of the Lunar Crater volcanic field, Nye County, Nevada: U. S. Geol. Survey Prof. Paper 599-I, 22 p.
- Serna-Isaza, M. J., 1971, Geology and geochemistry of Calico Peak, Dolores County, Colorado: M. S. thesis, Colorado School Mines, Golden, 88 p.
- Shaw, H. R., 1974, Diffusion of H₂O in granitic liquids: part I. Experimental data; part II. Mass transfer in magma chambers: in, Hofmann, A. W., Giletti, B. J., Yoder, H. S., Jr., and Yund, R. A., eds., Geochemical Transport and Kinetics, Carnegie Institute of Washington, Publication 634, p. 139-170.
- Sheppard, S. M. F., and Taylor, H. P., Jr., 1974, Hydrogen and oxygen isotope evidence for the origins of water in the Boulder batholith and the Butte ore deposits, Montana: Econ. Geol., v. 69, p. 926-946.
- Sheppard, S. M. F., Nielsen, R. L., and Taylor, H. P., Jr., 1969, Oxygen and hydrogen isotope ratios of clay minerals from porphyry copper deposits: Econ. Geol., v. 64, p. 755-777.

- Sheppard, S. M. F., Nielsen, R. L., and Taylor, H. P., Jr., 1971, Hydrogen and oxygen isotope ratios in minerals from porphyry copper deposits: *Econ. Geol.*, v. 66, p. 515-542.
- Silver, L. T., and Barker, F., 1967, Geochronology of Precambrian rocks of the Needle Mountains, southwestern Colorado: Part I, U-Pb zircon results [abstract]: *Geol. Soc. America Spec. Paper* 115, p. 204-205.
- Slack, J. F., 1980, Multistage vein ores of the Lake City district, western San Juan Mountains, Colorado: *Econ. Geol.*, v. 75, p. 963-991.
- Smith, R. L., and Bailey, R. A., 1968, Resurgent cauldrons: *Geol. Soc. America Memoir* 116, p. 613-662.
- Smith, R. L., Bailey, R. A., and Ross, C. S., 1970, Geologic map of the Jemez Mountains, New Mexico: U. S. Geol. Survey Map I-571 (1:125000).
- Snyder, R. P., Ekren, E. B., and Dixon, G. L., 1972, Geologic map of the Lunar Lake Crater quadrangle, Nye County, Nevada: U. S. Geol. Survey Map I-700 (1:48000).
- Solomon, G. C., and Taylor, H. P., Jr., 1981, The geographic distribution of $\delta^{18}\text{O}$ values in Mesozoic and early Cenozoic granitic rocks of the southwestern North American cordillera [abstract]: *Geol. Soc. America Abstracts with Programs*, v. 13, p. 558.
- Sorey, M. L., and Lewis, R. E., 1976, Convective heat flow from hot springs in the Long Valley caldera, Mono County, California: *Jour. Geophys. Research*, v. 81, p. 785-791.
- Steven, T. A., 1967, Geologic map of the Bristol Head quadrangle, Mineral and Hinsdale Counties, Colorado: U. S. Geol. Survey Map GQ-631 (1:62500).
- Steven, T. A., and Lipman, P. W., 1973, Geologic map of the Spar City quadrangle, Mineral County, Colorado: U. S. Geol. Survey Map GQ-1052 (1:62500).
- Steven, T. A., and Lipman, P. W., 1976, Calderas of the San Juan volcanic field, southwestern Colorado: U. S. Geol. Survey Prof. Paper 958, 35 p.
- Steven, T. A., and Ratte, J. C., 1960, Geology and ore deposits of the Summitville district, San Juan Mountains, Colorado: U. S. Geol. Survey Prof. Paper 343, 70 p.
- Steven, T. A., and Ratte, J. C., 1965, Geology and structural control of ore deposition in the Creede district, San Juan Mountains, Colorado: U. S. Geol. Survey Prof. Paper 487, 87 p.

- Steven, T. A., and Ratte, J. C., 1973, Geologic map of the Creede quadrangle, Mineral and Saguache Counties, Colorado: U. S. Geol. Survey Map GQ-1053 (1:62500).
- Steven, T. A., Mehnert, H. H., and Obradovich, J. D., 1967, Age of volcanic activity in the San Juan Mountains, Colorado: U. S. Geol. Survey Prof. Paper 575-D, p. 47-55.
- Steven, T. A., Luedke, R. G., and Lipman, P. W., 1974, Relation of mineralization to calderas in the San Juan volcanic field, southwestern Colorado: U. S. Geol. Survey Jour. Research, v. 2, p. 405-409.
- Stewart, J. H., 1978, Basin-Range structure in western North America: Geol. Soc. America Memoir 152, p. 1-31.
- Stormer, J. C., and Carmichael, I. S. E., 1971, Fluorine-hydroxyl exchange in apatite and biotite: a potential igneous geothermometer: Contr. Mineralogy Petrology, v. 31, p. 121-131.
- Stuckless, J. S., and O'Neil, J. R., 1973, Petrogenesis of the Superstition-Superior volcanic area as inferred from strontium and oxygen isotope studies: Geol. Soc. America Bull., v. 84, p. 1987-1997.
- Taylor, H. P., Jr., 1968, The oxygen isotope geochemistry of igneous rocks: Contr. Mineralogy Petrology, v. 19, p. 1-71.
- Taylor, H. P., Jr., 1971, Oxygen isotope evidence for large-scale interaction between meteoric ground waters and Tertiary granodiorite intrusions, Western Cascade Range, Oregon: Jour. Geophys. Research, v. 76, p. 7855-7874.
- Taylor, H. P., Jr., 1973, O^{18}/O^{16} evidence for meteoric-hydrothermal alteration and ore deposition in the Tonopah, Comstock Lode, and Goldfield mining districts, Nevada: Econ. Geol., v. 68, 747-764.
- Taylor, H. P., Jr., 1974a, Oxygen and hydrogen isotopic evidence for large-scale circulation and interactions between ground waters and igneous intrusions, with particular reference to the San Juan volcanic field, Colorado: in, Hofmann, A. W., Giletti, B. J., Yoder, H. S., Jr., and Yund, R. A., eds., Geochemical Transport and Kinetics, Carnegie Institute of Washington, Publication 634, p. 299-324.
- Taylor, H. P., Jr., 1974b, The application of oxygen and hydrogen isotope studies to problems of hydrothermal alteration and ore deposition: Econ. Geol., v. 69, p. 843-883.
- Taylor, H. P., Jr., 1977, Water/rock interactions and the origin of H_2O in granitic batholiths: Jour. Geol. Soc. London, v. 133, p. 509-558.

- Taylor, H. P., Jr., 1978, Oxygen and hydrogen isotope studies of plutonic granitic rocks: *Earth Planet. Sci. Letters*, v. 38, p. 177-210.
- Taylor, H. P., Jr., 1979, Oxygen and hydrogen isotope relationships in hydrothermal mineral deposits: in, Barnes, H. L., ed., *Geochemistry of Hydrothermal Ore Deposits*, John Wiley and Sons, New York, p. 236-277.
- Taylor, H. P., Jr., 1980a, Stable isotope studies of spreading centers and their bearing on the origin of granophyres and plagiogranites: *Colloques Internationaux du C. N. R. S.*, No. 272, Association Mafiques-Ultra Mafiques dans les Orogenes, p. 149-165.
- Taylor, H. P., Jr., 1980b, The effects of assimilation of country rocks by magmas on $^{18}\text{O}/^{16}\text{O}$ and $^{87}\text{Sr}/^{86}\text{Sr}$ systematics in igneous rocks: *Earth Planet. Sci. Letters*, v. 47, p. 243-254.
- Taylor, H. P., Jr., and Epstein, S., 1962a, Relationship between $^{18}\text{O}/^{16}\text{O}$ ratios in coexisting minerals in igneous and metamorphic rocks. Part 1. Principles and experimental results: *Geol. Soc. America Bull.*, v. 73, p. 461-480.
- Taylor, H. P., Jr., and Epstein, S., 1962b, Relationship between $^{18}\text{O}/^{16}\text{O}$ ratios in coexisting minerals of igneous and metamorphic rocks. Part 2. Application to petrologic problems: *Geol. Soc. America Bull.*, v. 73, p. 675-694.
- Taylor, H. P., Jr., and Forester, R. W., 1971, Low- ^{18}O igneous rocks from the intrusive complexes of Skye, Mull, and Ardnamurchan, western Scotland: *Jour. Petrology*, v. 12, p. 465-497.
- Taylor, H. P., Jr., and Forester, R. W., 1979, An oxygen and hydrogen isotope study of the Skaergaard intrusion and its country rocks: a description of a 55-m.y. old fossil hydrothermal system: *Jour. Petrology*, v. 20, p. 355-419.
- Taylor, H. P., Jr., and Magaritz, M., 1978, Oxygen and hydrogen isotope studies of the cordilleran batholiths of western North America: in, Robinson, B. W., ed., *Stable Isotopes in the Earth Sciences*, New Zealand Dept. of Sci. and Ind. Research Bull. 220, p. 151-174.
- Truesdell, A. H., Nathenson, M., and Rye, R. O., 1977, The effects of subsurface boiling and dilution on the isotopic compositions of Yellowstone thermal waters: *Jour. Geophys. Research*, v. 82, p. 3694-3704.
- Turi, B., and Taylor, H. P., Jr., 1971, An oxygen and hydrogen isotope study of a granodiorite pluton from the Southern California batholith: *Geochim. et Cosmochim. Acta*, v. 35, p. 383-406.

- Tuttle, O. F., and Bowen, N. L., 1958, Origin of granite in the light of experimental studies in the system $\text{NaAlSi}_3\text{O}_8\text{-KAlSi}_3\text{O}_8\text{-SiO}_2\text{-H}_2\text{O}$: Geol. Soc. America Memoir 74, 153 p.
- Vanderwilt, J. W., 1947, Mineral resources of Colorado: State of Colorado Mineral Resources Board, Denver, 547 p.
- Wenner, D. B., and Taylor, H. P., Jr., 1971, Temperatures of serpentinization of ultramafic rocks based on $\text{O}^{18}/\text{O}^{16}$ fractionation between coexisting serpentine and magnetite: Contr. Mineralogy Petrology, v. 32, p. 165-185.
- White, D. E., 1978, Conductive heat flows in research drill holes in thermal areas of Yellowstone National Park, Wyoming: U. S. Geol. Survey Jour. Research, v. 6, p. 765-774.
- White, D. E., Muffler, L. J. P., and Truesdell, A. H., 1971, Vapor-dominated hydrothermal systems compared with hot-water systems: Econ. Geol., v. 66, p. 75-97.
- White, D. E., Fournier, R. O., Muffler, L. P. J., and Truesdell, A. H., 1975, Physical results of research drilling in thermal areas of Yellowstone National Park, Wyoming: U. S. Geol. Survey Prof. Paper 892, 70 p.
- Whitney, J. A., and Stormer, J. C., Jr., 1983, Igneous sulfides in the Fish Canyon Tuff and the role of sulfur in calc-alkaline magmas: Geology, v. 11, p. 99-102.
- Williams, A. E., 1978, Circulation in a fossil geothermal area-- $\delta^{18}\text{O}$ study: U. S. Geol. Survey Open File Report 78-701, p. 453-455.
- Woolsey, L. H., 1907, Lake Fork extension of the Silverton mining area, Colorado: U. S. Geol. Survey Bull. 315, p. 26-30.